

Institut für Anorganische und Analytische Chemie  
der Justus-Liebig-Universität Gießen



# **Investigations on the Behavior of Zinc and Copper Complexes Containing Polydentate Amine Ligands**

Inaugural-Dissertation zur Erlangung des Doktorgrades der  
Naturwissenschaften im Fachbereich Biologie und Chemie der  
Justus-Liebig-Universität Gießen

Vorgelegt  
von  
Alexander Beitat  
aus Gießen

*For Simone, Nina, Ida  
and  
My parents*

## **Acknowledgement**

First of all I would like to thank my supervisor Siegfried Schindler for his great support, guidance and patience throughout the time of my thesis. He gave me enough room to develop and made me find my own way.

Furthermore I would like to express my gratitude for the financial support of the DFG and Prof. Schindlers group at the Institute of Inorganic and Analytic Chemistry of the Justus Liebig University Gießen that made my thesis possible.

Additionally, all of my colleagues and lab mates deserve a lot of gratefulness. Especially I have to thank my “roomies” Anja Henß, Sabrina Turba, Sabrina Schäfer, Jenny Blank, Jörg Müller, Thomas Nebe, and Christian Würtele for the discussion and good advice during that time, you made the daily routine worthwhile. Here, I found great friends that supported me during my time at the university and beyond.

This work would not have been possible without the support of all the members of the Institute of Inorganic and Analytical Chemistry of the Justus Liebig University, especially Christian Würtele, Michael Serafin and Günther Koch who told me a lot about crystallography and helped me carrying out the crystallographic measurements. Additionally, I would like to thank the external crystallographers Frank Hampel and Frank Heinemann at the University of Erlangen Nürnberg, Olaf Walter at the Karlsruhe Institute of Technology and Harald Kelm at the Technical University Kaiserslautern for the measurement of numerous crystal structures.

The magnetic measurements presented in chapter 2.1 were performed in cooperation with the group of Miguel Julve at the University of Valencia and Paul Müllers group at the University of Erlangen-Nürnberg as well. Special thanks due to my colleague Sabrina Turba, who performed great parts of the synthetic work for chapter 2.1 already published in her doctoral thesis.<sup>1</sup>

In chapter 4.1 emission spectroscopy measurements were performed in cooperation with the group of Günter Knör at the Johannes Kepler University Linz. Thanks to Heike Hausmann, who performed the elaborate NMR spectroscopic measurements at the Institute of Organic Chemistry at the Justus Liebig University. Special thanks due to Simon Foxon, who initiated the study in this chapter and Jing-Yuan Xu, who initiated the work presented in chapter 5.1.

I want to express my gratitude to Cornelius Brombach for the great support in the laboratory during the time of his Bachelor- and Master thesis. It was a real pleasure to work with you.

## Acknowledgement

---

Last but not least my warmest thanks belong to Simone, Nina, Ida and my whole family for their great support in every situation throughout my time at the university. Without you it would not have been possible.



## **Table of Contents**

Acknowledgement .....	I
Table of Contents.....	III
Table of Abbreviations.....	IX
Ligand Index.....	XI
<b>1 Introduction.....</b>	<b>1</b>
1.1 Motivation.....	1
1.2 Activation of Small Molecules.....	2
1.2.1 Activation of Dioxygen.....	2
1.2.1.1 C-H Bond Activation.....	4
1.2.2 Activation of Carbon Dioxide .....	6
1.3 Zinc Coordination Compounds as Selective Ion Sensors .....	7
1.4 Formation of Coordination Polymers.....	10
1.5 Goals .....	12
<b>2 Ligands Containing Bridged Bispicolylamine Units .....</b>	<b>14</b>
2.1 Syntheses, Characterization and Magnetic Studies of Copper(II) Complexes with the Ligand <i>N,N,N',N'</i> -Tetrakis(2-pyridylmethyl)-1,3-benzenediamine ( <b>1,3-tpbd</b> ) and its Phenol Derivative 2,6-Bis[bis(2-pyridylmethyl)amino]- <i>p</i> -cresol] ( <b>2,6-Htpcd</b> ).....	14
2.1.1 Introduction.....	15
2.1.2 Results and Discussion.....	16
2.1.2.1 Syntheses.....	16
2.1.2.2 Molecular Structures of Copper(II) Complexes.....	16
2.1.2.2.1 [Cu <sub>4</sub> ( <b>1,3-tpbd</b> ) <sub>2</sub> (H <sub>2</sub> O) <sub>4</sub> (NO <sub>3</sub> ) <sub>4</sub> ] <sub>n</sub> (NO <sub>3</sub> ) <sub>4n</sub> ·13nH <sub>2</sub> O ( <b>1</b> ) .....	16
2.1.2.2.2 [Cu <sub>4</sub> ( <b>1,3-tpbd</b> ) <sub>2</sub> (AsO <sub>4</sub> )(ClO <sub>4</sub> ) <sub>3</sub> (H <sub>2</sub> O)](ClO <sub>4</sub> ) <sub>2</sub> ·2H <sub>2</sub> O·0.5CH <sub>3</sub> OH ( <b>2</b> ) .....	18
2.1.2.2.3 [Cu <sub>4</sub> ( <b>1,3-tpbd</b> ) <sub>2</sub> (PO <sub>4</sub> )(ClO <sub>4</sub> ) <sub>3</sub> (H <sub>2</sub> O)](ClO <sub>4</sub> ) <sub>2</sub> ·2H <sub>2</sub> O·0.5CH <sub>3</sub> OH ( <b>3</b> ).....	20
2.1.2.2.4 [Cu <sub>2</sub> ( <b>1,3-tpbd</b> ){(PhO) <sub>2</sub> P(O) <sub>2</sub> } <sub>2</sub> ] <sub>2n</sub> (ClO <sub>4</sub> ) <sub>4n</sub> ( <b>4</b> ).....	20
2.1.2.2.5 [Cu <sub>2</sub> ( <b>1,3-tpbd</b> )((PhO)PO <sub>3</sub> ) <sub>2</sub> (H <sub>2</sub> O) <sub>0.69</sub> (CH <sub>3</sub> CN) <sub>0.31</sub> ] <sub>2</sub> (BPh <sub>4</sub> ) <sub>4</sub> ·Et <sub>2</sub> O·CH <sub>3</sub> CN ( <b>5</b> )... ..	21
2.1.2.2.6 [Cu <sub>2</sub> ( <b>2,6-tpcd</b> )(H <sub>2</sub> O)Cl](ClO <sub>4</sub> ) <sub>2</sub> ·2H <sub>2</sub> O ( <b>6</b> ) .....	22
2.1.2.3 Magnetic Properties of <b>2</b> , <b>3</b> , <b>4</b> , and <b>6</b> .....	23
2.1.3 Conclusions.....	28
2.1.4 Experimental Section.....	28
2.1.4.1 Materials.....	28
2.1.4.2 Syntheses of Copper Complexes <b>1–5</b> .....	28
2.1.4.2.1 [Cu <sub>4</sub> ( <b>1,3-tpbd</b> ) <sub>2</sub> (H <sub>2</sub> O) <sub>4</sub> (NO <sub>3</sub> ) <sub>4</sub> ] <sub>n</sub> (NO <sub>3</sub> ) <sub>4n</sub> ·13nH <sub>2</sub> O ( <b>1</b> ) .....	28

2.1.4.2.2	[Cu <sub>4</sub> (1,3-tpbd) <sub>2</sub> (AsO <sub>4</sub> )(ClO <sub>4</sub> ) <sub>3</sub> (H <sub>2</sub> O)](ClO <sub>4</sub> ) <sub>2</sub> ·2H <sub>2</sub> O·0.5CH <sub>3</sub> OH (2) / [Cu <sub>4</sub> ( <b>1,3-tpbd</b> ) <sub>2</sub> (PO <sub>4</sub> )(ClO <sub>4</sub> ) <sub>3</sub> (H <sub>2</sub> O)](ClO <sub>4</sub> ) <sub>2</sub> ·2H <sub>2</sub> O·0.5CH <sub>3</sub> OH (3) / [Cu <sub>2</sub> ( <b>1,3-tpbd</b> ){(PhO) <sub>2</sub> P(O) <sub>2</sub> } <sub>2</sub> ] <sub>2</sub> (ClO <sub>4</sub> ) <sub>4</sub> ( <b>4</b> ) .....	29
2.1.4.2.3	[Cu <sub>2</sub> ( <b>1,3-tpbd</b> ){(PhO)PO <sub>3</sub> } <sub>2</sub> (H <sub>2</sub> O) <sub>0.69</sub> (CH <sub>3</sub> CN) <sub>0.31</sub> ] <sub>2</sub> (BPh <sub>4</sub> ) <sub>4</sub> ·Et <sub>2</sub> O·CH <sub>3</sub> CN ( <b>5</b> )... ..	29
2.1.4.3	Magnetic Measurements .....	29
2.1.4.4	X-Ray Crystallographic Studies.....	29
2.1.4.5	Acknowledgements .....	30
2.2	Supporting Information and Unpublished Material .....	30
2.2.1	Reactivity of <b>1,3-tpbd</b> Copper(I) Complexes Towards Dioxygen .....	30
2.2.2	Synthesis and Characterization of a Dimeric, Hydroxido Bridged <b>1,3-tpbd</b> Zinc(II) Complex .....	33
2.2.3	Experimental Section .....	34
2.2.3.1	Synthesis of [Zn <sub>4</sub> (H <sub>2</sub> O) <sub>2</sub> (OH) <sub>3</sub> ( <b>1,3-tpbd</b> ) <sub>2</sub> ](BF <sub>4</sub> ) <sub>5</sub> ·CH <sub>3</sub> COCH <sub>3</sub> ·xH <sub>2</sub> O .....	35
2.2.3.2	“Benchtop” UV/Vis Experiments.....	35
2.2.3.2.1	Solution of [Cu <sub>2</sub> ( <b>1,3-tpbd</b> )](SO <sub>3</sub> CF <sub>3</sub> ) <sub>2</sub> .....	35
2.2.3.2.2	Solution of [Cu <sub>2</sub> ( <b>1,3-tpbd</b> )](SbF <sub>6</sub> ) <sub>2</sub> .....	35
2.2.3.2.3	Solution of [Cu <sub>2</sub> ( <b>1,3-tpbd</b> )] <sup>2+</sup> and Cl <sup>-</sup> .....	36
2.2.3.3	Preparation of Copper(I) Solutions for Low Temperature Stopped-Flow experiments .....	36
2.2.3.3.1	Solution of [Cu <sub>2</sub> ( <b>1,3-tpbd</b> )](SbF <sub>6</sub> ) <sub>2</sub> .....	36
<b>3</b>	<b>Functionalized Unspenp Derivatives .....</b>	<b>37</b>
3.1	Introduction .....	37
3.2	Results and Discussion.....	39
3.2.1	Reactivity of Copper(I) Complexes Using <b>Ant-unspenp</b> Ligands Towards Dioxygen .....	39
3.2.2	Reactivity of Copper(I) Complexes of Bridged <b>Unspenp</b> Derivatives Towards Dioxygen .....	42
3.2.2.1	Synthesis and Characterization of a Carbonate Bridged Copper(II) Dimer ....	45
3.3	Conclusions.....	46
3.4	Experimental Section.....	47
3.4.1	Low Temperature Stopped Flow Measurements.....	47
3.4.1.1	X-ant Unspenp Solutions .....	47
3.4.1.2	[Cu <sub>2</sub> ( <b>Imxyl-unspenp</b> )] <sup>2+</sup> Solution .....	47
3.4.1.3	[Cu <sub>2</sub> ( <b>Hxyl-unspenp</b> )] <sup>2+</sup> Solution .....	48
3.4.2	Synthesis of [Cu <sub>4</sub> (CO <sub>3</sub> ) <sub>2</sub> ( <b>Hxyl-unspenp</b> ) <sub>2</sub> ](SbF <sub>6</sub> ) <sub>4</sub> .....	48
<b>4</b>	<b>Bispicolylamine Relatives Closely Related to Tmpa.....</b>	<b>49</b>
4.1	Syntheses, Emission Properties and Intramolecular Ligand Exchange of Zinc Complexes with Ligands Belonging to the Tmpa Family .....	49

4.1.1	Introduction.....	49
4.1.2	Results and Discussion.....	50
4.1.2.1	Ligand Synthesis.....	50
4.1.2.2	Metal Complexes.....	50
4.1.2.3	Crystal Structure Determinations.....	51
4.1.2.3.1	[( <b>L2</b> )ZnCl <sub>2</sub> ] ( <b>1a</b> ) .....	51
4.1.2.3.2	[( <b>L2</b> )Zn(OTf)(H <sub>2</sub> O)]OTf ( <b>1b</b> ).....	52
4.1.2.3.3	[( <b>L2</b> ) <sub>3</sub> Cu <sub>2</sub> ](BPh <sub>4</sub> ) <sub>2</sub> ( <b>1c</b> ) .....	53
4.1.2.3.4	[( <b>Me-bispic</b> )ZnCl <sub>2</sub> ] ( <b>2</b> ) .....	54
4.1.2.3.5	[ <b>L1H</b> ]OTf ( <b>3a</b> ) .....	56
4.1.2.3.6	[( <b>L1</b> )ZnCl <sub>2</sub> ] ( <b>3b</b> ) .....	57
4.1.2.3.7	[( <b>L1</b> ) <sub>2</sub> Zn(MeOH) <sub>2</sub> ](OTf) <sub>2</sub> ( <b>3c</b> ).....	58
4.1.2.3.8	[( <b>L1</b> ) <sub>2</sub> Cu <sub>2</sub> ](OTf) <sub>2</sub> ·2DMF ( <b>3d</b> ).....	59
4.1.2.4	Rationale for the Displayed Coordination Preferences of the Metal Atom in <b>1–3</b> .....	60
4.1.2.5	Fluxional Behaviour of the Complexes in Solution .....	61
4.1.2.6	Luminescence .....	64
4.1.3	Conclusions.....	66
4.1.4	Experimental Section.....	66
4.1.4.1	X-ray Structure Determination of <b>1–3</b> .....	67
4.1.4.2	Synthesis of Ligands.....	68
4.1.4.3	Preparation of Zinc(II) Complexes .....	68
4.1.4.3.1	General Procedure.....	68
4.1.4.3.2	[( <b>L2</b> )ZnCl <sub>2</sub> ] ( <b>1a</b> ) .....	68
4.1.4.3.3	[( <b>L2</b> )Zn(H <sub>2</sub> O)(OTf)]OTf ( <b>1b</b> ).....	68
4.1.4.3.4	[( <b>Me-bispic</b> )ZnCl <sub>2</sub> ] ( <b>2</b> ) .....	69
4.1.4.3.5	[ <b>L1H</b> ]OTf ( <b>3a</b> ) .....	69
4.1.4.3.6	[( <b>L1</b> )ZnCl <sub>2</sub> ] ( <b>3b</b> ) .....	69
4.1.4.3.7	[( <b>L1</b> ) <sub>2</sub> Zn(MeOH) <sub>2</sub> ](OTf) <sub>2</sub> ( <b>3c</b> ).....	70
4.1.4.3.8	Mixture of <b>L1</b> and Zn(OTf) <sub>2</sub> ( <b>3e</b> ) .....	70
4.1.4.4	Preparation of Copper(I) Complexes.....	70
4.1.4.4.1	General Procedure.....	70
4.1.4.4.2	[( <b>L2</b> ) <sub>3</sub> Cu <sub>2</sub> ](BPh <sub>4</sub> ) <sub>2</sub> ( <b>1c</b> ) .....	70
4.1.4.4.3	[( <b>L1</b> ) <sub>2</sub> Cu <sub>2</sub> ](OTf) <sub>2</sub> ·2DMF ( <b>3d</b> ) .....	71
4.1.5	Acknowledgements.....	71
4.2	Supporting Information and Unpublished Material for Chapter 1.1.....	71
4.2.1	NMR Spectroscopy .....	71

4.2.1.1	$^1\text{H}$ NMR Spectra at Ambient Temperature .....	71
4.2.1.1.1	[ <b>L2</b> ZnCl <sub>2</sub> ] ( <b>1a</b> ) .....	71
4.2.1.1.2	[ <b>L2</b> Zn(OTf)(H <sub>2</sub> O)]OTf ( <b>1b</b> ) .....	72
4.2.1.1.3	[ <b>Mebispic</b> ZnCl <sub>2</sub> ] ( <b>2</b> ) .....	72
4.2.1.1.4	[ <b>L1</b> ZnCl <sub>2</sub> ] ( <b>3b</b> ) .....	73
4.2.1.1.5	[( <b>L1</b> ) <sub>2</sub> Zn(MeOH) <sub>2</sub> ]OTf <sub>2</sub> ( <b>3c</b> ) .....	73
4.2.1.1.6	Mixture of <b>L1</b> and Zn(OTf) <sub>2</sub> ( <b>3e</b> ) .....	74
4.2.1.1.7	[ <b>tpa</b> ZnCl <sub>2</sub> ] .....	74
4.2.1.2	Variable Temperature $^1\text{H}$ NMR and 2D spectra .....	75
4.2.1.2.1	[ <b>Mebispic</b> ZnCl <sub>2</sub> ] ( <b>2</b> ) .....	75
4.2.1.2.2	[ <b>L1</b> ZnCl <sub>2</sub> ] ( <b>3b</b> ) .....	75
4.2.1.2.3	Mixture of <b>L1</b> and Zn(OTf) <sub>2</sub> ( <b>3e</b> ) .....	80
4.2.1.2.4	[ <b>tpa</b> ZnCl <sub>2</sub> ] .....	84
<b>5</b>	<b>Copper and Zinc Complexes Using Ligands Closely Related to <b>L2</b> .....</b>	<b>87</b>
5.1	Ligand Effects on the Formation of Coordination Polymers Containing Copper and Zinc Complexes with Derivatives of Tris(2-pyridylmethyl)amine ( <b>tmpa</b> ) as Ligands .....	87
5.1.1	Introduction .....	87
5.1.2	Results and Discussion .....	88
5.1.2.1	Ligands <b>L3</b> , <b>L4</b> and <b>L5</b> .....	88
5.1.2.2	Copper(I) Complexes of the Ligands <b>L3</b> , <b>L4</b> and <b>L5</b> .....	89
5.1.2.2.1	[Cu( <b>L3</b> )(MeCN)] <sub>n</sub> (CF <sub>3</sub> SO <sub>3</sub> ) <sub>n</sub> ·MeCN ( <b>1</b> ) .....	89
5.1.2.2.2	[Cu <sub>2</sub> ( <b>L4</b> ) <sub>2</sub> ](CF <sub>3</sub> SO <sub>3</sub> ) <sub>2</sub> ·DMF ( <b>2</b> ) .....	92
5.1.2.2.3	[Cu( <b>L4</b> ) <sub>n</sub> ](ClO <sub>4</sub> ) <sub>n</sub> ·nDMF ( <b>3</b> ) .....	93
5.1.2.2.4	[Cu <sub>2</sub> ( <b>L5</b> ) <sub>2</sub> ](BPh <sub>4</sub> ) <sub>2</sub> ·2CH <sub>3</sub> COCH <sub>3</sub> ( <b>4</b> ) .....	94
5.1.2.2.5	Oxidation Reactions of Copper(I) Complexes .....	95
5.1.2.3	Zinc(II) Complexes of the Ligands <b>L3</b> , <b>L4</b> and <b>L5</b> .....	98
5.1.2.3.1	[Zn(DMF) <sub>4</sub> ( <b>L4</b> ) <sub>2</sub> ](ClO <sub>4</sub> ) <sub>2</sub> ( <b>5</b> ) .....	98
5.1.2.4	Copper(II) Complexes of the Ligands <b>L3</b> , <b>L4</b> and <b>L5</b> .....	100
5.1.2.4.1	[Cu <sub>3</sub> Cl <sub>6</sub> ( <b>L4</b> ) <sub>2</sub> ] <sub>n</sub> ·(xH <sub>2</sub> O) <sub>n</sub> ( <b>6</b> ) .....	100
5.1.2.4.2	[CuCl <sub>2</sub> ( <b>L5</b> )]·0.75 H <sub>2</sub> O ( <b>7</b> ) .....	101
5.1.2.5	Heterometallic Cu/Zn Complexes .....	101
5.1.3	Conclusions .....	103
5.1.4	Experimental Section .....	104
5.1.4.1	Materials and Methods .....	104
5.1.4.2	X-ray Structure Determination .....	105
5.1.4.3	Syntheses of the Ligands <b>L3</b> , <b>L4</b> and <b>L5</b> .....	105

5.1.4.3.1	General Procedure.....	105
5.1.4.3.2	Synthesis of N,N-[(2-pyridyl)methyl(4-pyridyl)methyl]-2-pyridylamine (L3).....	105
5.1.4.3.3	Synthesis of N,N-(4-pyridyl)(2-pyridylmethyl)amine .....	106
5.1.4.3.4	Syntheses of N-[Bis(2-pyridyl)methyl]-4-pyridylamine (L4).....	106
5.1.4.3.5	Syntheses of N,N-(3-pyridyl)(2-pyridylmethyl)amine .....	107
5.1.4.3.6	Syntheses of N-[Bis(2-pyridyl)methyl]-3-pyridylamine (L5).....	107
5.1.4.4	Synthesis of the Copper(I) Complexes of the Ligands L3, L4 and L5 .....	108
5.1.4.4.1	Synthesis of [Cu(L3)(MeCN)] <sub>n</sub> (CF <sub>3</sub> SO <sub>3</sub> ) <sub>n</sub> (1) .....	108
5.1.4.4.2	Synthesis of [Cu <sub>2</sub> (L4) <sub>2</sub> ](CF <sub>3</sub> SO <sub>3</sub> ) <sub>2</sub> ·DMF (2) .....	108
5.1.4.4.3	Synthesis of [Cu(L4)] <sub>n</sub> (ClO <sub>4</sub> ) <sub>n</sub> ·nDMF (3).....	108
5.1.4.4.4	Synthesis of [Cu <sub>2</sub> (L5) <sub>2</sub> ](BPh <sub>4</sub> ) <sub>2</sub> ·2CH <sub>3</sub> COCH <sub>3</sub> (4) .....	108
5.1.4.5	Synthesis of Zinc(II) Complexes of the Ligands L3, L4 and L5 .....	108
5.1.4.5.1	Synthesis of [Zn(DMF) <sub>4</sub> (L4) <sub>2</sub> ](ClO <sub>4</sub> ) <sub>2</sub> (5) .....	108
5.1.4.6	Synthesis of the Copper(II) Complexes of the Ligands L4 and L5.....	109
5.1.4.6.1	Synthesis of [Cu <sub>3</sub> Cl <sub>6</sub> (L4) <sub>2</sub> ] <sub>n</sub> ·(xH <sub>2</sub> O) <sub>n</sub> (7) .....	109
5.1.4.6.2	Synthesis of [CuCl <sub>2</sub> (L5)]·H <sub>2</sub> O (8).....	109
5.1.4.7	Preparation of Heterometallic Solutions Used for NMR Experiments .....	109
5.1.4.7.1	Preparation of L4 + Zn(SO <sub>3</sub> CF <sub>3</sub> ) <sub>2</sub> + Cu(SO <sub>3</sub> CF <sub>3</sub> ) .....	109
5.1.4.7.2	Preparation of a Mixture of L4 + Zn(ClO <sub>4</sub> ) <sub>2</sub> + Cu(ClO <sub>4</sub> ).....	109
5.1.5	Acknowledgements.....	109
5.2	Supporting Information for Chapter 5.1 .....	110
5.2.1	Crystal Structures of the Ligands L4 and L5.....	110
5.2.2	[Cu <sub>2</sub> (L4) <sub>2</sub> ](PF <sub>6</sub> ) <sub>2</sub> ·2CH <sub>3</sub> COCH <sub>3</sub> .....	112
5.2.3	[Cu <sub>2</sub> (L4) <sub>2</sub> ](PF <sub>6</sub> ) <sub>2</sub> ·DMF .....	113
5.2.4	[Cu <sub>3</sub> Cl <sub>6</sub> (L4) <sub>2</sub> ]·H <sub>2</sub> O (6) .....	114
5.2.5	[Zn(DMF) <sub>4</sub> (L4) <sub>2</sub> ](CF <sub>3</sub> SO <sub>3</sub> ) <sub>2</sub> .....	115
5.2.6	EDX Measurement.....	115
5.2.7	Low Temperature Stopped Flow Spectrum of the Oxidation Reaction of [Cu <sub>2</sub> (L4) <sub>2</sub> ](BF <sub>4</sub> ) <sub>2</sub> with mCPBA .....	116
5.2.8	UV/Vis Spectra of Copper(II) Complexes.....	117
5.2.9	Experimental Section of the Supporting Information .....	118
5.2.9.1	Synthesis of Ligands L4 and L5 .....	118
5.2.9.2	Synthesis of [Cu <sub>2</sub> (L4) <sub>2</sub> ](PF <sub>6</sub> ) <sub>2</sub> ·2CH <sub>3</sub> COCH <sub>3</sub> .....	118
5.2.9.3	Synthesis of [Cu <sub>2</sub> (L4) <sub>2</sub> ](PF <sub>6</sub> ) <sub>2</sub> ·DMF .....	118
5.2.9.4	Synthesis of [Zn(DMF) <sub>4</sub> (L4) <sub>2</sub> ](CF <sub>3</sub> SO <sub>3</sub> ) <sub>2</sub> .....	118
5.2.9.5	Low Temperature Stopped Flow Spectrum of the Oxidation Reaction of [Cu <sub>2</sub> (L4) <sub>2</sub> ](BF <sub>4</sub> ) <sub>2</sub> with mCPBA.....	118

5.2.9.6	UV/Vis Measurement of Copper(II) Complexes.....	118
<b>6</b>	<b>Summary/Zusammenfassung.....</b>	<b>119</b>
6.1	Summary.....	119
6.1.1	Unspenp Relatives as Ligands .....	120
6.1.2	Bispic Relatives as Ligands .....	121
6.1.2.1	<b>1,3-tpbd</b> Coordination Compounds .....	121
6.1.2.2	Coordination Compounds Using Ligands Related to <b>tmpa</b> .....	122
6.1.2.3	Coordination Polymers Using Derivatives of <b>bispic</b> as Ligands.....	123
6.2	Zusammenfassung .....	125
6.2.1	<b>Unspenp</b> verwandte Verbindungen als Liganden .....	126
6.2.2	<b>Bispic</b> verwandte Verbindungen als Liganden .....	127
6.2.2.1	<b>1,3-tpbd</b> Koordinationsverbindungen.....	127
6.2.2.2	Koordinationsverbindungen mit Liganden verwandt mit <b>tmpa</b> .....	128
6.2.2.3	Koordinationspolymere mit Derivaten des Liganden <b>bispic</b> .....	130
<b>7</b>	<b>Publications .....</b>	<b>132</b>
7.1	Journal Articles.....	132
7.1.1	Articles in Preparation .....	133
7.2	Oral Presentations .....	133
7.3	Poster Presentations.....	133
<b>8</b>	<b>References .....</b>	<b>134</b>

**Table of Abbreviations**

SOD	superoxide dismutase
D $\beta$ M	dopamine- $\beta$ -monooxygenase
PHM	peptidylglycine- $\alpha$ -hydroxylating monooxygenase
HOMO	highest occupied molecular orbital
LUMO	lowest unoccupied molecular orbital
PET	photoinduced electron transfer
DNA	desoxy-ribonucleic acid
ATP	adenosintriphosphate
1D CP	one-dimensional coordination polymer
MOF	metalorganic framework
$\tau$	trigonality index parameter $\tau = (\beta - \alpha)/60^\circ$ , with $\alpha$ and $\beta$ being the two largest coordination angles around the metal atom, $\tau = 0$ and 1 for ideal square-pyramidal and trigonal-bipyramidal coordination.
DFT	density functional theory
$\chi_M$	magnetic susceptibility
$J$	magnetic/exchange coupling
Å	Angstrom
°	degree
<i>et al.</i>	<i>et alii</i>
<i>p.a.</i>	<i>per analysis</i>
NMR	nuclear magnetic resonance
MeCN	acetonitrile
DMF	dimethylformamide
COSY	correlated spectroscopy
TOCSY	total correlated spectroscopy
EXSY	exchange spectroscopy
NOESY	nuclear overhauser enhancement spectroscopy
2D	two-dimensional
K	Kelvin
$\delta$	chemical shift
ppm	parts per million
s	singlet
d	doublet
t	triplet
q	quartet
br	broad
m	multiplet, for unresolved lines
$\lambda$	wavelength
UV	ultraviolet

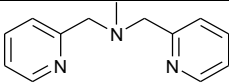
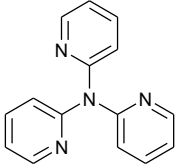
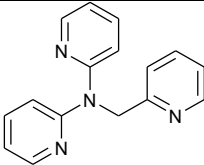
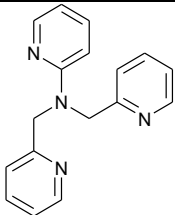
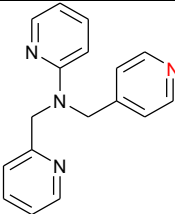
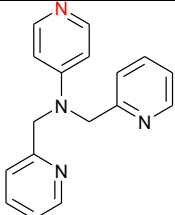
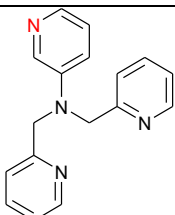
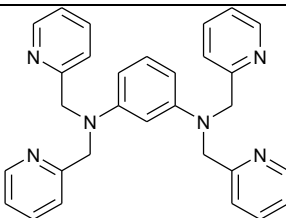
## Table of Abbreviations

---

vis	visible
$\Phi$	quantum yield
$\tau$	lifetime
MS	mass spectrometry
THF	tetrahydrofuran
TMS	tetramethylsilane



## Ligand Index

Name	Abbreviation	Structure	Sum Formula	Molecular Weight [g <sup>mol</sup> <sup>-1</sup> ]
<i>N</i> -methyl-[bis(2-pyridyl)methyl]amine	Me-bispic		C <sub>13</sub> H <sub>15</sub> N <sub>3</sub>	213.28
2,2',2''-Tripyridylamine	tpa		C <sub>15</sub> H <sub>12</sub> N <sub>4</sub>	248.28
<i>N</i> -[(2-pyridyl)methyl]-2,2'-dipyridylamine	L1		C <sub>16</sub> H <sub>14</sub> N <sub>4</sub>	262.31
<i>N</i> -[bis(2-pyridyl)methyl]-2-pyridyl amine	L2		C <sub>17</sub> H <sub>16</sub> N <sub>4</sub>	276.34
<i>N</i> -[(2-pyridyl)methyl]- <i>N</i> -[(4-pyridyl)methyl]-2-pyridylamine	L3		C <sub>17</sub> H <sub>16</sub> N <sub>4</sub>	276.34
<i>N</i> -[bis(2-pyridyl)methyl]-4-pyridyl amine	L4		C <sub>17</sub> H <sub>16</sub> N <sub>4</sub>	276.34
<i>N</i> -[bis(2-pyridyl)methyl]-3-pyridyl amine	L5		C <sub>17</sub> H <sub>16</sub> N <sub>4</sub>	276.34
<i>N,N,N',N'</i> -tetrakis(2-pyridylmethyl)-1,3-benzenediamine	1,3-tpbd		C <sub>30</sub> H <sub>28</sub> N <sub>6</sub>	472.58

Name	Abbreviation	Structure	Sum Formula	Molecular Weight [g $\text{mol}^{-1}$ ]
2,6-bis[bis(2-pyridylmethyl)amino]- <i>p</i> -cresolate	2,6-tpcd		$\text{C}_{31}\text{H}_{30}\text{N}_6\text{O}$	502.61
<i>N'</i> -1-{3-[2-bis(2-pyridylmethyl)amino-ethyliminomethyl]-phenyl}methyliden- <i>N,N</i> -bis(2-pyridylmethyl)-1,2-ethanediamine	Imxyl-unspenp		$\text{C}_{36}\text{H}_{38}\text{N}_8$	582.74
<i>N'</i> -{3-[2-bis(2-pyridylmethyl)amino-ethylaminomethyl]-benzyl}methyliden- <i>N,N</i> -bis(2-pyridylmethyl)-1,2-ethanediamine	Hxyl-unspenp		$\text{C}_{36}\text{H}_{42}\text{N}_8$	586.77
<i>N'</i> -(9-anthracenylmethylene)- <i>N,N</i> -bis(2-pyridylmethyl)-1,2-ethanediamine	Imant-unspenp		$\text{C}_{29}\text{H}_{26}\text{N}_4$	430.54
<i>N'</i> -(9-anthracenylmethyl)- <i>N,N</i> -bis(2-pyridylmethyl)-1,2-ethanediamine	Hant-unspenp		$\text{C}_{29}\text{H}_{28}\text{N}_4$	432.56

# 1 Introduction

## 1.1 Motivation

Copper and zinc complexes in general are interesting due to their importance in biological processes.<sup>2-7</sup> Proteins containing copper or zinc ions in their active centers participate in the metabolism of prokaryote and eukaryote organisms.<sup>8-9</sup> The functions of the different enzymes reach from selective DNA binding zinc finger proteins, where zinc dictates the structure of the active core, to copper proteins like tyrosinase that selectively oxidizes phenol to catechol. Additionally, there are essential enzymes with heterobinuclear active sites containing copper and zinc ions. Human copper zinc superoxide dismutase (Cu/Zn SOD) for example, rapidly binds and deactivates superoxide radicals occurring during respiration processes.<sup>10</sup> An excess amount of this highly reactive molecule causes severe cell damage leading to cell death. Therefore, it is involved in aging processes.<sup>11</sup> Binding and converting this radical into less reactive species like peroxide that is further deactivated by catalases, is crucial for living organisms. The structure of the active core of Cu/Zn SOD and a proposed reaction mechanism for its reaction with superoxide radicals is shown in Figure 1 to demonstrate the different functions of the two transition metals.<sup>8</sup>

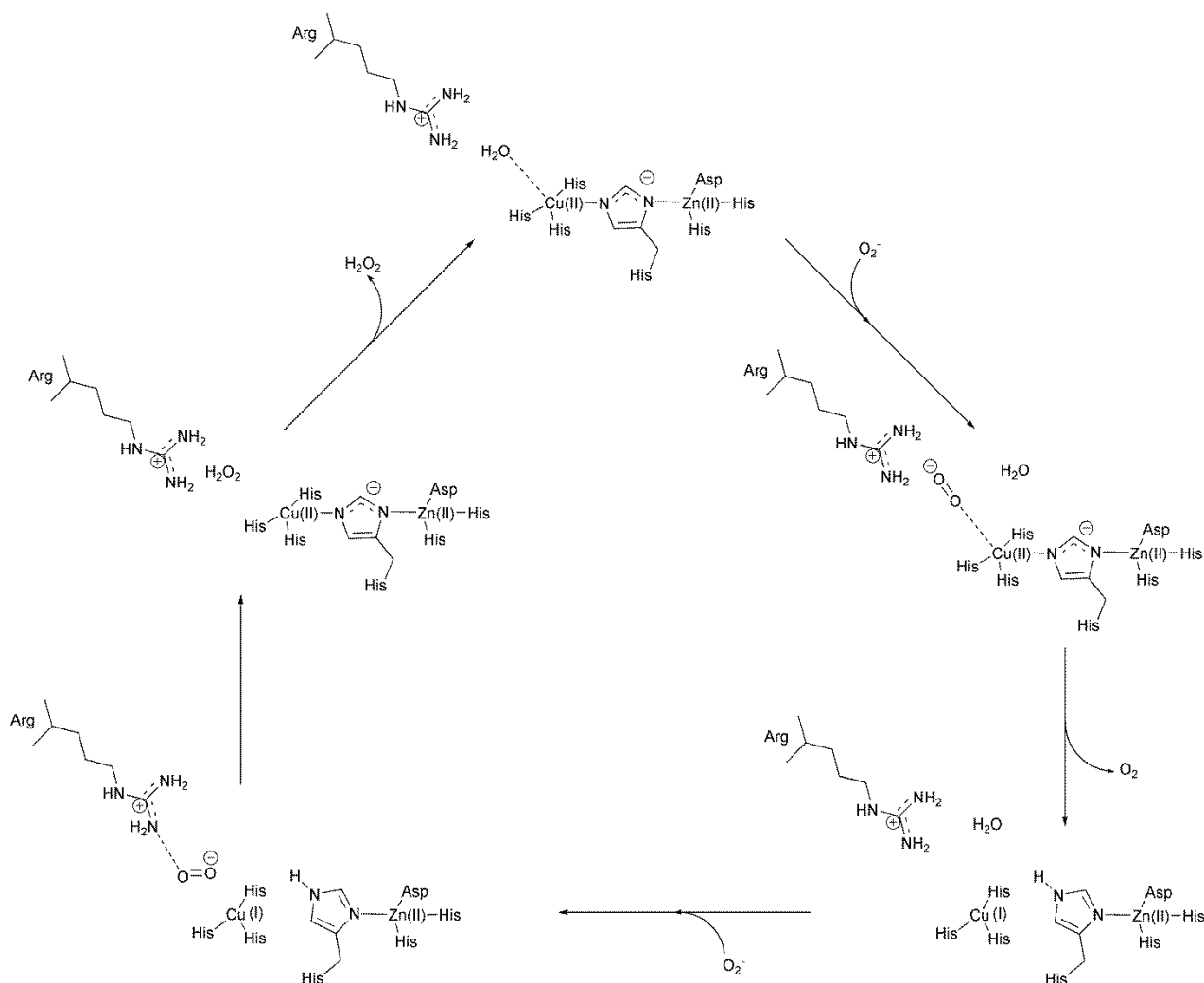


**Fig. 1** Catalytic cycle of human Cu/Zn SOD deactivating the highly reactive superoxide radical.<sup>8</sup>

While zinc(II) is important for the structure of the active core and influences the reduction potentials, the copper ion is involved in the redox chemistry of the enzyme.<sup>12-13</sup> Knowledge about the mechanisms of such biological processes is important, not only due to pharmaceutical aspects, but furthermore for possible application in chemical processes in industry.<sup>14-15</sup> Mimicking the active cores of enzymes is therefore of special interest for chemical researchers with regard to gain knowledge about natural processes and the synthesis of new coordination compounds with extraordinary properties.

Therefore, modeling the functionality of such metalloproteins using low molecular weight transition metal complexes has turned out to be an interesting research area in bioinorganic chemistry and homogeneous catalysis. In regard to obtain useful model compounds, ligand design plays an important role. Here, bispicolylamine (bispic) as binding motif for various transition metal complexes is well known and offers a great variety of different complex properties.<sup>16-18</sup> The facile selective derivatisation of bispicolylamine provides a coordination motive for transition metals with the possibility of combination with additional functionalities (e.g. electron donors for further coordination, hydrogen bond donors or tuning of the electronic properties of the ligand). Figure 2 shows the molecular formulas of bispicolylamine and some prominent relatives that are well-known for the extraordinary properties of the related metal complexes.

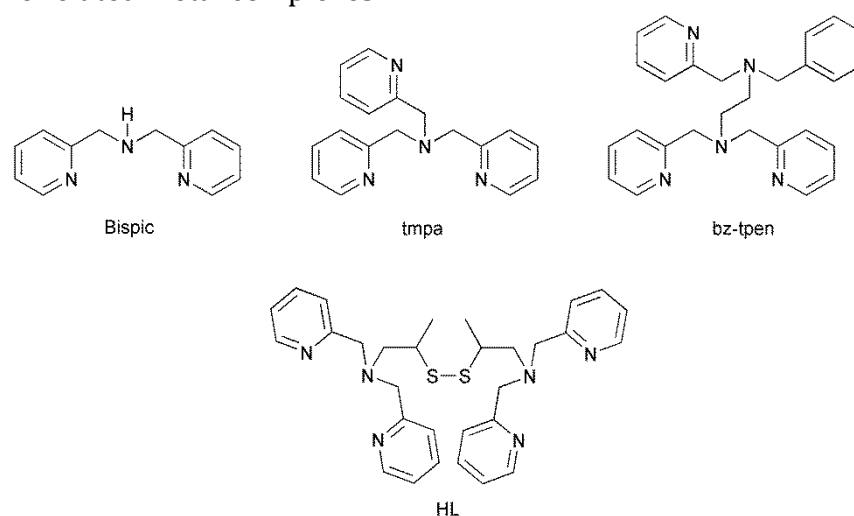


Fig. 2 Structures of bispicolylamine and related ligands.

Studies involving copper and zinc complexes using derivatives of bispicolylamine as ligand were performed previously and are described in more detail in the following chapters.

## 1.2 Activation of Small Molecules

### 1.2.1 Activation of Dioxygen

The redox chemistry of copper(I) coordination compounds as active cores in enzymes is of growing interest due to its catalyzing capability for selective oxidation reactions under mild conditions. Enzymes containing copper in their active site serve as catalysts for various reaction types. Figure 3 depicts a summary of the different functions of selected enzymes. Mimicking the active centers, or at least mimicking the functionalities of the natural

prototypes remains a challenging aim. Nevertheless, it is very promising in regard to the knowledge that is still to be gained about natural processes and the benefits of possible applications deriving from the new findings.

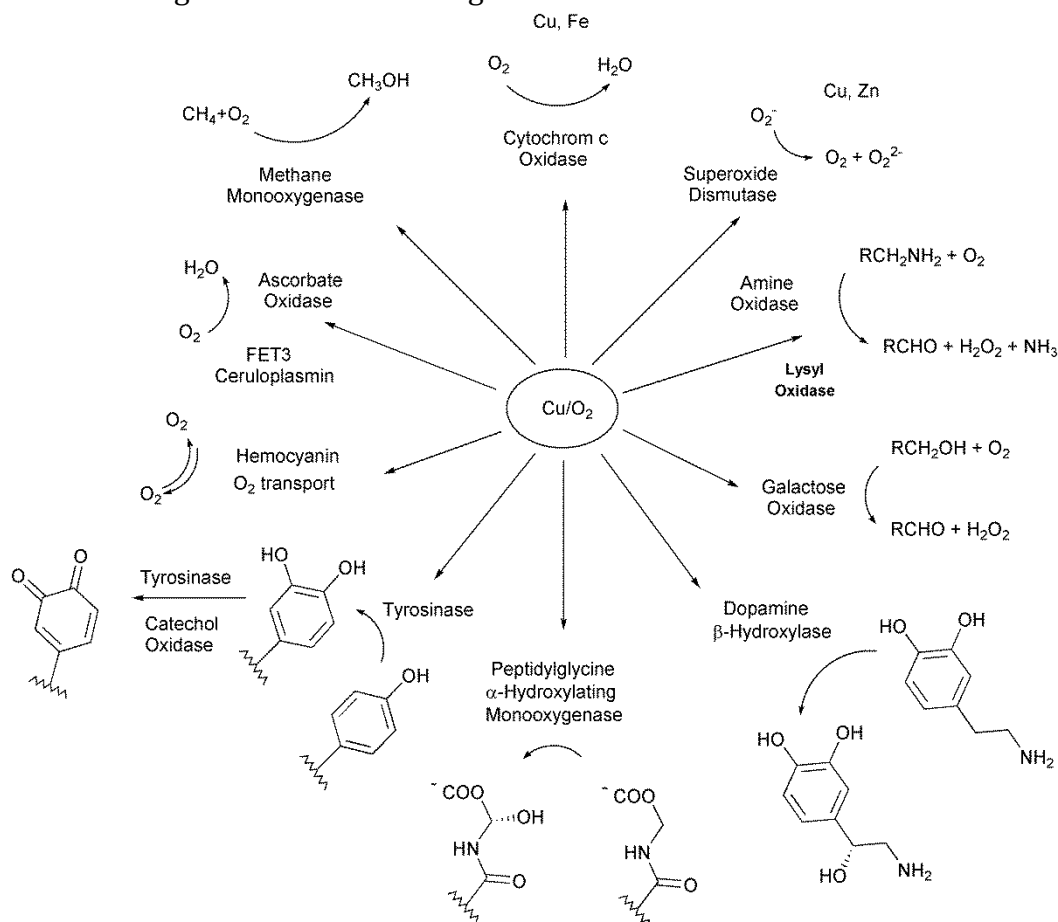


**Fig. 3** Selected reaction types catalyzed by copper containing enzymes.<sup>4</sup>

The activation of dioxygen by copper(I) complexes is well known and numerous active species could be isolated and were structurally characterized so far.<sup>4, 19-21</sup> Figure 4 gives an overview of the currently known species.

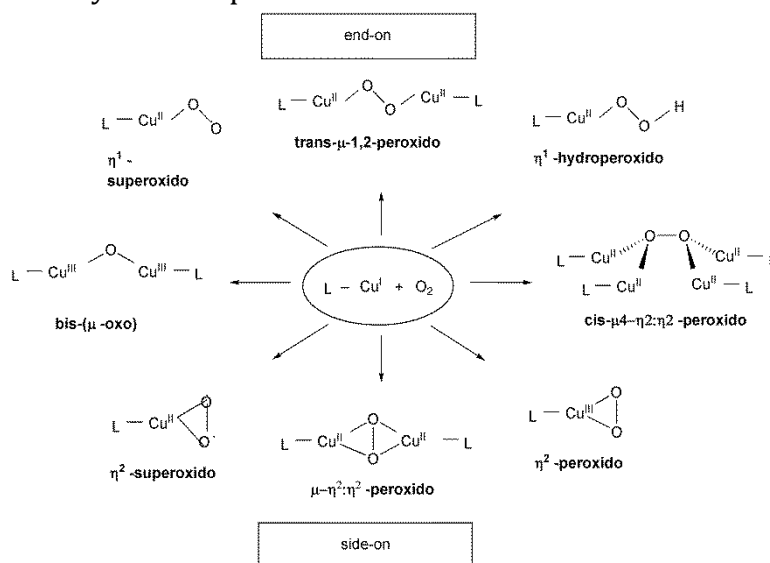


**Fig. 4** Side- and end-on copper dioxygen species.<sup>22</sup>

In contrast to related iron chemistry, a copper(III)-oxido species has not been isolated until now. This is interesting in so far that this species is regarded as an important intermediate in oxidation reactions.

To give an example of bispic related molecules involved in the studies of reactive oxygen intermediates, the tripodal ligand tris(methylpyridyl)amine (tmpa) (see Figure 1) is a perfect candidate. Tmpa has a fourth nitrogen donor group, however its close relationship to bispic is still obvious. Already in 1988 Karlin and co-workers reported the structure of a copper bis- $\mu$ -peroxido species stabilized by tmpa as ligand.<sup>23</sup> More recently, Würtele *et al.* were able to present a series of room temperature stable copper bis- $\mu$ -peroxido complexes with tmpa and selected derivatives as ligands.<sup>24</sup> In solid state the bulky tetraphenylborate anion was used to protect the active species leading to an extremely extended lifetime of the complexes. Furthermore, the catalytic activity of these complexes to oxidize toluene could be demonstrated.<sup>24</sup>

### 1.2.1.1 C-H Bond Activation

Oxidative C-H bond functionalization is crucial for the synthesis of many important organic compounds.<sup>25</sup> A challenging aim is the utilization of dioxygen as an oxidant in the synthesis of complex organic targets like pharmaceuticals. In that regard the biologically inspired oxidation reactions using copper or iron complex compounds that mimic the reactivity of the corresponding enzymes are very promising due to the advantages they provide: substrate specificity, regio- and stereoselectivity and the operation under mild conditions.<sup>26</sup> An overview of the proposed  $O_2$  activation mechanisms of various iron and copper compounds is shown in Figure 5.

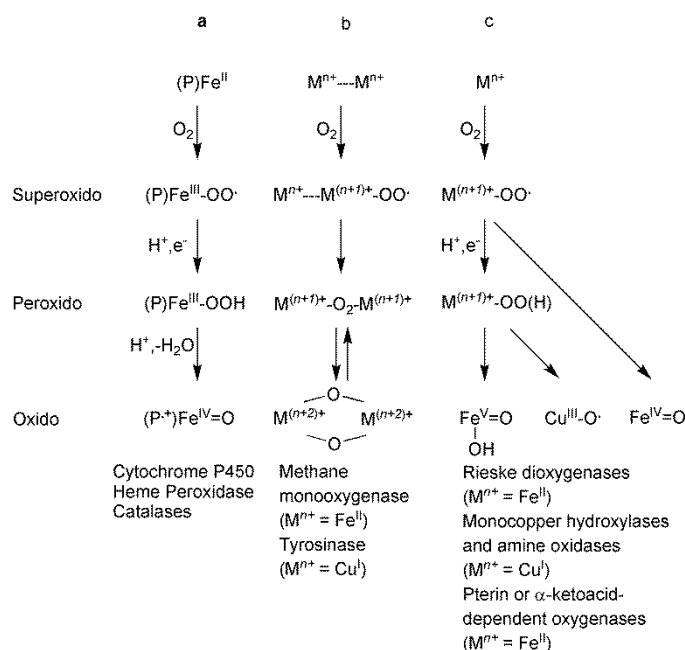


**Fig. 5** Proposed  $O_2$  activation mechanisms for heme (a), di-iron or dicopper metallo oxygenases (b) and mononuclear non heme iron and copper complexes.<sup>26</sup>

In contrast to heme iron chemistry understanding of related oxidation reactions in copper chemistry is limited. Especially the missing link, a copper-oxido species described above

awaits its detection and characterization. So far its occurrence is only postulated. Recently, Karlin and co-workers published the first example of an intermolecular C-H bond activation mediated by a copper(II) superoxido species, that could be of relevance for the reactivity of dopamine- $\beta$ -monooxygenase (D $\beta$ M) and peptidylglycine- $\alpha$ -hydroxylating monooxygenase (PHM) enzymes.<sup>18</sup> The presented superoxido compound is not reactive towards substrates with weak C-H bonds like dihydroanthracene. However, as a strong H atom (H $\cdot$ ) and hydride (H $^-$ ) donor it leads to the decay of the substrate that could be detected at -125 °C. In this case the homolytical cleavage of the activated C-H bond is most likely the initial step of the reaction. Figure 6 shows the proposed reaction mechanism.

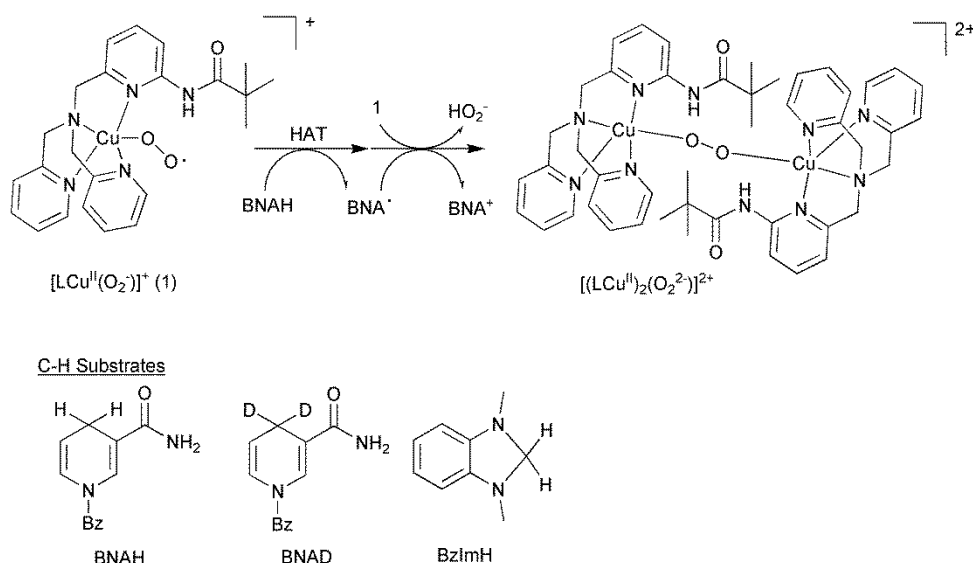


**Fig. 6** Reaction mechanism of the H- abstraction with a copper(II) superoxido complex using a ligand closely related to tmpa.<sup>18</sup>

More recently, Tolman and co-workers reported the synthesis and characterization of a new reactive copper(III) hydroxido intermediate that has been described by spectroscopy and theoretical calculations.<sup>27</sup> Formally, this intermediate could be considered as a protonated form of the copper(III) oxido species that is capable of rapid hydrogen abstraction from dihydroanthracene, leading to a copper(II) aqua complex. The rearomatisation of dihydroanthracene into anthracene is energetically rather simple. Never the less this species could be of importance in many oxidation reactions involving copper coordination compounds.

These two examples of model compounds for the enzymatic activation of C-H bonds illustrate, that mechanistic insights in this field are limited to systems that incorporate weak C-H bonds. So far reactive intermediates described above could not be observed and identified in the activation mechanism of C-H bonds with bond-strengths comparable to the substrates of their natural prototypes. To demonstrate the potential and importance of copper-catalyzed selective aerobic oxidation reactions for the synthesis of complicated targets e.g. in the pharmaceutical industry, Wendlandt *et al.* reported a good overview as an alternative to the widespread palladium catalysis.<sup>28</sup>

### 1.2.2 Activation of Carbon Dioxide

The fixation and activation of carbon dioxide has attracted increasing interest in the past due to limited amount of fossil resources. Efforts to use carbon dioxide as  $C_1$  source and to convert it into usable liquid fuels or other organic basic compounds are challenging. Figure 7 shows a generalized path from carbon dioxide to methanol in three steps.<sup>29</sup>

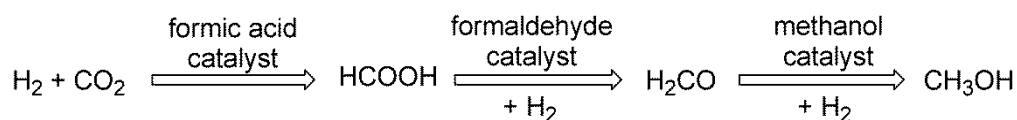


Fig. 7 Generalized pathway of the overall reduction of  $CO_2$  to methanol

Thus, numerous investigations are concerned with metal complexes that are able to reversibly bind and activate carbon dioxide from air. Examples of organic compounds, transition metals in complexes and simple salts are known that are able to transform it into carbonate salts or carbamates. Selective reductive conversion and the generation of  $CO_2^{\bullet-}$  as active species are more ambitious aims.<sup>29-30</sup>

In this regard Angamuthu *et al.* reported an interesting electrocatalytic conversion of carbon dioxide using a copper(I) complex with a bispicolylamine ligand unit.<sup>17</sup> They postulated a catalytic cycle presented in Figure 8, where carbon dioxide from air coordinates to a dinuclear copper(I) complex and is reduced to the reactive  $CO_2^{\bullet-}$  radical in a first step. The recombination of four radicals leads to the formation of two oxalate anions that build a tetranuclear coordination unit.

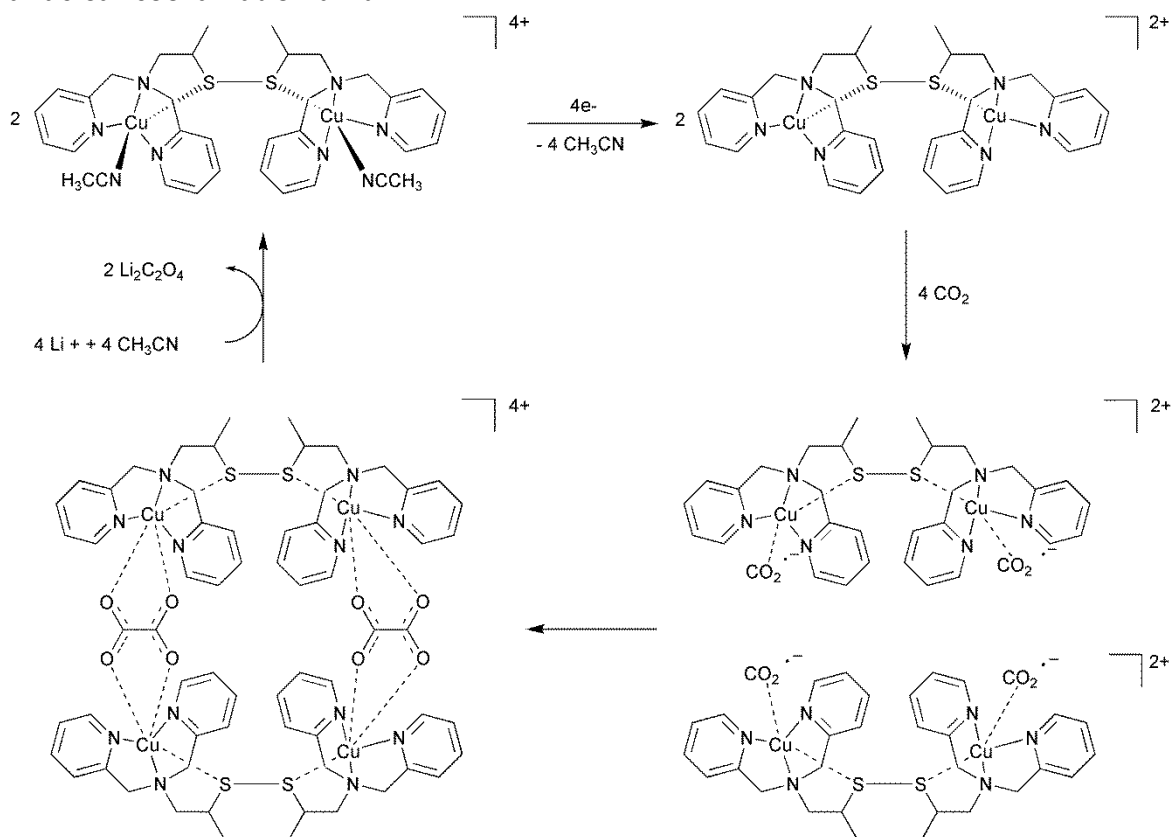


Fig. 8 Proposed catalytic cycle for the formation of oxalate from carbon dioxide.<sup>17</sup>



In order to recover the catalytic active copper(I) species, oxalate is removed by addition of  $\text{Li}^+$  and the formation of hardly soluble lithium oxalate in acetonitrile. The copper(II) complex coordinated by acetonitrile is electrochemically reduced to the active copper(I) species.<sup>17</sup> While there is room for improvement for this reaction the results clearly demonstrate that copper(I) complexes with dipicolylamine units are useful for the reduction of carbon dioxide leading to more useful organic compounds.

### 1.3 Zinc Coordination Compounds as Selective Ion Sensors

Selective detection of zinc or the sensing of different anions in solution by emission spectroscopy is of great importance for the research on natural processes and further insight into chemical reactions therein. Zinc is an essential element for living organisms and is crucial for the functionality of many enzymes involved in cellular processes.<sup>31</sup> Improved techniques to monitor zinc in these natural processes would provide an easy way of monitoring the progress of a specific reaction *in situ* or even *in vivo* by measuring the wavelength shift of emission or the enhanced or quenched emission intensity of the solution under changing conditions. This would help to answer numerous questions in chemical biology.<sup>32</sup> To achieve this goal, several obstacles have to be overcome: the compounds need to be soluble in aqueous solution; they have to be non toxic to cells and the emission properties have to change selectively upon reaction with the target molecules.

Derivatisation of potential organic sensor molecules again is a versatile instrument to influence the properties of the used compounds. One strategy is adding electron donating functionalities to strongly colored or fluorescent organic molecules to enable the specific binding of metal ions. Bispic binding units are used because of their affinity to zinc(II) ions compared to alkaline or alkaline-earth metal ions omnipresent in cellular milieu.<sup>33</sup> Upon complexation of the metal ion the highest occupied molecular orbital/lowest unoccupied molecular orbital (HOMO/LUMO) energy gap of the compound is influenced. Therefore, the emission wavelength is shifted or the emission intensity is quenched or enhanced. As an example, “Turn-on” sensors can often be explained with the photoinduced electron transfer (PET) effect depicted in Figure 9.<sup>34</sup>

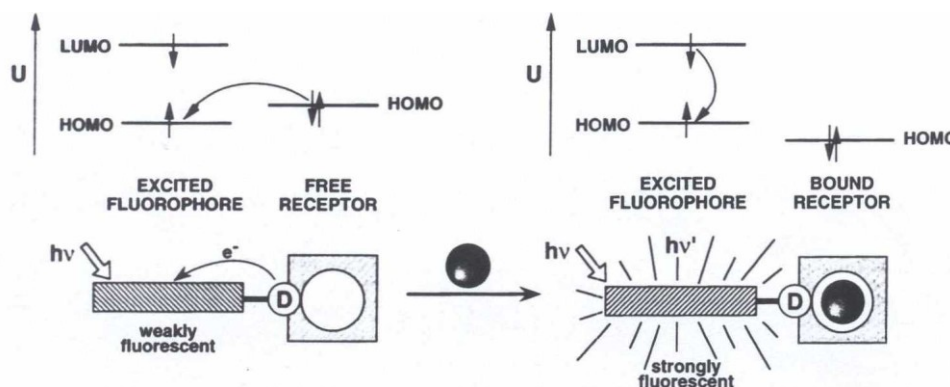


**Fig. 9** Photoinduced electron transfer effect of metal ion coordination on the emission of a fluorophore.<sup>34</sup>

The electron donating bispic units lead to a quenched emission, until the nitrogen atoms are coordinated to a metal ion. This inhibits the quenching PET process and the coordination compounds show a strong fluorescence.

Recently, Lippard and co-workers reported detailed studies on ditopic fluorescence sensors containing bispic as zinc(II) binding receptor.<sup>33</sup> The emission behavior of the archetype of the presented sensor molecule is strongly influenced by the pH and the changing protonation grade of the amine functions of the bispic receptors, shown earlier by the same group.<sup>35-36</sup> As a good example for the potential of rational ligand design, derivatisation of the latter lead to a decreased background fluorescence due to lowering of the basicity of the binding pockets. This enabled a larger pH spectrum, where the sensor could be applied. Figure 10 depicts the unbound sensor molecule consisting of two binding bispic pockets bound to a fluorophore body and their different proposed analogous emissive zinc complexes.<sup>35</sup>

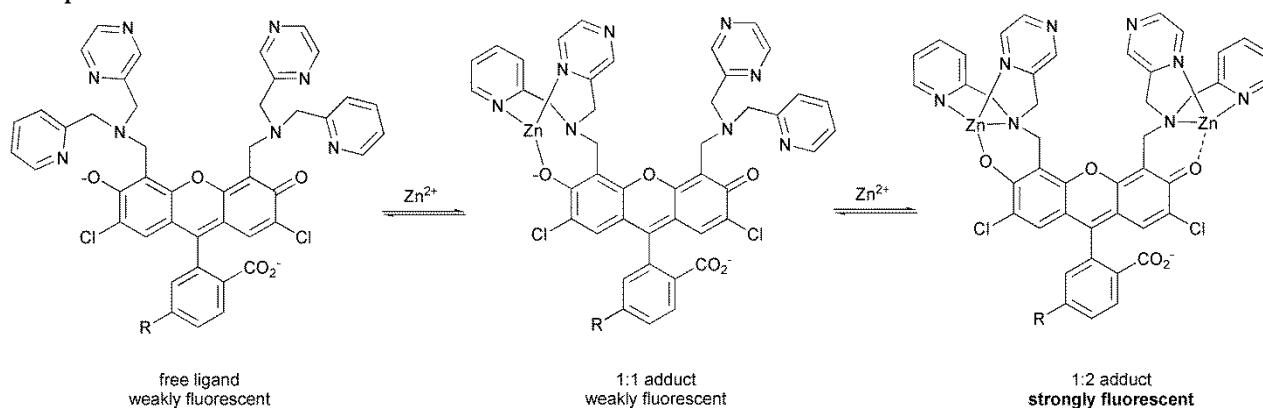


**Fig. 10** Free Sensor molecule and different zinc coordination compounds leading to altering emission behavior.

These receptors show an interesting OFF-ON-OFF behavior towards increasing zinc ion concentration. At lower concentrations only one binding site is occupied by a zinc(II) ion and upon coordination of the second ion, the compound exhibits a significantly enhanced fluorescence. The maximum intensity at a ligand/zinc(II) ratio of 0.5 provides an easy protocol to determine the zinc(II) concentration.<sup>35</sup>

Additional to metal ion sensing, ligand design for specific binding of the metal complexes to biomolecules can also lead to significant changes of the fluorescence and is therefore of great interest. Important targets are phosphate groups, present in many biomolecules. The real time detection of phosphorylated biomolecules by fluorescence sensors is an active field of research.<sup>37</sup> To achieve this goal one attempt is to mimic the recognition strategy of metalloenzymes containing more than one metal ion like alkaline phosphatase that carries two zinc(II) ions in its active site.<sup>38</sup> On this basis Hamachi and co-workers designed a set of chemosensors specific for phosphate derivatives that are based on two zinc ions coordinated by bispic.<sup>39</sup> They introduced three different recognition strategies: (a) simultaneous use of two zinc binding motifs for a monophosphorylated species; (b) cross linking interaction with a multi phosphorylated protein; (c) chemosensor combined with a phosphoprotein binding pocket (see Figure 11). Coordination of the zinc(II) ion to the phosphate functionality results in a change of the emission signal in different ways,

demonstrated with ATP detection. Principals of the sensing modes are depicted in Figure 12.

39

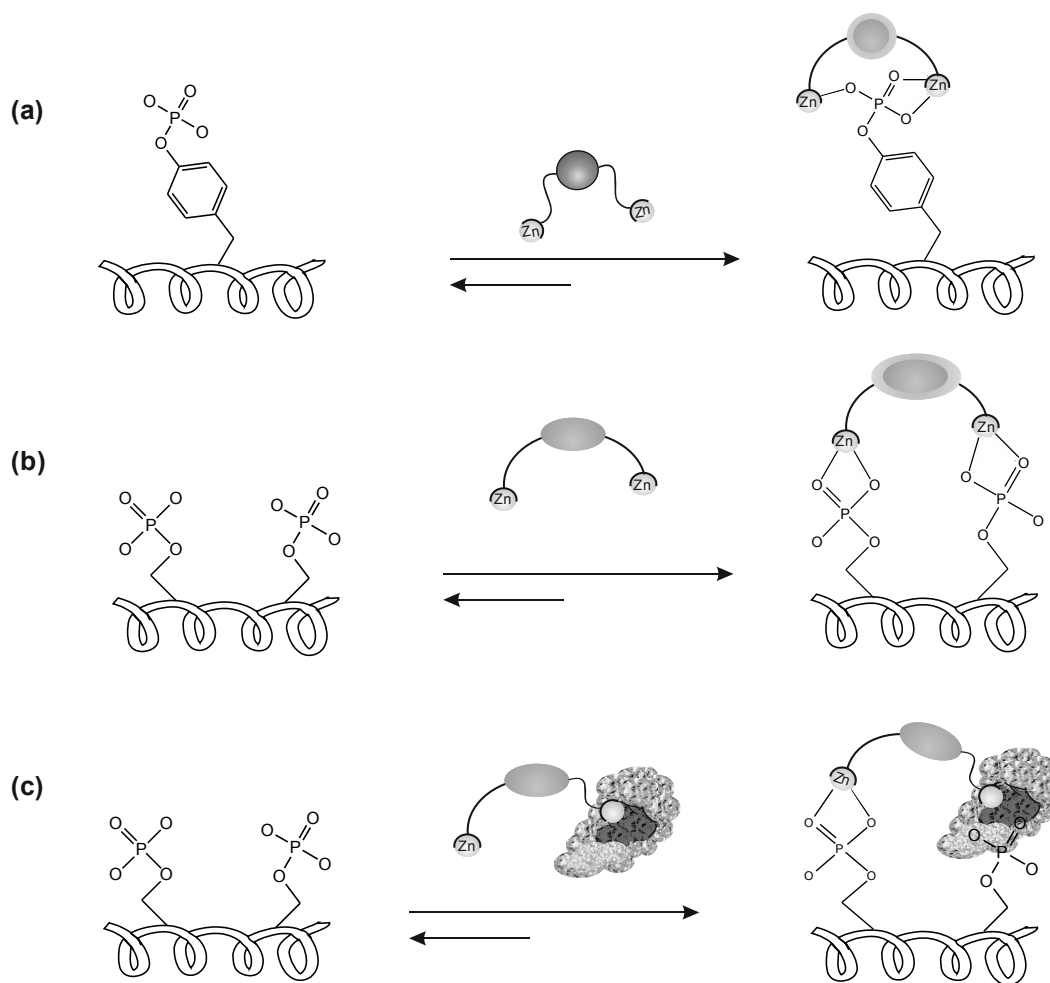


**Fig. 11** Recognition strategies of ditopic zinc coordination compounds.<sup>39</sup>

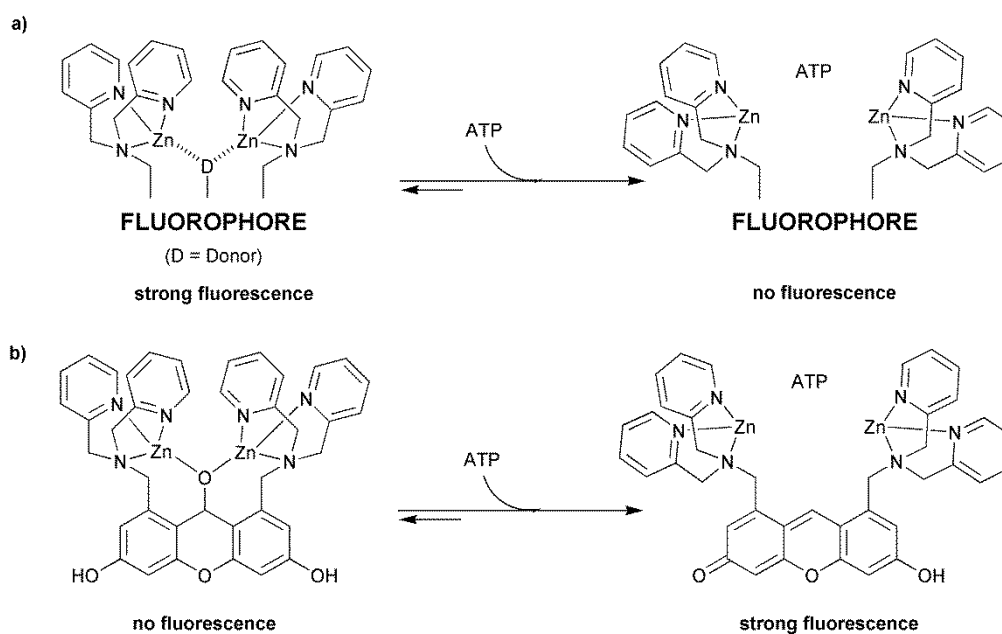


**Fig. 12** Different sensing modes.<sup>39</sup>

Nevertheless, phosphate recognition is not limited to the described mechanisms. Recently, Huang *et al.* reported a macrocyclic zinc(II) coordination compound where the coordination of phosphate causes a structural change inhibiting  $\pi$ -stacking of the two anthracene residues and thus the excimeric emission.<sup>40</sup> The strong monomeric emission wavelength of the new formed complex is hypsochromically shifted and can easily be distinguished from the excimer. More recently, Kim *et al.* published the first liposome based fluorescence sensor coupled with a zinc(II) bispic recognition unit on a micro array chip demonstrating the increasing applicability of artificial chemosensors of this type.<sup>41</sup>

The activity in this research field is furthermore described briefly in chapter 3.1. It demonstrates the importance of selective ion sensing for the understanding and monitoring of natural processes and gives an idea of bispic derivatives as versatile recognition units. Although great improvements could be achieved, there is still need for more basic research and the exploration of different residues that are capable of increasing the selectivity and applicability of this type of chemosensors.

## 1.4 Formation of Coordination Polymers

Organic Polymers are well known and of great importance for our daily life. More uncommon are coordination polymers, which were described for the first time about 50 years ago. At this time one-dimensional coordination polymers (1D CPs) consisting of metal ions linked *via* bridging organic molecules were introduced.<sup>42</sup> These compounds exhibit interesting electrochemical, optical or magnetic properties that could be exploited in new materials.<sup>43</sup>

Today, coordination polymers are an active field of research due to their extraordinary possibilities concerning functional materials. Hoskins *et al.* promoted the development of coordination compounds when they first described the synthesis of three-dimensional Metal-organic frameworks (MOFs) 20 years ago.<sup>44-45</sup> MOFs consist of a network of metal ions and organic linkers with definite topology leading to highly porous structures. Since that time coordination polymers have attracted a lot of attention due to their highly interesting properties. Functional properties are dominated by the pore sizes, shapes and environments.<sup>46</sup> Therefore, directed synthesis of such compounds is of special interest. Various strategies are applied to achieve the desired products. While metalorganic chemists prefer electrochemical, mechanochemical or precursor concepts as well as in situ linker synthesis, zeolite chemists use solvothermal reaction conditions, structure directing agents, mineralizers or microwave assisted synthesis instead.<sup>47</sup> Although great progress has been made in the synthetic strategies of MOFs, so far efforts to really design such materials were not successful. A recent review by Stock *et al.* describes the numerous routes to various MOFs.<sup>48</sup>

Due to the high number of possible applications deriving from the extraordinary high porosity, research in the field of coordination polymers concentrates on MOFs as targets.<sup>46</sup> Nevertheless, 1D CPs that initialized the field of research still attract attention due to their magnetical, optical electrical or mechanical properties. Only recently, Leong *et al.* gave a good overview on the variety of different types of 1D CPs with selected examples for

compounds with extraordinary properties.<sup>49</sup> In Figure 13 various common structure motifs for 1D CPs are depicted. The majority of compounds consist of linear or zigzag shaped building blocks that assemble in bigger superlattices mediated by solvent, anion or other attractive or repulsive interactions. Interestingly, there are 1D CPs exhibiting permanent porosity and gas storage/separation capability.<sup>49</sup>

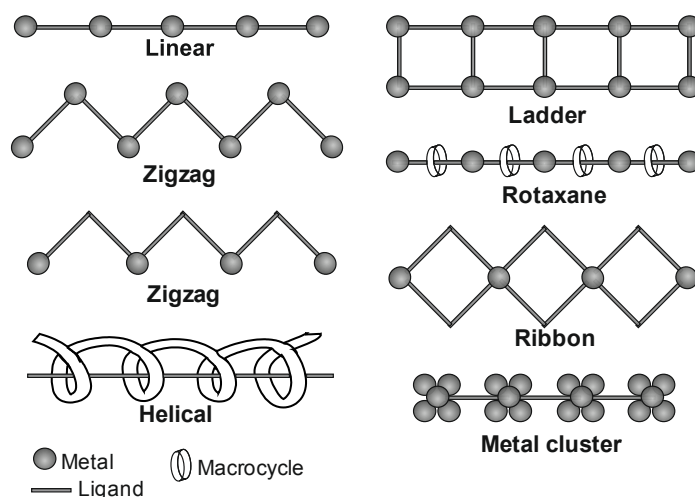


**Fig. 13** Common structure motifs of 1D CPs.<sup>49</sup>

Again, discrete structures are difficult to design due to the numerous possible interactions that influence the formation of coordination polymers. Schröder and co-workers described supramolecular interactions in coordination polymers based on silver bipyridine compounds and attempted to correlate these with structural characteristics.<sup>50</sup> There are in most cases too many different variables to consider. The crystallizing conditions as well as the solvent or the used anion, for example, participate in the structure forming process. Thus, serendipity is most likely to be the biggest driving force for the discovery of new, unexpected applications and structures.

In the following, some examples of 1D CPs with outstanding properties are presented to underline the relevance of this class of compounds beside the omnipresent MOFs. Cui and co-workers recently reported a zigzag-shaped CP, that is forming definite pores and is capable of separating cyclohexane from benzene utilizing the disability of aliphatic cyclohexane to adsorb on the hydrophobic pore surface in contrast to benzene that is strongly adsorbed.<sup>51</sup> Lee *et al.* described an example of a linear 1D CP that exhibits high porosity in the solid state and is capable of hydrogen storage. Interestingly, single crystals of the reported compound undergo reversible single crystal to single crystal (SCSC) transformation upon dehydration. Additionally, guest molecules capable of forming hydrogen bonds can be intercalated.<sup>52</sup> As an example for extraordinary properties of the more exotic ladder type structure, Mc Manus *et al.* reported a fluorescent zinc compound that intercalates aromatic solvent molecules into the cavities of the zinc bipyridine framework, leading to a conformational change observable through a shift of the emission wavelength.<sup>53</sup> Furthermore, 1D CPs are applicable as polymeric gels, fibers and nanostructures.<sup>49</sup> Only recently, Zamora and co-workers presented a good overview on the progress of 1D CPs on surfaces and their potential to be utilized as single molecule devices.<sup>54</sup>

Here again the bispicolylamine coordination motif can be applied. Thus, Lippard and co-workers reported on a two-dimensional coordination polymer containing a trimetallic copper(II) building block as binding motif for permethylate anions.<sup>55</sup> Figure 14 shows the bispicolylamine containing ligand and the trimetal unit. The copper(II) chlorido complex forms a two-dimensional structure with hexagonal pores ( $\varnothing = 20 \text{ \AA}$ ). The trimetallic units are connected through intermolecular chlorido bridges between two copper units.

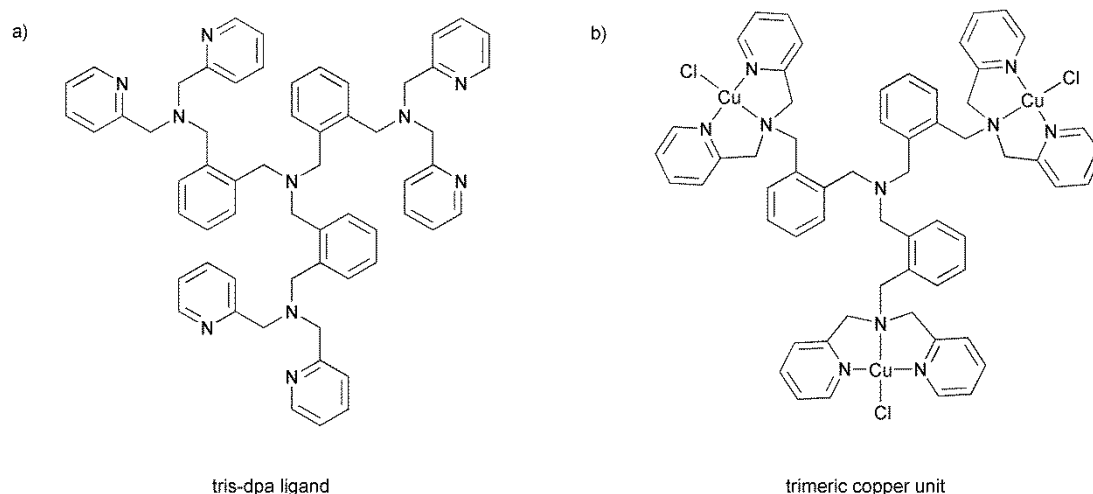


**Fig. 14** a) Ligand tris-dpa and b) the trimetallic copper(II) chlorido unit forming the two-dimensional coordination polymer.

Upon addition of perrhenate, the weakly bound  $\text{PF}_6^-$  anion is readily exchanged. The new formed compound exhibits two forms of anion trapping, one of which being the formation of a  $(\mu^3\text{-ReO}_4^-)$  bridge, where the anion is covalently bound to the copper(II) atoms. The second perrhenate anion is located in a cavity of the polymeric skeleton, immobilized by binding coulomb interactions. A possible application is trapping of anions that are able to disturb physiological processes and therefore affect human health. Pertechnetate occurring as nuclear fission waste product with a good environmental mobility is one of the addressed targets. Technetium reacts very similar to rhenium, hence the published work provides a first promising step towards pertechnetate trapping. Furthermore, both technetium as well as rhenium are applied as radionucleoides in medicine.<sup>55</sup>

## 1.5 Goals

This work is intended to provide further insight in the interesting and versatile chemistry of copper and zinc complexes using several derivatives of bispicolylamine as ligands. This class of ligands, including tripodale amine ligands closely related to tmpa (see Figure 1), have a high potential for useful applications of their transition metal complexes. Hence, basic research concerning the properties of new coordination compounds using this ligand type is promising. Starting point is the synthesis and characterization of new and well-known relatives of the parent amine bispicolylamine. Among the variety of transition metals this work focuses on copper(I), copper(II), and zinc(II) as central atoms for coordination compounds.

The synthesis and structural characterization of new, so far unknown metal complexes with the ligands as the next step is intended to enable studies on possibly interesting properties of these compounds. Amongst others, the reactivity of copper(I) complexes towards dioxygen, emission properties of zinc(II) complexes and the ability to form coordination polymers are topics that are addressed in the following.

## 2 Ligands Containing Bridged Bispicolylamine Units

### 2.1 Syntheses, Characterization and Magnetic Studies of Copper(II) Complexes with the Ligand *N,N,N',N'*-Tetrakis(2-pyridylmethyl)-1,3-benzenediamine (1,3-tpbd) and its Phenol Derivative 2,6-Bis[bis(2-pyridylmethyl)amino]-*p*-cresol (2,6-Htpcd)

This work has been published previously in *Inorganic Chemistry* **2012**, 51(1), 88-97.

*Sabrina Turba,<sup>a</sup> Simon P. Foxon,<sup>a</sup> Alexander Beitat,<sup>a</sup> Frank W. Heinemann,<sup>b</sup> Konstantin Petukhov,<sup>c</sup> Paul Müller,<sup>c</sup> Olaf Walter,<sup>d</sup> Francesc Lloret,<sup>e</sup> Miguel Julve,<sup>\*e</sup> and Siegfried Schindler<sup>\*a</sup>*

<sup>a</sup>Institut für Anorganische und Analytische Chemie, Justus-Liebig-Universität Gießen, Heinrich-Buff-Ring 58, 35392 Gießen, Germany

<sup>b</sup>Institut für Anorganische Chemie, Universität Erlangen-Nürnberg, Egerlandstrasse 1, 91058 Erlangen, Germany

<sup>c</sup>Physikalisches Institut III, Universität Erlangen-Nürnberg, Erwin-Rommel-Strasse 1, 91058 Erlangen, Germany

<sup>d</sup>Institut für Technische Chemie – Chemisch-Physikalische Verfahren (ITC-CPV), Forschungszentrum Karlsruhe, Postfach 3640, 76021 Karlsruhe, Germany

<sup>e</sup>Instituto de Ciencia Molecular, Universidad de Valencia, C/ Catedrático José Beltrán 2, 46980 Paterna (Valencia), Spain

The copper(II) complexes  $[\text{Cu}_4(1,3\text{-tpbd})_2(\text{H}_2\text{O})_4(\text{NO}_3)_4]_n(\text{NO}_3)_{4n} \cdot 13n\text{H}_2\text{O}$  (**1**),  $[\text{Cu}_4(1,3\text{-tpbd})_2(\text{AsO}_4)(\text{ClO}_4)_3(\text{H}_2\text{O})](\text{ClO}_4)_2 \cdot 2\text{H}_2\text{O} \cdot 0.5\text{CH}_3\text{OH}$  (**2**),  $[\text{Cu}_4(1,3\text{-tpbd})_2(\text{PO}_4)(\text{ClO}_4)_3(\text{H}_2\text{O})](\text{ClO}_4)_2 \cdot 2\text{H}_2\text{O} \cdot 0.5\text{CH}_3\text{OH}$  (**3**),  $[\text{Cu}_2(1,3\text{-tpbd})\{(\text{PhO})_2\text{P}(\text{O})_2\}_2](\text{ClO}_4)_4$  (**4**) and  $[\text{Cu}_2(1,3\text{-tpbd})\{(\text{PhO})\text{PO}_3\}_2(\text{H}_2\text{O})_{0.69}(\text{CH}_3\text{CN})_{0.31}]_2(\text{BPh}_4)_4 \cdot \text{Et}_2\text{O} \cdot \text{CH}_3\text{CN}$  (**5**) [1,3-tpbd = *N,N,N',N'*-tetrakis(2-pyridylmethyl)-1,3-benzenediamine,  $\text{BPh}_4^-$  = tetraphenylborate] were prepared and structurally characterized. Analyses of the magnetic data of **2**, **3**, **4**, and  $[\text{Cu}_2(2,6\text{-tpcd})(\text{H}_2\text{O})\text{Cl}](\text{ClO}_4)_2$  (**6**) [2,6-tpcd = 2,6-bis[bis(2-pyridylmethyl)amino]-*p*-cresolate] show the occurrence of weak antiferromagnetic interactions between the copper(II) ions, the bis-terdentate 1,3-tpbd/2,6-tpcd,  $\mu_4\text{-EO}_4$  (E = As and P)  $\mu_{1,2}\text{-OPO}$  and  $\mu\text{-O}_{\text{phenolate}}$  appearing as poor mediators of exchange interactions in this series of compounds. Simple orbital symmetry considerations based on the structural knowledge account for the small magnitude of the magnetic couplings found in these copper(II) compounds.



### 2.1.1 Introduction

Molecular magnetism is an important research field in coordination chemistry. Some highlights on molecular magnets have been summarized previously by Verdager and Linert.<sup>56</sup> Inorganic chemists are especially interested in the synthesis of polynuclear transition metal complexes with predictable magnetic properties. Here Kahn and others have provided extensive detailed experimental and theoretical studies in the past to allow some predictions on the magnetic properties of such compounds.<sup>57-67</sup> Blocking ligands and bridging groups play an important role in the synthesis of polynuclear complexes. In our own work we have used tetra-*N*-functionalized 1,3-benzenediamine (*m*-phenylenediamine) as a building block (together with copper(II) ions and co-ligands) for the formation of polynuclear complexes. Thus, the ligand *N,N,N',N'*-tetrakis(2-pyridylmethyl)-1,3-benzenediamine (1,3-tpbd) and a series of its dinuclear copper(II) complexes (Figure 15) has been prepared in the past by Schindler and co-workers.<sup>68-72</sup> 1,3-tpbd is a versatile ligand that binds various metal ions in a structurally rigid framework.<sup>69</sup> The phenol-based derivative of 1,3-tpbd, 2,6-bis[bis(2-pyridylmethyl) amino]-*p*-cresol (2,6-Htpcd), once deprotonated, forms dinuclear copper(II) complexes, too (Figure 15).<sup>69</sup>

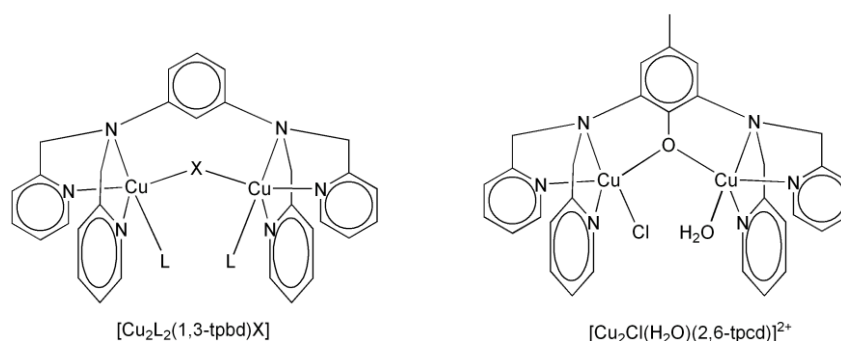


**Fig. 15** (left) 1,3-tpbd-bridged dicopper(II) complexes with X and L being possible ligands, L can also be a bridging ligand (right). Representation of compound 6 (charges are omitted).

A magnetic study of the structurally characterized perchlorate-bridged dicopper(II) complex  $[\text{Cu}_2(1,3\text{-tpbd})(\text{H}_2\text{O})_2(\text{ClO}_4)_3]\text{ClO}_4$ , with a large intramolecular Cu...Cu separation of 5.873(1) Å, had shown a significant ferromagnetic coupling ( $J = +9.3 \text{ cm}^{-1}$ , the Hamiltonian being defined as  $\hat{H} = -J\hat{S}_1 \cdot \hat{S}_2$ ), which is mediated by the *m*-phenylenediamine unit.<sup>70</sup> Ferromagnetic coupling (parallel spin alignment) is difficult to accomplish because the antiparallel alignment of the local spins (antiferromagnetic coupling) is the most common situation for the magnetic interaction between paramagnetic centers through diamagnetic bridging ligands. Ferromagnetic coupling between copper(II) ions arising from spin polarization effects across polyatomic bridges are rare. Taking into account that the values of the exchange coupling ( $J$ ) were quite large, we became interested in investigating such complexes further. However, more recent results with regard to magnetic properties of complexes with 1,3-tpbd as a bridging ligand were somewhat frustrating. No magnetic coupling was observed when the perchlorate group in  $[\text{Cu}_2(1,3\text{-tpbd})(\text{H}_2\text{O})_2(\text{ClO}_4)_3]\text{ClO}_4$  was replaced by acetate or by

sulfate in the tetranuclear complex  $[\text{Cu}_4(1,3\text{-tpbd})_2(\text{H}_2\text{O})_2(\text{SO}_4)_2](\text{SO}_4)_2$ .<sup>70</sup> Furthermore, substitution of the perchlorate anions in  $[\text{Cu}_2(1,3\text{-tpbd})(\text{H}_2\text{O})_2(\text{ClO}_4)_3](\text{ClO}_4)$  by azide afforded the dicopper(II) complex  $[\text{Cu}_2(1,3\text{-tpbd})(\text{N}_3)_4]$  for which only weak antiferromagnetic coupling was observed ( $J = -2.1 \text{ cm}^{-1}$ ).<sup>71</sup> On the other hand, when oxalate was used as an anion, it caused strong antiferromagnetic coupling between the copper(II) ions ( $J = -366 \text{ cm}^{-1}$ ).<sup>71</sup>

A further study that included copper complexes with the isomeric ligands 1,2-tpbd and 1,4-tpbd as well as a structurally related ligand capable of forming mononuclear complexes, clearly demonstrated the advantage of the 1,3-tpbd ligand system in mediating ferromagnetic interactions.<sup>72</sup> In spite of the finding that the dicopper(II) complex  $[\text{Cu}_2(1,3\text{-tpbd})\text{Cl}_4]$  did not show ferromagnetic coupling (the magnetic behavior is practically identical to the azide complex  $[\text{Cu}_2(1,3\text{-tpbd})(\text{N}_3)_4]$ ), we observed an intramolecular ferromagnetic interaction in  $[\text{Cu}_2(1,3\text{-tpbd})(\text{H}_2\text{O})_2(\text{S}_2\text{O}_6)]\text{S}_2\text{O}_6$  whose magnitude is very similar to the structurally related complex  $[\text{Cu}_2(1,3\text{-tpbd})(\text{H}_2\text{O})_2(\text{ClO}_4)_3](\text{ClO}_4)$ .<sup>72-74</sup>

Using the same 1,3-tpbd ligand, we thus had achieved magnetic properties ranging from antiferromagnetic to ferromagnetic coupling, which could be tuned by additional co-ligands. Therefore, we became interested in further developing this system by introducing co-ligands that would provide larger polynuclear complex units with interesting magnetic properties. Promising candidates as co-ligands were arsenate and phosphate. Both anions lead to three-dimensional frameworks. Arsenate more recently gained interest in that regard and different extended structural motifs of iron(III/II) and zinc(II) arsenates have been reported.<sup>75-76</sup>

## 2.1.2 Results and Discussion

### 2.1.2.1 Syntheses

*N,N,N',N'*-Tetrakis(2-pyridylmethyl)-1,3-benzenediamine (1,3-tpbd) was prepared in good yield according to a literature procedure.<sup>68</sup> The copper(II) complexes were obtained by mixing stoichiometric amounts of the respective copper(II) salts, 1,3-tpbd and co-ligands in water/methanol mixtures.

### 2.1.2.2 Molecular Structures of Copper(II) Complexes

#### 2.1.2.2.1 $[\text{Cu}_4(1,3\text{-tpbd})_2(\text{H}_2\text{O})_4(\text{NO}_3)_4]_n(\text{NO}_3)_{4n} \cdot 13n\text{H}_2\text{O}$ (**1**)

Previous efforts to obtain single crystals of a nitrate relative of  $[\text{Cu}_2(1,3\text{-tpbd})(\text{H}_2\text{O})_2(\text{ClO}_4)_3]\text{ClO}_4$  were unsuccessful. Whereas the perchlorate anions could be readily substituted, partially or completely by nitrate ions, the crystal structure obtained could not be refined satisfactorily. Finally, it was recognized that the isolated crystals were quickly deteriorating due to the loss of solvent molecules from the crystal lattice. Keeping the crystals in their mother liquor allowed **1** to be structurally characterized. A fragment of the cationic chain of **1** is depicted below in Figure 16. Crystallographic data

for **1**, together with those of the remaining structures reported in this work (complexes **2–5**), are listed in Table 1, whereas the main bond lengths and angles of **1–5** are displayed in Table 2.

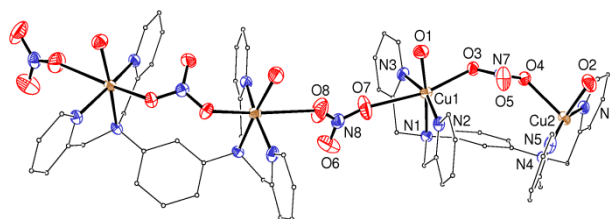


**Fig. 16** Perspective view of a fragment of the copper(II) chain  $[\text{Cu}_4(1,3\text{-tpbd})_2(\text{H}_2\text{O})_4(\text{NO}_3)_4]_n^{4n+}$  of **1**. Hydrogen atoms and solvent molecules are omitted for clarity.

Complex **1** crystallizes as a copper(II) chain that consists of dinuclear  $[\text{Cu}^{\text{II}}_2(1,3\text{-tpbd})]$  units with intra- and interdimer  $\mu_{1,2}$ -nitrate groups. Each of the copper(II) ions is surrounded by three nitrogen donor atoms, two nitrate ions and one oxygen atom of a water molecule forming a “4+2” distorted octahedral environment quite similar to  $[\text{Cu}_2(1,3\text{-tpbd})(\text{H}_2\text{O})_2(\text{ClO}_4)_3]\text{ClO}_4$ . The distance between the two copper(II) ions in one 1,3-tpbd-containing dicopper(II) unit is 5.7976 Å, a value which is close to 5.873(1) Å reported earlier for  $[\text{Cu}_2(1,3\text{-tpbd})(\text{H}_2\text{O})_2(\text{ClO}_4)_3]\text{ClO}_4$ .<sup>68</sup>

**Table 1** Crystallographic data of complexes **1–5**

Compound	1	2	3	4	5
Empirical Formula	$\text{C}_{30}\text{H}_{45}\text{Cu}_2\text{N}_{10}\text{O}_{19.5}$	$\text{C}_{60}\text{H}_{64}\text{AsCl}_5\text{Cu}_4\text{N}_{12}\text{O}_{27.5}$	$\text{C}_{60.5}\text{H}_{64}\text{Cl}_5\text{Cu}_4\text{N}_{12}\text{O}_{27.5}\text{PC}_{108}\text{H}_{104}\text{Cl}_4\text{Cu}_4\text{N}_{12}\text{O}_{32}\text{P}_4$		$\text{C}_{177.25}\text{H}_{166.63}\text{B}_4\text{Cu}_4\text{N}_{14.63}\text{O}_{10.38}\text{P}$
$M_r$	984.4	1905.57	1861.62	2601.87	3026.97
Temperature [K]	200(2)	200(2)	200(2)	200(2)	200(2)
Radiation ( $\lambda$ [Å])	Mo-K $\alpha$ , 0.71073	Mo-K $\alpha$ , 0.71073	Mo-K $\alpha$ , 0.71073	Mo-K $\alpha$ , 0.71073	Mo-K $\alpha$ , 0.71073
Crystal color and shape	green blocks	blue prisms	blue blocks	turquoise prisms	green rhombuses
Crystal size [mm]	0.4 × 0.4 × 0.4	0.3 × 0.2 × 0.045	0.4 × 0.3 × 0.3	0.33 × 0.25 × 0.04	0.3 × 0.2 × 0.045
Crystal system	monoclinic	monoclinic	monoclinic	triclinic	monoclinic
Space group	$C2/c$ (No. 15)	$P2_1/c$ (No. 14)	$P2_1/c$ (No. 14)	$P-1$ (No. 2)	$P2_1/n$ (No. 14)
$a$ [Å]	36.691(2)	18.662(2)	18.566(2)	16.312(2)	15.664(2)
$b$ [Å]	8.9054(6)	19.355(2)	19.326(2)	18.040(2)	27.742(3)
$c$ [Å]	24.997(2)	22.504(2)	22.596(2)	22.835(3)	17.767(1)
$\alpha$ [°]	90.0	90.0	90.0	105.968(2)	90.0
$\beta$ [°]	96.667(1)	109.639	109.328(1)	103.670(2)	94.20(1)
$\gamma$ [°]	90.0	90.0	90.0	105.645(2)	90.0
$V$ [Å <sup>3</sup> ]	8112.7(9)	7655.9(8)	7650(1)	5080(1)	7700(2)
$Z$	8	4	4	2	2
$\rho_{\text{calcd}}$ [g cm <sup>-3</sup> ]	1.613	1.653	1.616	1.474	1.306
$\mu$ [mm <sup>-1</sup> ]	1.140	1.787	1.379	0.944	0.632
$F(000)$	4072	3860	3788	2672	3163
Scan range $\theta$ [°]	1.64 to 28.29	1.42 to 28.32	1.42 to 28.32	1.29 to 28.34	3.35 to 25.68
Index ranges	$-48 \leq h \leq 48$ $-11 \leq k \leq 11$ $-33 \leq l \leq 32$	$-24 \leq h \leq 24$ $-25 \leq k \leq 25$ $-29 \leq l \leq 29$	$-24 \leq h \leq 24$ $-25 \leq k \leq 25$ $-30 \leq l \leq 29$	$-21 \leq h \leq 21$ $-24 \leq k \leq 23$ $-30 \leq l \leq 30$	$-19 \leq h \leq 19$ $-33 \leq k \leq 33$ $-21 \leq l \leq 21$
Reflections collected	46831	92298	90912	59537	69542
Unique reflections	9915	18858	18761	27966	14426
$R_{\text{int}}$	0.0437	0.1445	0.1039	0.2432	0.1062
Data/restraints/parameters	9915/36/572	18858/43/1056	18.761/56/1047	27966/28/1492	14426/1950/1331
Goodness-of-fit on $F^2$	1.059	1.019	1.018	0.928	1.006
Final $R$ indices [ $I > 2\sigma(I)$ ]	$R1 = 0.0665$ $wR2 = 0.1927$	$R1 = 0.0776$ $wR2 = 0.2133$	$R1 = 0.0761$ $wR2 = 0.2150$	$R1 = 0.1021$ $wR2 = 0.1957$	$R1 = 0.0648$ $wR2 = 0.1225$
$R$ indices (all data)	$R1 = 0.0924$ $wR2 = 0.2100$	$R1 = 0.1967$ $wR2 = 0.2585$	$R1 = 0.1667$ $wR2 = 0.2586$	$R1 = 0.3480$ $wR2 = 0.2940$	$R1 = 0.1495$ $wR2 = 0.1478$
Largest diff. peak/hole [eÅ <sup>-3</sup> ]	2.087/−0.950	1.496/−1.320	1.556/−2.091	1.639/−0.830	0.653/−0.420

The terminal nitrate ions are weakly coordinated to the copper(II) ions as one terminal nitrate ion has been replaced by a water molecule, an effect which was observed

previously for the crystallographically characterized copper(II) acetate complexes with 1,3-tpbd.<sup>70</sup> Similar polynuclear compounds with copper(II) ions coordinated by nitrogen donors that are intramolecularly linked by nitrate anions were published earlier.<sup>77-79</sup>

#### 2.1.2.2.2 $[\text{Cu}_4(1,3\text{-tpbd})_2(\text{AsO}_4)(\text{ClO}_4)_3(\text{H}_2\text{O})](\text{ClO}_4)_2 \cdot 2\text{H}_2\text{O} \cdot 0.5\text{CH}_3\text{OH}$ (**2**)

Initially it was attempted to prepare a dinuclear complex by mixing 1,3-tpbd,  $\text{Cu}(\text{ClO}_4)_2 \cdot 6\text{H}_2\text{O}$  and  $\text{Na}_2\text{HAsO}_4$  in a stoichiometric ratio of 1:2:1. However, given that the tetranuclear copper(II) complex **2** was always isolated as the product, the reaction conditions were modified accordingly. Blue crystals of **2** obtained were analyzed by X-ray diffraction studies and the tetracopper(II) cationic unit of **2** is shown in Figure 17. Three copper(II) ions Cu(1), Cu(2) and Cu(4) are coordinated by three nitrogen atoms of the 1,3-tpbd ligand, one arsenate oxygen atom and a perchlorate oxygen atom, whereas for the remaining copper atom [Cu(3)], the perchlorate anion has been replaced by a water molecule. Each of the four copper(II) ions is “4+1” coordinated in a slightly distorted square-pyramidal arrangement. The intramolecular distance between the copper(II) atoms bridged by 1,3-tpbd in **2** [ $\text{Cu}(1) \cdots \text{Cu}(2) = 4.358 \text{ \AA}$ ] is much shorter than in **1**. The separation between the copper(II) atoms (not bridged by 1,3-tpbd) [ $\text{Cu}(1) \cdots \text{Cu}(4) = 6.139 \text{ \AA}$ ] is considerably longer.

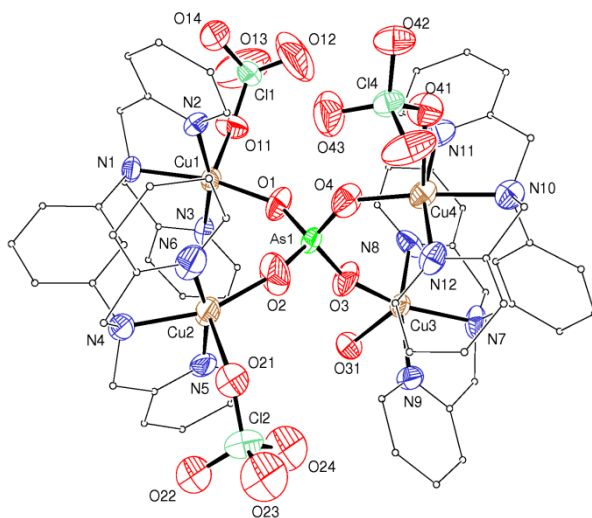


**Fig. 17** Molecular structure of the  $[\text{Cu}_4(1,3\text{-tpbd})_2(\text{AsO}_4)(\text{ClO}_4)_3(\text{H}_2\text{O})]^{2+}$  cation of **2**. Hydrogen atoms and solvent molecules are omitted for clarity.

The trigonality index parameter  $\tau$ <sup>80</sup> ranges from 0.08 for Cu(1) to 0.13 for Cu(4) [ $\tau = (\beta - \alpha)/60^\circ$ , with  $\alpha$  and  $\beta$  being the two largest coordination angles around the metal atom) ( $\tau = 0$  and 1 for ideal square-pyramidal and trigonal-bipyramidal coordination, respectively)]. The basal plane of the coordination sphere around each copper(II) ion in **2** is formed by the two pyridyl nitrogen atoms of 1,3-tpbd, which are *trans* to each other, the tertiary amine nitrogen of 1,3-tpbd and the coordinated arsenate oxygen atom. The apical position is occupied by a perchlorate oxygen atom [Cu(1), Cu(2) and Cu(4)] and the oxygen atom of a coordinated water molecule [Cu(3)].

Only a small number of complexes containing a Cu–O–As moiety have been structurally characterized. For example, Doyle *et al.* described a copper(II) 2,2'-bipyridine (bipy) complex, in which two copper(II) ions are bridged by two H<sub>2</sub>AsO<sub>4</sub><sup>−</sup> anions.<sup>81</sup> Furthermore, some polyoxidometallates are known that contain this binding mode.<sup>82–84</sup>

**Table 2** Selected bond lengths [Å] and angles of **1–5**

Atoms	1	Atoms	2	3	Atoms	4	Atoms	5
Cu(1)–O(1)	1.972(3)	Cu(1)–O(1)	1.865(6)	1.874(4)	Cu(1)–O(4)	1.964(7)	Cu(1)–O(11)	1.941(3)
Cu(1)–N(2)	1.972(3)	Cu(1)–N(3)	1.986(7)	1.988(6)	Cu(1)–N(3)	1.970(9)	Cu(1)–N(10)	2.026(3)
Cu(1)–N(3)	1.986(3)	Cu(1)–N(2)	1.990(7)	1.989(5)	Cu(1)–N(2)	1.971(9)	Cu(1)–N(20)	2.002(3)
Cu(1)–N(1)	2.091(3)	Cu(1)–N(1)	2.039(6)	2.061(5)	Cu(1)–N(1)	2.072(9)	Cu(1)–N(1)	2.086(3)
Cu(1)–O(3)	2.313(3)	Cu(1)–O(11)	2.40(2)	2.36(2)	Cu(1)–O(1)	2.168(7)	Cu(1)–O(14*)	2.115(3)
Cu(1)–O(7)	2.729(3)	Cu(2)–O(2)	1.877(6)	1.884(5)	Cu(2)–O(8)	1.958(7)	Cu(2)–O(12)	1.935(3)
Cu(2)–N(5)	1.966(4)	Cu(2)–N(5)	1.978(8)	1.990(8)	Cu(2)–N(6)	1.967(9)	Cu(2)–N(50)	1.991(4)
Cu(2)–N(6)	1.974(4)	Cu(2)–N(6)	2.003(8)	1.988(7)	Cu(2)–N(5)	1.980(9)	Cu(2)–N(40)	1.992(3)
Cu(2)–O(2)	1.979(4)	Cu(2)–N(4)	2.055(7)	2.066(6)	Cu(2)–N(4)	2.057(8)	Cu(2)–N(2)	2.081(3)
Cu(2)–N(4)	2.097(3)	Cu(2)–O(21)	2.383(8)	2.410(8)	Cu(2)–O(5)	2.152(7)	Cu(2)–O(2)	2.221(7)
Cu(2)–O(4)	2.313(3)	Cu(3)–O(3)	1.906(6)	1.885(5)				
Cu(2*)–O(8)	2.792(4)	Cu(3)–N(8)	1.999(7)	1.994(6)				
		Cu(3)–N(9)	2.016(8)	2.011(6)				
		Cu(3)–N(7)	2.050(7)	2.057(5)				
		Cu(3)–O(31)	2.268(6)	2.269(5)				
		Cu(4)–O(4)	1.888(6)	1.871(5)				
		Cu(4)–N(12)	1.994(8)	1.999(6)				
		Cu(4)–N(11)	2.012(8)	2.014(6)				
		Cu(4)–N(10)	2.069(7)	2.051(6)				
		Cu(4)–O(41)	2.369(6)	2.424(5)				
N(2)–Cu(1)–O(1)	94.97(2)	O(1)–Cu(1)–N(3)	94.6(3)	95.7(2)	O(11)–Cu(1)–N(3)	95.4(3)	O(11)–Cu(1)–N(20)	91.0(2)
N(2)–Cu(1)–N(3)	161.13(2)	O(1)–Cu(1)–N(2)	100.7(3)	99.1(2)	O(11)–Cu(1)–N(2)	97.2(3)	O(11)–Cu(1)–N(10)	100.9(2)
O(1)–Cu(1)–N(3)	96.41(2)	N(3)–Cu(1)–N(2)	163.7(3)	164.0(2)	N(20)–Cu(1)–N(2)	165.3(4)	N(20)–Cu(1)–N(10)	161.2(2)
N(2)–Cu(1)–N(1)	83.58(2)	O(1)–Cu(1)–N(1)	168.7(3)	165.7(2)	O(11)–Cu(1)–N(1)	148.2(3)	O(11)–Cu(1)–N(1)	145.6(2)
O(1)–Cu(1)–N(1)	174.09(2)	N(3)–Cu(1)–N(1)	82.0(3)	82.6(2)	N(20)–Cu(1)–N(1)	82.7(4)	N(20)–Cu(1)–N(1)	80.9(2)
N(3)–Cu(1)–N(1)	83.57(2)	N(2)–Cu(1)–N(1)	81.9(3)	81.6(2)	N(10)–Cu(1)–N(1)	82.6(4)	N(10)–Cu(1)–N(1)	81.1(2)
N(2)–Cu(1)–O(3)	106.59(2)	O(1)–Cu(1)–O(11)	96.0(6)	101.4(4)	O(11)–Cu(1)–O(1)	113.8(3)	O(11)–Cu(1)–O(14*)	108.8(2)
O(1)–Cu(1)–O(3)	87.33(2)	N(3)–Cu(1)–O(11)	78.9(6)	78.3(3)	N(20)–Cu(1)–O(1)	91.9(3)	N(20)–Cu(1)–O(14*)	94.6(2)
N(3)–Cu(1)–O(3)	88.95(2)	N(2)–Cu(1)–O(11)	105.1(4)	104.4(4)	N(10)–Cu(1)–O(1)	90.0(3)	N(10)–Cu(1)–O(14*)	95.2(2)
N(1)–Cu(1)–O(3)	98.57(2)	N(1)–Cu(1)–O(11)	94.0(6)	92.2(4)	N(1)–Cu(1)–O(1)	98.0(3)	N(1)–Cu(1)–O(14*)	105.2(2)
N(5)–Cu(2)–N(6)	160.58(2)	O(2)–Cu(2)–N(5)	102.1(3)	99.6(3)	O(8)–Cu(2)–N(6)	99.7(3)	P(1)–O(11)–Cu(1)	150.4(2)
N(5)–Cu(2)–O(2)	94.91(2)	O(2)–Cu(2)–N(6)	92.7(3)	95.5(3)	O(8)–Cu(2)–N(5)	93.6(3)	P(1)–O(14)–Cu(1*)	125.1(2)
N(6)–Cu(2)–O(2)	96.24(2)	N(5)–Cu(2)–N(6)	164.9(3)	164.7(3)	N(6)–Cu(2)–N(5)	165.2(4)	O(12)–Cu(2)–N(50)	93.0(2)
N(5)–Cu(2)–N(4)	83.39(2)	O(2)–Cu(2)–N(4)	159.0(3)	158.6(3)	O(8)–Cu(2)–N(4)	157.8(3)	O(12)–Cu(2)–N(40)	102.3(2)
N(6)–Cu(2)–N(4)	83.94(2)	N(5)–Cu(2)–N(4)	82.8(3)	82.4(3)	N(6)–Cu(2)–N(4)	83.3(4)	N(50)–Cu(2)–N(40)	164.1(2)
O(2)–Cu(2)–N(4)	174.26(2)	N(6)–Cu(2)–N(4)	82.3(3)	82.6(3)	N(5)–Cu(2)–N(4)	82.0(4)	O(12)–Cu(2)–N(2)	162.7(2)
N(5)–Cu(2)–O(4)	106.66(2)	O(2)–Cu(2)–O(21)	102.9(3)	104.9(3)	O(8)–Cu(2)–O(5)	106.6(3)	N(50)–Cu(2)–N(2)	81.6(2)
N(6)–Cu(2)–O(4)	89.46(2)	N(5)–Cu(2)–O(21)	95.8(3)	101.3(3)	N(6)–Cu(2)–O(5)	92.4(3)	N(40)–Cu(2)–N(2)	82.5(2)
O(2)–Cu(2)–O(4)	88.65(2)	N(6)–Cu(2)–O(21)	83.4(3)	77.0(3)	N(5)–Cu(2)–O(5)	89.8(3)	O(12)–Cu(2)–O(2)	105.4(2)
N(4)–Cu(2)–N(4)	97.09(2)	N(4)–Cu(2)–O(21)	96.9(3)	95.5(3)	N(4)–Cu(2)–O(5)	95.2(3)	N(50)–Cu(2)–O(2)	89.0(2)
		O(3)–Cu(3)–N(8)	104.4(3)	101.3(3)			N(40)–Cu(2)–O(2)	91.3(3)
		O(3)–Cu(3)–N(9)	91.8(3)	95.0(2)			N(2)–Cu(2)–O(2)	91.0(2)
		N(8)–Cu(3)–N(9)	163.3(3)	163.2(3)			P(1)–O(12)–Cu(2)	132.9(2)
		O(3)–Cu(3)–N(7)	156.0(3)	154.8(2)				
		N(8)–Cu(3)–N(7)	82.8(3)	82.6(3)				
		N(9)–Cu(3)–N(7)	80.8(3)	80.9(3)				
		O(3)–Cu(3)–O(31)	94.4(3)	97.5(2)				
		N(8)–Cu(3)–O(31)	91.9(3)	91.2(2)				
		N(9)–Cu(3)–O(31)	90.5(3)	90.6(2)				
		N(7)–Cu(3)–O(31)	108.4(3)	107.3(2)				
		O(4)–Cu(4)–N(12)	101.7(3)	100.3(3)				
		O(4)–Cu(4)–N(11)	94.3(3)	96.4(3)				
		N(12)–Cu(4)–N(11)	163.8(3)	163.1(3)				
		O(4)–Cu(4)–N(10)	171.5(3)	171.6(2)				
		N(12)–Cu(4)–N(10)	81.6(3)	81.1(2)				
		N(11)–Cu(4)–N(10)	82.2(3)	82.0(3)				
		O(4)–Cu(4)–O(41)	96.7(2)	101.0(2)				
		N(12)–Cu(4)–O(41)	96.4(3)	96.1(2)				
		N(11)–Cu(4)–O(41)	84.6(2)	82.8(2)				
		N(10)–Cu(4)–O(41)	90.7(2)	87.0(2)				

\* denotes a symmetry equivalent atom

However, to the best of our knowledge **2** represents the first example of a  $\mu_4$ -AsO<sub>4</sub><sup>3-</sup> coordination mode in a copper(II) complex.

#### 2.1.2.2.3 $[\text{Cu}_4(1,3\text{-tpbd})_2(\text{PO}_4)(\text{ClO}_4)_3(\text{H}_2\text{O})](\text{ClO}_4)_2 \cdot 2\text{H}_2\text{O} \cdot 0.5\text{CH}_3\text{OH}$ (**3**)

Complex **3** was prepared in an analogous manner to **2**, with NaH<sub>2</sub>AsO<sub>4</sub> being replaced by NaH<sub>2</sub>PO<sub>4</sub>. The blue needles obtained were analyzed by single crystal X-ray diffraction. The molecular structure of the tetracopper(II) cationic unit of **3** (see Figure 18) is isostructural to that of **2**. The separation of the copper(II) ions bridged by 1,3-tpbd [Cu(1)⋯Cu(2) = 4.226 Å] is similar to that found in **2**. However, the separation between the copper(II) ions not bridged by 1,3-tpbd [Cu(1)⋯Cu(4) = 5.869 Å] is shorter than the distance found in **2**.

Dinuclear copper(II) complexes with bridging phosphate groups are well known and they have been used in the past to model the active site of purple acid phosphatases.<sup>85-88</sup> In contrast, the  $\mu_4$ -binding mode is less common and is usually limited to phosphate groups embedded in polyoxidometallates<sup>89-92</sup> and sheet-like structures.<sup>93-95</sup> To the best of our knowledge, so far only two other structurally characterized complexes with a discrete  $\mu_4$ -PO<sub>4</sub>-Cu<sub>4</sub> coordination mode (as in **3**) have been reported in the literature.<sup>96-97</sup> Furthermore, it deserves to be noted that Anslyn *et al.* prepared copper(II) complexes of tripodal ligands, which act as receptors with an extraordinary capacity for binding phosphate and arsenate ions as well as various phosphate esters in neutral aqueous solutions.<sup>98-101</sup>

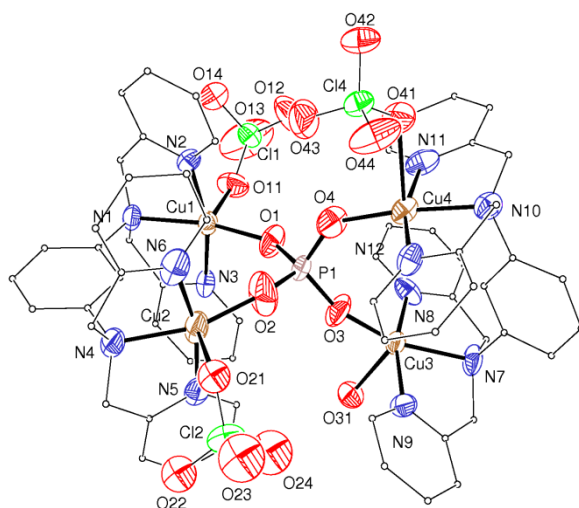


**Fig. 18** Molecular structure of the  $[\text{Cu}_4(1,3\text{-tpbd})_2(\text{PO}_4)(\text{ClO}_4)_3(\text{H}_2\text{O})]^{2+}$  cation of **3**. Hydrogen atoms and solvent molecules are omitted for clarity.

#### 2.1.2.2.4 $[\text{Cu}_2(1,3\text{-tpbd})\{(\text{PhO})_2\text{P}(\text{O})_2\}_2]_{2n}(\text{ClO}_4)_{4n}$ (**4**)

Introducing sterically demanding organic groups on the phosphate anion should suppress formation of a tetranuclear complex such as **3**. Therefore, diphenylphosphate was chosen as a bridging group. The complex  $[\text{Cu}_2(1,3\text{-tpbd})\{(\text{PhO})_2\text{P}(\text{O})_2\}_2]_{2n}(\text{ClO}_4)_{4n}$  (**4**) was obtained by mixing diphenylphosphate, 1,3-tpbd and  $\text{Cu}(\text{ClO}_4)_2 \cdot 6\text{H}_2\text{O}$  in a stoichiometric ratio. The turquoise crystals obtained were analyzed by X-ray diffraction

studies and demonstrated that a coordination polymer had formed. A view of the repeating unit including the copper(II) ions connecting the individual units of **4** is shown in Figure 19.

The coordination environment around the crystallographic independent copper(II) ions in **4** is best described as “4+1” distorted square-pyramidal with  $\tau$  values<sup>80</sup> of 0.285 at Cu(1) and 0.123 at Cu(2). Interestingly, the diphenylphosphate ligands neither act as bridges between the two adjacent copper(II) ions nor form a tetranuclear unit such as observed in **2** and **3**. Instead, they connect to another dinuclear complex unit, resulting in a chain-like structure, most likely due to the consequence of the steric crowding of the phenyl groups around the phosphorus atom. An eight-membered ring is formed between the two dinuclear units that are made up by two copper(II) ions, two phosphorus atoms and four oxygen atoms.

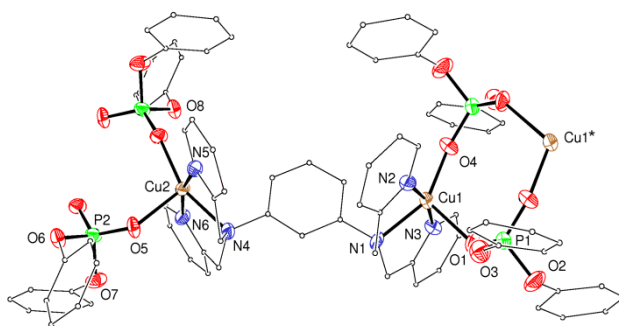


**Fig. 19** Perspective view of a fragment of the  $[\text{Cu}_2(1,3\text{-tpbd})\{(\text{PhO})_2\text{P}(\text{O})_2\}_2]_n^{2n+}$  cationic chain of **4**. Hydrogen atoms are omitted for clarity.

A copper(II) complex forming a similar six-membered ring was published earlier by Chin and co-workers.<sup>102</sup> They studied the phosphate diester cleavage capability of this dicopper(II) complex in a similar fashion to that reported for **6**.<sup>69</sup> The ring formed by two copper-, one phosphorus- and three oxygen atoms plays an important role in the postulated diester cleavage mechanism.<sup>102</sup>

#### 2.1.2.2.5 $[\text{Cu}_2(1,3\text{-tpbd})((\text{PhO})\text{PO}_3)_2(\text{H}_2\text{O})_{0.69}(\text{CH}_3\text{CN})_{0.31}]_2(\text{BPh}_4)_4\cdot\text{Et}_2\text{O}\cdot\text{CH}_3\text{CN}$ (**5**)

In order to relieve some of the steric strain shown in **4**, a monophenylphosphate was used in the synthesis of complex **5**. The molecular structure of the tetracopper(II) cationic part of **5** is shown in Figure 20.

The tetranuclear unit of **5** comprises two 1,3-tpbd molecules, each of them coordinating two copper(II) ions, and two monophenylphosphate molecules. As in **4**, an eight-membered ring with two copper(II) ions, two phosphorus atoms and four oxygen atoms is formed. Moreno *et al.* and Phuengphai *et al.* both reported a similar structural motif with the 1,10-phenanthroline ligand (phen) where mono-/diphenylphosphate was replaced by dihydrogenphosphate.<sup>103-104</sup> The Cu–O bond lengths reported therein are in good agreement with those of **4** and **5**. Complex **5** crystallizes with an inversion center located in the middle of the Cu–P–O eight-membered ring. The four copper(II) ions are



connected *via* the monophenylphosphate groups resulting in a tetranuclear complex, which is built up of two dinuclear symmetry-related units.

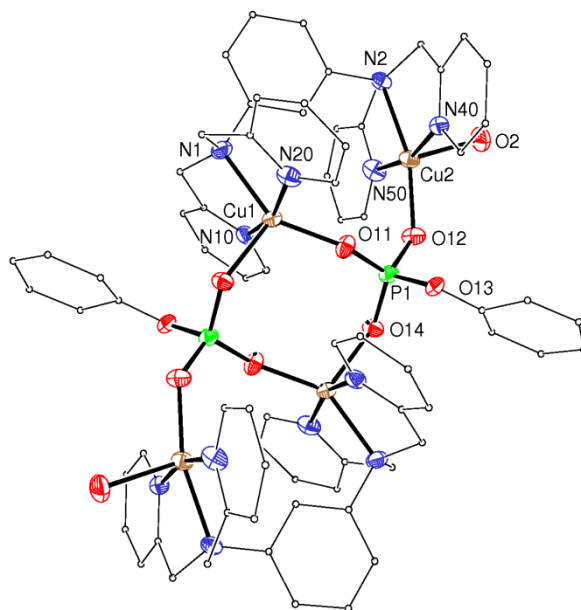


**Fig. 20** Molecular structure of the  $[\text{Cu}_2(1,3\text{-tpbd})\{(\text{PhO})\text{PO}_3\}_2(\text{H}_2\text{O})_{0.69}(\text{CH}_3\text{CN})_{0.31}]^{2+}$  cation of **5**. Hydrogen atoms and solvent molecules are omitted for clarity.

The coordination environment around the copper(II) ions in one of the two units in **5** is again “4+1” distorted square-pyramidal. The distortion differs remarkably for Cu(1) and Cu(2). The trigonality index parameter  $\tau^{80}$  has values of 0.263 [at Cu(1)] and 0.023 [at Cu(2)].

#### 2.1.2.2.6 $[\text{Cu}_2(2,6\text{-tpcd})(\text{H}_2\text{O})\text{Cl}](\text{ClO}_4)_2 \cdot 2\text{H}_2\text{O}$ (**6**)

The crystal structure of the dinuclear complex **6** was previously reported.<sup>69</sup> Its structure is reproduced in Figure 21, the pertinent feature being that the phenolate oxygen atom occupies the apical position at each copper(II) ion.

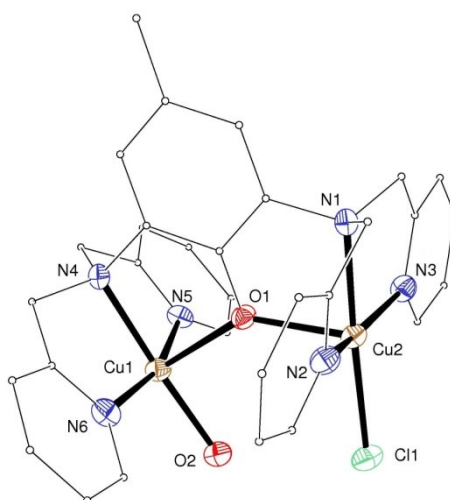


**Fig. 21** Molecular structure of  $[\text{Cu}_2(2,6\text{-tpcd})(\text{H}_2\text{O})\text{Cl}]^{2+}$  cation of **6**. Hydrogen atoms, solvent molecules and uncoordinated anions are omitted for clarity.



The magnetic properties of this compound are reported here as a model compound in the interpretation of the magnetic properties of **2–5**.

### 2.1.2.3 Magnetic Properties of **2**, **3**, **4**, and **6**

The ferromagnetic coupling observed in  $[\text{Cu}_2(1,3\text{-tpbd})(\text{H}_2\text{O})_2(\text{ClO}_4)_3]\text{ClO}_4$ , following the spin polarization mechanism, was successfully interpreted using density functional theory (DFT) calculations.<sup>70</sup> This finding is in good agreement with a related benzenediamine-based dinuclear complex that also showed ferromagnetic coupling ( $J = +16.8 \text{ cm}^{-1}$ ) between two copper(II) ions over a large distance.<sup>105</sup> More recently, ferromagnetic coupling has been observed in *m*-phenylenediamine-bridged tris(2-aminoethyl)amine copper(II) complex units<sup>106</sup> and oligo-*m*-phenyleneoxalamide copper(II) mesocates.<sup>107</sup> These last examples can be viewed as electro-switchable ferromagnetic metal organic wires. For the nitrate complex **1**, the fast deterioration that it undergoes due to the loss of solvent precludes its magnetic study. However, a structural comparison between **1** and  $[\text{Cu}_2(1,3\text{-tpbd})(\text{H}_2\text{O})_2(\text{ClO}_4)_3]\text{ClO}_4$  suggests that most likely a ferromagnetic coupling would occur between the copper(II) ions through the 1,3-tpbd bridging ligand. Here the loss of solvent molecules in the copper(II) complex can cause subtle structural changes, which prevent detailed magnetic analysis, a situation experienced previously for the acetate system.<sup>70</sup> Therefore, magnetic measurements were only performed on **2**, **3**, **4**, and **6**.

The magnetic properties of complex **6** (Figure 21) under the form of the  $\chi_{\text{M}}T$  versus  $T$  plot [ $\chi_{\text{M}}$  is the magnetic susceptibility per two copper(II) ions] are shown in Figure 22. At room temperature,  $\chi_{\text{M}}T$  is equal to  $0.80 \text{ cm}^3 \text{ mol}^{-1} \text{ K}$ , a value which is as expected for two magnetically isolated spin doublets ( $\chi_{\text{M}}T = 0.75 \text{ cm}^3 \text{ mol}^{-1} \text{ K}$  with  $g = 2.0$ ). A Curie law behavior is observed upon cooling until ca. 30 K.  $\chi_{\text{M}}T$  decreases sharply in the low temperature domain and a value of  $0.55 \text{ cm}^3 \text{ mol}^{-1} \text{ K}$  at 1.9 K is attained. A maximum of the magnetic susceptibility is quasi reached, the temperature of such a maximum being slightly below 1.9 K (see the inset of Figure 23). These features are consistent with the occurrence of a weak intramolecular antiferromagnetic interaction between two local spin doublets leading to a singlet ground spin state.

In light of the discrete dinuclear structure of compound **6**,<sup>69</sup> its magnetic data were analyzed through a simple Bleaney–Bowers expression [eq (1)], which was derived through the isotropic Hamiltonian  $\mathbf{H} = -J\mathbf{S}_1 \cdot \mathbf{S}_2$

$$\chi_{\text{M}} = (2N\beta^2g^2/kT) [3 + \exp(-J/kT)]^{-1} \quad (1)$$

where  $J$  and  $g$  are the singlet-triplet energy gap and the average  $g$  factor for the dicopper(II) unit, and  $N$ ,  $\beta$  and  $k$  have their usual meanings. Least-squares fitting leads to the following parameters:  $J = -1.70(1) \text{ cm}^{-1}$ ,  $g = 2.07(1)$  and  $R = 1.2 \times 10^{-5}$  ( $R$  is the agreement factor defined as  $\Sigma[(\chi_{\text{M}})_{\text{obs}} - (\chi_{\text{M}})_{\text{calc}}]^2 / \Sigma[(\chi_{\text{M}})_{\text{obs}}]^2$ ). The computed curve matches well the experimental one in the temperature range investigated. The small value of the weak intramolecular magnetic interaction in **6** can be understood by looking

at the respective orientation of the magnetic orbitals involved. In fact, each copper(II) ion of this compound is found in a square pyramidal environment, the basal plane being defined by the N(4), N(5), N(6) and O(2) [at Cu(1)] and N(1), N(2), N(3) and Cl(1) [at Cu(2)] set of atoms (see Figure 26). A phenolate oxygen atom [O(1)] fills the apical position, the copper to O(1) bond distances being longer than 2.1 Å. In such a case, the unpaired electron at each copper(II) ion is located in the equatorial plane (the magnetic orbital) and a weak overlap is predicted between the two magnetic orbitals through the phenolate oxygen atom because of the small spin density at the apical position. Also the magnetic coupling through the long  $\sigma$  in-plane Cu(1)–N(4)–C(17)–C(18)–C(13)–N(3)–Cu(2) pathway [*syn-syn* conformation according to the relative orientation of the Cu(1)–N(4) and Cu(2)–N(1) bonds] is expected to be very weak.<sup>70</sup> The low efficiency of both exchange pathways in **6** accounts for the weak magnetic coupling observed.

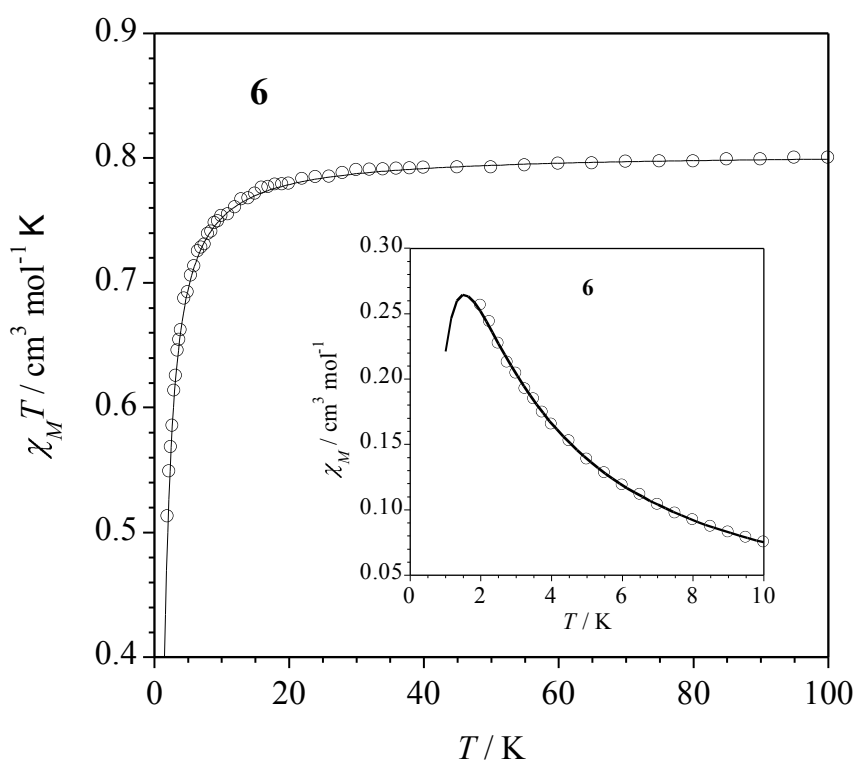


**Fig. 22** Temperature dependence of the  $\chi_M T$  product for **6**: (o) experimental data; (–) best-fit curves through eq (1) (see text). The inset shows the  $\chi_M$  versus  $T$  plot for  $T < 10$  K.

The magnetic properties of complex **4** under the form of the  $\chi_M T$  versus  $T$  plot [ $\chi_M$  is the magnetic susceptibility per two copper(II) ions] are shown in Figure 23. At room temperature,  $\chi_M T$  is equal to 0.80 cm³ mol⁻¹ K, a value which is as expected for two magnetically non-interacting spin doublets. A Curie law behavior is observed upon cooling until ca. 70 K and afterwards  $\chi_M T$  decreases sharply at lower temperatures to attain a value of 0.17 cm³ mol⁻¹ K at 1.9 K. A maximum of the magnetic susceptibility occurs at 3.5 K (see the inset of Figure 23). These features are characteristic of an overall weak antiferromagnetic behavior.

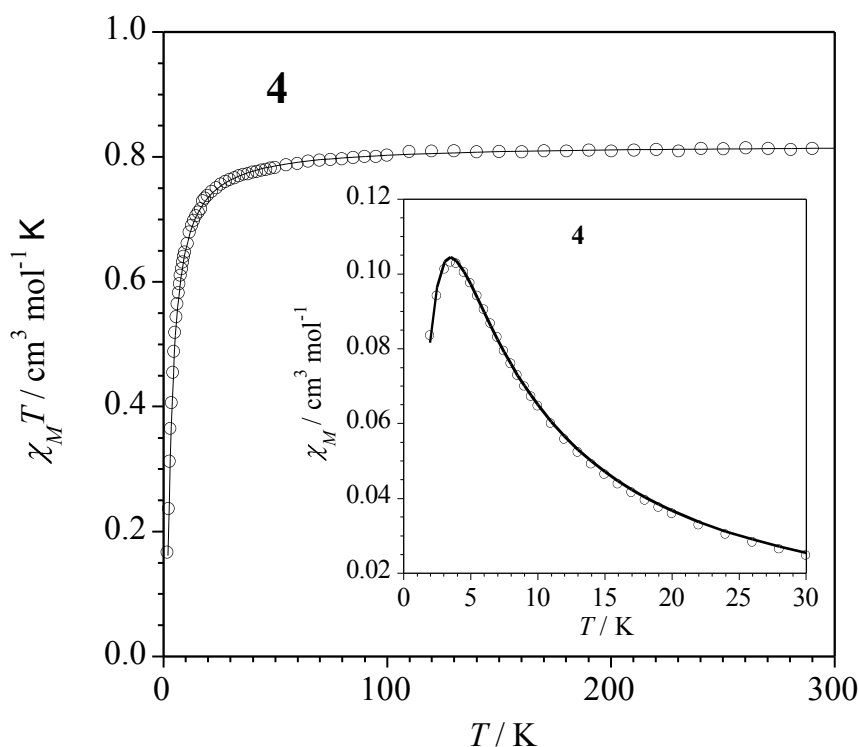


**Fig. 23** Temperature dependence of the  $\chi_M T$  product for **4**: (o) experimental data; (–) best-fit curves through eq. (2) (see text). The inset shows the  $\chi_M$  versus  $T$  in the vicinity of the maximum.

In agreement with the chain structure of **4** where the regular alternating bis-terdentate 1,3-tpbd and doubly bis-monodenate  $(\text{PhO})_2\text{P}(\text{O})_2$  bridges occurs, its magnetic data were analyzed through the alternating chain spin exchange model [eq (2)] and the development of Hatfield *et al.*<sup>108</sup>

$$H = -J\sum(\mathbf{S}_{2i}\cdot\mathbf{S}_{2i-1} + \alpha\mathbf{S}_{2i}\cdot\mathbf{S}_{2i+1}) \quad (2)$$

where  $J$  and  $\alpha$  are the exchange coupling and alternation parameter, respectively. Least-squares fit minimizing  $R = \Sigma[(\chi_M)_{\text{obs}} - (\chi_M)_{\text{calc}}]^2 / \Sigma[(\chi_M)_{\text{obs}}]^2$ , led to the following set of values :  $J = -3.90(1) \text{ cm}^{-1}$ ,  $\alpha J = -1.79(2) \text{ cm}^{-1}$ ,  $g = 2.09(1)$  and  $R = 2.3 \times 10^{-5}$ . The calculated curves reproduce the magnetic data very well in the whole temperature range investigated. The two intrachain magnetic couplings in **4** are weak and antiferromagnetic and their assignment to the two exchange pathways involved is not evident at first sight. Their weakness is not surprising bearing in mind the two exchange pathways involved: the extended bis-terdentate 1,3-tpbd molecule, which links equatorial positions at the Cu(1) and Cu(2) [ $\text{Cu}(1)\cdots\text{Cu}(2) = 8.12 \text{ \AA}$ ] and the pair of bis-monodenate  $(\text{PhO})_2\text{P}(\text{O})_2$  bridges connecting an equatorial position of a copper atom with the apical one of the adjacent copper [ $\text{Cu}(1)\cdots\text{Cu}(1A) = 4.59 \text{ \AA}$  and  $\text{Cu}(2)\cdots\text{Cu}(2A) = 4.67 \text{ \AA}$ ].

The former one is a  $\sigma$  in-plane exchange pathway as in **6**, the Cu(1)–N(1)–C(13)–C(18)–C(17)–N(4)–Cu(2) fragment exhibiting the *anti-anti* conformation instead of the *syn-syn* occurring for such a fragment in **6**. Most likely, the weaker antiferromagnetic interaction [ $\alpha J = -1.79(2) \text{ cm}^{-1}$ ] is mediated by this bridging pathway, whereas the somewhat larger

antiferromagnetic coupling [ $J = -3.90(1) \text{ cm}^{-1}$ ] would involve the double equatorial-apical  $\mu_{1,2}\text{-O-P-O}$  skeleton involving a much shorter copper–copper separation.

The magnetic properties of the complexes **2** and **3** under the form of  $\chi_M T$  versus  $T$  plots [ $\chi_M$  is the magnetic susceptibility per four copper(II) ions] are shown in Figure 24. At room temperature,  $\chi_M T$  for **2** and **3** is ca.  $1.60 \text{ cm}^3 \text{ mol}^{-1} \text{ K}$ , a value which is as expected for four magnetically isolated spin doublets [ $\chi_M T = \text{cm}^3 \text{ mol}^{-1} \text{ K}$  with  $g = 2.0$ ]. Upon cooling, a Curie law behavior is observed until ca. 100 K, which is followed by an abrupt decrease of  $\chi_M T$  to reach values of 0.9 (**2**) and 0.55  $\text{cm}^3 \text{ mol}^{-1} \text{ K}$  (**3**) at 1.9 K. No maximum in the magnetic susceptibility is observed for **2** and **3** in the temperature range explored. This decrease of  $\chi_M T$  in the low temperature domain is due to relatively weak intramolecular antiferromagnetic interactions.

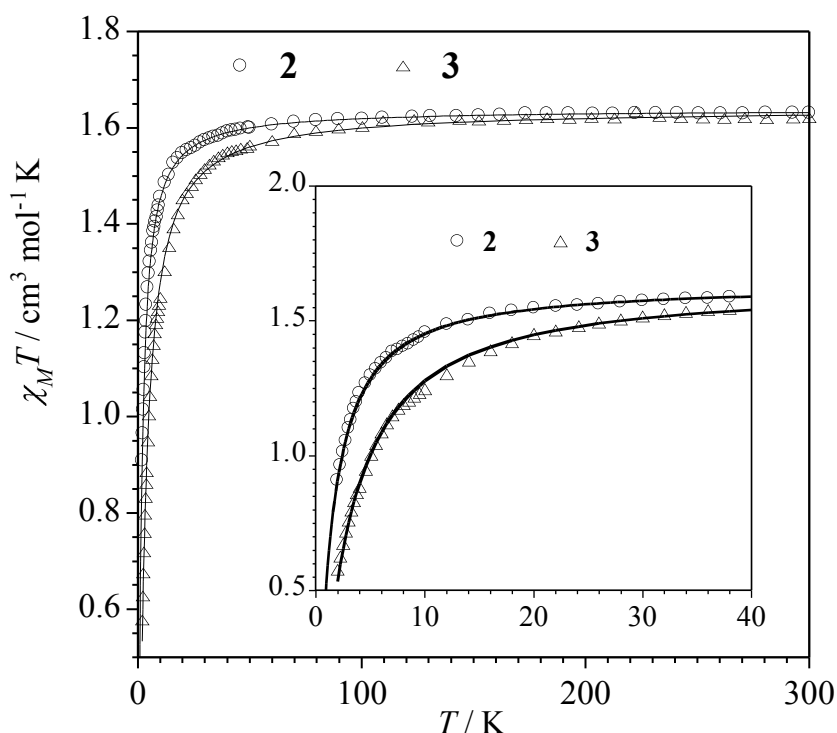


**Fig. 24** Temperature dependence of the  $\chi_M T$  product for **2** and **3**: (○,△) experimental data; (–) best-fit curves through eq (3) (see text). The inset shows a detail of the low temperature region.

In agreement with the tetrahedral arrangement of the four copper(II) ions in **2** and **3**, their magnetic data were analyzed through the isotropic spin Hamiltonian of eq (3).

$$\mathbf{H} = -J_a (\mathbf{S}_1 \cdot \mathbf{S}_2 + \mathbf{S}_3 \cdot \mathbf{S}_4) - J_b (\mathbf{S}_1 \cdot \mathbf{S}_4 + \mathbf{S}_2 \cdot \mathbf{S}_3) - J_c (\mathbf{S}_1 \cdot \mathbf{S}_3 + \mathbf{S}_2 \cdot \mathbf{S}_4) - g\beta H (\mathbf{S}_1 + \mathbf{S}_2 + \mathbf{S}_3 + \mathbf{S}_4) \quad (3)$$

where  $J_a$ ,  $J_b$  and  $J_c$  are the magnetic coupling parameters (see Figure 25, right) and  $g$  is the average Landé factor which is assumed to be identical for the four copper(II) ions. Numerical matrix diagonalization techniques using a Fortran program<sup>109</sup> (conducting extensive mappings with the aim of locating the global minimum of each system among a large number of local minima) led to the following set of parameters through least-squares fitting of the data:  $J_a = J_b = J_c = -1.11(1) \text{ cm}^{-1}$ ,  $g = 2.09(1)$  and  $R = 1.6 \times 10^{-6}$  (**2**),  $J_a = J_b = J_c = -2.27(1) \text{ cm}^{-1}$ ,  $g = 2.09(1)$  and  $R = 1.5 \times 10^{-6}$  (**3**) ( $R$  is the agreement factor

defined as  $R = \Sigma[(\chi_M T)_{\text{obs}} - (\chi_M T)_{\text{calc}}]^2 / \Sigma[(\chi_M T)_{\text{obs}}]^2$ . An excellent agreement between the experimental data and the calculated curves is obtained in the two cases.

It deserves to be noted that although we tried different sets of starting values for the  $J_i$  parameters (even of different nature), the best fit is always achieved with the same value for the three magnetic couplings in each complex. This means that the magnetic coupling through the  $\mu_4\text{-XO}_4$  motif is dominant and then, the interaction through the extended 1,3-tpbd involving the pairs Cu(1)/Cu(2) and Cu(3)/Cu(4) pairs would be negligible. Looking at the structure of **2** and **3**, this can be easily understood because of the common Cu–O–X–O–Cu' [X = As (**2**) and P (**3**)] five-atoms-set involved in the intramolecular exchange pathways connecting equatorial positions (see the orbital picture in Figure 25). The somewhat shorter values of the intramolecular Cu...Cu' separation for **3** with respect to those in **2** (dictated by the shorter P–O bond lengths compared to the As–O ones) would account for the slightly larger antiferromagnetic coupling in **3**.

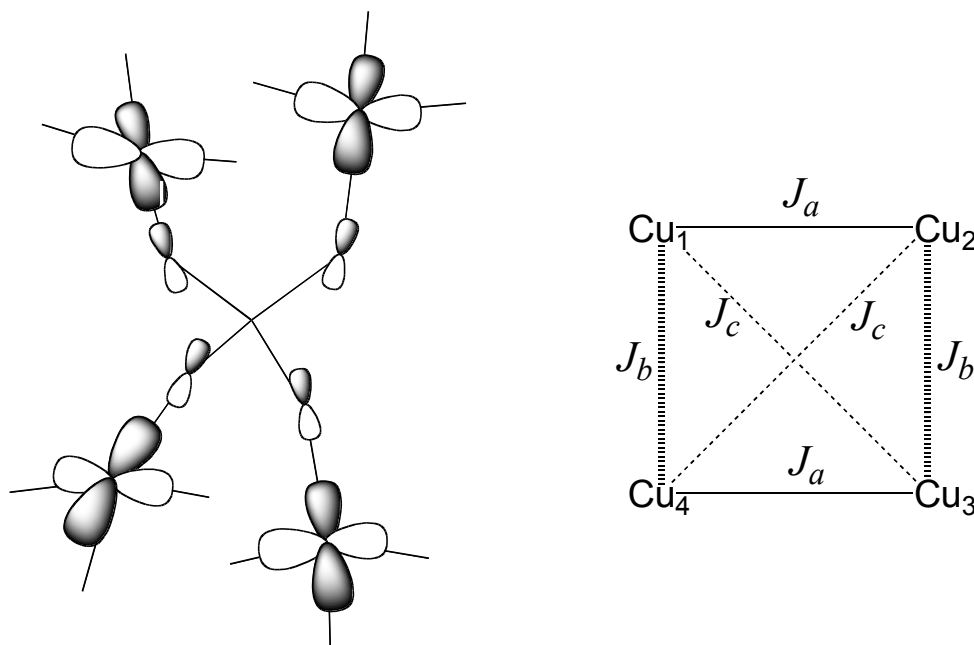


**Fig. 25** (Left) Orbital picture illustrating the exchange pathways through the  $\mu_4\text{-XO}_4$  with X = As (**2**) and P (**3**). (Right) Intramolecular spin coupling pattern in **2** and **3**.

Finally, a brief comment concerning the weak magnetic interactions in these two complexes is warranted. To the best of our knowledge, the case of **2** is the first magneto-structurally characterized example of a  $\mu_4\text{-AsO}_4$ -bridged copper(II) complex and this precludes any comparison. A similarly related complex is the copper(II) complex  $\{[\text{Cu}(\text{bipy})(\text{H}_2\text{AsO}_4)](\mu_{1,2}\text{-H}_2\text{AsO}_4)\}$  where a very weak antiferromagnetic coupling between the copper(II) ions ( $J = -0.58 \text{ cm}^{-1}$ ) is mediated by a pair of bis-monodentate dihydroarsenate bridges, the copper–copper separation being  $5.287 \text{ \AA}$ .<sup>81</sup> The case of complex **3** is also a special one because no correlation between the structural parameters and the magnetic coupling exists and the magnetic coupling through the Cu–O–P–O–Cu pathway covers a wide range of significant values either negative or positive.<sup>110</sup> In fact, only two other structurally characterized complexes with a tetrakis-

monodentate-coordination mode of the phosphate group are known but their magnetic properties were not investigated.<sup>96-97</sup>

### 2.1.3 Conclusions

The copper(II) 1,3-tpbd complexes **1–5** exhibit interesting structural properties. Two of them (**2** and **3**) show rare or even unique coordination modes of copper(II) ions with the arsenate (**2**) or phosphate (**3**) co-ligands. Furthermore, an eight-membered ring between two copper(II) ions and two phosphate molecules occurs in complexes **4** and **5**. The study of the magnetic behavior of **2**, **3**, **4**, and the related compound [Cu<sub>2</sub>(2,6-tpcd)(H<sub>2</sub>O)Cl](ClO<sub>4</sub>)<sub>2</sub> (**6**) shows that the bis-terdentate 1,3-tpbd, 2,6-tpcd, bis-monodentate O–P–O and tetrakis-monodentate-XO<sub>4</sub><sup>3-</sup> (X = P and As) bridges appear as poor mediators of magnetic interactions between the copper(II) atoms in these species. Simple magnetic orbital considerations, which are based on the structural knowledge and previous theoretical calculations, account for the weak magnetic interactions. Larger polynuclear copper(II) 1,3-tpbd complexes containing anionic co-ligands were prepared, although the magnetic interactions in these new compounds turned out to be weak and antiferromagnetic. Finally, this work demonstrates methods to increase the nuclearity and/or dimensionality of the 1,3-tpbd-containing copper(II) complexes, the achievement of stronger magnetic couplings being the goal to be achieved varying the nature of the co-ligand.

### 2.1.4 Experimental Section

#### 2.1.4.1 *Materials*

All chemicals were obtained from commercial sources and used without further purification. The 1,3-tpbd ligand was prepared according to a literature procedure.<sup>68</sup>

**Caution!** The syntheses and procedures described below involve compounds that contain perchlorate ions, which can detonate explosively and without warning. Although we have not encountered any problems with the compounds used in this study, they should be handled with extreme caution.

#### 2.1.4.2 *Syntheses of Copper Complexes 1–5*

##### 2.1.4.2.1 [Cu<sub>4</sub>(1,3-tpbd)<sub>2</sub>(H<sub>2</sub>O)<sub>4</sub>(NO<sub>3</sub>)<sub>4</sub>]<sub>n</sub>(NO<sub>3</sub>)<sub>4n</sub>·13nH<sub>2</sub>O (**1**)

1,3-tpbd (329 mg, 0.68 mmol) dissolved in methanol (15 mL) was added to an aqueous solution (10 mL) of Cu(NO<sub>3</sub>)<sub>2</sub>·3H<sub>2</sub>O (328 mg; 1.36 mmol). The reaction mixture was stirred for 5 min during which time the solution turned to a dark green color. Single crystals of **1** were obtained after two days. UV/Vis (MeOH) λ<sub>max</sub> = 383 nm (ε = 2800 M<sup>-1</sup> cm<sup>-1</sup>), 684 nm (ε = 600 M<sup>-1</sup> cm<sup>-1</sup>).

**2.1.4.2.2**      $[Cu_4(1.3\text{-tpbd})_2(AsO_4)(ClO_4)_3(H_2O)](ClO_4)_2 \cdot 2H_2O \cdot 0.5CH_3OH$  (**2**) /  
 $[Cu_4(1.3\text{-tpbd})_2(PO_4)(ClO_4)_3(H_2O)](ClO_4)_2 \cdot 2H_2O \cdot 0.5CH_3OH$  (**3**) /  
 $[Cu_2(1,3\text{-tpbd})\{(PhO)_2P(O)_2\}_2](ClO_4)_4$  (**4**)

1.3-tpbd (100.0 mg, 0.21 mmol) dissolved in methanol (15 mL) was added to aqueous solutions (5 mL) of  $Cu(ClO_4)_2 \cdot 6H_2O$  (155 mg, 0.42 mmol) and  $Na_2HAsO_4$  (65.5 mg, 0.21 mmol) for **2**,  $Cu(ClO_4)_2 \cdot 6H_2O$  (155.0 mg, 0.42 mmol) and  $Na_2HPO_4$  (56.3 mg, 0.21 mmol) for **3**, and  $Cu(ClO_4)_2 \cdot 6H_2O$  (155.0 mg, 0.42 mmol) and diphenylphosphate (52.5 mg; 0.21 mmol) for **4**. The green reaction solutions were each stirred for 5 min. Crystals suitable for X-ray diffraction were formed after two days. Intense blue crystals of **2** (UV/Vis (MeOH)  $\lambda_{max} = 380$  nm (shoulder,  $\epsilon = 900 \text{ M}^{-1}\text{cm}^{-1}$ ), 713 nm ( $\epsilon = 500 \text{ M}^{-1}\text{cm}^{-1}$ )) and of **3** (UV/Vis (MeOH)  $\lambda_{max} = 706$  nm ( $\epsilon = 600 \text{ M}^{-1}\text{cm}^{-1}$ )), and light blue crystals of **4** (UV/Vis (MeCN)  $\lambda_{max} = 308$  nm (shoulder,  $\epsilon = 4100 \text{ M}^{-1}\text{cm}^{-1}$ ), 379 nm ( $\epsilon = 1500 \text{ M}^{-1}\text{cm}^{-1}$ ), 734 nm ( $\epsilon = 500 \text{ M}^{-1}\text{cm}^{-1}$ )).

**2.1.4.2.3**      $[Cu_2(1,3\text{-tpbd})\{(PhO)PO_3\}_2(H_2O)_{0.69}(CH_3CN)_{0.31}]_2(BPh_4)_4 \cdot Et_2O \cdot CH_3CN$  (**5**).

Aqueous solutions (5 mL) of  $Cu(ClO_4)_2 \cdot 6H_2O$  (78.4 mg, 0.210 mmol) and the sodium salt of phenylphosphate (27.0 mg, 0.105 mmol) were added to a mixture of 1,3-tpbd (50.0 mg, 0.105 mmol) and  $NaBPh_4$  dissolved in methanol. The turquoise precipitate was filtered and dissolved in  $CH_3CN$ . Crystals suitable for X-ray diffraction analyses were obtained by slow diffusion of diethyl ether into the solution. (UV/Vis (MeCN)  $\lambda_{max} = 380$  nm ( $\epsilon = 1700 \text{ M}^{-1}\text{cm}^{-1}$ ), 701 nm ( $\epsilon = 500 \text{ M}^{-1}\text{cm}^{-1}$ ))

**2.1.4.3**     *Magnetic Measurements*

Variable-temperature (1.9–300 K) magnetic susceptibility measurements on polycrystalline samples of **2**, **3**, **4** and **6** were collected with a SQUID susceptometer under applied dc magnetic fields of 1 T ( $T \geq 100$  K) and 500 G ( $T < 100$  K). Corrections of the diamagnetism for the constituent atoms of **2**, **3**, **4**, and **6** were done by means of the Pascal's constants.<sup>111</sup> Corrections for the sample holder as well as for the temperature-independent paramagnetism [ $60 \times 10^{-6} \text{ cm}^3 \text{ mol}^{-1} \text{ K}$  per copper(II) ion] were also applied.

**2.1.4.4**     *X-Ray Crystallographic Studies*

Intensity data of **1–4** were collected with a Siemens SMART CCD 1000 diffractometer by the  $\omega$ -scan technique collecting a full sphere of data with irradiation times of 10 to 20 s per frame and  $\Delta\omega$  ranges between  $0.3^\circ$  and  $0.45^\circ$ . The collected reflections were corrected for absorption, Lorentz and polarization effects.<sup>112</sup> All structures were solved by direct methods and refined by least-squares techniques using the SHELX-97 program package.<sup>113</sup> The hydrogen atoms were positioned geometrically and all non-hydrogen

atoms, if not mentioned otherwise, were refined anisotropically. Further data collection parameters are summarized in Table 1.

Intensity data of **5** were collected with a Bruker-Nonius Kappa CCD diffractometer. Absorption effects were corrected by semi-empirical methods based on equivalent reflections.<sup>112</sup> The structure was solved by direct methods; full-matrix least-squares refinement was carried out on  $F^2$  using SHELXTL NT 6.12.<sup>112</sup> All non-hydrogen atoms were refined anisotropically. The high residual electron density in **5** is due to the high amount of solvent molecules and the poor quality of the crystals. Hydrogen atoms were geometrically positioned, their isotropic displacement parameters were tied to those of their corresponding carrier atoms by a factor of 1.2 or 1.5. Both of the BPh<sub>4</sub><sup>-</sup> anions show disordered phenyl groups. SIMU and SAME restraints were applied in the refinement of these anions. The co-ligand at Cu(2) is disordered. The sixth coordination site is either occupied by an aqua ligand [O(2), 69(2)%] for which no hydrogen atoms have been included in the structural model or by an acetonitrile molecule [N(520)–C(522), 31(2)%]. A disordered Et<sub>2</sub>O molecule [O(500)–C(504)] is partially present when the aqua ligand is coordinated to Cu(2). SIMU, SADI, SAME and ISOR restraints were applied in the treatment of this disordered part of the structure.

CCDC Nos. 661254 (**1**), 661255(**2**), 661256(**3**), 661257(**4**) and 658344 (**5**) contain the supplementary crystallographic data for this paper. These data can be obtained free of charge at [www.ccdc.cam.ac.uk/conts/retrieving.html](http://www.ccdc.cam.ac.uk/conts/retrieving.html) [or from the Cambridge Crystallographic Data Centre, 12, Union Road, Cambridge CB2 1EZ, UK; Fax: (internat.) +44-1223-336-033; E-mail: [deposit@ccdc.cam.ac.uk](mailto:deposit@ccdc.cam.ac.uk)].

#### **2.1.4.5 Acknowledgements**

This work was supported by the Ministerio Español de Ciencia e Innovación through projects CTQ2010-15364 and Molecular Nanoscience (Consolider Ingenio CSD-2007-00010).

## **2.2 Supporting Information and Unpublished Material**

Reactivity of copper(I) compounds of 1,3-tpbd towards oxygen has only been described by Creutz and co-workers in methanol.<sup>68</sup> Therefore, a closer look at the behavior in different solvents might be interesting as well as the characterization of an isoelectronic zinc(II) complex in comparison to the copper(I) species.

### **2.2.1 Reactivity of 1,3-tpbd Copper(I) Complexes Towards Dioxygen**

Although copper complexes of 1,3-tpbd are issue of several publications<sup>68-72, 74, 114</sup>, a detailed work on the reactivity has not been reported so far. Only Schindler and co-workers reported oxidation reactions of complexes using 1,3-tpbd as ligand. In methanol solution, copper(I) complexes decay to unidentified copper(II) species upon reaction



with oxygen. A ligand hydroxylation is not likely due to Schindler and co-workers could only separate 1,3-tpbd from the reaction mixture.<sup>68</sup>

Therefore, experiments concerning the reactivity of copper(I) complexes with 1,3-tpbd towards oxygen in different solvents or at lower temperatures are interesting. Unfortunately, low temperature stopped flow experiments at various temperatures with acetone solutions of  $[\text{Cu}_2(1,3\text{-tpbd})](\text{SO}_3\text{CF}_3)_2$  showed no hint for intensive charge transfer bands of possible reactive oxygen intermediates.

The use of propionitrile as coordinating solvent led to interesting UV/Vis spectra. "Bench top" experiments showed a change of color from yellow to green, when bubbling oxygen through a solution of  $[\text{Cu}_2(1,3\text{-tpbd})]^{2+}$ , as one would expect. Unexpectedly, the solution turned red after one day at room temperature. Figure 26 shows the UV/Vis spectrum of the red species measured after one day reaction time.

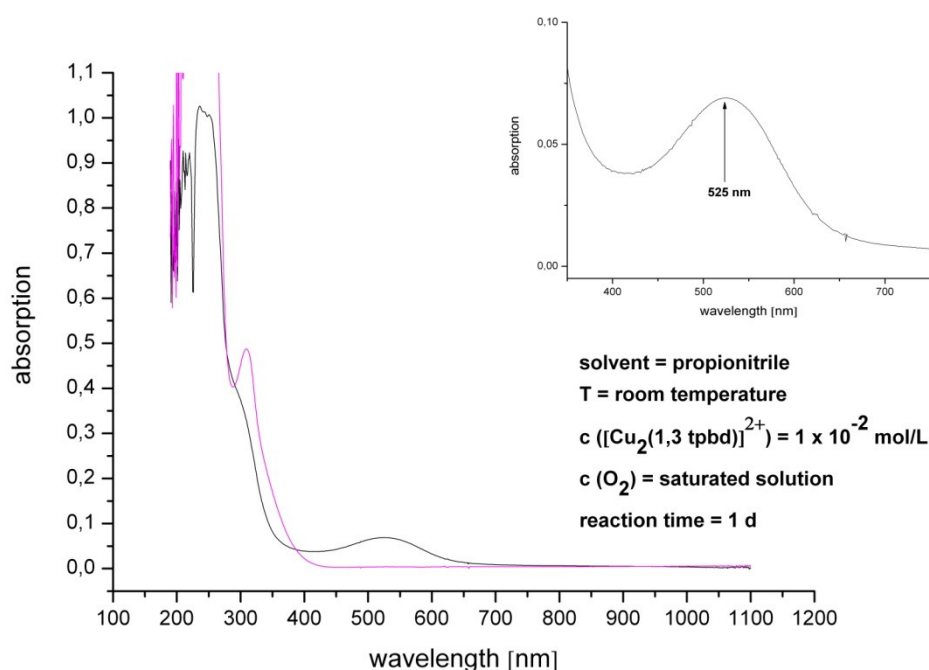


**Fig. 26** UV/Vis spectra of the copper(I) complex (magenta) and the red species (black) occurring during the reaction with dioxygen.

The expanded part of the spectrum shown in the inset of Figure 26 shows a band at 525 nm derived from the oxidation reaction. Spectra recorded earlier during the day of reaction time already showed a weak band at 525 nm proving the ongoing oxidation reaction. Although products could not be identified so far, an oxidation of the ligand is probable due to literature examples of similar reactions with bridged dinuclear copper complexes. Upon a longer period of time the solution turns brown.

Only recently, Müller *et al.* reported about conversion of nitriles to aldehydes with cobalt(II) complexes of salmdpt derivatives.<sup>115</sup> Additionally, Karlin and co-workers reported earlier about an interesting nitrile oxidation reaction using a close relative of 1,3-tpbd as ligand for a copper(I) complex.<sup>116-117</sup> Here, an interesting dicopper hydroperoxide coordination compound could be detected. Thus, experiments to detect possible reaction products deriving from the nitrile were performed. One attempt of

Müller *et al.* was to use higher nitriles as butyro- or benzonitrile to get more stable aldehydes that would have been easier to detect. Using butyronitrile as solvent led to similar reactivities as in aceto- or propionitrile resulting in a brown solution. It was possible to perform stopped flow experiments at room temperature. The gathered UV/Vis spectra are shown in Figure 27. Unfortunately, GC-MS spectra of the reaction mixture showed no hint for butyraldehyde anyway.

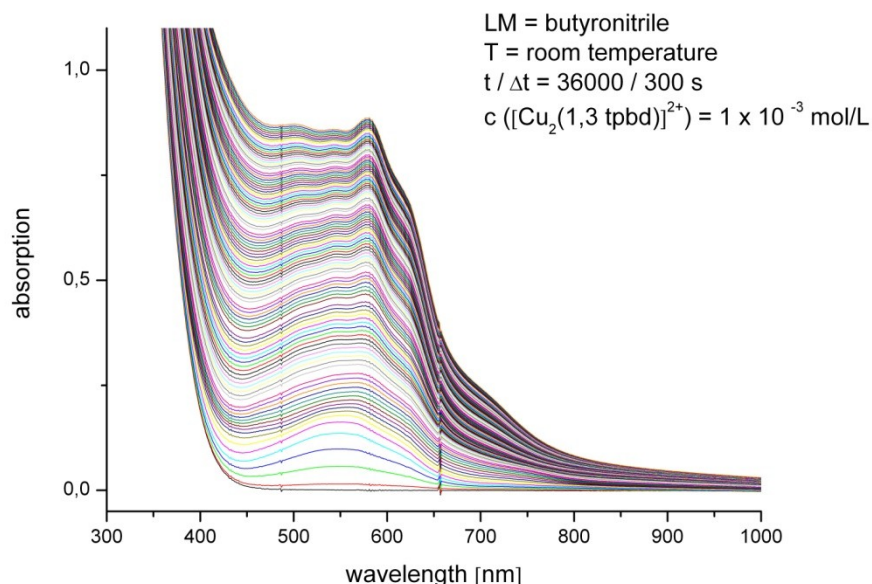


**Fig. 27** Room temperature UV/Vis spectra of the reaction of  $[\text{Cu}_2(1,3\text{-tpbd})]^{2+}$  with dioxygen in butyronitrile.

Over a period of approximately half an hour there is one dominating band at 552 nm rising that is responsible for the red color of the solution. With time the visible color more and more changes to brown obvious through the steady rising bands at 501, 542 and 581 nm respectively. Moreover, there are two shoulders at 623 and 715 nm detectable. The reaction did not cease after 10 h but continued for at least 7.5 h with rising bands at the same wavelengths leading to a deeply colored solution. Unfortunately it was not possible to assign the different bands to a specific electron transition or an active species. A comparison with the reactivity in propionitrile shows acceleration in butyronitrile and a shift of the initially formed band from 525 nm in propionitrile to 552 nm in butyronitrile. This shift is most likely explainable by the influence of the different anions used. Triflate is capable of coordinating the copper atom or forming hydrogen bridges with the oxidized product. Hexafluoroantimonate used in butyronitrile is hardly coordinating or forming hydrogen bridges. Thus, a shift may be due to the formation of bigger subunits due to the triflate anion. That would give a possible explanation for the hindrance of the reaction with oxygen, too.

The aromatic benzonitrile did not lead to a red intermediate as detected in the other nitriles. This is possibly due to the aromatic character of the nitrile or simply it is too bulky to coordinate to the metal center and interact thereby in the reaction. Thus, benzaldehyde could not be detected in the reaction mixture.

As a concluding remark it should be allowed to say, that the work concerning the reactivity of copper(I) complexes towards dioxygen using 1,3-tpbd as ligand can only be regarded as initiation for further studies. In regard of the special interest in nitrile oxidation reactions and the probable active oxygen intermediates, more detailed information about the possible ligand oxidation should be gathered.<sup>115-117</sup>

### 2.2.2 Synthesis and Characterization of a Dimeric, Hydroxido Bridged 1,3-tpbd Zinc(II) Complex

In order to avoid problems deriving from the redox chemistry of the copper(I) complexes of 1,3-tpbd copper(I) was substituted by the isoelectronic zinc(II) ion. In contrast to all the shown copper complexes, zinc complexes with the ligand 1,3-tpbd did not readily crystallize from various solvents. They exhibited a very sluggish solution behavior. One attempt at least led to the formation of crystals that were suitable to only a limited extent for single crystal X-ray crystallography.

Due to the bad crystal quality the structure refinement only lead to high R values. Therefore, crystallographic details (Table 3) as well as bond lengths and angles given in Table 4 are poorly reliable. Never the less the ORTEP drawing shown in Figure 28 is capable of showing the structure motif of the crystallized zinc(II) species.

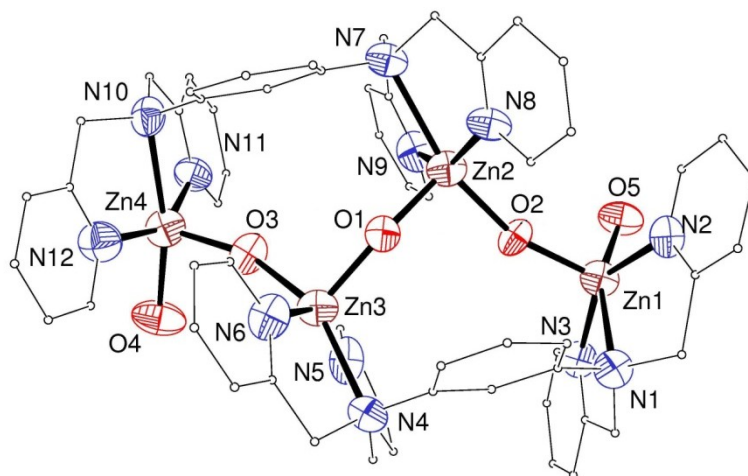


**Fig. 28** Molecular structure of  $[Zn_4(H_2O)_2(OH)_3(1,3\text{-tpbd})_2](BF_4)_5 \cdot CH_3COCH_3 \cdot xH_2O$ . Anions, hydrogen atoms and solvent molecules have been omitted for clarity. Thermal ellipsoids set to 50%.

Interestingly a dimer bridged by the three hydroxido oxygen atoms O1, O2 and O3. Each of the four zinc(II) ions are coordinated by three nitrogen atoms of one arm of the 1,3-tpbd ligand and two oxygen atoms, one of which occupying the apical position in the square pyramidal coordination sphere ( $\tau^{118} = 0.25$  (Zn1); 0.30 (Zn2); 0.20 (Zn3); 0.29 (Zn4)). The zinc(II) ions Zn1 and Zn4 are coordinated by a bridging hydroxido and a water oxygen atom that acts as “stopper”. Thus, coordination of an additional bridging hydroxido group instead of water could lead to the formation of a polymeric structure. Unfortunately none of the hydrogen atoms bond to the different oxygen atoms could be found during the structure refinement again due to the bad crystal quality. Zn-O bond

lengths are all similar and can therefore not be used as reliable criteria to differentiate between hydroxido and water ligands.

**Table 3** Crystallographic details for  $[\text{Zn}_4(\text{H}_2\text{O})_2(\text{OH})_3(1,3\text{-tpbd})_2](\text{BF}_4)_5 \cdot \text{CH}_3\text{COCH}_3 \cdot x\text{H}_2\text{O}$

Empirical Formula	$[\text{Zn}_4(\text{H}_2\text{O})_2(\text{OH})_3(1,3\text{-tpbd})_2](\text{BF}_4)_5 \cdot \text{CH}_3\text{COCH}_3 \cdot x\text{H}_2\text{O}$	$\alpha$ [°]	90.0	Reflections collected	25254
$M_r$	485.54	$\beta$ [°]	100.10(3)	Unique reflections	12815
Temperature [K]	193(2)	$\gamma$ [°]	90.0	$R_{\text{int}}$	0.1528
Radiation ( $\lambda$ [Å])	0.71073	$V$ [Å <sup>3</sup> ]	8633(3)	Data/restraints/parameters	12815/1/1038
Crystal color and shape	colorless, block	$Z$	4	Goodness-of-fit on $F^2$	0.871
Crystal size [mm]		$\rho_{\text{calc}}$ [g cm <sup>-3</sup> ]	1.401	Final $R$ indices [ $I > 2\sigma(I)$ ]	$R1 = 0.1077$
Crystal system	monoclinic	$\mu$ [mm <sup>-1</sup> ]	1.194	$R$ indices (all data)	$wR2 = 0.2629$
Space group	P21/c	$F(000)$	3676		$R1 = 0.2187$
		Scan range $\theta$ [°]	1.87 to 24.30		$wR2 = 0.3150$
$a$ [Å]	20.274(4)	Index ranges	$-23 \leq h \leq 23$	Largest diff. peak/hole [eÅ <sup>-3</sup> ]	1.645/−1.112
$b$ [Å]	24.366(5)		$-24 \leq k \leq 27$		
$c$ [Å]	17.750(4)		$-20 \leq l \leq 15$		

Thus, the only remaining hint is given by the number of  $\text{BF}_4^-$  anions in the cell. Three positive charges need to be neutralized most likely by the coordinated hydroxido groups that bridge the two monomeric units. Additionally the coordination of two zinc(II) ions should be favored using an oxygen atom bearing a negative charge.

Water and hydroxido groups derive most likely from the crystal water of the  $\text{Zn}(\text{BF}_4)_2$  salt used in the synthesis. The formation of hydroxide anions can easily be explained because zinc containing complexes are well known as weak cationic acids that are capable of deprotonizing water.<sup>119</sup>

**Table 4** Selected Bond Lengths and Angles of  $[\text{Zn}_4(\text{H}_2\text{O})_2(\text{OH})_3(1,3\text{-tpbd})_2](\text{BF}_4)_5 \cdot \text{CH}_3\text{COCH}_3 \cdot x\text{H}_2\text{O}$  [Å, °]

Atoms		Atoms		Atoms	
Zn(1)-N(1)	2.404(12)	Zn(2)-O(2)	1.971(8)	Zn(4)-O(3)	1.946(8)
Zn(1)-N(2)	2.026(11)	Zn(3)-N(4)	2.439(12)	Zn(4)-O(4)	2.079(11)
Zn(1)-N(3)	2.024(12)	Zn(3)-N(5)	2.041(11)	N(1)-Zn(1)-N(2)	77.5(5)
Zn(1)-O(2)	1.936(7)	Zn(3)-N(6)	2.013(11)	N(1)-Zn(1)-N(3)	78.2(4)
Zn(1)-O(5)	2.038(9)	Zn(3)-O(1)	1.931(9)	N(1)-Zn(1)-O(2)	102.4(4)
Zn(2)-N(7)	2.441(12)	Zn(3)-O(3)	1.961(8)	N(1)-Zn(1)-O(5)	159.4(4)
Zn(2)-N(8)	2.017(10)	Zn(4)-N(10)	2.373(12)	N(2)-Zn(1)-N(3)	144.3(5)
Zn(2)-N(9)	2.036(11)	Zn(4)-N(11)	2.038(12)	N(2)-Zn(1)-O(2)	102.0(4)
Zn(2)-O(1)	1.939(9)	Zn(4)-N(12)	2.023(12)	N(2)-Zn(1)-O(5)	96.5(4)
N(3)-Zn(1)-O(2)	108.4(4)	N(9)-Zn(2)-O(2)	98.0(4)	O(1)-Zn(3)-O(3)	96.3(4)
N(3)-Zn(1)-O(5)	97.2(4)	O(1)-Zn(2)-O(2)	94.4(4)	N(10)-Zn(4)-N(11)	78.5(5)
O(2)-Zn(1)-O(5)	98.2(4)	N(4)-Zn(3)-N(5)	76.9(4)	N(10)-Zn(4)-N(12)	76.8(5)
N(7)-Zn(2)-N(8)	76.4(4)	N(4)-Zn(3)-N(6)	76.2(5)	N(10)-Zn(4)-O(3)	101.8(4)
N(7)-Zn(2)-N(9)	76.8(4)	N(4)-Zn(3)-O(1)	108.1(4)	N(10)-Zn(4)-O(4)	165.9(4)
N(7)-Zn(2)-O(1)	103.4(4)	N(4)-Zn(3)-O(3)	155.6(4)	N(11)-Zn(4)-N(12)	148.7(6)
N(7)-Zn(2)-O(2)	162.2(4)	N(5)-Zn(3)-N(6)	143.4(6)	N(11)-Zn(4)-O(3)	105.9(4)
N(8)-Zn(2)-N(9)	144.4(5)	N(5)-Zn(3)-O(1)	107.6(4)	N(11)-Zn(4)-O(4)	97.9(5)
N(8)-Zn(2)-O(1)	101.6(4)	N(5)-Zn(3)-O(3)	96.5(4)	N(12)-Zn(4)-O(3)	97.7(4)
N(8)-Zn(2)-O(2)	100.4(4)	N(6)-Zn(3)-O(1)	104.0(4)	N(12)-Zn(4)-O(4)	101.4(5)
N(9)-Zn(2)-O(1)	107.1(4)	N(6)-Zn(3)-O(3)	97.9(4)	O(3)-Zn(4)-O(4)	92.3(4)

## 2.2.3 Experimental Section

Solvents were of *p.a.* grade and used as commercially available. For the copper(I) chemistry solvents of extra dry quality were used and distilled under inert atmosphere prior to use. Propionitrile was purified according to a literature procedure.<sup>120</sup> The ligand 1,3-tpbd was synthesized according to a published procedure and recrystallized from

acetone prior to use.<sup>68</sup> O<sub>2</sub> saturated solutions for the stopped-flow measurements were prepared by bubbling O<sub>2</sub> for 10 min through the extra dry solvent.

**Caution!** *The syntheses and procedures described below involve compounds that contain perchlorate ions, which can detonate explosively and without warning. Although we have not encountered any problems with the compounds used in this study, they should be handled with extreme caution.*

Room temperature UV/Vis experiments were performed using an Agilent 8453 spectrophotometer using the UV/Vis Chemstation program (Agilent) for collecting and processing of data. Low temperature stopped-flow spectra were recorded on a Hightec Scientific SF-61SX2 stopped-flow system. Data were collected and processed with the Kinetic Studio (1.12) program by TgK Scientific.

Single crystal X-ray structure determination in chapter 2.2 was performed using a STOE IPDS equipped with a low temperature unit built by Karlsruher Glastechnisches Werk. Data was processed using the implemented STOE software and structures were solved and refined with the ShelX 97 program package.<sup>113</sup> Crystals were covered with perfluoropolyether and mounted on a glass fiber.

### 2.2.3.1 *Synthesis of [Zn<sub>4</sub>(H<sub>2</sub>O)<sub>2</sub>(OH)<sub>3</sub>(1,3-tpbd)<sub>2</sub>](BF<sub>4</sub>)<sub>5</sub>·CH<sub>3</sub>COCH<sub>3</sub>·xH<sub>2</sub>O*

To an acetone solution (2 mL) of 1,3-tpbd (50 mg, 1.1×10<sup>-4</sup> mol), Zn(BF<sub>4</sub>)<sub>2</sub>·H<sub>2</sub>O (55 mg, 2.1×10<sup>-4</sup> mol) solved in 2 mL acetone was added dropwise. After several days of slow ether diffusion at -30 °C colorless block shaped crystals suitable for single crystal X-ray determination formed.

### 2.2.3.2 *“Benchtop” UV/Vis Experiments*

#### 2.2.3.2.1 *Solution of [Cu<sub>2</sub>(1,3-tpbd)](SO<sub>3</sub>CF<sub>3</sub>)<sub>2</sub>*

To a solution of 1,3-tpbd (50 mg, 1.1×10<sup>-4</sup> mol) in propionitrile (5 mL) was added [Cu(CH<sub>3</sub>CN)<sub>4</sub>]SO<sub>3</sub>CF<sub>3</sub> (176 mg, 2.1×10<sup>-4</sup> mol) in propionitrile (5 mL) dropwise under inert conditions. The resulting solution was reacted with oxygen, bubbled through at -80 °C. The solution was allowed to warm to room temperature. After one day the yellow solution turned red.

#### 2.2.3.2.2 *Solution of [Cu<sub>2</sub>(1,3-tpbd)](SbF<sub>6</sub>)<sub>2</sub>*

[Cu(CH<sub>3</sub>CN)<sub>4</sub>]SbF<sub>6</sub> (12 mg, 3×10<sup>-5</sup> mol) was dissolved in Butyronitrile (25 mL) and 1,3-tpbd (6 mg, 1×10<sup>-5</sup> mol) was added to the solution. Oxygen was bubbled through the yellow solution for 5 min. After one day the solution had turned brown.

**2.2.3.2.3      *Solution of  $[\text{Cu}_2(1,3\text{-tpbd})]^{2+}$  and  $\text{Cl}^-$*** 

1,3-tpbd (5 mg,  $1 \times 10^{-5}$  mol) and CuCl (2 mg,  $2 \times 10^{-5}$  mol) were dissolved in propionitrile (1.5 mL). The yellow solution was diluted with propionitrile and oxygen was bubbled through. The resulting green solution turned brown-red after one day.

**2.2.3.3      *Preparation of Copper(I) Solutions for Low Temperature Stopped-Flow experiments*****2.2.3.3.1      *Solution of  $[\text{Cu}_2(1,3\text{-tpbd})](\text{SbF}_6)_2$*** 

To an acetone solution of 1,3-tpbd (6 mg,  $1 \times 10^{-5}$  mol)  $[\text{Cu}(\text{CH}_3\text{CN})_4]\text{SO}_3\text{CF}_3$  (9 mg,  $3 \times 10^{-5}$  mol) was added under inert conditions. The resulting yellow solution was diluted under inert conditions to a complex concentration of  $2 \times 10^{-4}$  mol/L. UV/Vis spectra were recorded after the mixture with oxygen saturated acetone solution (1:1 ratio) at various temperatures.

### 3 Functionalized Unspenp Derivatives

#### 3.1 Introduction

In a different approach to synthesize bridging ligands similar to 1,3-tpbd (see chapter 2) we obtained the xylyl bridged unspenp derivatives *N'*-1-{3-[2-bis(2-pyridylmethyl)aminoethyliminomethyl]phenyl}methyliden-*N,N*-bis(2-pyridylmethyl)-1,2-ethanediamine (**Imxyl-unspenp**), *N'*-{3-[2-bis(2-pyridylmethyl)aminoethylaminomethyl]benzyl}methyliden-*N,N*-bis(2-pyridylmethyl)-1,2-ethanediamine (**Hxyl-unspenp**) and *N'*-{3-[2-bis(2-pyridylmethyl)aminoethyl(methyl)aminomethyl]benzyl}methyliden-*N,N*-bis(2-pyridylmethyl)-1,2-ethanediamine (**Me<sub>2</sub>xyl unspenp**) (Figure 29). Here, each of the bispicolylamine units bears an additional ethylamine residue resulting in a tripodale ligand.<sup>121-122</sup> The synthesis of the ligands is well known,<sup>122-124</sup> but until today only one copper(I) complex could be structurally characterized.<sup>123</sup>

This type of bridged bispicolylamine units can be used successfully for to provide a ligand environment that affords space for two metal ions. Thus, studies on the reactivity towards dioxygen of the dinuclear copper(I) compounds are interesting with regard to the extraordinary properties of the parent mononuclear amine *tris*-(2-methylpyridyl)amine.<sup>23</sup> Additionally, the zinc(II) complexes and the heterometallic species are of special interest, due to the extraordinary superoxide reducing capabilities of human Cu/Zn SOD bearing a heterobimetallic active core.<sup>12-13</sup>

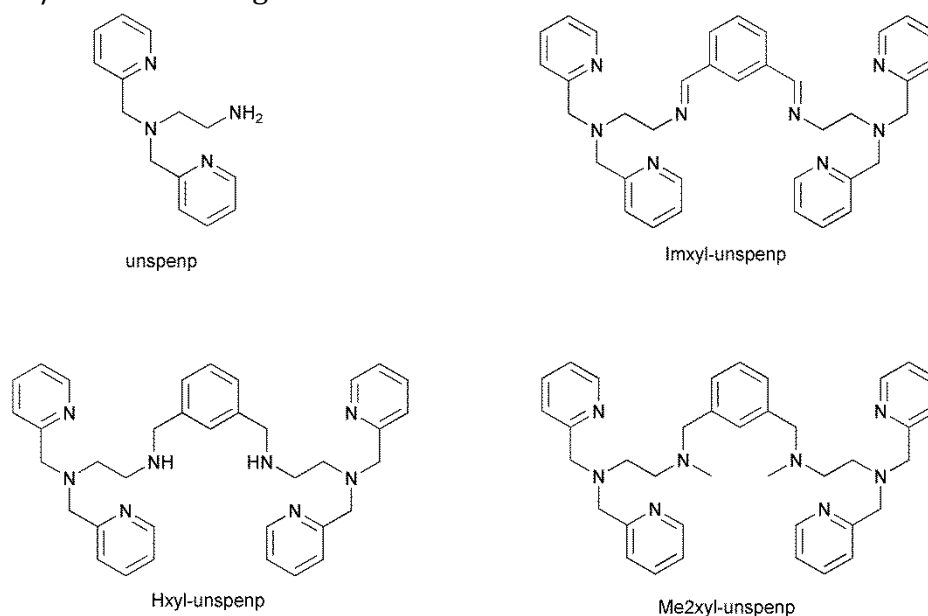


**Fig. 29** Xylyl bridged unspenp derivatives related to 1,3-tpbd.

Derivatisation of unspenp is a versatile instrument to combine the excellent tripodal binding site for copper or zinc ions with other functionalities such as extended  $\pi$ -systems for example. From various examples it is known, that anthracene can be easily derivatised with bispic as binding site for zinc. The zinc(II) complexes of these ligands

are known to exhibit fluorescent phosphate sensing capabilities.<sup>39, 125</sup> Hence, the condensation reaction of unspenp with anthracenecarboxaldehyde to form the imine bond was performed earlier in order to synthesize and characterize zinc(II) complexes and especially study their emission behavior.<sup>126</sup> Figure 30 depicts the structures of the formed *N'*-(9-anthracenylmethylene)-*N,N*-bis(2-pyridylmethyl)-1,2-ethanediamine (**Imant-unspenp**) and the related *N'*-(9-anthracenylmethyl)-*N,N*-bis(2-pyridylmethyl)-1,2-ethanediamine (**Hant-unspenp**) derived from a simple reduction with borohydride.

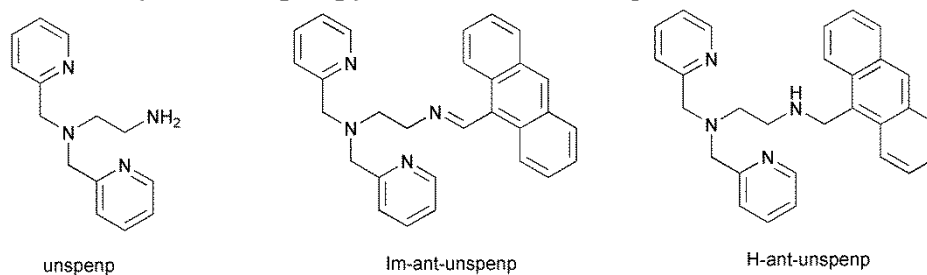


**Fig. 30** Structures of **Imant-unspenp** and **Hant-unspenp** and the parent **unspenp** ligand.

The molecular structure of a zinc(II) complex using **Imant-unspenp** as a ligand could be reported (Figure 31). The single crystals derived from a solution of **Imant-unspenp**, stoichiometric amount of zinc(II)chloride and dichloroethane as solvent. An *in situ* formed  $[\text{ZnCl}_4]^{2-}$  molecule serves as anion and eight solvent molecules are located in the smallest independent unit. The trigonal-bipyramidal coordination around the zinc(II) ion is not affected by the fluorophore group.<sup>126</sup>

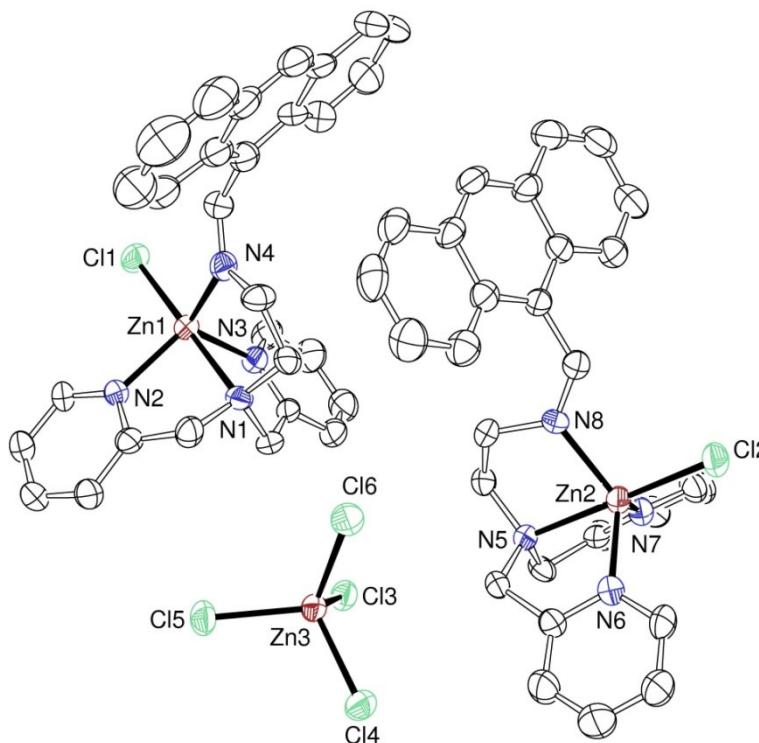


**Fig. 31** Structure of  $[\text{Zn}(\text{Imant-unspenp})\text{Cl}]_2[\text{ZnCl}_4] \cdot 8\text{C}_2\text{H}_4\text{Cl}_2$ . Solvent molecules and hydrogen atoms omitted for clarity. Thermal ellipsoids set to 50% probability.

Due to the lability of the imine bond, it remains unclear, which species is present in solution. Therefore, emission studies were not performed until today. The emission



behavior of **Hant-unspenp** has neither been studied in detail but simple emission spectra showed an enhancement of the emission intensity upon addition of zinc. Further addition of hydrogenphosphate anions led to a lowered intensity. A significant shift of the emission maxima at 392 nm, 411 nm and 432 nm, generated by the fluorophore anthracene residue, could not be observed. The enhanced emission intensity is most likely explainable by the inhibition of the PET process (see chapter 1.3) upon complexation of zinc(II). The addition of hydrogenphosphate, that most likely leads to a conformational change and serves as electron donating group, then again promotes the PET process and causes a lowered intensity.<sup>126</sup>

Until today no copper complexes of the ligands **Hant-unspenp** and **ant-im-unspenp** are known. Unfortunately, all attempts to obtain single crystals of a copper(I) or copper(II) species remained unsuccessful so far. Recently, photocatalysis using transition metal complexes has attracted a great deal of attention due to the offered possibilities with regard to reactions under mild conditions ("green chemistry") or the production of hydrogen by watersplitting.<sup>127-130</sup> Basic investigation on this field of research is therefore of growing importance. The implementation of photosensitizing groups (e.g. anthracene as shown in Figure 30) to the ligand **unspenp** is one attempt to influence the reactions of related copper(I) complexes towards dioxygen. This chapter provides first results with the copper(I) complexes of the already known ligands **Imant-unspenp** and **Hant-unspenp**.

## 3.2 Results and Discussion

In order to detect reactive intermediates during the reaction of the copper(I) complexes towards dioxygen, low temperature stopped-flow experiments were performed. Studies on the reactivity of the copper(I) complex of **unspenp** towards dioxygen were reported earlier by Schatz *et al.*<sup>131</sup> A copper(I) species that had been structurally characterized as dimer in the solid, led to the formation of a copper superoxido intermediate followed by a peroxido species. The rate constants were strongly influenced by the used solvents (acetone, propionitrile). Additional reactions occurred most likely due to the dimeric nature of the compound that prevented a full kinetic analysis. In the case of the parent ligand **unspenp**, methylation of the aliphatic amine led to **Me<sub>2</sub>unspenp** which enabled a full kinetic analysis of the reaction towards dioxygen and to a stabilized peroxido species.<sup>132-133</sup>

### 3.2.1 Reactivity of Copper(I) Complexes Using Ant-unspenp Ligands Towards Dioxygen

Following the strategy of Schatz *et al.*<sup>131</sup> methylation of the ligand **Hant-unspenp** (see Figure 30) most likely enables kinetic analysis of the reactivity of the copper(I) complex towards dioxygen. Unfortunately, the pure methylated **ant-unspenp** ligand could not be synthesized so far. Therefore, the problems that arise by the lability of the imine bond of **Imant-unspenp** and the presence of protons in **Hant-unspenp** were inevitable for the

UV/Vis measurements. Nevertheless, Figure 32 depicts the obtained low temperature stopped-flow spectra of the copper(I) complexes of **Hant-unspenp**.

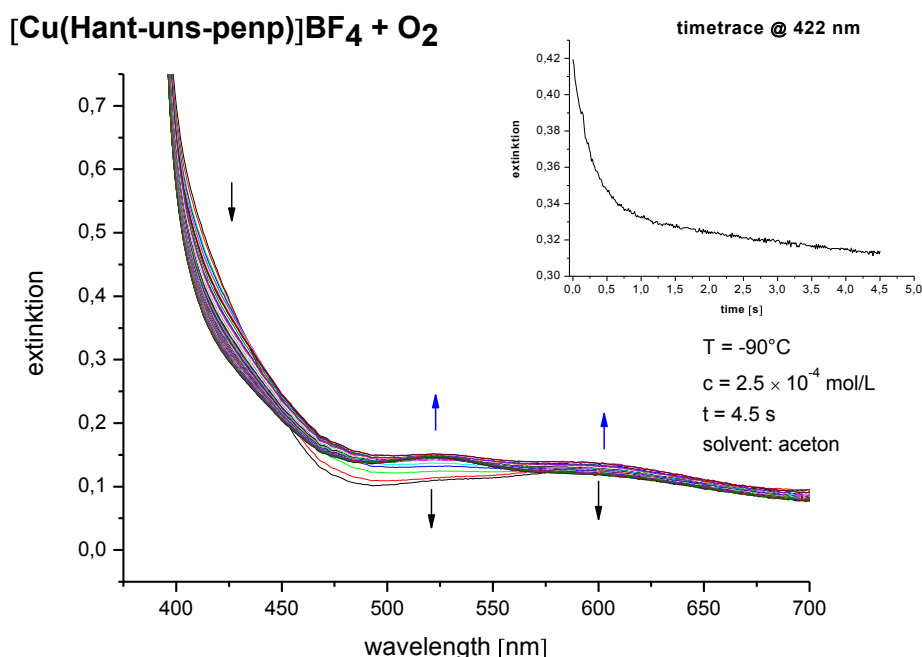


**Fig. 32** Low temperature UV/Vis spectra of the reaction of  $[\text{Cu}(\text{Hant-unspenp})]^+$  with dioxygen in acetone solution. Inset: Timetrace of the assumed superoxido shoulder at 422 nm.

In addition to the problems arising from the labile nature of the ligands itself, upon addition of oxygen always an unidentified precipitate formed even at very low concentrations that prevented detailed kinetic studies. Thus, the imine could not be measured.

Below 400 nm the very intensive bands deriving from the anthracene residue are visible in the spectra and overlay the band at 422 nm, assumed to be a superoxido charge transfer band that is only detectable as a shoulder. The inset of Figure 32 depicts a timetrace at 422 nm over a period of 4.5 s. At the given temperature of  $-90^\circ\text{C}$  the superoxido species is decaying fast and identification is not possible after this period. Compared to the spectra of the copper(I) superoxido species using unspenp as a ligand, the weaker bands at higher wavelength that are visible in the first few spectra, support the assumption of an initially formed superoxido complex with a very short lifetime.<sup>131</sup>

In Figure 33, an enlarged section of Figure 32 that concentrates on the bands at 524 nm and the broad one around 600 nm is depicted. These bands are assigned to the charge transfer bands of a formed peroxido species. The inset of Figure 33 depicts the timetrace at 524 nm showing a fast formation, followed by a period of approximately 1.5 s of non-distinctive behavior and a very slow decay afterwards. Normally, charge transfer bands are very intense. Therefore, a very low concentration of peroxido species in solution can be assumed.

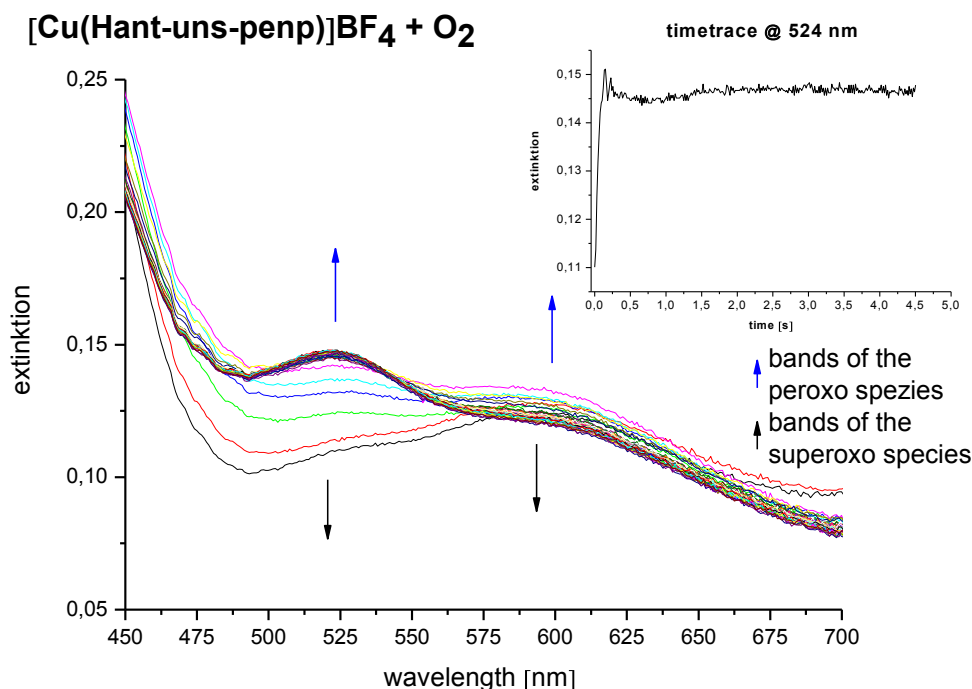


**Fig. 33** Section of Fig. 32 Inset: Timetrace at 524 nm of the assumed peroxido band.

From the results of the studies using unspenp as a ligand it is known that hydrogen atoms of the aliphatic amine most likely lead to side reactions. Additionally, possible products of an oxidation reaction could not be identified yet. Hence, a statement about the reaction pathway is hardly drawable. The first two steps, the initially formed superoxido complex followed by a  $\mu$ -1,2 peroxido species, are reasonable from the results of the UV/Vis spectra but the further progress of the reaction remains unclear. Figure 34 depicts drawings of the assumed species.

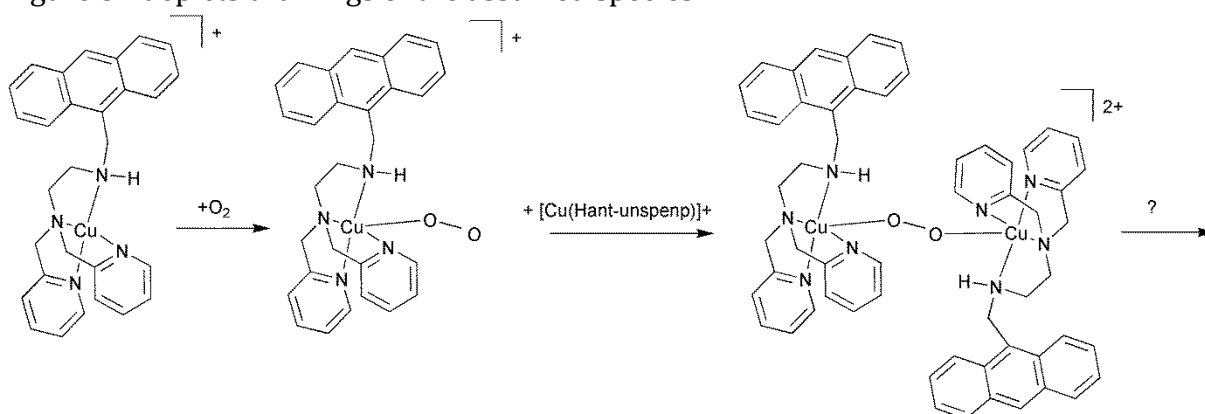


**Fig. 34** Assumed structures of the superoxido and peroxido species most likely occurring during the reaction of  $[\text{Cu}(\text{Hant-uns-pen})]^+$  with oxygen.

Abstraction of the hydrogen atom at the aliphatic amine function possibly leads to the formation of dihydrogenperoxide that is capable of further oxidation reactions, for example the formation of acetone peroxide. This remains highly speculative but could explain the formation of a precipitate during the reaction.

At  $-90\text{ }^{\circ}\text{C}$  the decay of the peroxido species is very slow. After 450 s the intensities of the assigned bands are only very slightly lowered. At  $-35\text{ }^{\circ}\text{C}$  still weak peroxido bands are visible, that are overlaid during 450 s by a broad starting around 600 nm, typical for copper(II) dd transfers. An indefinite decay of the peroxido species is therefore the only assumption that is possible from these initial results of the study.

### 3.2.2 Reactivity of Copper(I) Complexes of Bridged Unspenp Derivatives Towards Dioxygen

Copper(I) salts react readily with all three ligands (**Imxyl-unspenp**, **Hxyl-unspenp**, **Me<sub>2</sub>xyl-unspenp**, see Figure 29) in various solvents to form yellow complexes under inert conditions. The copper(I) complexes of unspenp and closely related amines like tmpa, Me<sub>2</sub>unspenp, Me<sub>4</sub>apme or Me<sub>6</sub>tren are known to form end on superoxide and  $\mu$ -peroxido oxygen species, that can be identified by the intensive charge transfer bands caused by the coordination of oxygen in the region of visible light.<sup>22</sup>

In order to examine the reactivity of the copper(I) complexes with the bridged ligands and to determine the active oxygen species, low temperature stopped flow experiments were performed. Only recently, Garcia-Bosch *et al.* reported about a  $\mu$ -peroxido species of **Imxyl-unspenp** and its oxidizing capability towards selected substrates.<sup>123</sup> The low temperature stopped flow experiments (see Figure 35) with the copper(I) complex of **Imxyl-unspenp** showed the typical bands for this oxygen species and affirmed their results. Unlike complexes with the related amines of the tmpa family and even at very low temperatures around  $-90\text{ }^{\circ}\text{C}$ , a formation of a superoxido intermediate could not be observed.

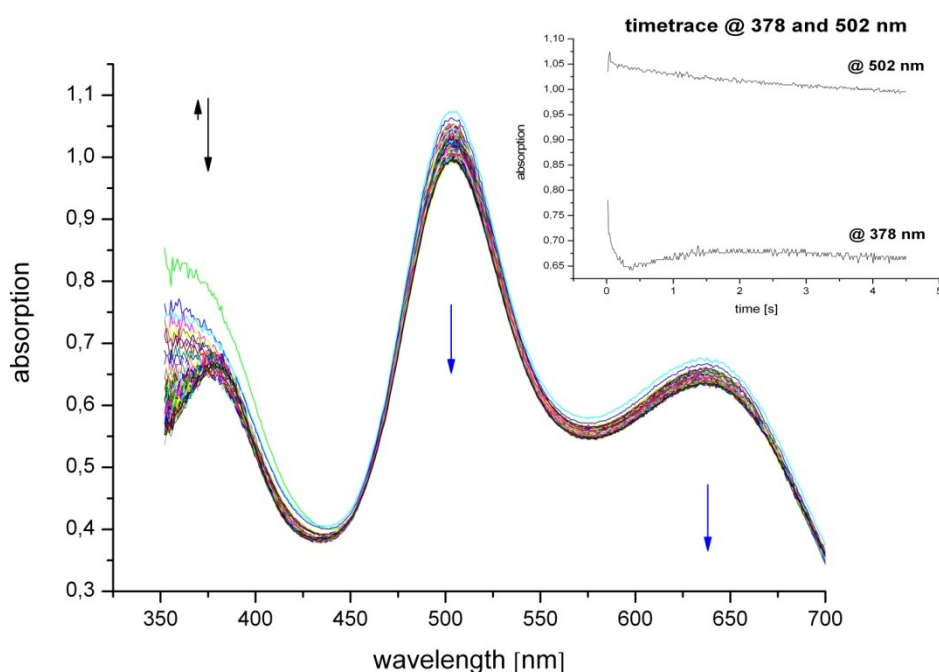


**Fig. 35** UV/Vis spectra and timetraces of the reaction of  $[\text{Cu}_2\text{Imxyl-unspenp}]^{2+}$  with oxygen in propionitrile at  $T = -90\text{ }^{\circ}\text{C}$  ( $t = 4.5\text{ s}$ ;  $c(\text{O}_2) = \text{saturated solution}$ ;  $c([\text{Cu}_2\text{ImXyl-unspenp}]\text{ClO}_4) = 5 \times 10^{-4}\text{ mol/L}$ ).

Unfortunately, the complexes were badly soluble after the oxidation reaction. Thus, a kinetic analysis of the gained UV/Vis spectra was not possible and activation parameters could not be determined. Nevertheless, a comparison of the observed bands during the reaction with dioxygen with the ones characteristic for specific oxygen intermediates provided information on the possible reaction pathway. As expected, the  $\mu$ -peroxido complex is formed very rapidly even at very low temperatures. This is most likely due to the second intramolecular copper(I) atom that leads to a fast monomolecular reaction once a superoxido complex is formed. In consequence, neither the formation nor the decay of a possible end-on superoxido complex is observable.

A closer look at the band at 378 nm that most likely derives from ligand-centered imine transitions, reveals a rapid decay followed by a period of approximately one second where an increasing absorption is observable. After a reaction time of 1.5 to 2 seconds the absorption is again decreasing slowly. Unfortunately, no explanation for this phenomenon can doubtlessly be provided since there is more than one rational possibility. One of which is a rapid decay of the imine followed by a formation of a side-on bis- $\mu$ -peroxido deriving from the initially formed end-on- $\mu$ -peroxido complex. These two species are known to exist in an equilibrium. Both are decaying slowly to so far unknown products. Ligand hydroxylation at the Xylyl-bridge or the cleavage of the aliphatic amine bond are the most likely pathways for oxidation reactions. A similar hydroxylation is known from an 1,3-tpbd derivative.<sup>68</sup>

An underlying, intensive charge transfer band of a small amount of formed superoxido complex is also not completely deniable, but compared to the spectra of other superoxido species of similar coordination compounds or the ones of the copper(I) complex **Hxyl-unspenp** the superoxido band should be redshifted (compare Figure 36). Here, only educated guesses can be made concerning the detailed reaction pathway, due to the missing kinetic analysis. The rapid formation of an end-on- $\mu$ -peroxido complex stable for more than 250 seconds at  $-90\text{ }^{\circ}\text{C}$  in propionitrile is the only conclusion of the stopped flow spectra that can be proved. Until today neither oxidized ligand nor other possible oxidation products of the reaction could be isolated and characterized.

In contrast to these findings the reaction of the copper(I) complex of **Hxyl-unspenp** as ligand with oxygen is comparable to the properties of the related amines of the tmpa family. The depicted spectra in Figure 36 reveal charge transfer bands of both end-on superoxido and  $\mu$ -peroxido species as reactive intermediates. A kinetic analysis was again impossible due to the bad solubility of the oxidation products leading to a cloudy solution, making an observation over a longer time period or in a broad temperature range impossible. From a comparison of the timetraces of the complexes bearing only one copper(I) atom and that of the copper(I) atom of **Hxyl-unspenp** it is obvious that the reaction rates for the formation and the decay of both superoxido and peroxido species are faster for the complex bearing two metal atoms. This is again most likely due to the acceleration of the reaction by the change between bi- and monomolecular reaction type minimizing the effects of solvent molecules.

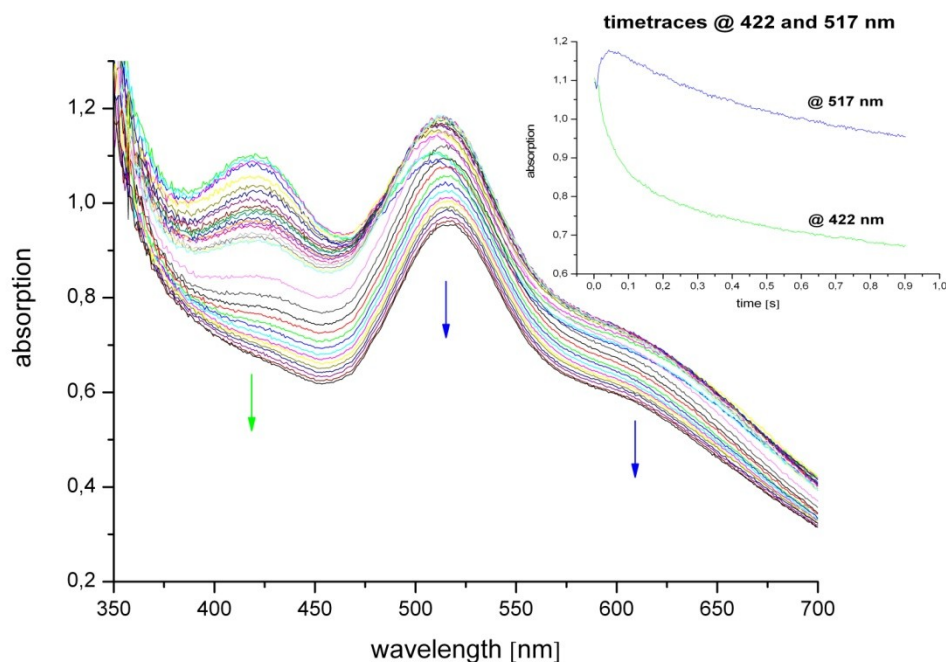


**Fig. 36** UV/Vis spectra and timetraces of the reaction of  $[\text{Cu}_2\text{Hxyl-unspenp}]^{2+}$  with oxygen in propionitrile at  $T = -93\text{ }^\circ\text{C}$  ( $t = 0.9\text{ s}$ ;  $c(\text{O}_2) = \text{saturated solution}$ ;  $c([\text{Cu}_2\text{Hxyl-unspenp}]\text{SbF}_6) = 5 \times 10^{-4}\text{ mol/L}$ ).

The decreasing band at 422 most likely derives from an intensive charge transfer transition of an end-on superoxido complex already known from the tmpa derivatives.<sup>22</sup> The formation is too fast, to observe even at  $-93\text{ }^\circ\text{C}$ , while the formation of the  $\mu$ -peroxido species is detectable at least in the very first spectra of the stopped-flow experiment forming strong charge transfer bands at 517 and 602 nm, respectively. Both species are very reactive and decay rapidly, over a period of only some seconds. The comparison of these spectra with the related data for the related monomolecular species leads to the postulation of a possible reaction pathway shown in Figure 37. It follows the well known mechanism for the mononuclear complexes.<sup>134-135</sup> Due to the excess amount of solvated oxygen in the saturated propionitrile, a pseudo first order reaction leads to the formation of the very reactive superoxido species. The initially formed intermediate reacts intramolecular with the second copper(I) atom most likely in a first order reaction leading to the formation of a more stable end-on  $\mu$ -peroxido species. Their slow decay leads to so far unknown products. Side reactions, involving the direct decay of the superoxido complex are plausible.<sup>18</sup>

A concerted reaction of both copper(I) atoms with the oxygen molecule leading directly to the end-on  $\mu$ -peroxido species is not impossible but improbable due to the result already published for the comparable monomolecular copper(I) complexes.<sup>22, 131</sup> To the best of our knowledge, the formation of the end-on superoxido complex is the initial step during the reaction of comparable copper(I) complexes with oxygen. Using these bridged ligands most likely only accelerates the formation of the  $\mu$ -peroxido complex, making lower temperatures or faster spectroscopy necessary to observe the superoxido complex.

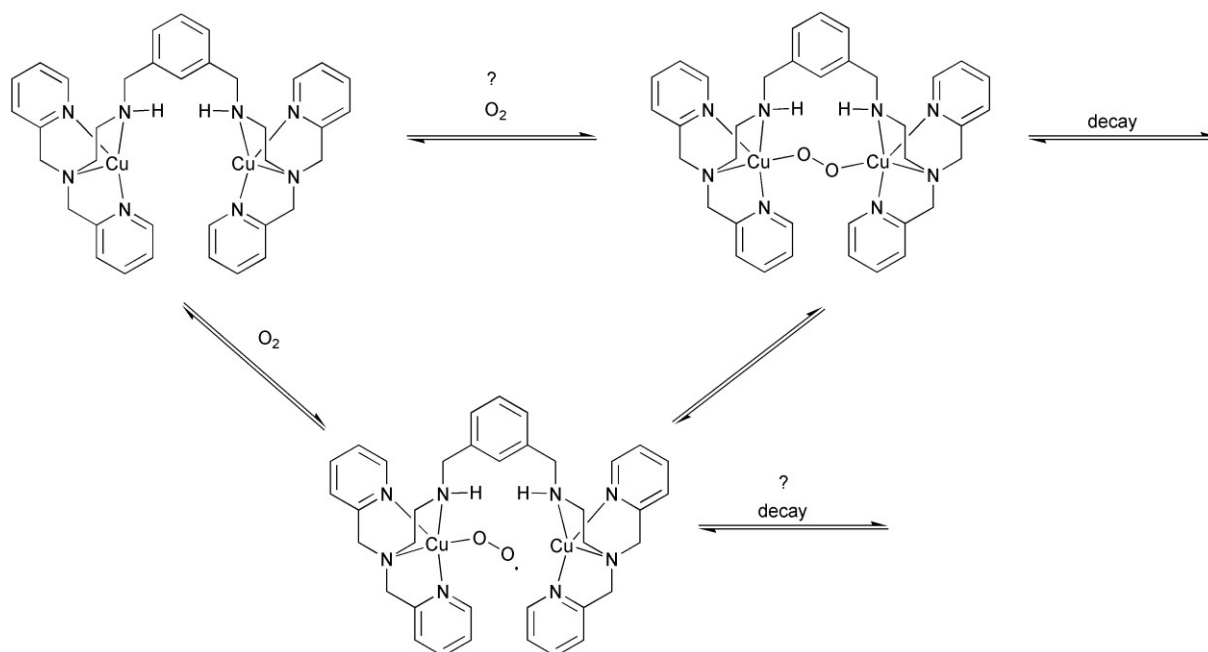


**Fig. 37** Proposed mechanism for the reaction of **Hxyl-unspenp** with oxygen following the reaction pathway published earlier.<sup>131</sup>

From the comparison of the different timetraces (see insets of Figures 35 and 36) it is obvious that the peroxido adduct of Imxyl-unspenp is more stable than the Hxyl-unspenp adduct, possibly due to the existence of an equilibrium between end-on and side-on bound peroxido species.

### 3.2.2.1 Synthesis and Characterization of a Carbonate Bridged Copper(II) Dimer

The copper(II) complex shown in Figure 38 derived from a solution containing copper(I) and hexafluoroantimony ions. The solution was oxidized with dioxygen and allowed to stand several days. Unexpectedly a carbonato bridged copper(II) complex formed, that could be determined by single crystal X-ray crystallography. Unfortunately the single crystals were of minor quality resulting in high R-values. Thus, the structure could not be solved properly. Nevertheless, the structure motive was determinable and is obvious from Figure 38.

Although the position of some of the carbon atoms of the ligand was not refinable, the carbonato bridges between the copper atoms are clearly recognizable. During the synthesis of the complex no carbonate was added. Therefore, the coordinated carbonate is most likely the reaction product of an reaction of carbon dioxide from air activated by the copper(I) complex and dioxygen or *vice versa*. Copper and zinc complexes are known for stoichiometric transition of carbon dioxide into carbonate.<sup>136-137</sup> There are many examples for coordinated bridging carbonates, but the conversion of carbon dioxide from air into carbonate is rather rare.<sup>138</sup> Due to the great interest of utilizing carbon dioxide from air as carbon source for chemical processes, knowledge about fixation and oxidation of carbon dioxide is essential. Copper complexes that are capable of catalyzing such reactions are therefore promising study objects.<sup>139</sup>

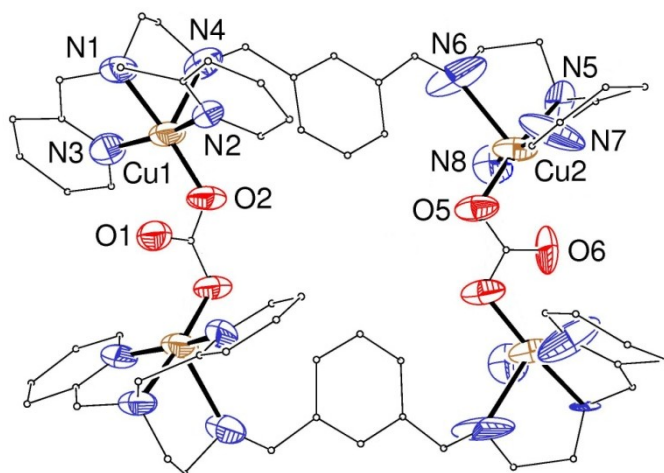


**Fig. 38** Fragments of the molecular structure of the cation  $[\text{Cu}_4(\text{CO}_3)_2(\text{Hxyl-unspenp})_2]^{4+}$ . Hydrogen atoms have been omitted for clarity. Thermal ellipsoids set to 50 %.

Only recently Angamuthu *et al.* reported the activation of carbon dioxide from air by a similar copper(I) complex containing two bridged dipicolyl subunits as ligand.<sup>17</sup> Even a catalytic cycle recovering the active copper(I) species electrochemically could be demonstrated (see chapter 1.2.2).

Although the presented structure is not more than a first hint for the carbon dioxide activating capability of  $[\text{Cu}_2(\text{Hxyl-unspenp})](\text{SbF}_6)_2$ , it should serve as initiator for further studies concerning this topic.

### 3.3 Conclusions

To draw a conclusion, it was unfortunately not possible to clarify the reaction pathway of the reaction of the copper(I) complexes using anthracenyl ligands towards dioxygen. Nevertheless, the formation of a superoxido and a peroxido species could successfully be observed in the UV/Vis spectra at very low temperatures.

There are still many open questions: Why is the equilibrium concentration of the formed intermediates that low? How does the peroxido species decompose? Does the complex catalyze oxidation reactions? These questions have to be solved in further studies initialized during this work. Additionally, studying the influence of light on the reactions still remains a challenging but very interesting aim.

In terms of the xylyl bridged unspenp imine studies on the reactivity towards dioxygen resulted in the approval of data published most recently by Garcia-Bosch *et al.* As expected only a  $\mu$ -peroxido compound could be observed even at low temperatures. In contrast the copper(I) complex of the related amine formed most likely an observable superoxido species.

Unexpectedly, the copper(II) complex formed a bis- $\mu$ -carbonato dimer most likely deriving from carbon dioxide from air.



### 3.4 Experimental Section

Ligands unspenp, ant-im-unspenp and Hant-unspenp were synthesized according to literature procedures.<sup>126, 131</sup> The synthesis for Ligands Imxyl-unspenp and Hxyl-unspenp has been recently published.<sup>123-124</sup> Here a slightly modified procedure published earlier by Würtele *et al.* was applied.<sup>122</sup> Solvents were of p.a. grade and used without further purification as commercially available. Water-free copper(I) salts with weakly coordinating anions were synthesized following a well-known procedure.<sup>140</sup>

**Caution!** *The syntheses and procedures described below involve compounds that contain perchlorate ions, which can detonate explosively and without warning. Although we have not encountered any problems with the compounds used in this study, they should be handled with extreme caution.*

Single crystal X-ray structure determination in chapter 3 was performed using a STOE IPDS equipped with a low temperature unit built by Karlsruher Glastechnisches Werk. Data was processed using the implemented STOE software and structures were solved and refined with the ShelX 97 program package.<sup>113</sup> Crystals were covered with perfluoropolyether and mounted on a glass fiber.

#### 3.4.1 Low Temperature Stopped Flow Measurements

For the copper(I) chemistry, solvents of extra dry quality were used and distilled under inert atmosphere prior to use. Propionitrile was purified according to a literature procedure.<sup>120</sup> Low temperature stopped-flow spectra were recorded on a Hi Tech Scientific system using kinetic studio program for data processing. Dioxygen saturated solutions were prepared by bubbling dioxygen (grade 5.5) through the solvent for 10 min.

##### 3.4.1.1 *X-ant Unspenp Solutions*

The copper(I) solutions for the low temperature stopped flow experiments were prepared by mixing stoichiometric amounts of ligand  $[\text{Cu}(\text{CH}_3\text{CN})_4]\text{BF}_4$  presolved in acetone and filled up to 25 mL to yield a  $5 \times 10^{-4}$  mol/L acetone solution. In the cuvette, the complex solution was mixed with dioxygen saturated acetone solution.

##### 3.4.1.2 *$[\text{Cu}_2(\text{Imxyl-unspenp})]^{2+}$ Solution*

**Imxyl-unspenp** (15 mg,  $2.5 \times 10^{-5}$  mol) and  $[\text{Cu}(\text{CH}_3\text{CN})_4]\text{ClO}_4$  (16 mg,  $5.0 \times 10^{-5}$  mol) were dissolved in absolute propionitrile (25 mL). To record a copper(I) spectrum at low temperatures, the solution was mixed with dry and oxygen-free solvent 1:1. For the stopped flow experiments to observe reactive intermediates, the complex solution was mixed with  $\text{O}_2$ -saturated propionitrile in 1:1 ratio and measured *in situ* at various temperatures.

### 3.4.1.3 $[Cu_2(Hxyl-unspenp)]^{2+}$ Solution

**Hxyl-unspenp** (14.7 mg,  $2.5 \times 10^{-5}$  mol) and  $[Cu(CH_3CN)_4]SbF_6$  (23.1 mg,  $5.0 \times 10^{-5}$  mol) were dissolved in absolute propionitrile (25 mL). To record a copper(I) spectrum at low temperatures, the solution was mixed with dry and oxygen-free solvent 1:1. For the stopped-flow experiments to observe reactive intermediates, the complex solution was mixed with  $O_2$ -saturated propionitrile in 1:1 ratio and measured *in situ* at various temperatures.

### 3.4.2 Synthesis of $[Cu_4(CO_3)_2(Hxyl-unspenp)_2](SbF_6)_4$

Under inert atmosphere a solution of  $[Cu(CH_3CN)_4]SbF_6$  (318 mg,  $6.86 \times 10^{-4}$  mol) in acetone (2mL) was added dropwise to an acetone solution (4mL) of **Hxyl-unspenp** (200 mg,  $3.41 \times 10^{-4}$  mol). After 15 min  $O_2$  was bubbled through the solution and the resulting turquoise solution was allowed to stand for one day. After several additional days of ether diffusion at room temperature, blue, plate like single crystals suitable for X-ray structure determination formed.

## 4 Bispicolylamine Relatives Closely Related to Tmpa

### 4.1 Syntheses, Emission Properties and Intramolecular Ligand Exchange of Zinc Complexes with Ligands Belonging to the Tmpa Family

This chapter has been published previously in *Dalton Transactions* **2011**, 40, 5090-5101

Alexander Beitat,<sup>a</sup> Simon P. Foxon,<sup>a</sup> Christoph-Cornelius Brombach,<sup>a</sup> Heike Hausmann,<sup>b</sup> Frank W. Heinemann,<sup>c</sup> Frank Hampel,<sup>d</sup> Uwe Monkowius,<sup>e</sup> Christa Hirtenlehner,<sup>e</sup> Günther Knör<sup>\*e</sup> and Siegfried Schindler<sup>\*a</sup>

a Institut für Anorganische Chemie, Justus-Liebig-Universität Gießen, Heinrich-Buff-Ring 58, 35392 Gießen, Germany, E-mail: Siegfried.Schindler@anorg.chemie.uni-giessen.de

b Institut für Organische Chemie, Justus-Liebig-Universität Gießen, Heinrich-Buff-Ring 58, 35392 Gießen, Germany

c Department Chemie und Pharmazie, Anorganische Chemie, Universität Erlangen-Nürnberg, Egerlandstr. 1, 91058 Erlangen, Germany

d Department Chemie und Pharmazie, Organische Chemie, Universität Erlangen-Nürnberg, Henkestr. 42, 91054 Erlangen, Germany

e Institut für Anorganische Chemie, Johannes Kepler Universität Linz, Altenbergerstr. 69 A-4040 Linz, Austria, E-mail: Guenther.Knoer@jku.at

The zinc complexes  $[(\mathbf{L1})_2\text{Zn}(\text{MeOH})_2](\text{OTf})_2$ ,  $[(\mathbf{L1})\text{ZnCl}_2]$ ,  $[(\mathbf{L2})\text{ZnCl}_2]$ ,  $[(\mathbf{L2})\text{Zn}(\text{OTf})(\text{H}_2\text{O})]\text{OTf}$  and  $[(\mathbf{Me-bispic})\text{ZnCl}_2]$  of the ligands *N*-[(2-Pyridyl)methyl]-2,2'-dipyridylamine (**L1**), *N*-[bis(2-pyridyl)methyl]-2-pyridylamine (**L2**) and *N*-methyl-[bis(2-pyridyl)methyl]amine (**Me-bispic**) were synthesised and characterised. The first copper(I) complexes of the ligands **L1** and **L2** were also synthesised and structurally characterised.  $[(\mathbf{L1})\text{ZnCl}_2]$  showed unexpected fluxional behaviour in solution and revealed an interesting intramolecular ligand exchange mechanism in the coordination sphere of the zinc ion. Furthermore, strong blue emission was observed under UV-light excitation.

#### 4.1.1 Introduction

Metalloproteins containing zinc in their active sites play an important role in the metabolism of eukaryote and prokaryote cells. There are examples in nearly every fundamental class of enzymes i.e. oxidoreductases, transferases or hydrolases.<sup>2-3, 141</sup>

The function of such enzymes is intimately related to the structural and geometric properties of their active sites. In the past, complexes containing derivatives of tris(2-pyridylmethyl)amine (**tmpa**, Figure 39) as ligands were used as model compounds for zinc enzymes.<sup>142-150</sup> Detailed studies of ligands closely related to **tmpa** revealed a strong effect of the chelate ring size on the

properties of related copper complexes.<sup>134, 151</sup> When the "ligand arms" of **tmpa** were systematically shortened, ligands *N*-[(2-pyridyl)methyl]-2,2'-dipyridylamine (**L1**), *N*-[bis(2-pyridyl)methyl]-2-pyridyl amine (**L2**) and 2,2',2''-tripyridylamine (**tpa**) were obtained. Additionally, *N*-methyl-[bis(2-pyridyl)methyl]amine (**Me-bispic** also abbreviated as **Me-bpa**) missing one "arm" and thus a donor atom (compared with **tmpa**) was prepared.

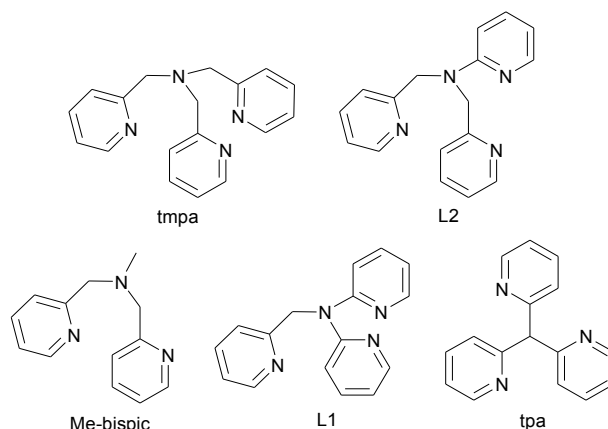


**Fig. 39** The ligands **tmpa**, **L2**, **Me-bispic**, **L1** and **tpa**

Herein we report the synthesis, characterisation and the properties of the zinc complexes containing ligands **L1**, **L2** and **Me-bispic**. Furthermore, copper(I) complexes of the ligands **L1** and **L2** have been structurally characterised and compared to their analogous zinc complexes.

#### 4.1.2 Results and Discussion

##### 4.1.2.1 Ligand Synthesis

The ligands **L1**, **L2** and **tpa** were synthesised according to recently reported procedures.<sup>151-152</sup> The ligand *N*-methyl-[bis(2-pyridyl)methyl]amine (**Me-bispic**) can be synthesised by various published procedures:<sup>153-155</sup> (treating an aqueous solution of 2-(chloromethyl)pyridine hydrochloride and  $K_2CO_3$  with 2-(*N*-methylaminomethyl)pyridine,<sup>155</sup> reacting an aqueous solution of 2-(chloromethyl)pyridine hydrochloride and NaOH with methylamine hydrochloride<sup>153</sup> or by the reductive methylation of bis[(2-pyridyl)methyl]amine under Eschweiler-Clark conditions.)<sup>154</sup> As described previously, we used an alternative method to prepare **Me-bispic** in a direct reductive amination reaction leading to much better yields.<sup>156</sup> The required product bis[(2-pyridyl)methyl]amine was synthesised in high yield according to a procedure described earlier.<sup>157</sup>

##### 4.1.2.2 Metal Complexes

Zinc complexes of **tmpa** are well-known and their properties and crystal structures have been described.<sup>158-163</sup> In contrast, only 3 different zinc complexes of **tpa** have been investigated and structurally characterised.<sup>152, 164-165</sup>

Ligands **L1**, **L2** and **Me-bispic** coordinate readily with zinc salts to form complexes of which 4 are presented herein. All of the zinc complexes are air stable with the exception of  $[(\mathbf{L2})\text{Zn}(\text{OTf})(\text{H}_2\text{O})]\text{OTf}$ , which is hygroscopic.

In contrast, copper(I) complexes of **L1** and **L2** were found to be air sensitive and, although their reactivities were investigated previously, it was not possible to structurally characterise them by X-ray diffraction analysis at this time.<sup>151</sup>

#### 4.1.2.3 Crystal Structure Determinations

Crystals suitable for structural characterisation were obtained for  $[(\mathbf{L2})\text{ZnCl}_2]$  (**1a**),  $[(\mathbf{L2})\text{Zn}(\text{OTf})(\text{H}_2\text{O})]\text{OTf}$  (**1b**),  $[(\mathbf{L2})_3\text{Cu}_2](\text{BPh}_4)_2$  (**1c**),  $[(\mathbf{Me-bispic})\text{ZnCl}_2]$  (**2**),  $[\mathbf{L1H}]\text{OTf}$  (**3a**),  $[(\mathbf{L1})\text{ZnCl}_2]$  (**3b**),  $[(\mathbf{L1})_2\text{Zn}(\text{MeOH})_2](\text{OTf})_2$  (**3c**) and  $[(\mathbf{L1})_2\text{Cu}_2](\text{OTf})_2 \times 2 \text{ DMF}$  (**3d**). A summary of the relevant crystallographic data and refinement parameters for the zinc complexes **1a**, **1b**, **2**, **3b**, **3c** and the protonated ligand **3a** can be found in Table 5 and for the copper(I) complexes **1c** and **3d** in Table 6, respectively. Selected bond lengths and angles for all compounds are provided in Table 7.

##### 4.1.2.3.1 $[(\mathbf{L2})\text{ZnCl}_2]$ (**1a**)

Colourless block-shaped crystals of **1a** suitable for single-crystal X-ray analysis were obtained and Figure 40 shows a thermal ellipsoid plot of the molecular structure.

Two of the pyridyl rings of **L2** coordinate to the zinc atom in **1a**. The zinc atom is tetracoordinated by the pyridyl nitrogen atoms N(11) and N(21),  $[\text{Zn}(1)\text{--N}(11) = 2.082(2) \text{ \AA}$ ,  $\text{Zn}(1)\text{--N}(21) = 2.051(2) \text{ \AA}]$  and two chloride ions Cl(1) and Cl(2)  $[\text{Zn}(1)\text{--Cl}(1) = 2.214(1) \text{ \AA}$ ,  $\text{Zn}(1)\text{--Cl}(2) = 2.294(1) \text{ \AA}]$ .

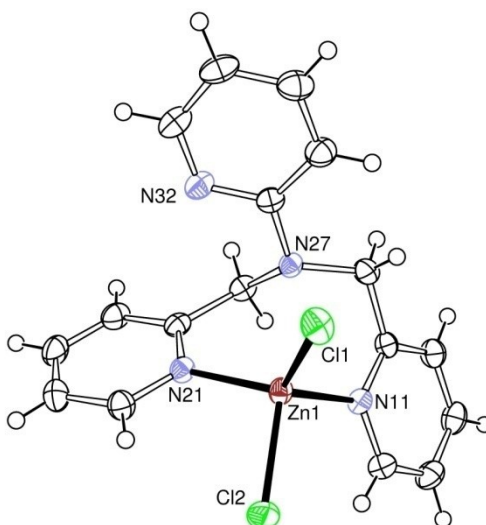


**Fig. 40** Thermal ellipsoid representation (50 % probability ellipsoids) of the molecular structure of  $[(\mathbf{L2})\text{ZnCl}_2]$  (**1a**)

The coordination environment around the zinc atom is best described as close to tetrahedral with only small deviations from the ideal value of  $109^\circ$ . Only two of the pyridyl rings of **L2** are coordinated to the zinc atom.

The two coordinated pyridyl rings are far from being coplanar with one another as is evident by a dihedral angle of  $69.75^\circ$  between the two rings. Two nitrogen atoms of **L2** remain uncoordinated to the zinc(II) atom, the tertiary amine nitrogen N(27) [ $N(27)\cdots Zn(1) = 2.69 \text{ \AA}$ ], and the pyridyl nitrogen N(32) atom [ $N(32)\cdots Zn(1) = 4.11 \text{ \AA}$ ]. In contrast to **1a**, the metal ion in the corresponding structurally characterised copper(II) chloride complex of **L2** [**(L2)**CuCl<sub>2</sub>] was found to be penta-coordinate.<sup>151</sup>

#### 4.1.2.3.2 [(L2)Zn(OTf)(H<sub>2</sub>O)]OTf (**1b**)

The three ligands were also reacted with a zinc salt containing a weakly coordinating anion - zinc triflate. Colourless prism-shaped crystals of **1b** were grown at  $-20^\circ\text{C}$  from a solution containing MeCN/CH<sub>2</sub>Cl<sub>2</sub>/Et<sub>2</sub>O. A thermal ellipsoid plot of the molecular structure of **1b** is displayed in Figure 41.

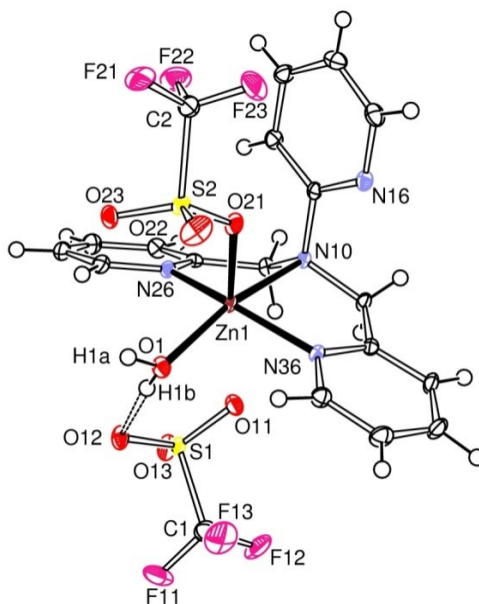


**Fig. 41** Thermal ellipsoid representation (50 % probability ellipsoids) of the molecular structure of [(L2)Zn(OTf)(H<sub>2</sub>O)]OTf (**1b**)

As is depicted in Figure 41, and as was observed for **1a**, only two of the pyridyl rings of **L2** coordinate to the zinc atom. The zinc atom is pentacoordinated by the pyridyl nitrogen atoms N(26) and N(36), the tertiary amine nitrogen atom N(10), O(21) of one of the triflate anions and O(1) of the coordinated water molecule. The coordination environment around the zinc atom is best described as distorted square pyramidal ( $\tau = 0.22$  as described by the trigonality parameter  $\tau$ :<sup>118</sup>  $\tau = 0$  denotes perfect square pyramidal;  $\tau = 1$  denotes perfect trigonal bipyramidal), with N(10), N(26), N(36) and O(1) forming the basal plane [ $Zn(1)-N(10) = 2.319(2) \text{ \AA}$ ,  $Zn(1)-N(26) = 2.033(2) \text{ \AA}$ ,  $Zn(1)-N(36) = 2.023(2) \text{ \AA}$  and  $Zn(1)-O(1) = 2.058(2) \text{ \AA}$ ]. The apical coordination site

is occupied by the oxygen atom O(21) of a triflate anion [Zn(1)–O(21) = 2.070(2) Å]. Zn(1) deviates from the mean plane of the square pyramid towards the apical O(21) atom by ca. 0.35 Å. A second triflate anion, which remains uncoordinated [Zn(1)–O(11) = 2.60 Å] forms an *intramolecular* hydrogen bond with the coordinated water molecule [O(1)···O(12) = 2.702(2) Å, O(1)–H(1B)···O(12) = 172(3)°]. The coordinated water molecule also forms an *intermolecular* hydrogen bond with the coordinated triflate anion of a neighbouring molecule of **1c** in the unit cell [O(1)···O(23)# = 2.755(2) Å, O(1)–H(1A)···O(23)# = 164(2)°].

#### 4.1.2.3.3 [(L2)<sub>3</sub>Cu<sub>2</sub>](BPh<sub>4</sub>)<sub>2</sub> (**1c**)

Single crystals of **1c** suitable for X-ray structure determination were grown from an acetone solution at –40 °C under an inert atmosphere. The molecular structure of the dimer is depicted in Figure 42.

Three **L2** ligand molecules and two copper(I) ions form the dimer. As observed in the triflate complex **1b**, **L2** coordinates

**Table 5** Crystallographic data for zinc compounds **1a**, **1b**, **2**, **3b**, **3c** and the protonated ligand **3a**

	<b>1a</b>	<b>1b</b>	<b>2</b>	<b>3a</b>	<b>3b</b>	<b>3c</b>
Molecular formula	C <sub>17</sub> H <sub>16</sub> Cl <sub>2</sub> N <sub>4</sub> Zn	C <sub>19</sub> H <sub>18</sub> F <sub>6</sub> N <sub>4</sub> O <sub>7</sub> S <sub>2</sub> Zn	C <sub>13</sub> H <sub>15</sub> Cl <sub>2</sub> N <sub>3</sub> Zn	C <sub>17</sub> H <sub>17</sub> F <sub>3</sub> N <sub>4</sub> O <sub>4</sub> S	C <sub>16</sub> H <sub>14</sub> Cl <sub>2</sub> N <sub>4</sub> Zn	C <sub>36</sub> H <sub>36</sub> F <sub>6</sub> N <sub>8</sub> O <sub>8</sub> S <sub>2</sub> Zn
CCDC no.	724313	796270	724312	796272	796273	796274
<i>M<sub>r</sub></i>	412.61	657.86	349.55	430.41	398.58	952.22
Temperature [K]	173(2)	100(2)	173	193(2)	100(2)	193(2)
Wavelength [Å]	0.71073	0.71073	0.71073	0.71073	0.71073	0.71073
Crystal description	colourless block	colourless prism	colourless block	colourless block	colourless prism	yellow block
Crystal size [mm]	0.30 × 0.30 × 0.30	0.28 × 0.23 × 0.17	0.20 × 0.20 × 0.10	0.52 × 0.48 × 0.36	0.29 × 0.19 × 0.19	0.38 × 0.24 × 0.12
Crystal system	monoclinic	triclinic	monoclinic	triclinic	monoclinic	monoclinic
Space group	<i>P</i> 2 <sub>1</sub> / <i>c</i> (No. 14)	<i>P</i> -1 (No. 2)	<i>P</i> 2 <sub>1</sub> / <i>n</i> (No. 14)	<i>P</i> -1 (No. 2)	<i>C</i> 2/ <i>c</i> (No. 15)	<i>C</i> 2/ <i>c</i> (No. 15)
<i>a</i> [Å]	9.2065(18)	9.4941(1)	8.5048(1)	9.2409(18)	15.2535(4)	23.404(5)
<i>b</i> [Å]	11.230(2)	10.8919(2)	13.0128(1)	9.5985(19)	7.4124(1)	12.220(2)
<i>c</i> [Å]	17.138(3)	12.8792(2)	13.1424(1)	10.721(2)	29.1536(6)	17.155(3)
$\alpha$ [°]	90	100.878(1)	90	75.35(3)	90	90
$\beta$ [°]	101.09(3)	94.965(2)	95.250(1)	83.59(3)	92.344(2)	123.83(3)
$\gamma$ [°]	90	108.341(1)	90	88.29(3)	90	90.0
<i>V</i> [Å <sup>3</sup> ]	1738.7(6)	1226.14(3)	1448.38(4)	914.2(3)	3293.5(2)	4075.8(14)
<i>Z</i>	4	2	4	2	8	4
<i>F</i> (000)	840	664	712	444	1616	1952
$\rho_{\text{calc}}$ [g cm <sup>–3</sup> ]	1.576	1.782	1.603	1.564	1.608	1.552
$\mu$ [mm <sup>–1</sup> ]	1.725	1.267	2.053 mm <sup>–1</sup>	0.241	1.819	0.794
Total reflections	7223	33004	5650	8133	32273	14581
Unique reflections	3519	7118	3228	3970	5707	4942
<i>R</i> (int)	0.0773	0.0574	0.0179	0.0715	0.0699	0.1493
Scan range $\theta$ [°]	2.89 to 26.30	3.42 to 30.00	2.21 to 27.48	3.12 to 28.06	3.34 to 32.00	2.43 to 28.13
Completeness to $\theta_{\text{max}}$ [%]	99.9	99.3	97.5	89.3	99.8	99.1
Index ranges	–11 ≤ <i>h</i> ≤ 11 –7 ≤ <i>k</i> ≤ 13 –21 ≤ <i>l</i> ≤ 21	–13 ≤ <i>h</i> ≤ 13 –15 ≤ <i>k</i> ≤ 15 –18 ≤ <i>l</i> ≤ 18	–9 ≤ <i>h</i> ≤ 10 –16 ≤ <i>k</i> ≤ 15 –17 ≤ <i>l</i> ≤ 17	–12 ≤ <i>h</i> ≤ 11 –12 ≤ <i>k</i> ≤ 12 –12 ≤ <i>l</i> ≤ 13	–22 ≤ <i>h</i> ≤ 22 –11 ≤ <i>k</i> ≤ 11 –43 ≤ <i>l</i> ≤ 41	–30 ≤ <i>h</i> ≤ 30 –16 ≤ <i>k</i> ≤ 16 –22 ≤ <i>l</i> ≤ 22
Data / restraints / parameters	3519 / 0 / 273	7118 / 0 / 406	3228 / 0 / 232	3970 / 0 / 275	5707 / 1 / 254	4942 / 0 / 326
Goodness-of-fit on <i>F</i> <sup>2</sup> [c]	0.873	1.125	1.122	1.108	1.015	0.860
<i>R</i> <sub><i>I</i></sub> [a][b] <i>wR</i> <sub>2</sub> [ <i>I</i> > 2σ( <i>I</i> )] [c]	0.0292, 0.0683	0.0323, 0.0856	0.0262, 0.0754	0.0573, 0.1593	0.0359, 0.0705	0.0588, 0.1183
<i>R</i> <sub><i>I</i></sub> [a][d] <i>wR</i> <sub>2</sub> (all data) [c][d]	0.0459, 0.0789	0.0479, 0.0910	0.0311, 0.0781	0.0631, 0.1656	0.0714, 0.0762	0.1456, 0.1453
Max./min. el. density [e·Å <sup>–3</sup> ]	+0.331, –0.458	+0.470, –0.558	+0.272, –0.536	+0.471, –0.913	+0.488, –0.427	+0.566, –0.592

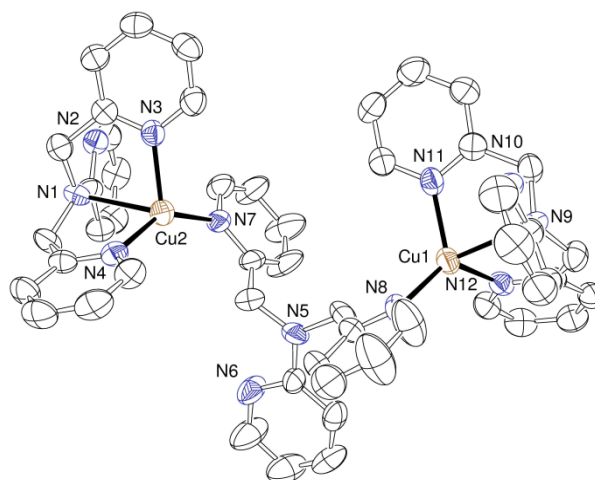


**Fig. 42** Thermal ellipsoid plot (50 % probability ellipsoids) of the molecular structure of  $[(\mathbf{L2})_3\text{Cu}_2](\text{BPh}_4)_2$  (**1c**). Hydrogen atoms and anions are omitted for clarity

with three nitrogen atoms to the metal atom. Two of them are from the methylpyridyl moieties and one being the tertiary amine. The bridging ligand molecule coordinates with one nitrogen of the methylpyridyl moieties to each copper(I) atom leading to four-coordinate metal atoms in the dimer. The geometry around the copper(I) atoms are best described as distorted tetrahedral.

#### 4.1.2.3.4 $[(\text{Me-bispic})\text{ZnCl}_2]$ (**2**)

The ligand **Me-bispic** acts as a tridentate ligand to the zinc atom in **2**. A thermal ellipsoid plot of the molecular structure of **2** is displayed in Figure 43.

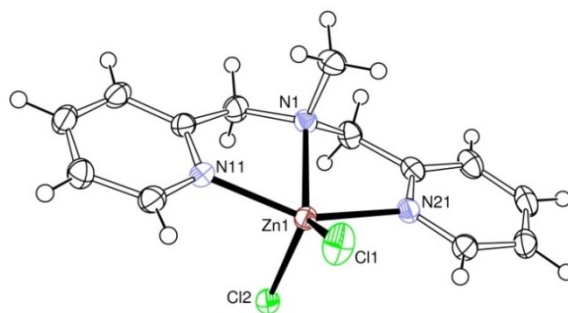


**Fig. 43** Thermal ellipsoid representation (50 % probability ellipsoids) of the molecular structure of  $[(\text{Me-bispic})\text{ZnCl}_2]$  (**2**)

The zinc atom is pentacoordinate, being ligated by the tertiary amine N(1) [ $\text{Zn(1)-N(1)} = 2.215(1) \text{ \AA}$ ] and the two pyridyl nitrogen atoms N(11) and N(21) [ $\text{Zn(1)-N(11)} = 2.148(2) \text{ \AA}$ ,  $\text{Zn(1)-N(21)} = 2.150(2) \text{ \AA}$ ] of the ligand. The coordination sphere around the zinc atom is completed by two chloride anions Cl(1) and Cl(2) [ $\text{Zn(1)-Cl(1)} = 2.271(1) \text{ \AA}$ ,  $\text{Zn(1)-Cl(2)} = 2.278(1) \text{ \AA}$ ]. Examination of the coordination around the zinc atom reveals that it is best described as distorted square pyramidal ( $\tau = 0.35$ ). The corresponding copper(II) complex has a similar coordination geometry ( $\tau = 0.38$ ) where the bonds of the nitrogen atoms to the metal



atom are about 0.14 Å shorter. In this complex the bond length of only one of the coordinated chlorides is similar to that in **2**, the other bond is significantly longer [2.419(2) Å].<sup>156</sup>

Only one further copper(II) complex with **Me-bispic** as ligand has been structurally characterised. Until now efforts to obtain single crystals of the copper(I) complex [(**Me-bispic**)CuCl], have been unsuccessful.<sup>156, 163</sup>

Ligands **L2** and **Me-bispic** are derivatives of the parent amine bis[(2-pyridyl)methyl]amine (**bispic**, also abbreviated as dipica or bpa). It is therefore informative to compare the zinc complexes of **L2**, **Me-bispic** and **bispic**. Copper complexes of **bispic** have been described previously<sup>166-168</sup> and show similar modes of coordination as observed in copper(II) complexes with **L2**.<sup>151</sup> The complex [(**bispic**)ZnCl<sub>2</sub>] has been structurally characterised by single-crystal X-ray crystallography.<sup>169</sup>

**Table 6** Crystallographic data for copper(I) complexes **1c** and **3d**

	<b>1c</b>	<b>3d</b>
Molecular formula	C <sub>102</sub> H <sub>94</sub> B <sub>2</sub> Cu <sub>2</sub> N <sub>12</sub> O	C <sub>40</sub> H <sub>42</sub> Cu <sub>2</sub> F <sub>6</sub> N <sub>10</sub> O <sub>8</sub> S <sub>2</sub>
CCDC no.	796271	796275
<i>M<sub>r</sub></i>	1652.59	1096.04
Temperature [K]	193(2)	203(2)
Wavelength [Å]	0.71073	0.71073
Crystal description	yellow block	yellow block
Crystal size [mm]	0.52 × 0.24 × 0.24	0.80 × 0.32 × 0.24
Crystal system	monoclinic	monoclinic
Space group	Cc (No. 9)	P2 <sub>1</sub> /n (No. 14)
<i>a</i> [Å]	17.762(4)	13.411(3)
<i>b</i> [Å]	20.211(4)	9.5300(19)
<i>c</i> [Å]	24.377(5)	17.636(4)
$\alpha$ [°]	90	90
$\beta$ [°]	100.35(3)	95.72(3)
$\gamma$ [°]	90	90
<i>V</i> [Å <sup>3</sup> ]	8609(3)	2242.8(8)
<i>Z</i>	4	2
<i>F</i> (000)	3464	1120
$\rho_{\text{calc}}$ [g cm <sup>-3</sup> ]	1.275	1.623
$\mu$ [mm <sup>-1</sup> ]	0.552	1.130
Total reflections	27816	19621
Unique reflections	13806	5123
<i>R</i> (int)	0.0517	0.0624
Scan range $\theta$ [°]	2.02 to 25.02	2.81 to 28.09
Completeness to $\theta_{\text{max}}$ [%]	99.3	93.6
Index ranges	-21 ≤ <i>h</i> ≤ 21 -22 ≤ <i>k</i> ≤ 23 -28 ≤ <i>l</i> ≤ 28	-17 ≤ <i>h</i> ≤ 17 -11 ≤ <i>k</i> ≤ 11 -23 ≤ <i>l</i> ≤ 23
Data / restraints / parameters	13806 / 2 / 1074	5123 / 0 / 340
Goodness-of-fit on <i>F</i> <sup>2</sup> [c]	0.924	1.070
<i>R</i> [a][b] <i>wR</i> 2 [ <i>I</i> > 2σ( <i>I</i> )] [c]	0.0461, 0.0941	0.0410, 0.1126
<i>R</i> [a][d] <i>wR</i> 2 (all data) [c][d]	0.0795, 0.1057	0.0502, 0.1182
Max./min. el. density [e.Å <sup>-3</sup> ]	+0.459 / -0.237	+0.624 / -0.585

The zinc atom is penta-coordinate and the coordination around the zinc atom is best described as distorted square-based pyramidal having a trigonality index  $\tau$  of 0.15. The three Zn–N bond lengths are identical within error [average Zn–N distance = 2.166(5) Å] as are the Zn–Cl distances [average Zn–Cl distance = 2.270(1) Å]. In stark contrast to [(**bispic**)ZnCl<sub>2</sub>], the zinc atom in **1a** remains tetra-coordinate and has close to tetrahedral geometry with the tertiary amine nitrogen atom remaining uncoordinated to the zinc atom as described above. There are

only a few minor differences in the geometric parameters in complex **2** compared to those in [(**bispic**)ZnCl<sub>2</sub>].

It is interesting to observe how derivatisation of the secondary amine group of the parent **bispic** ligand structure can cause drastic changes in the coordination environment around the zinc atom in the respective derivatised ligand complexes. **L2** and **Me-bispic** both contain tertiary amine groups. The tertiary amine nitrogen atom in **L2** is less basic than the corresponding tertiary amine in **Me-bispic**. In **L2** the lone-pair electron density of the tertiary amine nitrogen atom (N1) is reduced through delocalisation onto the pyridine ring, thus making it less available for coordination to a metal atom.

Finally, a zinc complex of **L2** (**1b**) with triflate – a well-known “weakly interacting” counter anion – was prepared. However only one ligand molecule **L2** coordinates to the zinc atom and the zinc atom forms a strong interaction with one triflate anion.

#### 4.1.2.3.5 [L1H]OTf (**3a**)

The structure of the protonated ligand **L1** is depicted in Figure 44. Surprisingly, one of the pyridyl moieties is protonated and not, as we expected, the aliphatic bridging nitrogen N1. The two pyridyl moieties of the ligand are co-planar and the nitrogen atoms N3 and N4 are facing each other to allow the proton to be covalently bonded to N4. Thus they form an intramolecular hydrogen bond to N3 with a distance of 1.827 Å. Due to this stabilisation the pyridyl nitrogen is the favoured position for protonation.

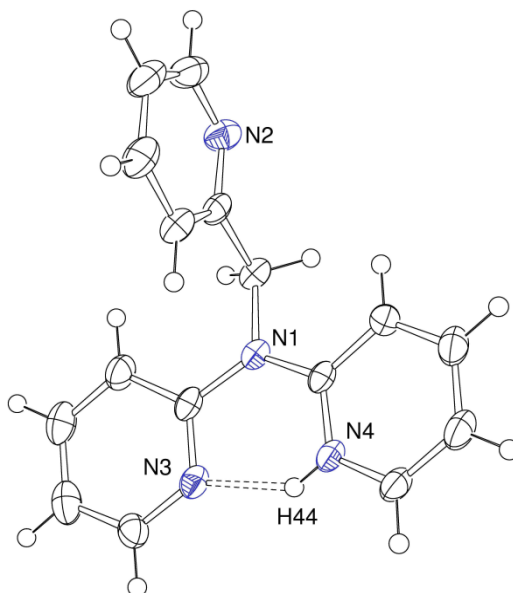


**Fig. 44** Thermal ellipsoid representation (50 % probability ellipsoids) of the molecular structure of [L1H]OTf. Anion and solvent molecules are omitted for clarity. (**3a**)

#### 4.1.2.3.6 [(L1)ZnCl<sub>2</sub>] (3b)

The molecular structure of **3b** is shown in Figure 45. In this figure it can clearly be seen that only two of the pyridyl rings of **L1** are ligated to the zinc atom. The zinc atom is four-coordinate, being coordinated by the pyridyl nitrogen atoms N(26) and N(36), [Zn(1)–N(26) = 2.039(2) Å, Zn(1)–N(36) = 2.075(2) Å] and two chloride ions Cl(1) and Cl(2) [Zn(1)–Cl(1) = 2.241(1) Å, Zn(1)–Cl(2) = 2.240(1) Å]. The coordination environment around the zinc atom is close to tetrahedral as is noted by only small variations from the ideal value of 109°. It is clear that the two pyridyl rings which are coordinated to the zinc atom are not coplanar as is evident by a dihedral angle of 26.77° between the two rings. During the crystallographic refinement of the structure of **3b**, the non coordinating pyridyl ring was found to be disordered over two positions. The positions of each orientation were successfully refined with occupancies of 67(2)% and 33(2)%. Two nitrogen atoms of **L1** remain uncoordinated, the tertiary amine nitrogen N(10) [N(10)⋯Zn(1) = 3.18 Å], and the pyridyl nitrogen N(16) atom [N(16)⋯Zn(1) = 3.72 Å].

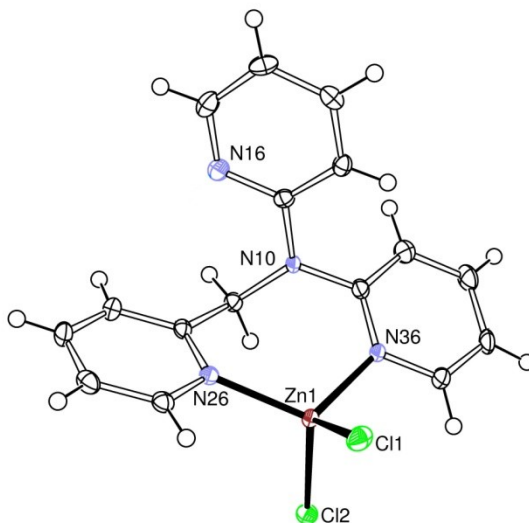


**Fig. 45** Thermal ellipsoid representation (50 % probability ellipsoids) of the molecular structure of [(**L1**)ZnCl<sub>2</sub>] (**3b**)

The ligand **L1** is structurally closely related to **tpa**, **L1** differing in that a methylene spacer group has been inserted into one of the ligand “arms”. The corresponding ZnCl<sub>2</sub> complex of **tpa** [Zn(**tpa**)Cl<sub>2</sub>] has been structurally characterised by X-ray crystallography.<sup>152</sup> There are similarities between the two structures, only two of the three pyridyl rings are found coordinated to the zinc atom. The coordination around the zinc atom in [Zn(**tpa**)Cl<sub>2</sub>] is close to tetrahedral, only the angle between the two coordinating pyridyl nitrogen atoms and the zinc atom [N(36)–Zn(1)–N(26) = 88.39(14)°] differs drastically from 109°, a consequence of the small chelate angle enforced by the 2,2′-dipyridylamine moiety.

However, in contrast to [Zn(**tpa**)Cl<sub>2</sub>], both pyridyl rings of the 2,2′-dipyridylamine moiety do not coordinate to the zinc atom in **3b**. Instead, the pyridyl ring of the “longer” arm with the

methylene spacer coordinates to the zinc atom. This is in striking contrast to what was observed for the copper(II) complexes of **L1** reported previously.<sup>151</sup> In the four structurally characterised copper(II) complexes of **L1**, the copper(II) ion was always found to be coordinated to the dipyridylamine moiety of **L1** with the “longer” arm of **L1** remaining uncoordinated. These observations might be important in regard to the highly dynamic solution behaviour of **1** described below.

#### 4.1.2.3.7 $[(\mathbf{L1})_2\text{Zn}(\text{MeOH})_2](\text{OTf})_2$ (**3c**)

In Figure 46 the molecular structure of **3c** is shown. The coordination around the zinc atom is best described as octahedral. The zinc ion is coordinated by two **L1** and two solvent molecules in the axial positions.

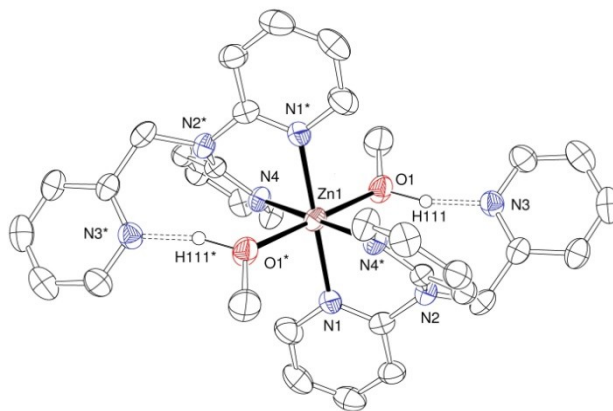


**Fig. 46** Thermal ellipsoid representation (50 % probability ellipsoids) of the molecular structure of  $[(\mathbf{L1})_2\text{Zn}(\text{MeOH})_2](\text{OTf})_2$  (**3c**). Hydrogen atoms and anions omitted for clarity. Equivalent atoms are generated using the symmetry operation  $-x+1/2, -y+1/2, -z+1$

In contrast to the structure of **3c** and all other metal complexes presented herein only the pyridyl nitrogens of the “short arms” of the two **L1** ligands are coordinated to the zinc atom forming the plane of the octahedron.

The nitrogen atoms N(3) and N(3)\* of the “long arm” of the ligands form hydrogen bonds (1.59(7) Å) with the hydroxyl hydrogen atoms H(111) and H(111)\* of the coordinated methanol molecules, resulting in an elongated O-H bond. Therefore the bond length between O(1) and the hydrogen atom H(111) that has been found and isotropically refined was not restrained to more standard values. The aliphatic nitrogen atoms N(2) remain uncoordinated [ $\text{N}(2)\cdots\text{Zn}(1) = 4.342$  Å]. In all other zinc and copper(I) complexes the metal atom is tetra- or penta-coordinate differing from the zinc atom in **3c** which is hexa-coordinate. Interestingly, the corresponding copper(II) complex from methanolic solution, that has been structurally characterised earlier, is nearly superimposable upon **3c**.<sup>151</sup>

4.1.2.3.8  $[(L1)_2Cu_2](OTf)_2 \cdot 2DMF$  (**3d**)

An ORTEP plot of the molecular structure of **3d** is displayed in Figure 47. The copper(I) complex of **L1** with triflate as a weakly coordinating anion is dimeric when crystallised from DMF. Although to date, it has not been possible to crystallise a monomer of **3d** so far, the molecular structure of **3d** shows that copper(I), being isoelectronic to zinc(II), coordinates to the same pyridyl moieties of **L1** as the chloride complex **3b**. The nitrogen atoms N(4) and N(4)\* of the dipyridylamine moiety bind to the second copper atom to form a cage-like dimer. The two copper(I) ions, unlike the zinc atom in **3b**, are three-coordinate with a copper(I)···copper(I) distance of 4.11 Å. The copper atom is positioned 0.10 Å out of the plane formed by the three coordinated nitrogen atoms. The coordination is best described as distorted trigonal planar. Although there should be enough room for oxygen to attack the three coordinate copper(I) atoms, **3d** in the solid is

**Table 7** Selected bond lengths [Å] and angles [°] for compounds **1a** – **3d**

<b>1a</b>							
Zn(1)–N(11)	2.0819(18)	Zn(1)–N(21)	2.0513(19)	N(11)–Zn(1)–N(21)	110.59(8)	N(21)–Zn(1)–Cl(2)	100.00(6)
Zn(1)–Cl(2)	2.2941(8)	Zn(1)–Cl(1)	2.2143(7)	N(11)–Zn(1)–Cl(2)	101.07(6)	N(21)–Zn(1)–Cl(1)	119.93(6)
				N(11)–Zn(1)–Cl(1)	114.39(6)		
<b>1b</b>							
Zn(1)–N(36)	2.023(2)	Zn(1)–O(1)	2.058(2)	O(1)–Zn(1)–O(11)	81.93(5)	O(21)–Zn(1)–O(11)	173.26(5)
Zn(1)–O(21)	2.070(2)	Zn(1)–O(11)	2.599(2)	O(1)–H(1B)...O(12)	172(3)	O(1)–H(1A)...O(23)*	164(2)
O(1)...O(12)	2.703(2)	N(36)–Zn(1)–N(26)	150.73(6)	N(36)–Zn(1)–O(1)	97.23(6)	N(26)–Zn(1)–O(1)	97.88(6)
Zn(1)–N(26)	2.033(2)	N(36)–Zn(1)–O(21)	97.07(6)	N(26)–Zn(1)–O(21)	105.95(6)	O(1)–Zn(1)–O(21)	96.44(6)
Zn(1)–N(10)	2.319(2)	N(36)–Zn(1)–N(10)	79.80(6)	N(26)–Zn(1)–N(10)	78.71(6)	O(1)–Zn(1)–N(10)	163.79(6)
O(1)...O(23)*	2.755(2)	O(21)–Zn(1)–N(10)	99.78(5)	N(36)–Zn(1)–O(11)	76.73(5)	N(26)–Zn(1)–O(11)	80.76(5)
*Symmetry operation used to generate equivalent atoms: $-x+1, -y+1, -z$							
<b>1c</b>							
Cu(1)–N(8)	1.979(4)	Cu(2)–N(7)	1.954(4)	N(8)–Cu(1)–N(11)	116.68(18)	N(4)–Cu(2)–N(7)	141.53(17)
Cu(1)–N(12)	1.995(4)	Cu(2)–N(3)	2.051(4)	N(12)–Cu(1)–N(11)	115.88(16)	N(4)–Cu(2)–N(3)	110.74(16)
Cu(1)–N(11)	2.007(4)	Cu(2)–N(1)	2.417(5)	N(8)–Cu(1)–N(9)	123.22(17)	N(7)–Cu(2)–N(3)	107.33(16)
Cu(1)–N(9)	2.424(5)	Cu(1)...Cu(2)	7.364	N(12)–Cu(1)–N(9)	77.74(15)	N(4)–Cu(2)–N(1)	78.06(16)
Cu(2)–N(4)	1.952(4)	N(8)–Cu(1)–N(12)	126.25(16)	N(11)–Cu(1)–N(9)	78.47(16)	N(7)–Cu(2)–N(1)	116.54(16)
N(3)–Cu(2)–N(1)	76.81(15)						
<b>2</b>							
Zn(1)–N(11)	2.1483(15)	Zn(1)–N(1)	2.2151(14)	Cl(1)–Zn(1)–Cl(2)	120.62(2)	N(21)–Zn(1)–N(1)	76.04(6)
Zn(1)–Cl(1)	2.2709(5)	N(11)–Zn(1)–N(21)	152.01(6)	N(11)–Zn(1)–N(1)	76.37(6)	N(1)–Zn(1)–Cl(1)	130.80(4)
Zn(1)–N(21)	2.1497(15)	N(11)–Zn(1)–Cl(1)	97.95(5)	N(21)–Zn(1)–Cl(1)	96.44(4)	N(1)–Zn(1)–Cl(2)	108.58(4)
Zn(1)–Cl(2)	2.2783(5)	N(11)–Zn(1)–Cl(2)	95.16(4)	N(21)–Zn(1)–Cl(2)	97.97(4)		
<b>3a</b>							
N(3)...H(44)	1.827(4)						
<b>3b</b>							
Zn(1)–N(36)	2.075(2)	Zn(1)–Cl(1)	2.2413(5)	N(36)–Zn(1)–Cl(1)	108.70(4)	N(26)–Zn(1)–Cl(1)	108.43(5)
Zn(1)–Cl(2)	2.2399(5)	N(36)–Zn(1)–N(26)	112.42(6)	N(26)–Zn(1)–Cl(2)	110.37(4)	Cl(1)–Zn(1)–Cl(2)	114.65(2)
Zn(1)–N(26)	2.039(2)	N(36)–Zn(1)–Cl(2)	102.24(5)				
<b>3c</b>							
N(1)–Zn(1)	2.130(4)	N(3)–H(111)	1.59(7)	N(1)–Zn(1)–N(1)*	180.0	N(4)*–Zn(1)–O(1)	91.69(12)
N(4)–Zn(1)	2.108(3)	N(4)*–Zn(1)–N(4)	180.0(2)	N(4)*–Zn(1)–O(1)*	88.31(13)	N(4)–Zn(1)–O(1)	88.31(12)
O(1)–Zn(1)	2.158(3)	N(4)*–Zn(1)–N(1)	83.68(14)	N(4)–Zn(1)–O(1)*	91.69(12)	N(1)–Zn(1)–O(1)	90.89(13)
Zn(1)–N(4)*	2.108(3)	N(4)–Zn(1)–N(1)	96.32(14)	N(1)–Zn(1)–O(1)*	89.11(13)	N(1)*–Zn(1)–O(1)	89.11(13)
Zn(1)–N(1)*	2.130(4)	N(4)*–Zn(1)–N(1)*	96.32(14)	N(1)*–Zn(1)–O(1)*	90.89(13)	O(1)*–Zn(1)–O(1)	180.0
Zn(1)–O(1)*	2.158(3)	N(4)–Zn(1)–N(1)*	83.68(14)				
*Symmetry operation used to generate equivalent atoms: $-x+1/2, -y+1/2, -z+1$							
<b>3d</b>							
Cu(1)–N(2)	1.956(2)	Cu(1)–N(3)	2.0725(19)	N(2)–Cu(1)–N(4)*	140.54(8)	N(4)*–Cu(1)–N(3)	100.98(8)
Cu(1)–N(4)*	1.9834(17)	Cu(1)...Cu(1)*	4.114	N(2)–Cu(1)–N(3)	117.56(7)		
*Symmetry operation used to generate equivalent atoms: $-x+1, -y+2, -z$							

quite air stable and decomposition proceeds within a few days. Solutions of **3d** are much more sensitive towards oxygen, but still retain their typical yellow colour for about 15 minutes. Unfortunately no copper "dioxygen adduct" complexes could be crystallised or be detected spectroscopically by UV/Vis measurements.<sup>151</sup>

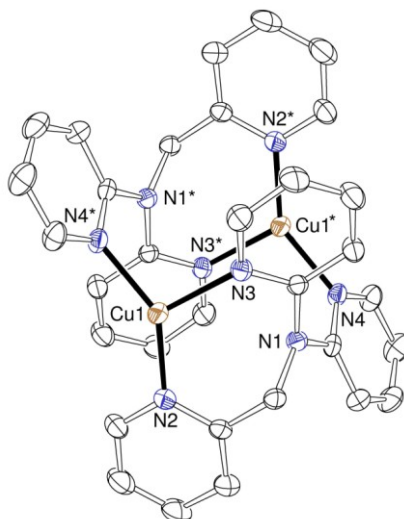


**Fig. 47** Thermal ellipsoid plot (50 % probability ellipsoids) of the molecular structure of  $[(\mathbf{L1})_2\text{Cu}_2](\text{OTf})_2 \cdot 2\text{DMF}$  (**3d**). Hydrogen atoms and counterions omitted for clarity. Equivalent atoms are generated using the symmetry operation  $-x+1, -y+2, -z$ .

In compounds **1b** and **1c** the metal atom is only four-coordinate, but in the absence of strong coordinating anions such as chloride, the aliphatic nitrogen of **L2** coordinates readily to the metal atom because of the lack of electron donation by the anion. In these cases the lack of negative charge is supposed to dominate the electronic repulsion between the ligands and the smaller chelate bite angles.

#### 4.1.2.4 Rationale for the Displayed Coordination Preferences of the Metal Atom in 1–3

The zinc(II) ion has a closed outer-shell electronic configuration of  $3d^{10}$ . In coordination compounds of zinc there is no crystal field stabilisation energy. Therefore, zinc can be tetra-, penta-, or hexa-coordinate without a particularly marked preference for octahedral coordination. The coordination number around the zinc(II) ion is determined by a balance between the bonding interactions of the ligands ligated to the zinc(II) ion and the repulsion amongst the ligands coordinated to the zinc(II) ion. The origin of the repulsion between the ligands coordinated to the zinc(II) ion in coordination compounds can be both steric and electronic. Tetrahedral tetra-coordinate complexes have shorter metal-ligand bond lengths on average than penta-coordinate zinc complexes, which have shorter metal-ligand bonds than hexa-coordinate zinc complexes. The repulsive interactions between the ligands increase in the same order. The isoelectronic copper(I) compounds have similar preferences. In the complexes **3b** and **3c** the metal ions coordinate to the "longer" pyridylmethyl "arm" rather than through the 2,2'-dipyridylamine moiety, as the 2,2'-dipyridylamine moiety would enforce a smaller chelate bite angle at the metal atom. In stark contrast the zinc complex

**3c** is hexa-coordinate, ligated by two **L1** molecules and two methanols in the axial positions. The nitrogen atoms of the methyl pyridyl moieties remain uncoordinated to the metal atom, but form intramolecular hydrogen bonds with the coordinated methanol solvent molecules. Ligation by the “longer arm” of **L2** ensures that the zinc(II) ion can adopt a close to tetrahedral geometry thus minimising repulsions between the coordinated chloride ions and the coordinated pyridyl donors. The zinc atom in **1a** is also found to be tetra-coordinate rather than adopting a penta-coordinate geometry for similar reasons. The reason why the zinc atom in **1a** remains tetra-coordinate and the zinc atom in **2** is penta-coordinate is that the bonding interaction offered by the more basic aliphatic tertiary amine donor of **Me-bispic** in **2** presumably offsets the gain in repulsion energy between the coordinated ligands on going from a tetrahedral to a penta-coordinate zinc coordination geometry.

#### 4.1.2.5 Fluxional Behaviour of the Complexes in Solution

All zinc complexes except for **3b** display sharp signals in their respective room temperature  $^1\text{H}$  NMR spectra. The resonances in the complexes **1a**, **1b** and **2** are comparable, but shifted, with respect to the uncoordinated ligands **L2** and **Me-bispic** (see Experimental Section). No evidence for dynamic processes occurring in solution is here apparent.

The crystal structure of **3b** (Figure 45) depicts two of the pyridyl rings of **L1** coordinating to the zinc atom with the third pyridyl ring remaining uncoordinated. What is unusual about the solid-state structure of **3b** is that **L1** does not chelate in a symmetrical fashion to the zinc atom through the 2,2'-dipyridylamine moiety. If **3b** retains the same structure in solution as in the solid state, one would expect to see a maximum of 12 different pyridyl proton resonances in the  $^1\text{H}$  NMR spectrum. Selected variable temperature  $^1\text{H}$  NMR spectra of **3b** are presented in Figure 48. For the full set of NMR spectra and signal assignment see Supporting Information. However, at room temperature the  $^1\text{H}$  NMR spectrum of **3b** displays only seven resonances in the aromatic region, three of which are very broad and hard to assign – indicative of some dynamic exchange process occurring in solution. In order to confirm this observation, we measured the  $^1\text{H}$  NMR spectrum of **3b** in  $\text{CD}_2\text{Cl}_2$  within the temperature range 180–300 K.

The other resonance observed in the  $^1\text{H}$  NMR spectra that occurs close to the position of the residual  $\text{CH}_2\text{Cl}_2$  solvent signal in  $\text{CD}_2\text{Cl}_2$  is a singlet at  $\delta = 5.49$  ppm [2H,  $-\text{CH}_2\text{py}$ ] which remains sharp down to 253 K. Upon further lowering of the temperature it broadens and finally splits into two signals at 180 K. This is attributed to the immobility of the molecule at low temperatures and the hindered rotation around the carbon bonds of the methylene bridge. As a result, the two hydrogen atoms become diastereotopic. To obtain sharp signals even lower temperatures would have been necessary but could unfortunately not be achieved because of the freezing point of the solution. Above 233 K the  $[-\text{CH}_2\text{py}]$  resonance and the signal due to residual  $\text{CH}_2\text{Cl}_2$  are distinguishable from one another.

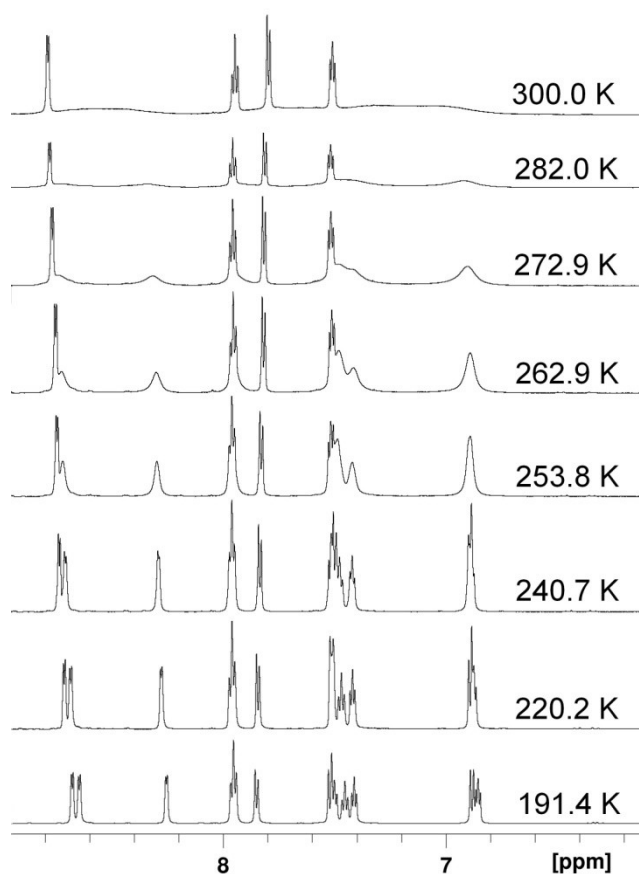


**Fig. 48**  $^1\text{H}$  NMR spectra of **3b** at variable temperatures in  $\text{CD}_2\text{Cl}_2$

At 180 K, 11 of the 12 expected resonances are observed in the aromatic region of the  $^1\text{H}$  NMR spectrum and can, except one overlap of the resonances of two protons at  $\delta = 7.95$  ppm, clearly be distinguished. With two-dimensional COSY, TOCSY and EXSY NMR experiments we are able to assign the signals of the different hydrogen atoms (for the full set of one- and two-dimensional NMR spectra and signal assignment see Supporting Information). At 253 K, the resonances at  $\delta = 8.6, 8.2, 7.5, 7.4$  and  $6.8$  ppm begin to broaden. As the temperature is increased these resonances begin to broaden further and at 300 K have nearly reached the fast exchange of the pyridyl rings. A further increase of the temperature was not possible due to the low boiling point of  $\text{CD}_2\text{Cl}_2$ .

The proposed exchange mechanism to account for the observed fluxional behaviour in solution is presented in Figure 49.

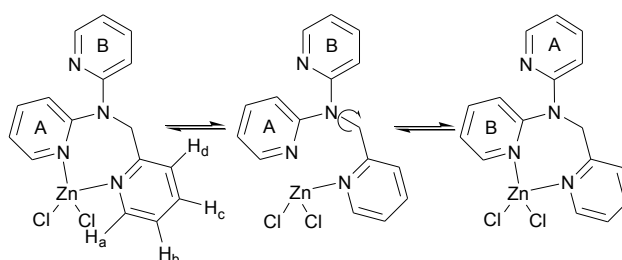


**Fig. 49** Exchange mechanism in the coordination sphere of  $[(\text{L1})\text{ZnCl}_2]$  (**3b**)

We propose that the “long arm” of **L1**, *i.e.* the 2-pyridylmethyl “arm” remains coordinated to the zinc atom, and that the 2,2′-dipyridylamine moiety of **L1** rotates



around the carbon-carbon bond shown in Figure 54. The protons ( $H_a$ – $H_d$ ) of the pyridyl ring of the “long arm” of **L1** in complex **3b** are labeled in Scheme 1. The assignments are based on the splitting patterns and the two-dimensional NMR spectroscopy. Assignments of  $H_c$  and  $H_b$  are additionally based on greater stabilisation of electron withdrawal in the *para* position, compared to the *meta* position, and previous assignments of pyridine hydrogen atoms in similar metal complexes.<sup>169-170</sup>

The proposed exchange mechanism accounts for the fact that the  $H_a$ – $H_d$  signals always remain sharp and the other 8 proton signals broaden at higher temperatures, due to an exchange process occurring between the coordinated and uncoordinated pyridyl rings (labelled A and B in Figure 49) of the 2,2'-dipyridylamine moiety. The mechanism becomes evident from the exchange signals in the 2D-EXSY spectrum depicted in Figure 50 (for assignment of the labelled exchange peaks see Supporting Information).

A very similar exchange process was described previously for  $[Zn(\text{tpa})Cl_2]$ .<sup>152</sup> However, a complete assignment of the NMR signals was not presented. In order to compare the exchange mechanisms of **tpa**- and **L1**-zinc complexes additional NMR experiments with  $[Zn(\text{tpa})Cl_2]$  and a mixture of **L1** and  $Zn(OTf)_2$  (**3e**) were performed. Therefore, the resonances for these zinc complexes can be clearly assigned, and it is possible to inspect the differences of the exchange in these molecules. Further information on the NMR spectroscopic data of  $[Zn(\text{tpa})Cl_2]$  and **3e** are provided in the Supporting Information. **3e** has reached the fast exchange at 300 K. Above 253 K all signals broaden and no sharp resonances can be observed. Furthermore, a shift of some resonances occurs. Therefore, the mode of coordination of this compound in solution at room temperature cannot be clearly defined.

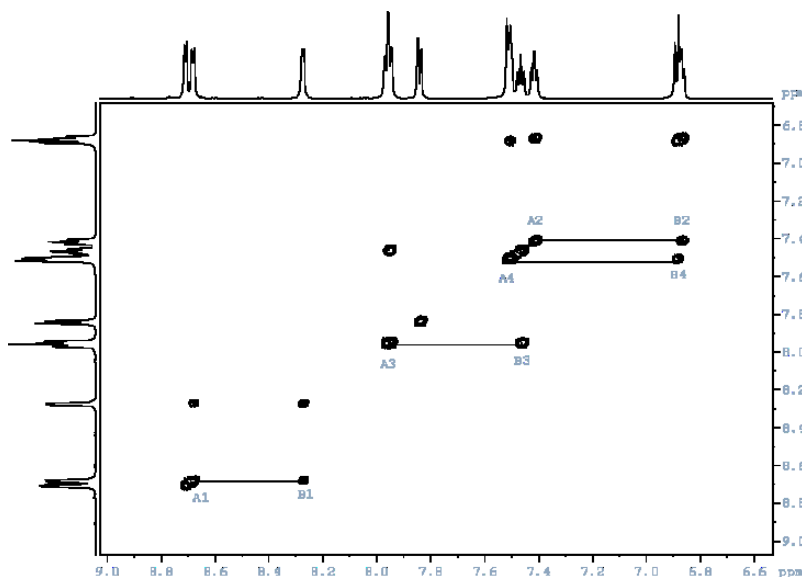
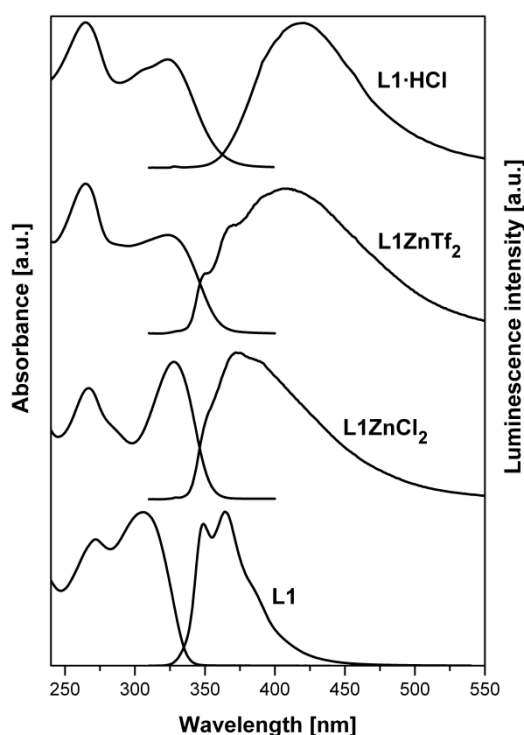


Fig. 50 2D-EXSY spectrum in  $CD_2Cl_2$  of **3b** at 219 K

Below 205 K the 8 expected resonances of the chloride complex of **tpa** are clearly observable and sharpen until they can be definitely assigned at 186 K.

#### 4.1.2.6 Luminescence

Wang and co-workers reported that zinc complexes of **tpa** and a derivative in THF solution showed strong blue emission when excited with UV-light.<sup>152</sup> Because **L1** is structurally related to **tpa** we became interested in studying the luminescence behaviour of our complexes. Indeed, strong blue luminescence under UV-excitation was observed for **3b**. To avoid complications due to potential solvent effects on the luminescence properties, dichloromethane was chosen to compare the emission spectra of the uncoordinated ligand **L1**, the protonated ligand **L1·HCl**, and the compounds **3b** and **3e**. Figure 51 displays the overlaid absorption and emission spectra of the four compounds.



**Fig. 51** Electronic absorption and emission spectra of the uncoordinated ligand **L1**, **L1·HCl**, and the compounds **3b** and **3e** in dichloromethane

The absorption spectra of the free and the protonated ligand **L1** and the corresponding zinc complexes are dominated by intraligand  $\pi$ - $\pi^*$  transitions with UV-maxima in the 250–350 nm region. The emission spectrum of **L1** at room temperature in solution shows a well-resolved vibronic structure with two main peaks at 349 nm and 364 nm ( $\lambda_{\text{max}}$ ) and a quantum yield of  $\Phi = 0.05$ , assigned to a fluorescence of  $\pi$ - $\pi^*$  origin from the lowest excited singlet state, which is typical for the presence of a 2-aminopyridine related chromophore where  $n$ - $\pi^*$  transitions are expected to be higher in energy.<sup>171</sup> When **L1** is protonated *in-situ* with HCl gas, a broad, unstructured luminescence band with a maximum at 439 nm is observed (Figure 51). This strong bathochromic shift of about 6000  $\text{cm}^{-1}$  is tentatively ascribed to the effects of intramolecular hydrogen-bond formation, which forces two of the pyridine rings into a coplanar configuration, thus

forming a more delocalized blue fluorescent 2,2'-dipyridylamine subunit (Figure 44). This interaction is also reflected in the absorption spectral changes which accompany the interconversion between **L1** and **L1·HCl**. A quite similar mechanism for tuning the excited state properties of luminescent materials by protonation of pyridine nitrogens and intramolecular hydrogen bonding has recently been proposed in the literature.<sup>172</sup>

The more complex luminescence behaviour of the zinc derivatives **3b** and **3e** (Figure 45) is best described as an intermediate situation between the free ligand **L1** and the protonated species **L1·HCl**. On the one-hand, the metal complexation induces a coplanar configuration of pyridyl and methylpyridyl subunits with a broad, red-shifted luminescence as observed for the protonated ligand. On the other hand, the dynamics of the coordination sphere in solution (Figure 49) leads to a significant equilibrium contribution of non-coordinated 2-aminopyridine chromophores similar to the situation in the **L1** system. This behaviour is reflected by the occurrence of a vibronic fine structure in the steady-state emission spectra, which overlays the broad unstructured luminescence band ascribed to the presence of a metal coordinated dipyridyl-type moiety (Figure 51). The emission in the visible spectral region with lifetimes in the nanosecond regime ( $\tau = 4.2$  ns,  $\Phi = 0.06$  for **3b** and  $\tau = 4.4$  ns,  $\Phi = 0.04$  for **3e**) is therefore assigned to an intraligand fluorescence from the lowest  $\pi$ - $\pi^*$  excited singlet state of the coordinatively saturated zinc complexes. A similar blue photoluminescence was also observed for zinc cyanido complexes with the ligand 2,2'-dipyridylamine.<sup>173</sup>

The different emission maxima of the chlorido compound **3b** (372 nm) and the triflate derivative **3e** (409 nm) clearly indicate that the features of the intraligand fluorescence of the **L1** metal complexes are quite sensitive to electronic effects induced by variations in the zinc coordination sphere. Due to the weakly coordinating triflate ion the net positive charge of the zinc atom of **3e** is much higher than in **3b**. This is reflected in the larger bathochromic shift of the emission maximum of  $4200\text{ cm}^{-1}$  relative to the free ligand. Coordinating solvents may also modify the luminescence features of these compounds. Due to the solid state structure of compound **3c** differing drastically from that of comparable zinc complexes we additionally performed fluorescence measurements using methanol as a solvent. Here **3b** showed only a bathochromic shift of  $3900\text{ cm}^{-1}$  compared to the uncoordinated ligand **L1**.

In THF solution compound **3b** shows strong emission at 423 nm when excited with light of wavelength 324 nm. Surprisingly we could observe the large bathochromic shift reported by Wang et al. for the emission band of the zinc complex of **tpa** in THF compared to the emission of the ligand only at unusual high concentrations.<sup>152</sup>

In general, the structural differences of the ligands **Me-bispic**, **tmpa**, **L2**, **L1**, and **tpa** are supposed to have a great influence on the emission properties of these compounds as well as on their zinc complexes. Thus, the emission of comparable zinc complexes of **L2**, **tmpa** and **Me-bispic** in methanol solution is much weaker compared to the corresponding complexes of **tpa** and **L1** respectively. This may be due to the fact that only **tpa** and **L1** provide the possibility of forming a rigid subunit consisting of two coplanar pyridyl groups which are connected by only one bridging atom.

### 4.1.3 Conclusions

In this work the synthesis and characterisation of zinc complexes of a set of nitrogen-containing ligands, which can all be derived from **tmpa** or **tpa**, has been reported. It turned out to be quite interesting – that in contrast to our expectations – the zinc complexes with the ligands **L1** and **L2** showed significant differences in their molecular structures in comparison to the according copper(II) complexes investigated previously.<sup>151</sup> Furthermore, fluxional behaviour of complex **3b** in solution could be observed by NMR spectroscopic measurements. Similar observations have been made for the related tpa complexes studied by Yang et. al.<sup>152</sup> We were now able to assign all resonances in the NMR spectroscopic experiments of the zinc complexes **3b** and **3e** as well as of [Zn(**tpa**)Cl<sub>2</sub>] by one- and two-dimensional NMR spectroscopy at variable temperatures. Most interestingly are the luminescence properties of these compounds. In dichloromethane the bathochromic shift of the emission band increases with the positive charge of the coordinated zinc atom at the conjugated  $\pi$ -system of **L1**. Thus, a dependence of the emission wavelengths and the positive charge of the metal atom in the examined compounds could be demonstrated. Additionally, the chloride complex in methanol exhibits a large bathochromic shift in the emission of 40 nm compared to the uncoordinated ligand and **3e**. One could therefore think of an application of zinc complexes with weakly coordinating anions as fluorescent chloride sensors in protic solvents. Intensive blue fluorescence is also important in regard to the development of blue light emitting diodes.

### 4.1.4 Experimental Section

*Materials and Methods.* Reagents and solvents used were of commercially available reagent quality.

The <sup>1</sup>H NMR spectra of **1a**, **1b** and **3c** were measured on a Bruker Avance II 400 spectrometer equipped with a 5 mm BBO Z-gradient probe.

All one-dimensional and two-dimensional <sup>1</sup>H NMR experiments for compound **2**, **3b**, **3e** and [Zn(**tpa**)Cl<sub>2</sub>] were performed on a Bruker Avance III 600 spectrometer equipped with a 5 mm BBO Z-gradient probe. To obtain the complete <sup>1</sup>H chemical shift assignments the structure elucidation was based on the application of homonuclear <sup>1</sup>H,<sup>1</sup>H correlation spectroscopy (COSY, TOCSY (not shown)) and 2D exchange NMR (EXSY). The data were collected and processed by TOPSPIN software (Bruker) running on a PC with Microsoft Windows<sup>XP</sup>. The two-dimensional experiments were performed using Bruker standard pulse sequences and parameters. The temperatures for all measurements were calibrated with the Bruker methanol sample and were controlled by a Bruker BVT 3000 temperature unit.

Chemical shifts are reported in ppm ( $\delta$  scale) using TMS as internal standard or the solvent signal as secondary standard. Multiplicities of NMR signals are designated as s (singlet), d (doublet), t (triplet), q (quartet), br (broad), m (multiplet, for unresolved lines), etc.

IR spectra were recorded as KBr pellets using a Bruker *IFS 25*.

The luminescence measurements were carried out in spectrograde solvents at room temperature using a Horiba Jobin Yvon Fluorolog-3 spectrofluorometer equipped with two double-grating monochromators, a R928P photomultiplier, and an FL-1040 phosphorimeter. All emission spectra were corrected for wavelength-dependent instrument and detector response and verified by collecting the corresponding excitation spectra. Emission quantum yields were measured relative to quinine sulfate ( $\Phi = 0.55$  in 0.5 M H<sub>2</sub>SO<sub>4</sub>).<sup>174</sup> Lifetime data were obtained by time-correlated single photon counting (TCSPC) experiments on a PicoQuant lifetime fluorescence spectrophotometer (FluoTime 100) equipped with a TimeHarp 200 PCI-board and a PDL 800-B pulsed diode laser driver at 10 MHz repetition rate. A sub-nanosecond pulsed LED (PLS-340-10) with an excitation wavelength of 334 nm was used as the light-source. The instrument response function (IRF) was 30 ps.

Elemental Analysis was carried out using Carlo Erba EA 1108 instrument.

FDMS spectra were performed on a Jeol JM 700 mass spectrometer.

#### 4.1.4.1 X-ray Structure Determination of 1–3

Single crystals were coated with protective perfluoropolyether oil and mounted on a glass fiber. Data for **1a** were collected on a Nonius MACH3 diffractometer at 173(2) K and for **1b**, **2** and **3b** on a Nonius Kappa CCD diffractometer at 100(2) K and 173(2), respectively. The remaining crystallographic data was collected on a STOE IPDS at 193(2) K or 203(2) K for **3d** respectively (MoK $\alpha$ ,  $\lambda = 0.71073$  Å, graphite-monochromator). An absorption correction was not applied for compounds **1c**, **3a**, **3c**, and **3d** measured on the STOE IPDS due to poor apperative possibilities. Furthermore the rather little effect that can be expected on the crystal structures of the copper and zinc salts presented herein did not justify the effort. Unfortunately, all attempts to receive better single crystals, that should lead to better *R*-values for these four compounds, failed. In addition apparative deficits are accountable for the poor *R*-values of some of the compounds.

Except for **3c** space groups were determined from systematic absences. All structures were solved by direct methods and refined on *F*<sup>2</sup> using full-matrix least-squares techniques.<sup>112-113</sup> All non-hydrogen atoms were refined with anisotropic thermal parameters.

Crystallographic data for the structures reported in this paper have been deposited with the Cambridge Crystallographic Data Centre as supplementary publication no. CCDC-724313 for **1a**, CCDC-724312 for **2** and CCDC-796270 – CCDC-796275 for **1b** – **3d**. Copies of the data can be obtained, free of charge from The Cambridge Crystallographic Data Centre via [www.ccdc.cam.ac.uk/data\\_request/cif](http://www.ccdc.cam.ac.uk/data_request/cif).

#### 4.1.4.2 Synthesis of Ligands

Ligands **L1** and **L2** were prepared as previously reported.<sup>151</sup> Bis(2-pyridylmethyl)amine was prepared according to a literature procedure with slight modifications.<sup>166</sup> **Me-bispic** was prepared according to a new method described recently.<sup>156</sup>

#### 4.1.4.3 Preparation of Zinc(II) Complexes

##### 4.1.4.3.1 General Procedure

A methanol solution of the respective zinc(II) salt was added to a solution of ligand **L1** or **L2** in methanol (5.0 mL). Precipitation of the respective zinc(II) complex of **L1** or **L2** occurred within a few minutes. In all cases the complexation reactions were allowed to stir for 1 h before the product was collected.

##### 4.1.4.3.2 [(L2)ZnCl<sub>2</sub>] (1a)

ZnCl<sub>2</sub>·2H<sub>2</sub>O (0.062 g, 0.36 mmol) dissolved in methanol (2.0 mL) was added to a solution of **L2** (0.10 g, 0.36 mmol) in methanol (5.0 mL). The pale yellow solution was stirred at room temperature and within 1 min a white precipitate formed. The reaction was allowed to continue for 1 h, stopped, and the product collected by filtration, washed with a little methanol, dried *in vacuo* to yield **2a** as a white solid (0.090 g, 0.22 mmol, 56%). Anal. Calcd for C<sub>17</sub>H<sub>16</sub>Cl<sub>2</sub>N<sub>4</sub>Zn (412.63): C, 49.48; H, 3.91; N, 13.58%. Found: C, 49.34; H, 3.68; N, 13.28%. FD MS (CH<sub>3</sub>CN) *m/z* = 377 (*M* – Cl<sup>–</sup>). IR (KBr disc / cm<sup>–1</sup>): 3444 (m, br), 3100 (m), 3067 (m), 2946 (w), 2909 (w), 1611 (s), 1591 (s), 1573 (m), 1480 (s), 1434 (s), 1426 (s), 1387 (m), 1335 (m), 1318 (m), 1309 (m), 1286 (m), 1273 (m), 1247 (m), 1222 (m), 1161 (m), 1154 (m), 1103 (w), 1093 (w), 1065 (m), 1057 (m), 1043 (w), 1025 (m), 984 (w), 960 (w), 941 (w), 895 (w), 866 (w), 841 (w), 830 (w), 799 (m), 778 (s), 740 (m), 725 (w), 648 (w), 630 (w), 574 (w), 536 (m), 465 (w), 427 (w), 419 (w), 409 (w). <sup>1</sup>H-NMR at 297 K (DMSO-*d*<sub>6</sub>, 400 MHz) δ ppm: 8.54 (d, 2H) 8.03 (d, 1H) 7.75 (t, 2H) 7.45 (t, 1H) 7.28 (m, 4H) 6.61 (m, 2H) 4.92 (s, 4H).

##### 4.1.4.3.3 [(L2)Zn(H<sub>2</sub>O)(OTf)]OTf (1b)

Solid Zn(OTf)<sub>2</sub> (0.13 g, 0.36 mmol) was added to a solution of **L2** (0.10 g, 0.36 mmol) in acetonitrile (5.0 mL). The colourless solution was stirred at room temperature. The reaction was allowed to continue for 1 h and then stopped. The acetonitrile was removed *in vacuo*. Dichloromethane and the minimal amount of acetonitrile were added to re-dissolve the white semi-solid. Diethyl ether was added, and the addition was stopped just before precipitation of the complex commenced. The reaction flask was then transferred to the freezer compartment of the refrigerator and within the period of one week large transparent blocks of **2b** formed. (0.090 g, 0.14 mmol, 38%).

FD MS (CH<sub>2</sub>Cl<sub>2</sub>) *m/z* = 491 [(**L2**)Zn(OTf)]<sup>+</sup>. IR (KBr disc / cm<sup>–1</sup>): 3386 (m, br), 3092 (w), 3022 (w), 2952 (w), 2319 (w), 2252 (w), 1993 (w), 1909 (w), 1869 (w), 1665 (m), 1612

(s), 1592 (s), 1575 (m), 1493 (s), 1477 (s), 1455 (s), 1435 (s), 1411 (m), 1390 (m), 1366 (m), 1335 (m), 1292 (s), 1231 (s), 1192 (s), 1165 (s), 1109 (m), 1096 (m), 1059 (m), 1025 (s), 958 (m), 938 (m), 850 (w), 817 (w), 791 (s), 783 (m), 769 (m), 724 (m), 629 (s), 576 (m), 554 (m), 536 (m), 517 (s), 465 (w), 456 (w), 420 (m).  $^1\text{H}$  NMR at 296 K ( $\text{CD}_6\text{CO}$ , 400 MHz)  $\delta$  ppm: 8.87 (d, 2H py-H) 8.27 (d, 1H, py-H) 8.23 (t, 2H, py-H) 7.92 (t, 1H, py-H) 7.78 (d, 2H, py-H) 7.74 (t, 2H, py-H) 7.53 (d, 1H, py-H) 7.27 (t, 1H, py-H) 5.21 (s, 4H,  $\text{CH}_2$ ).

#### 4.1.4.3.4 [(Me-bispic)ZnCl<sub>2</sub>] (2)

$\text{ZnCl}_2$  (0.064 g, 0.47 mmol) in methanol (1 mL) was added dropwise to a stirred solution of **Me-bispic** (0.10 g, 0.47 mmol) in methanol (2 mL). On addition of the metal salt a pale-coloured precipitate formed. The precipitate was collected, washed with a little diethyl ether and methanol, and dried to yield **2** as a cream coloured solid (0.13 g, 0.37 mmol, 80%). Analysis for  $\text{C}_{13}\text{H}_{15}\text{Cl}_2\text{N}_3\text{Zn}$  (349.57): calcd C 44.67, H 4.33, N 12.02, found C 44.62, H 4.56, N 11.91. IR (KBr disc /  $\text{cm}^{-1}$ ): 3453 (w, br), 3072 (w), 3060 (w), 3027 (w), 3001 (w), 2964 (w), 2914 (w), 2859 (w), 1602 (s), 1574 (m), 1478 (m), 1449 (m), 1441 (m), 1412 (w), 1384 (w), 1351 (w), 1361 (w), 1294 (m), 1285 (w), 1265 (w), 1248 (w), 1224 (w), 1187 (w), 1160 (m), 1131 (w), 1120 (w), 1102 (m), 1051 (m), 1019 (s), 991 (w), 972 (w), 963 (w), 906 (w), 869 (m), 819 (w), 780 (m), 773 (m), 732 (w), 649 (w), 641 (m), 515 (w), 480 (w), 451 (w), 420 (w).  $^1\text{H}$  NMR at 295 K ( $\text{CDCl}_3$ , 600 MHz)  $\delta$  ppm: 9.21 (d, 2H) 7.87 (dt, 2H) 7.49 (t, 2H) 7.31 (d, 2H) 4.36 (s, 2H) 3.93 (s, 2H) 2.29 (s, 3H). Needle shaped crystals suitable for single crystal X-ray diffraction analysis were grown by carefully layering a chloroform containing solution of **2** with diethyl ether.

#### 4.1.4.3.5 [L1H]OTf (3a)

Single crystals of **3a** suitable for single crystal X-ray structure analysis were grown in a methanol solution of 0.10 g (0.37 mmol) **L1** and 0.69 g (0.19 mmol)  $\text{Zn}(\text{OTf})_2$  by slow ether diffusion at  $-30^\circ\text{C}$ . After several days colourless block shaped crystals of **3a** and a white precipitate formed.

#### 4.1.4.3.6 [(L1)ZnCl<sub>2</sub>] (3b)

$\text{ZnCl}_2 \cdot 2\text{H}_2\text{O}$  (0.066 g, 0.38 mmol) dissolved in methanol (2.0 mL) was added to a solution of **L1** (0.10 g, 0.38 mmol) in methanol (3 mL). The pale yellow solution was stirred at room temperature and within 1 min a cream-coloured precipitate formed. The reaction was allowed to continue for 1 h, stopped, and the product collected by filtration, washed with a little methanol, dried *in vacuo* to yield **1** as a cream coloured solid (0.12 g, 0.28 mmol, 72%). Anal. Calcd for  $\text{C}_{16}\text{H}_{14}\text{Cl}_2\text{N}_4\text{Zn}$  (398.60): C, 48.21; H, 3.54; N, 14.06%. Found: C, 48.14; H, 3.38; N, 13.80%. FDMS ( $\text{CH}_3\text{CN}$ )  $m/z = 363$  ( $M - \text{Cl}^-$ ). IR (KBr disc /  $\text{cm}^{-1}$ ): 3232 (br), 3230 (w), 3215 (w), 3148 (w), 3073 (w), 3029 (w), 2968 (w), 2937 (w), 2861 (w), 1606 (m), 1590 (m), 1564 (m), 1475 (s), 1429 (s), 1378 (m), 1320 (m),

1288 (m), 1249 (w), 1211 (m), 1158 (m), 1108 (w), 1079 (w), 1058 (w), 1028 (m), 1000 (w), 980 (w), 877 (w), 832 (w), 800 (w), 772 (m), 649 (w), 610 (w), 589 (w), 527 (w), 419 (w).  $^1\text{H}$  NMR at 296 K ( $\text{CD}_2\text{Cl}_2$ , 600 MHz)  $\delta$  ppm: 8.79 (d, 1H) 8.70-8.32 (broad s) 7.95 (dt, 1H) 7.80 (d, 1H) 7.51 (t, 1H) 7.43-6.81 (broad m) 5.44 (s, 2H)

#### 4.1.4.3.7 $[(\text{L1})_2\text{Zn}(\text{MeOH})_2](\text{OTf})_2$ (**3c**)

$\text{Zn}(\text{OTf})_2$  (0.14 g, 0.38 mmol) in methanol (2.0 mL) was added to a solution of **L1** (0.10 g, 0.38 mmol) in methanol (2.0 mL). Colourless block-shaped crystals were obtained by diethyl ether diffusion into the yellow solution at  $-20^\circ\text{C}$ .  $^1\text{H}$  NMR of the crystals at 295 K was performed without further drying steps. ( $\text{CH}_3\text{OH} + \text{D}_2\text{O}$ , 400 MHz), methylpyridyl arm = mpy; pyridyl arm = py, methyl bridge = mb)  $\delta$  ppm: 8.48 (d, 1H mpy-H meta) 8.16 (s br, 2H py-H meta) 7.96 (t, 3H mpy-, py-H, para) 7.76 (d, 1H mpy-H, ortho) 7.51 (d, 2H py-H) 7.38 (t, 1H mpy-H, ortho) 7.26 (s broad, 2H py-H) 5.52 (s, 2H mb-H).

#### 4.1.4.3.8 Mixture of **L1** and $\text{Zn}(\text{OTf})_2$ (**3e**)

$\text{Zn}(\text{OTf})_2$  (0.28 g, 0.76 mmol) was added dropwise to a solution of **L1** (0.20 g, 0.76 mmol) in methanol (4 mL). The pale yellow solution was added dropwise to diethyl ether (100 mL). A white precipitate formed, which was left to stand overnight at  $-30^\circ\text{C}$ . The precipitate was decanted and solvent residues removed *in vacuo* to yield **3e** (0.04 g, 0.06 mmol, 8 %). IR (KBr disc /  $\text{cm}^{-1}$ ): 3382 (m, br), 3072 (m, br), 2309 (w), 1601 (s), 1578 (m), 1471 (s), 1444 (s), 1380 (m), 1346 (m), 1251 (s, br), 1162 (s), 1085 (m), 1030 (s), 898 (w), 877 (w), 834 (w), 799 (m), 776 (m), 759 (m), 641 (s), 602 (m), 590 (m), 575 (m), 517 (m), 472 (w), 422 (m).  $^1\text{H}$  NMR at 295 K: ( $\text{CD}_2\text{Cl}_2$ , 600 MHz)  $\delta$  ppm: 8.56 (s br, 1H) 8.02 (t br, 1H) 7.81 (d, 1H) 7.72 (t br, 3H) 7.45 (s, 1H) 7.10 (s, 2H) 6.96 (s, 2H) 5.42 (s, 2H).

#### 4.1.4.4 Preparation of Copper(I) Complexes

##### 4.1.4.4.1 General Procedure

The copper(I) complexes were prepared under inert atmosphere in the glove box. Only commercially available extra dry solvents were used and diluted under argon prior to use. The copper(I) salts were prepared according to a well-known procedure.

##### 4.1.4.4.2 $[(\text{L2})_3\text{Cu}_2](\text{BPh}_4)_2$ (**1c**)

$[\text{Cu}(\text{CH}_3\text{CN})_4]\text{PF}_6$  (0.12 g, 0.33 mmol) in acetone (3.0 mL) was added to **L2** (0.10 g, 0.36 mmol) dissolved in acetone (3.0 mL). A solution of  $\text{Na}(\text{BPh}_4)$  (0.11 g, 0.33 mmol) in acetone (2.0 mL) was added to the yellow solution. Diethyl ether diffused in at  $-40^\circ\text{C}$ . Within a period of 6 weeks yellow crystals suitable for X-ray crystallography formed.



#### 4.1.4.4.3 $[(L1)_2Cu_2](OTf)_2 \cdot 2DMF$ (**3d**)

**L1** (0.72 g, 0.19 mmol) was dissolved in DMF (1 mL). The solution was added dropwise to **L1** (0.050 g, 0.19 mmol) dissolved in DMF (1 mL). After several days at  $-40\text{ }^{\circ}\text{C}$  yellow block shaped crystals formed.

#### 4.1.5 Acknowledgements

We are grateful for the funding of the DFG within the project number SCHI 377/11-1. We would like to thank Prof. Martin Bröring (Phillips University Marburg) and his co-workers for their assistance with our preliminary fluorescence measurements.

### 4.2 Supporting Information and Unpublished Material for Chapter 1.1

#### 4.2.1 NMR Spectroscopy

##### 4.2.1.1 $^1\text{H}$ NMR Spectra at Ambient Temperature

Chemical shifts and multiplicity of the  $^1\text{H}$  NMR spectra for the compounds **1a**, **1b**, **2**, **3b**, **3c** and **3e** reported in the experimental section are taken from the spectra at ambient temperature depicted in the following Figures. Furthermore, the  $^1\text{H}$  NMR spectrum of the compound [**tpa**ZnCl<sub>2</sub>] at ambient temperature is shown in order to compare our data with data already published by Wang *et al.*<sup>152</sup>

##### 4.2.1.1.1 $[L2ZnCl_2]$ (**1a**)

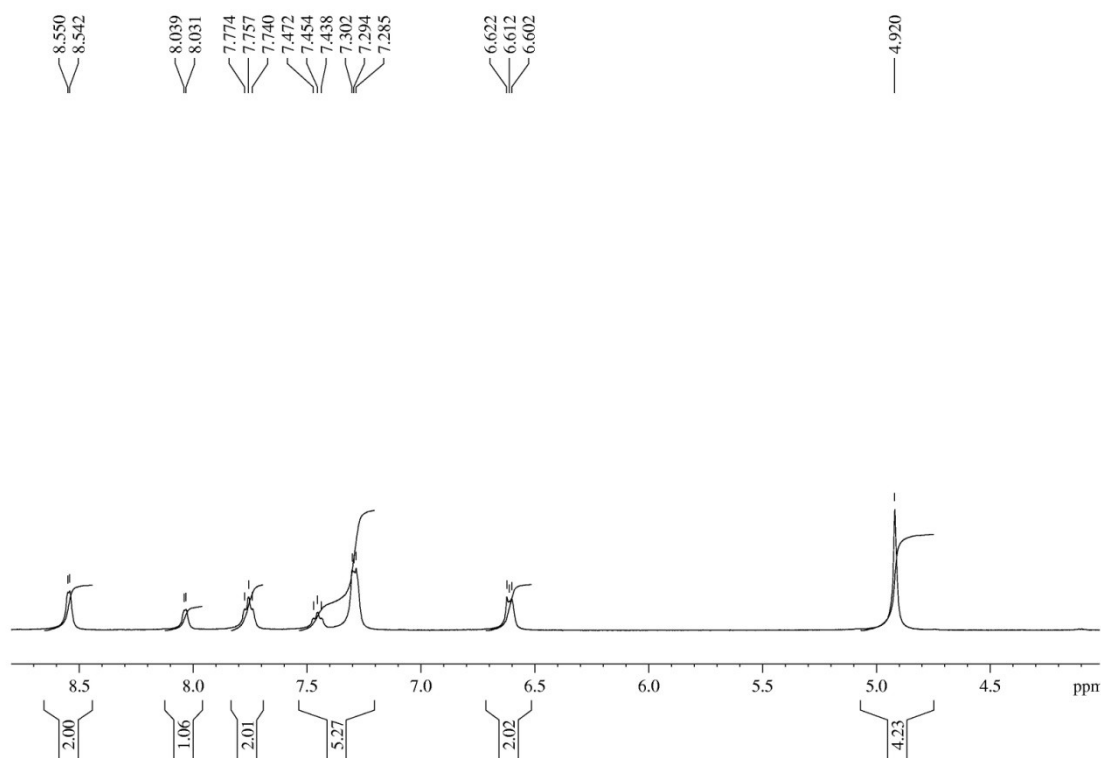
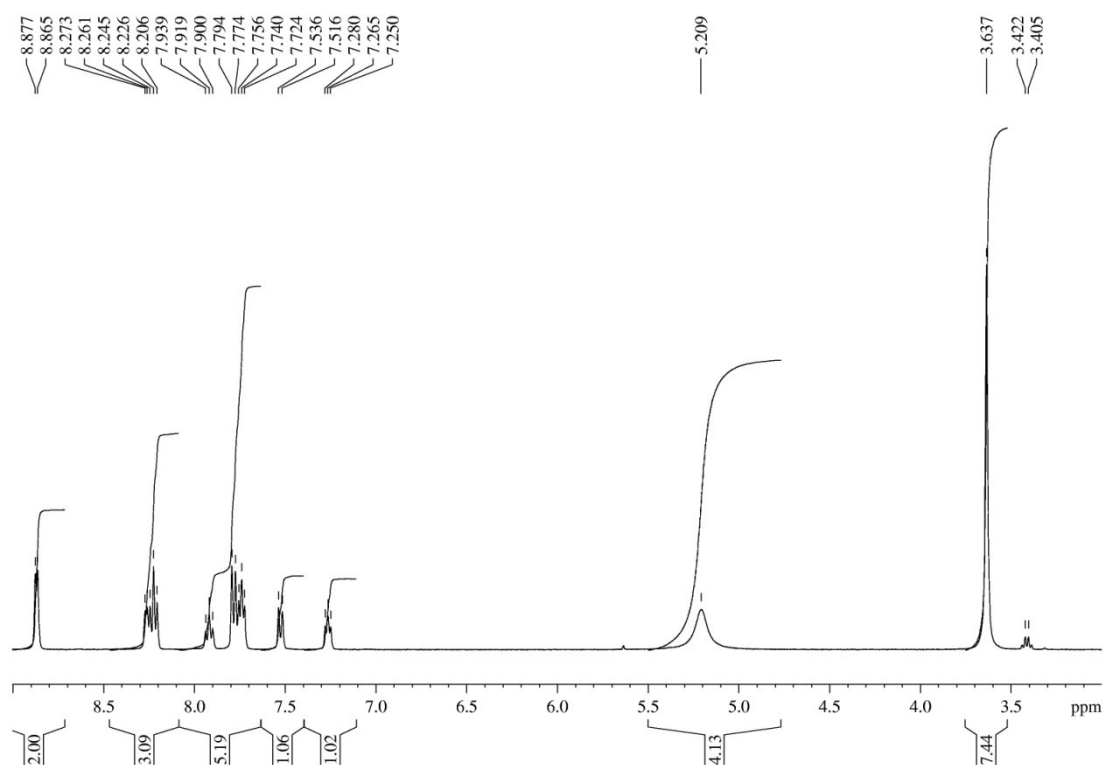
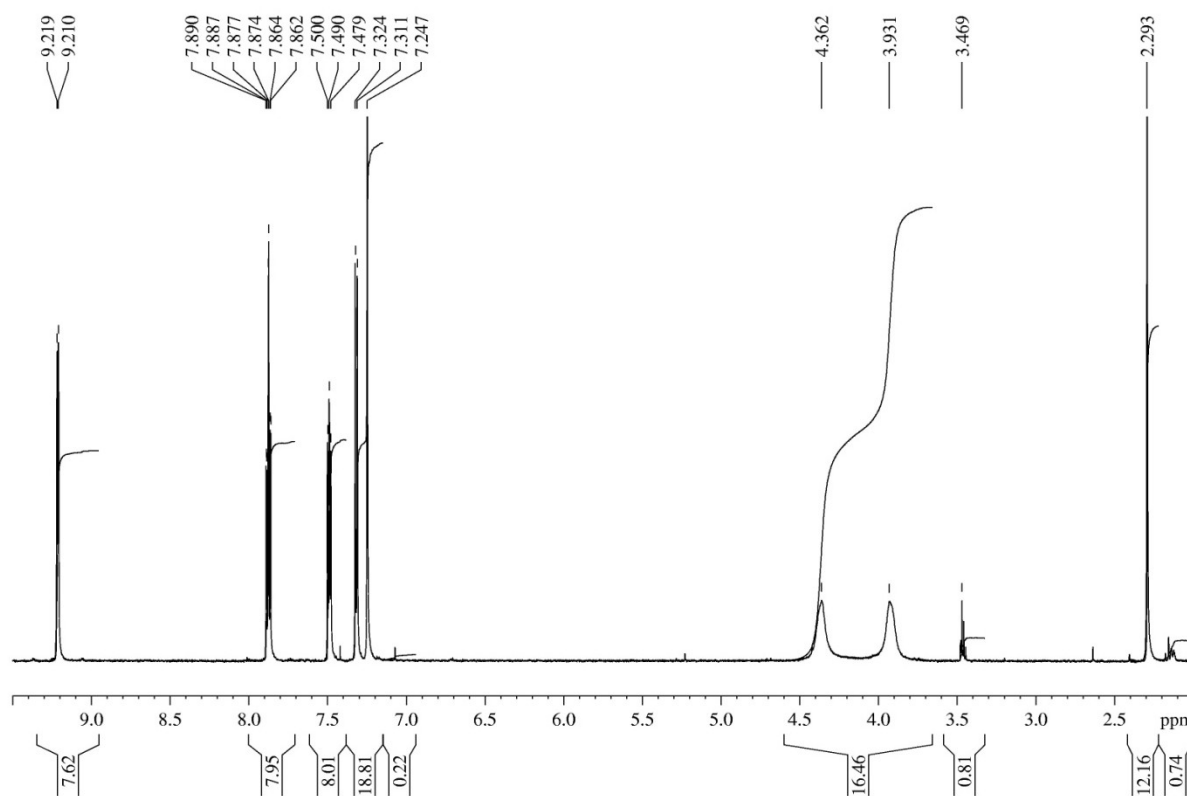
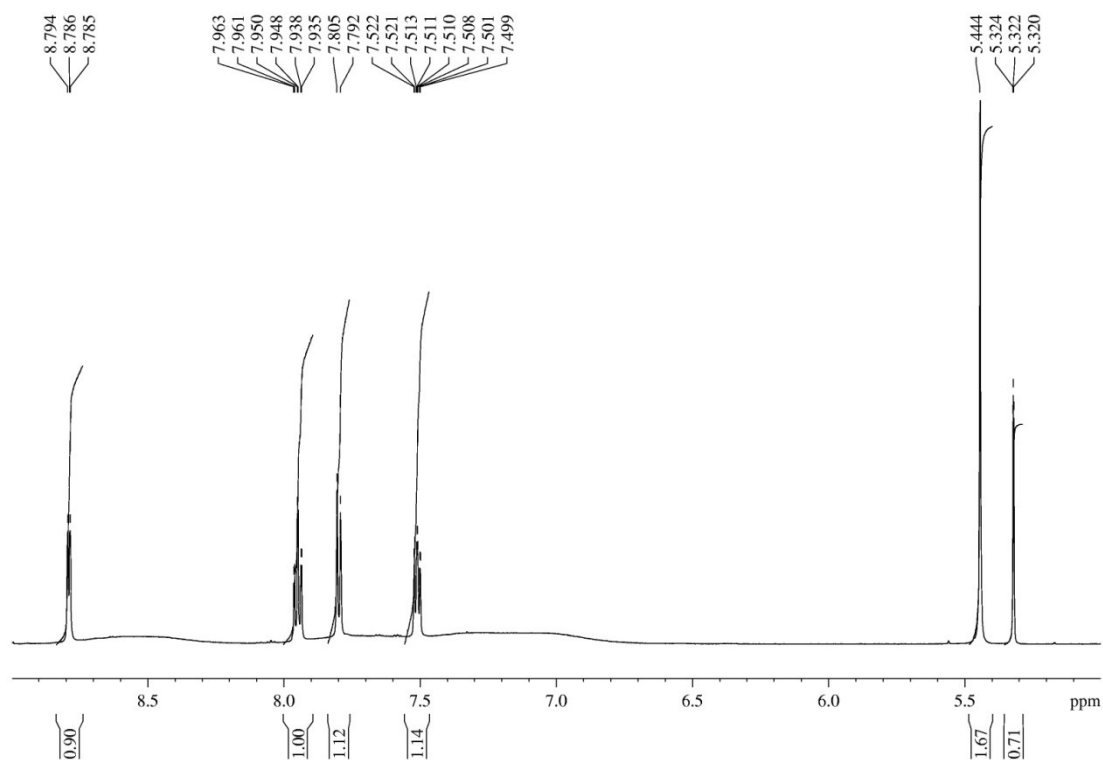
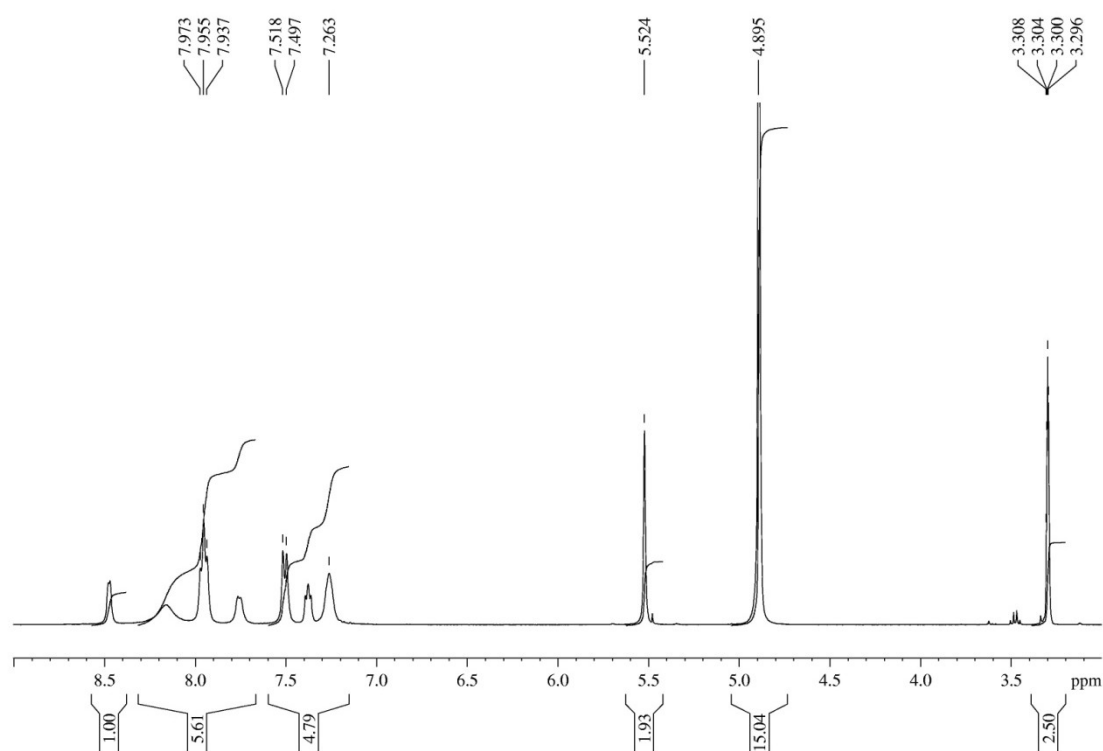
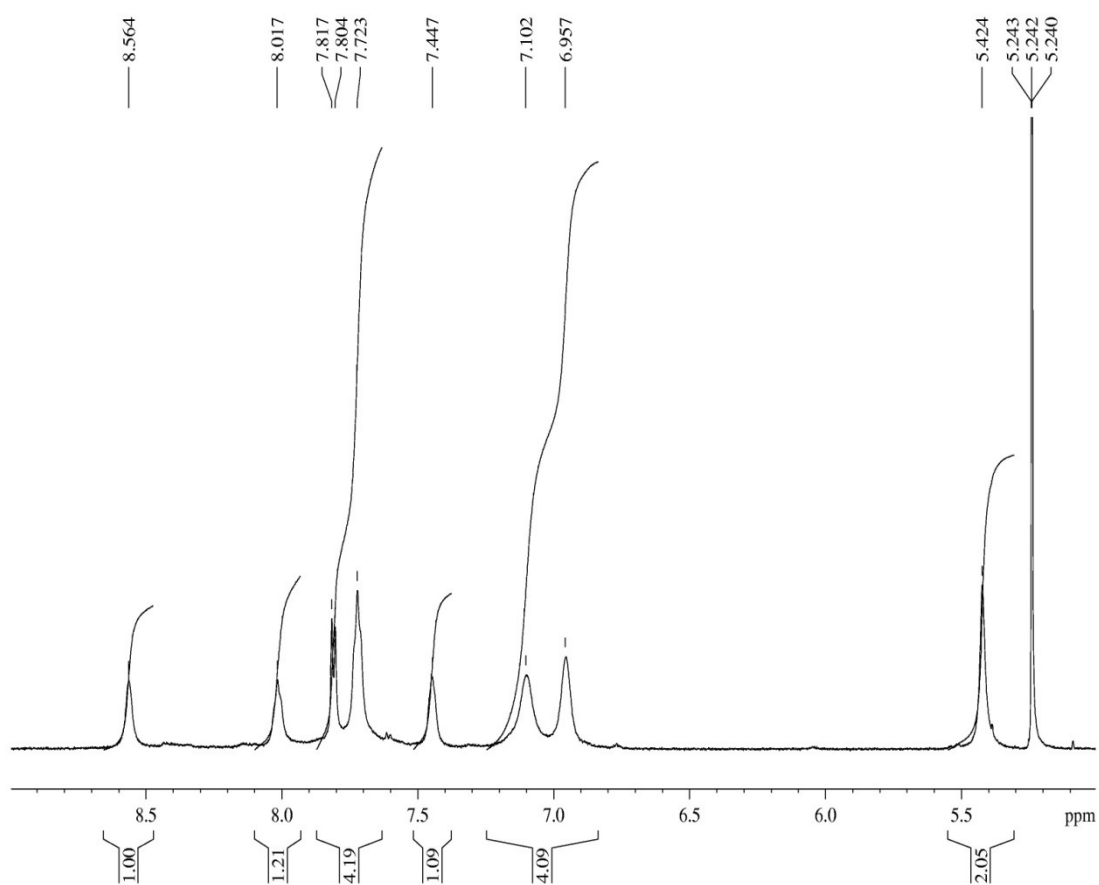
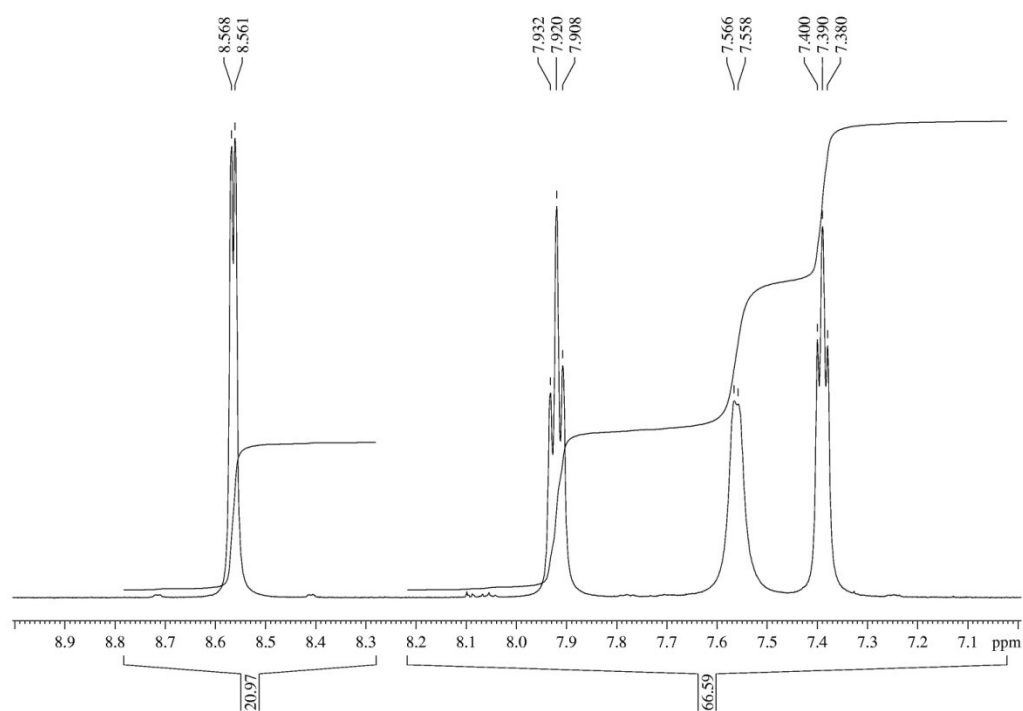


Fig. 52 Section of the  $^1\text{H}$  NMR spectrum of **1a** at 296 K in DMSO- $\text{D}_6$

4.2.1.1.2  $[L2Zn(OTf)(H_2O)]OTf$  (**1b**)Fig. 53 Section of the  $^1H$  NMR spectrum of **1b** at 296 K in  $C_2D_6CO$ 4.2.1.1.3  $[MebispicZnCl_2]$  (**2**)Fig. 54 Section of the  $^1H$  NMR spectrum of **2** at 295 K in  $CDCl_3$

4.2.1.1.4  $[L1ZnCl_2]$  (**3b**)Fig. 55 Section of the  $^1\text{H}$  NMR spectrum of **3b** at 296 K in  $\text{CD}_2\text{Cl}_2$ 4.2.1.1.5  $[(L1)_2Zn(\text{MeOH})_2]\text{OTf}_2$  (**3c**)Fig. 56 Section of the  $^1\text{H}$  NMR spectrum of **3c** at 295 K in  $\text{CH}_3\text{OH} + \text{D}_2\text{O}$

4.2.1.1.6 Mixture of L1 and Zn(OTf)<sub>2</sub> (3e)Fig. 57 Section of the <sup>1</sup>H NMR spectrum of **3e** at 296 K in CD<sub>2</sub>Cl<sub>2</sub>4.2.1.1.7 [tpaZnCl<sub>2</sub>]Fig. 58 Section of the <sup>1</sup>H NMR spectrum of [tpaZnCl<sub>2</sub>] at 296 K in CD<sub>2</sub>Cl<sub>2</sub>

### 4.2.1.2 Variable Temperature $^1\text{H}$ NMR and 2D spectra

All spectra depicted in the following were measured in  $\text{CD}_2\text{Cl}_2$  at 600 MHz using a Bruker Avance III spectrometer if not mentioned otherwise.

#### 4.2.1.2.1 $[\text{MebispicZnCl}_2]$ (**2**)

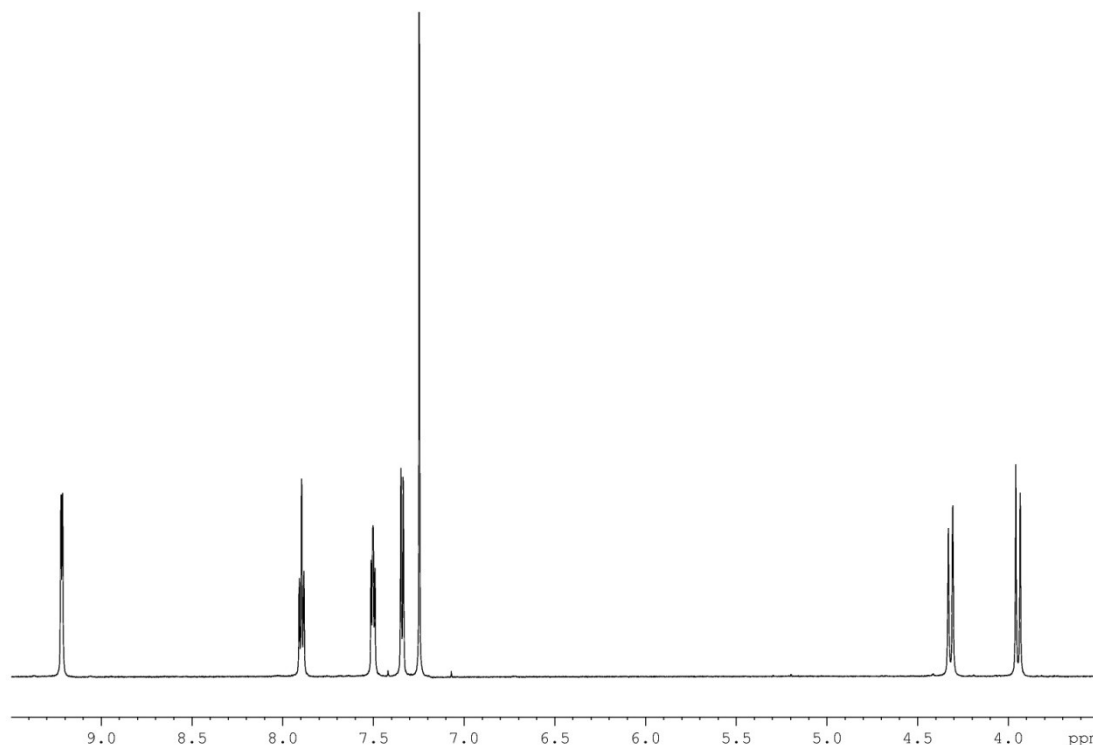


**Fig. 59** Section of the  $^1\text{H}$  NMR spectrum of **2** at 260 K in  $\text{CDCl}_3$

Unlike the  $^1\text{H}$  NMR spectrum of **2** at ambient temperature in Figure 54, the spectrum at 260 K (Figure 59) shows the resolved AB pattern of the diastereotope methylene protons (d, 4.32; d, 3.95).

#### 4.2.1.2.2 $[\text{L1ZnCl}_2]$ (**3b**)

Due to the unusual fluxional behaviour of **3b** in solution that leads to the proposed rotation mechanism (Figure 60), the assignment of protons in the NMR spectroscopy becomes difficult.

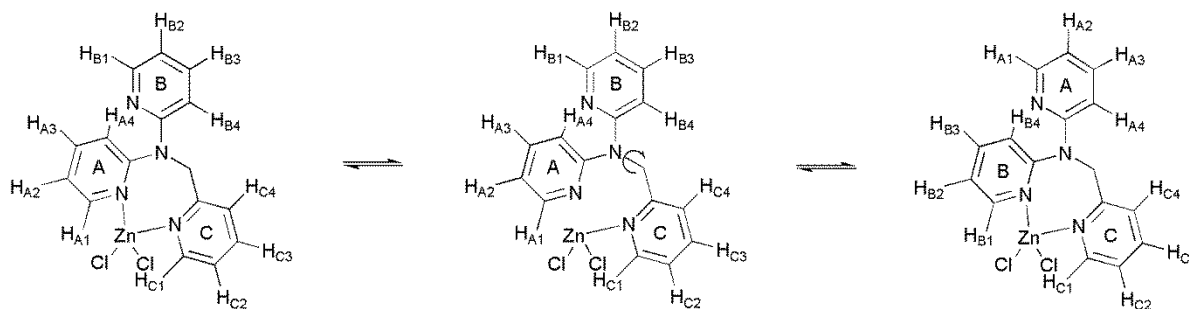


**Fig. 60** Proposed rotation mechanism of **3b** in solution

With low temperature NMR measurements and 2D NMR spectroscopic measurements, we are now able not only to clearly assign all protons to the according resonances but also to prove the rotation mechanism by the exchange signals in the 2D-EXSY spectrum at 219 K. At this temperature, the exchange of protons due to the rotation of the pyridyl rings labelled A and B is slow enough to follow by NMR spectroscopy. All expected exchange signals are visible in the depicted 2D-EXSY spectrum (Figure 65), assignable and labelled with the number of the according proton in Figure 60.

Starting point of the assignment is the COSY signal of  $H_{C4}$  at  $\delta = 7.84$  ppm that shows  $^4J$  coupling to the methylene protons. Combining of COSY and 2D-EXSY signals finally leads to the assignment of  $^1H$  NMR resonances to the full set of protons presented in the following Table 8. Due to an overlap of the signals of  $H_{A3}$  and  $H_{C3}$  at  $\delta = 7.95$ , 11 of the 12 expected resonances can be observed at 180 K.

In the  $^1H$  NMR spectra at variable temperatures depicted in Figures 61, 62 and 63, another interesting phenomenon can be detected. At 253 K, the signal for the methylene protons at a chemical shift of 5.36 starts to broaden and finally splits at 180 K. Two doublets indicate an AB system. Due to the lowered temperature, the two methylene protons become diastereotopic.

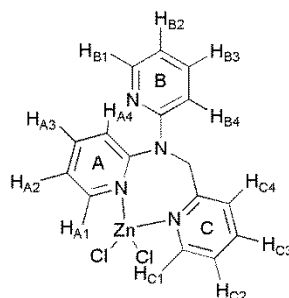


**Fig. 61** ChemDraw representation of **3b** with H labelled A1 to C4

**Table 8** Proton assignment to  $^1H$  signals of **3b** at 180 K

Proton No.	multiplicity	$\delta$ / ppm
$H_{A1}$	d	8.63
$H_{A2}$	t	7.41
$H_{A3}$	t	7.95
$H_{A4}$	d	7.52
$H_{B1}$	d	8.24
$H_{B2}$	t	6.84
$H_{B3}$	t	7.45
$H_{B4}$	d	6.88
$H_{C1}$	d	8.66
$H_{C2}$	t	7.50
$H_{C3}$	t	7.95
$H_{C4}$	d	7.86
methylene H	s	5.90; 4.74

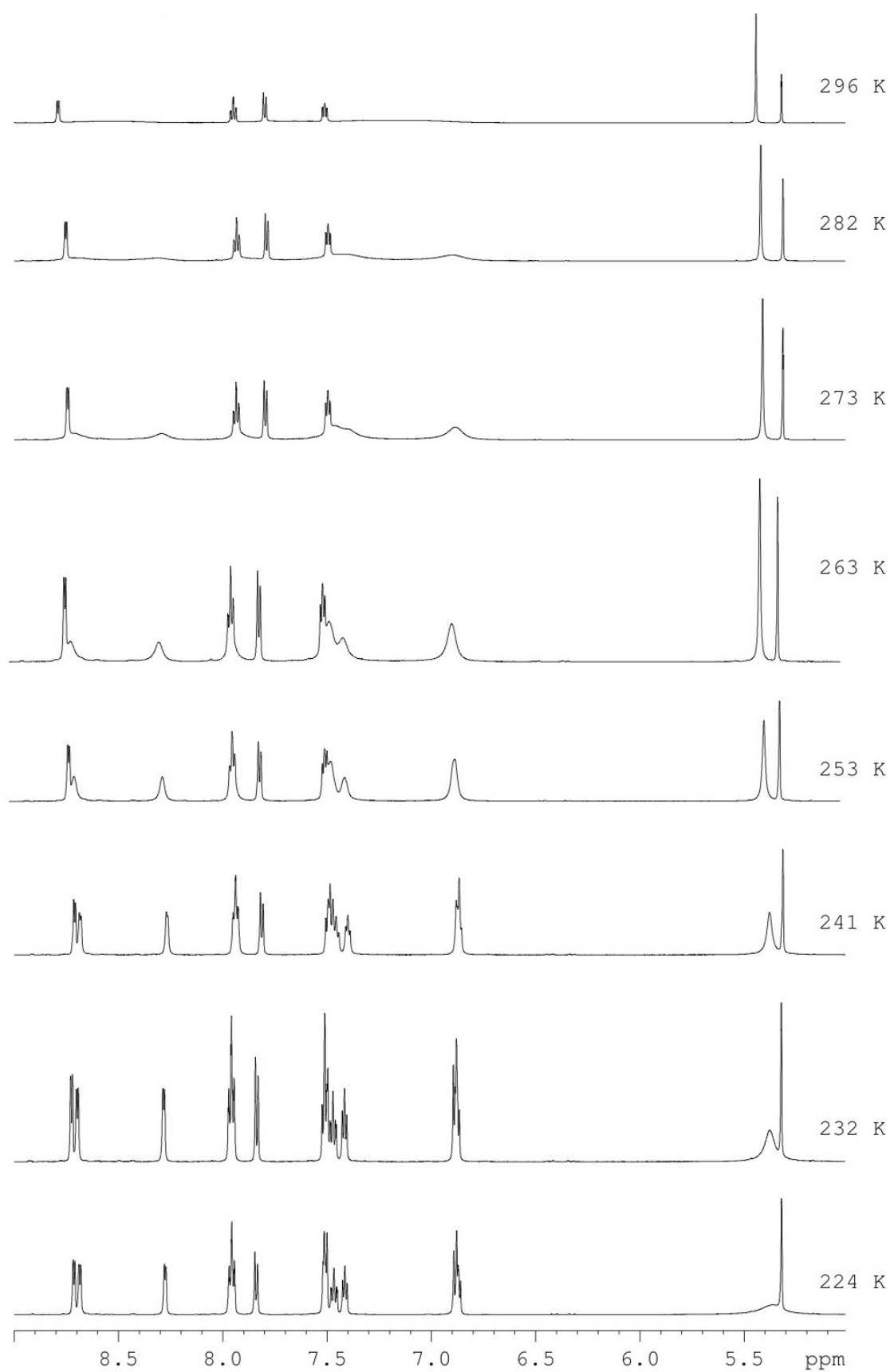


**Fig. 62** Sections of the  $^1\text{H}$  NMR spectra of **3b** from 296 K to 224 K in  $\text{CD}_2\text{Cl}_2$

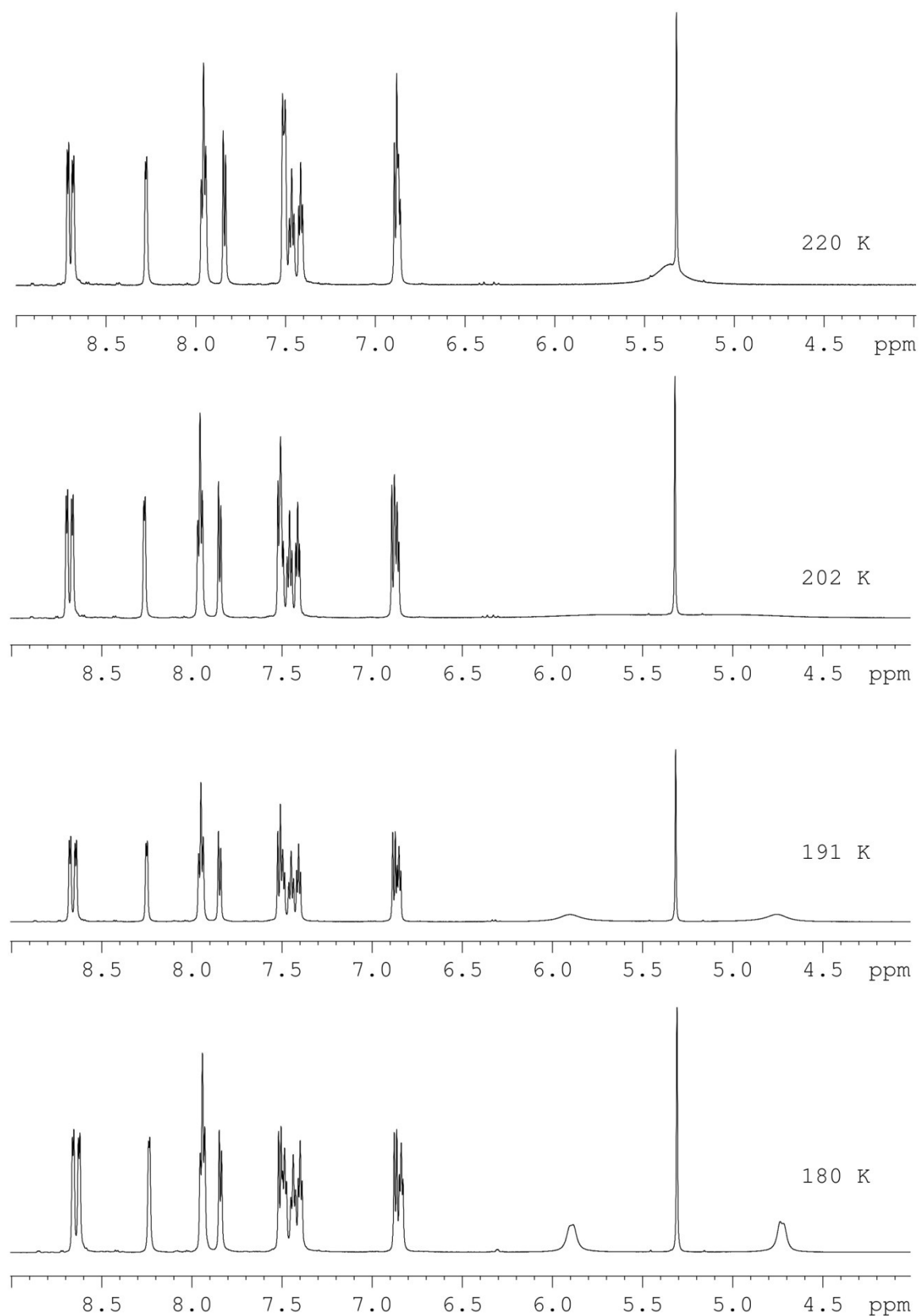


**Fig. 63** Sections of the  $^1\text{H}$  NMR spectra of **3b** from 220K to 180 K in  $\text{CD}_2\text{Cl}_2$



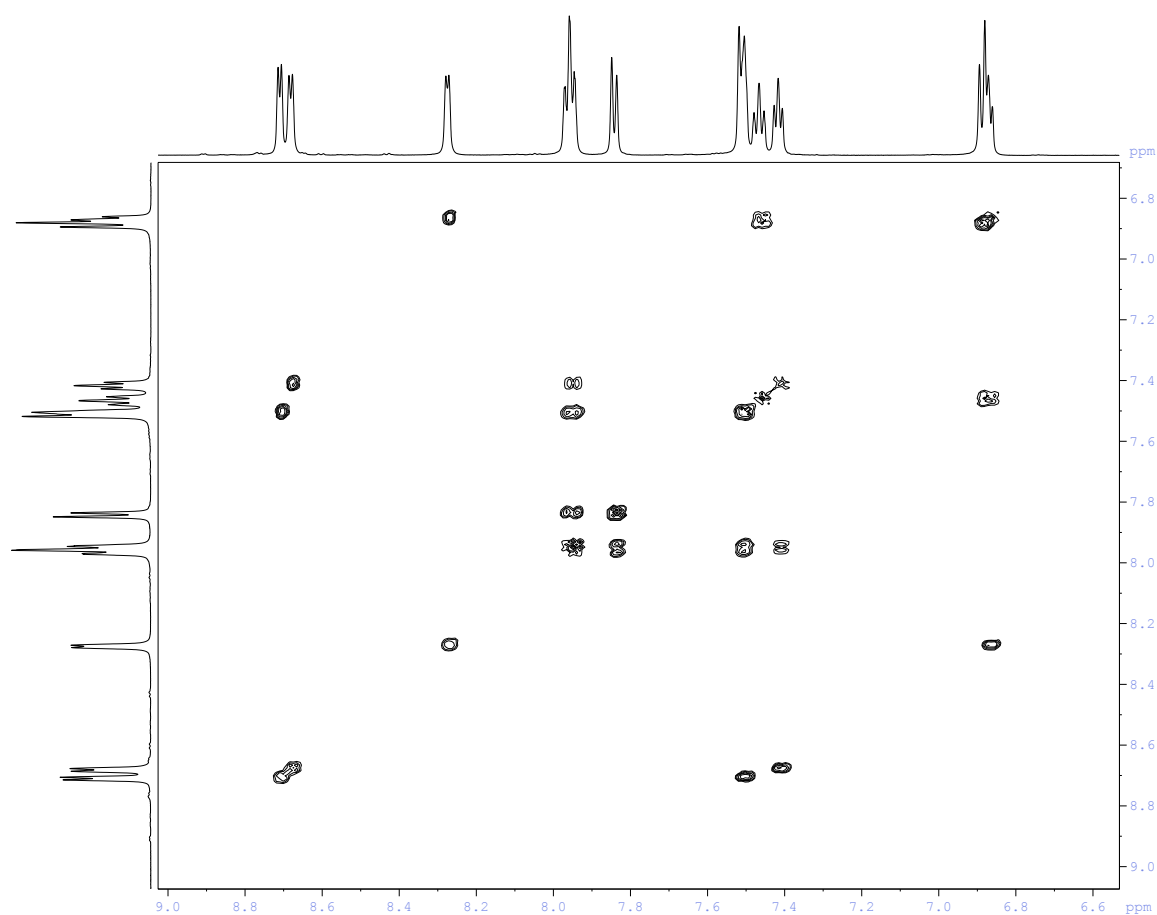


**Fig. 64** Section of the COSY spectrum of **3b** at 219 K in CD<sub>2</sub>Cl<sub>2</sub>

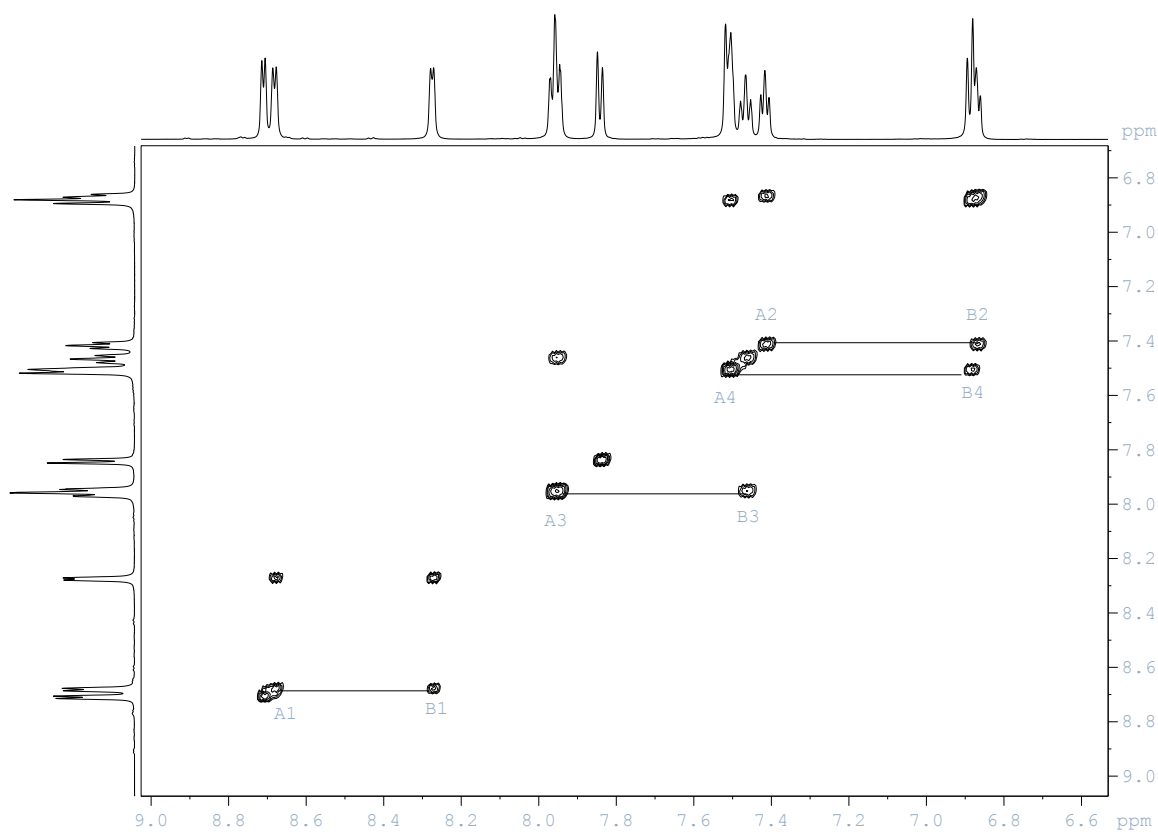


**Fig. 65** Section of the 2D-EXSY spectrum of **3b** at 219 K in CD<sub>2</sub>Cl<sub>2</sub>

#### 4.2.1.2.3 Mixture of **L1** and **Zn(OTf)<sub>2</sub>** (**3e**)

Unlike the spectra of **3b**, the <sup>1</sup>H NMR spectra of **3e** in CD<sub>2</sub>Cl<sub>2</sub> show no sign of diastereotope protons at low temperatures. The proton resonances in the room temperature spectrum are broad and not clearly assignable. Lowering of the temperature leads to a shift of signals and additional signals sharpen. At 230 K, the COSY (Figure 69) and 2D-EXSY (Figure 70) spectra of **3e** point to an exchange mechanism as is shown for **3b** in Figures 67 and 68. The exchange signals that prove the proposed mechanism are labelled with the number of the according proton in Figure 66. Again, all exchange signals are visible and an assignment of the full set of protons at 230 K is possible. Starting point of the assignment is the proton C4 close to the methylene protons. The chemical shifts and multiplicity of the signals are reported in the following Table 9.

Further decrease of temperature to 213 K clearly shows a broad underlying signal at 7.66 (most likely assignable as coordinated water) that disappears again at 186 K. The 2D-EXSY spectrum (Figure 71) at 213 K shows additional exchange signals indicating of a second dynamic process. Therefore, we unfortunately have not been able to clearly state the coordination mode so far. Additional experiments to prove the coordination mode of the complex **3e** are in progress.

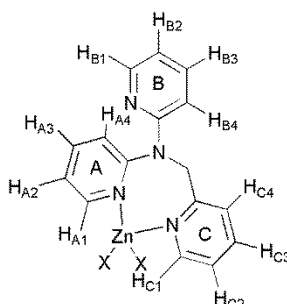


**Fig. 66** ChemDraw representation of **3e** with H-atoms labelled A1 to C4

**Table 9** Proton assignment to <sup>1</sup>H signals of **3e** at 213 K

Proton No.	multiplicity	δ / ppm
H <sub>A1</sub>	d	8.04
H <sub>A2</sub>	t	7.12
H <sub>A3</sub>	t	7.85
H <sub>A4</sub>	d	7.31
H <sub>B1</sub>	d	7.31
H <sub>B2</sub>	t	6.85
H <sub>B3</sub>	t	7.79
H <sub>B4</sub>	d	7.37
H <sub>C1</sub>	d	8.35
H <sub>C2</sub>	t	7.22
H <sub>C3</sub>	t	7.79
H <sub>C4</sub>	d	7.59
methylene H	s	4.49

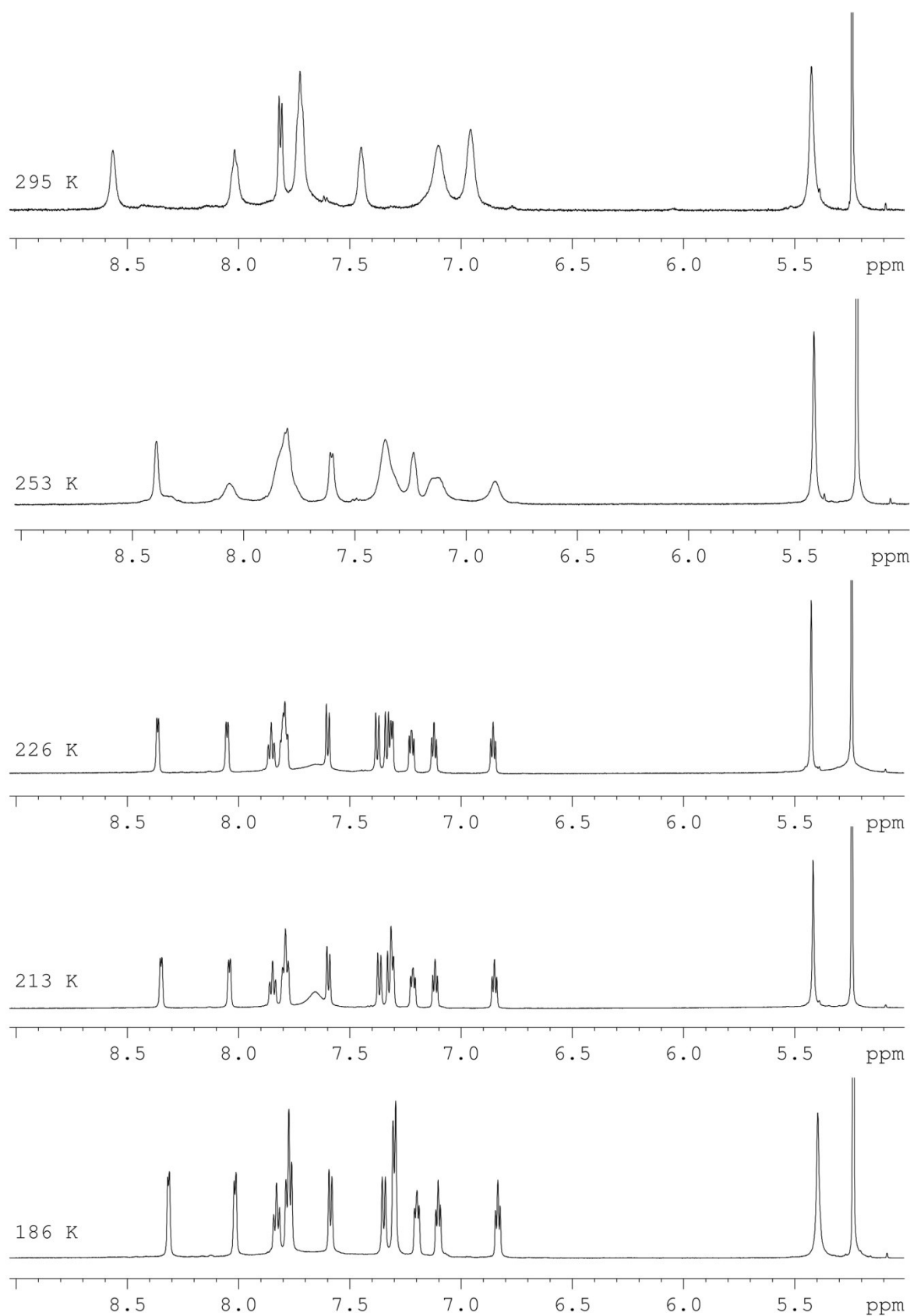


**Fig. 67** Sections of the  $^1\text{H}$  NMR spectra of **3e** in  $\text{CD}_2\text{Cl}_2$  at variable temperature

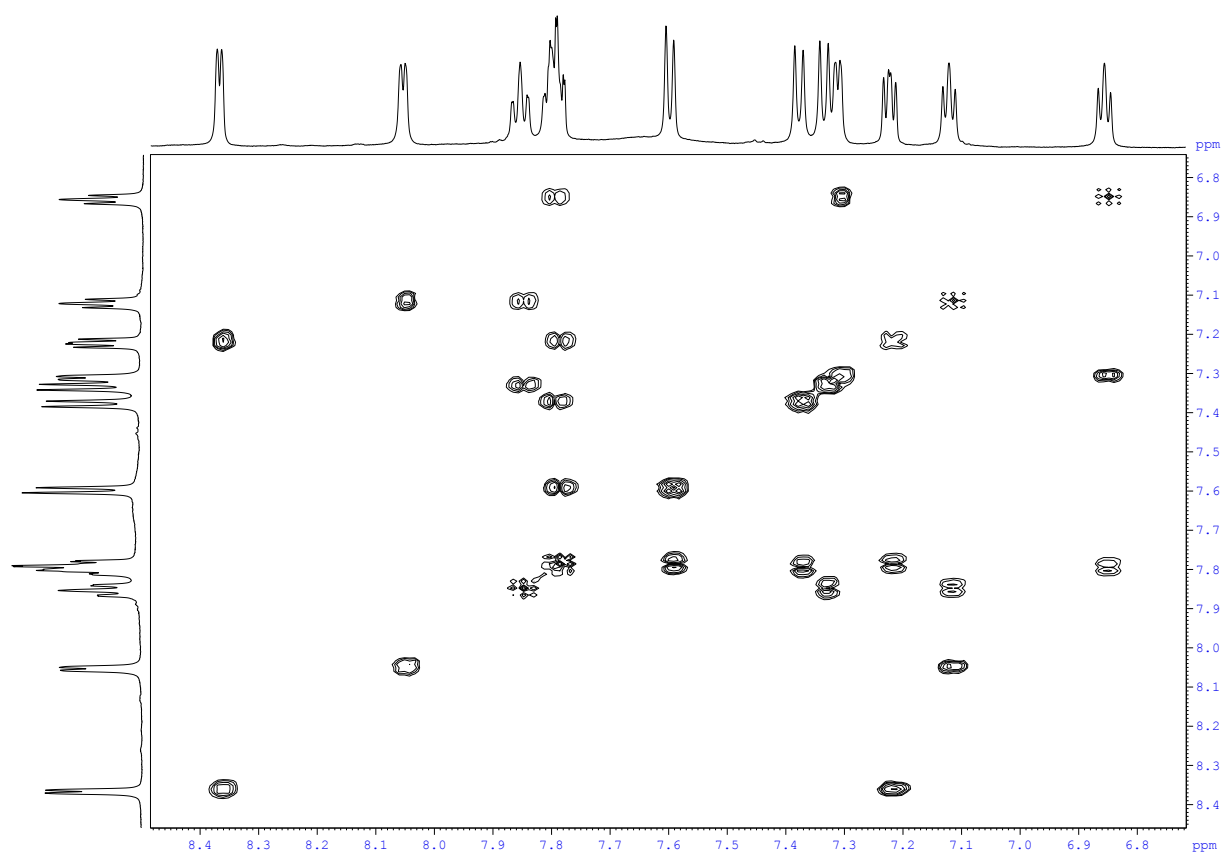


**Fig. 68** Section of the COSY spectrum of **3e** at 230 K in CD<sub>2</sub>Cl<sub>2</sub>

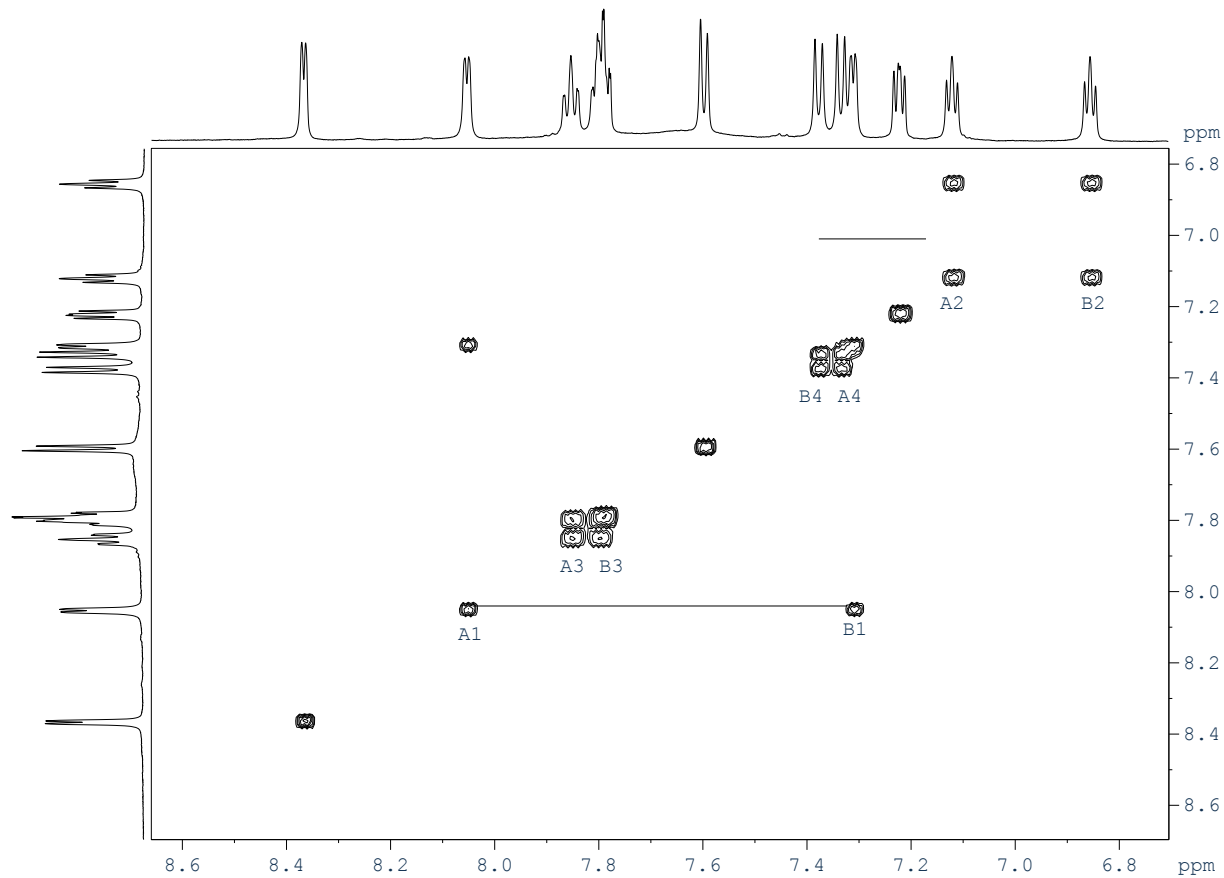


**Fig. 69** Section of the 2D-EXSY spectrum of **3e** at 230 K in CD<sub>2</sub>Cl<sub>2</sub>

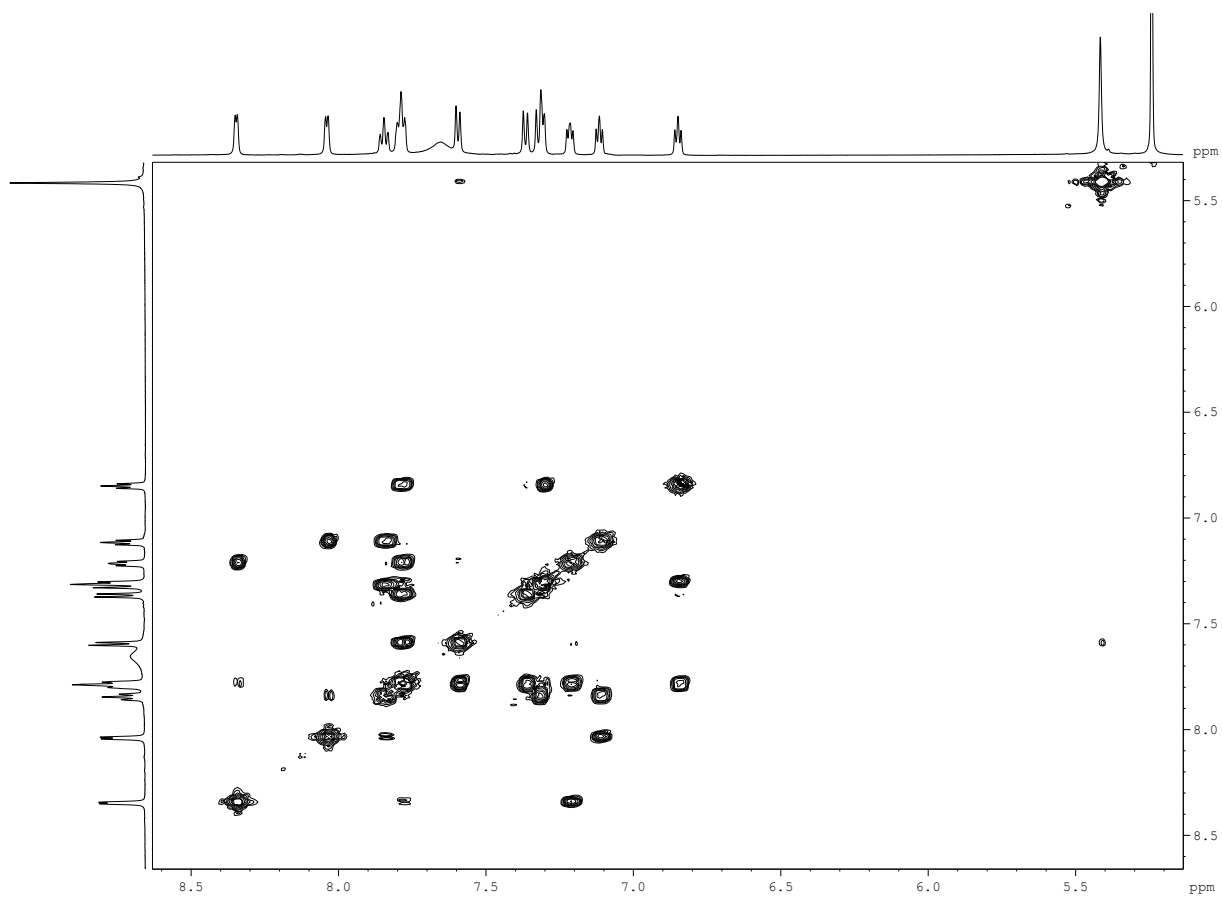


**Fig. 70** Section of the COSY spectrum of **3e** at 213 K in CD<sub>2</sub>Cl<sub>2</sub>

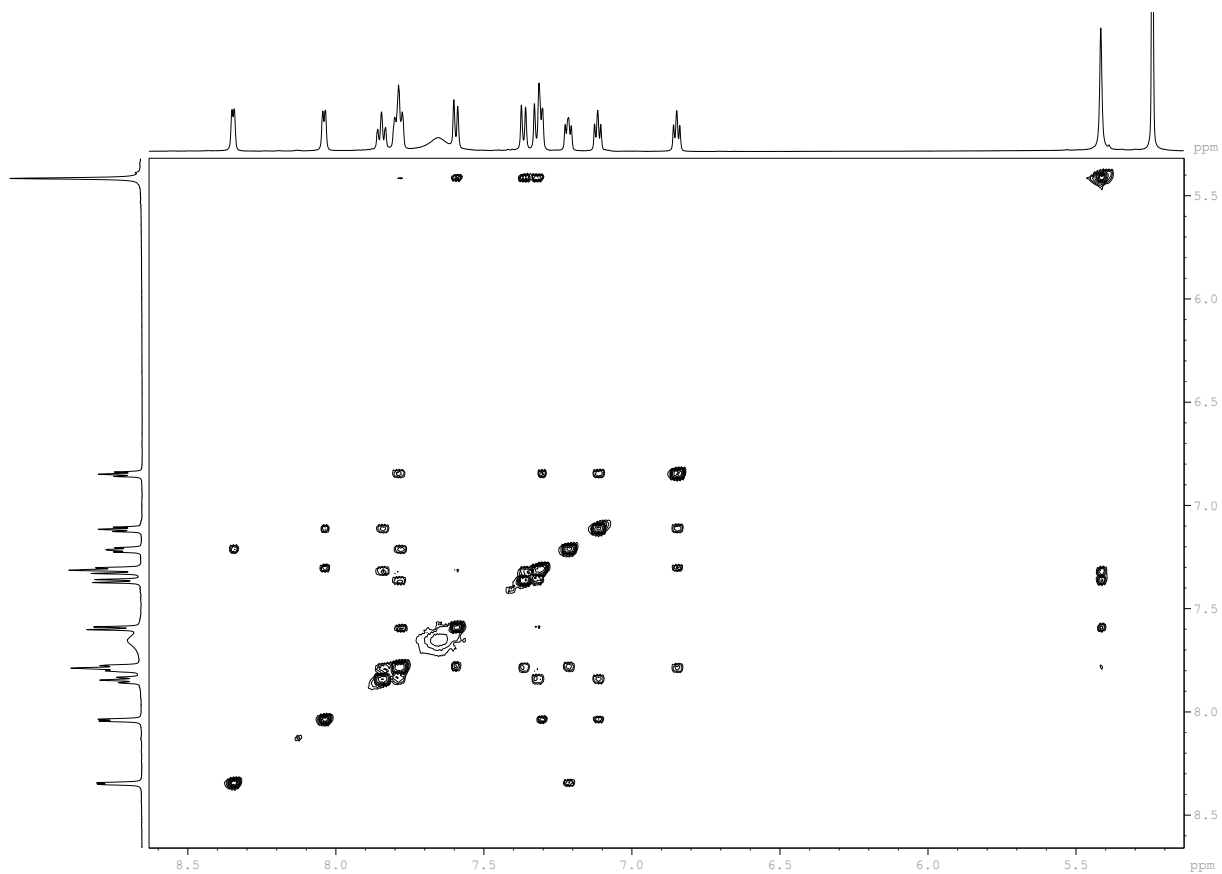


**Fig. 71** Section of the 2D-EXSY spectrum of **3e** at 213 K in CD<sub>2</sub>Cl<sub>2</sub>

4.2.1.2.4 [tpaZnCl<sub>2</sub>]

This complex has already been reported by Wang and co-workers.<sup>152</sup> A complete interpretation of the NMR spectroscopic data has not been possible so far. However, we are now able to clearly assign the full set of protons and prove the proposed exchange mechanism by the exchange signals occurring in the depicted 2D-EXSY spectrum at 186 K (Figure 75). Again, all expected resonances are detectable and assignable. They are labelled with the number of the according proton in Figure 72. As herein shown for **3b**, the <sup>1</sup>H NMR spectrum at ambient temperature of [tpaZnCl<sub>2</sub>] only shows the signals of the uncoordinated pyridyl residue indicating the rotation mechanism already published<sup>152</sup> The COSY spectrum depicted in Figure 74 proves the expected 3 ABCD spin systems of the different pyridyl rings.

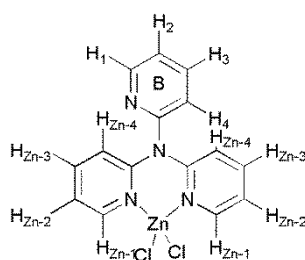


**Fig. 72** Representation of [tpaZnCl<sub>2</sub>]

**Table 10** Proton assignment to <sup>1</sup>H signals of [tpaZnCl<sub>2</sub>] at 186 K

Proton No.	multiplicity	δ / ppm
H <sub>A1</sub>	d	8.60
H <sub>A2</sub>	t	7.57
H <sub>A3</sub>	t	8.11
H <sub>A4</sub>	d	7.85
H <sub>B1</sub>	d	8.18
H <sub>B2</sub>	t	7.02
H <sub>B3</sub>	t	7.65
H <sub>B4</sub>	d	6.83

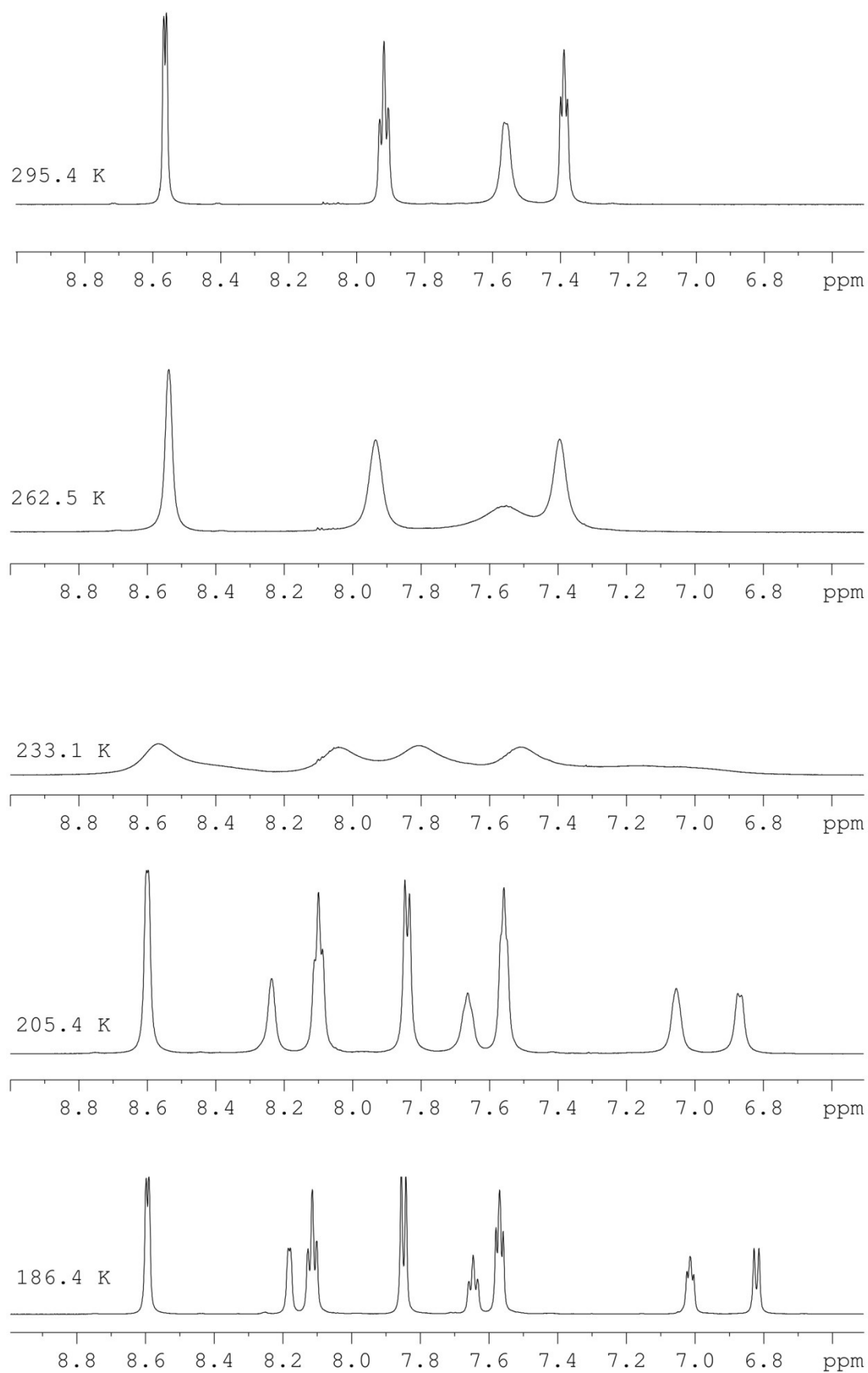


**Fig. 73** Sections of the  $^1\text{H}$  NMR spectra of  $[\text{tpaZnCl}_2]$  in  $\text{CD}_2\text{Cl}_2$  at variable temperature

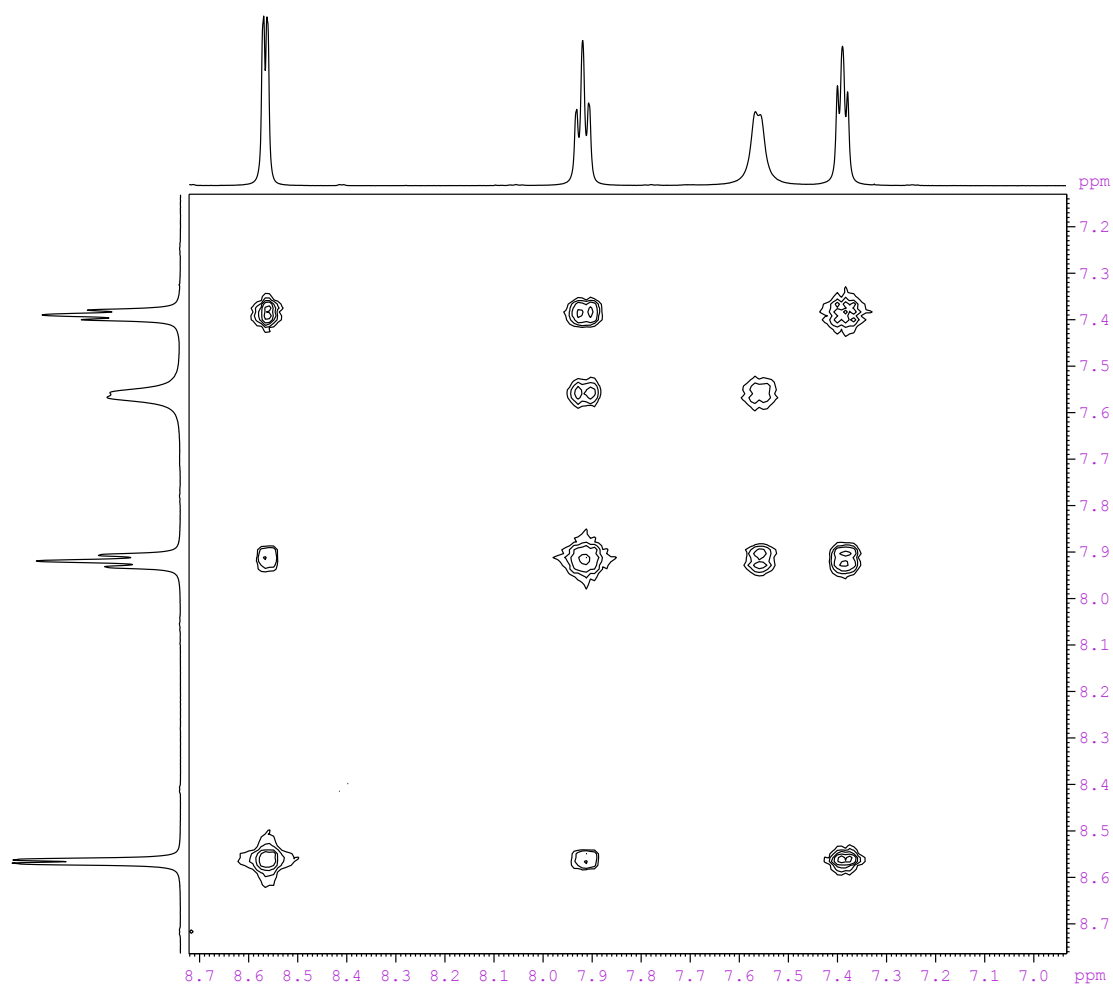


**Fig. 74** Section of the COSY spectrum of  $[\text{tpaZnCl}_2]$  at 296 K in  $\text{CD}_2\text{Cl}_2$

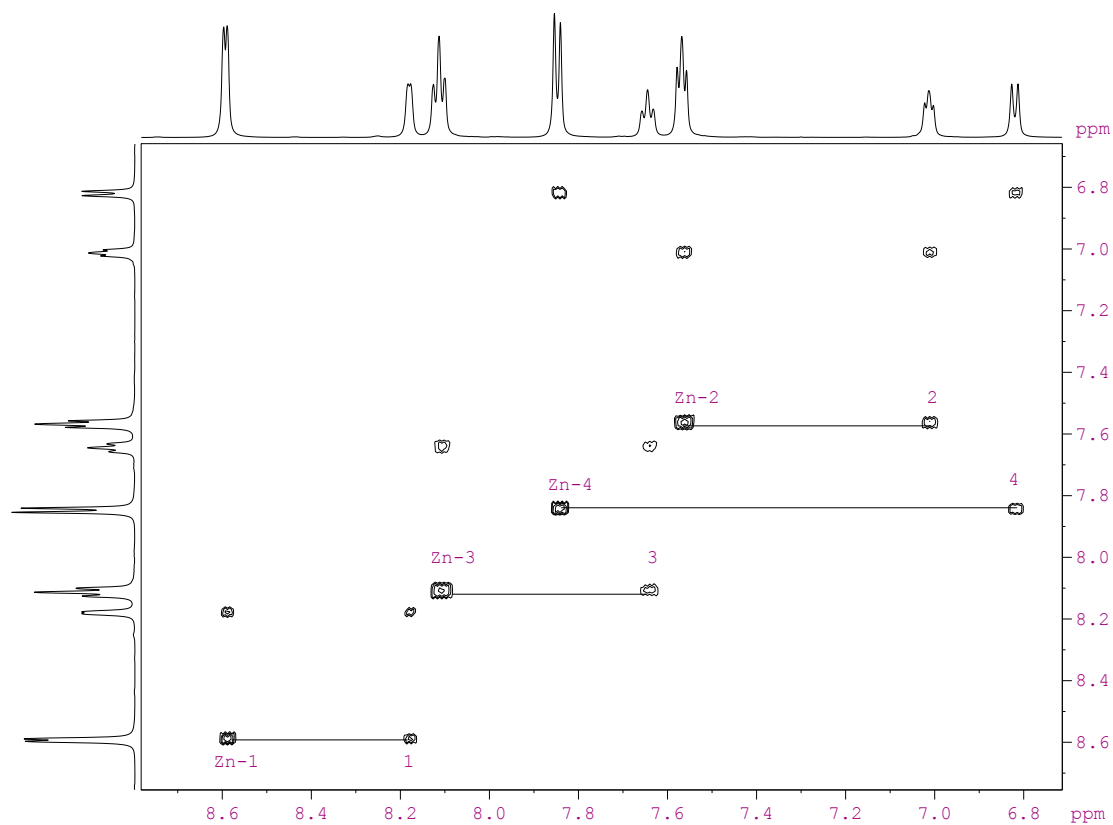


**Fig. 75** Section of the 2D-EXSY spectrum of  $[\text{tpaZnCl}_2]$  at 186 K in  $\text{CD}_2\text{Cl}_2$



## **5 Copper and Zinc Complexes Using Ligands Closely Related to L2**

### **5.1 Ligand Effects on the Formation of Coordination Polymers Containing Copper and Zinc Complexes with Derivatives of Tris(2-pyridylmethyl)amine (tmpa) as Ligands**

This chapter is ready for submission to the journal *Inorganic Chemistry*.

Alexander Beitat,<sup>a</sup> Jing-Yuan Xu,<sup>b</sup> Christoph-Cornelius Brombach,<sup>a</sup> Harald Kelm,<sup>c</sup>  
Christian Würtele,<sup>a</sup> and Siegfried Schindler\*<sup>a</sup>

*a* Institut für Anorganische und Analytische Chemie, Justus-Liebig-Universität Gießen,  
Heinrich-Buff-Ring 58, 35392 Gießen/Germany  
siegfried.schindler@anorg.chemie.uni-giessen.de

*b* School Pharmaceutical Sciences, Tianjin Medical University, Tianjin 300070, P. R.  
China

*c* Fachbereich Chemie, Technische Universität Kaiserslautern, Gebäude 54, Erwin-  
Schrödinger Straße, 67663 Kaiserslautern/Germany

#### **5.1.1 Introduction**

In our efforts to better understand dioxygen binding and substrate oxidation of copper enzymes we have successfully investigated copper complexes with tripodal ligands based on derivatives of the parent ligand tris(2-pyridylmethyl)amine (tmpa, Scheme 1). Tmpa is a versatile ligand in bioinorganic chemistry that turned out to be very useful in copper, iron and zinc chemistry. Copper tmpa complexes have been employed previously in order to explore the thermodynamic and kinetic aspects of the reaction of copper(I) compounds with dioxygen.<sup>22-23, 134-135</sup> Due to the fact that the function of a metalloprotein is closely related to the structure of its active site there has been considerable interest in the modification of the tmpa ligand system. Chelate ring sizes play an important role for the reactivity of copper(I) complexes towards dioxygen. Systematic lengthening of the pyridyl arms by the insertion of methylene spacer groups finally led to a copper(I) complex with tris[2-(2-pyridyl)ethyl]amine tepa as a ligand that was stable towards dioxygen.<sup>134</sup> In an effort to possibly obtain a different class of oxygen binding copper(I) complexes we furthermore investigated the effect of decreasing the chelate ring sizes. Unfortunately it turned out that using the new ligands N-2-pyridylmethyl-2,2-dipyridylamine (L1) and N-[bis(2-pyridyl)methyl]-2-pyridylamine (L2) (Figure 76) did not allow the observation of interesting intermediates during the reactions of dioxygen with the according copper(I) complexes.<sup>151, 175</sup>

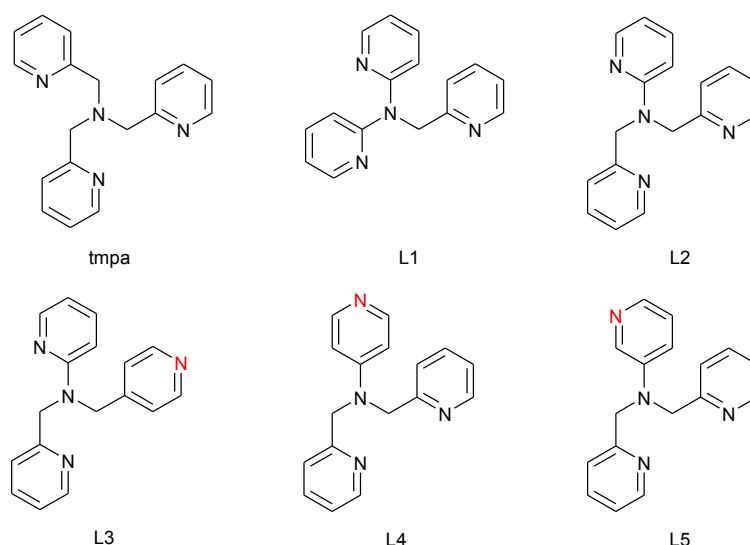


**Fig. 76** Derivatives of the parent amine tmpa

Most likely the reason for the sluggish behavior of these complexes towards dioxygen is a consequence of the formation of dimeric complexes as described by us more recently.<sup>175</sup> However, during the course of this study we observed that coordination polymers could be formed when copper(II) salts were reacted with L1. When reacting  $\text{CuCl}_2$  with L1 in acetonitrile a linear polymeric chain of  $[\text{Cu}(\text{L1})\text{Cl}_2]_n$  formed. However, if the reaction was performed in DMF only a trimeric copper complex was obtained. Here the DMF molecules act as “stoppers” and block formation of a polymeric complex.<sup>151</sup> Based on these results we considered it quite interesting to extend our experiments to ligands related to L1 and to prepare new polymeric copper complexes. Thus we synthesized the so far unknown ligands L3, L4 and L5 (Figure 76) and investigated the according copper and zinc complexes with these ligands.

### 5.1.2 Results and Discussion

#### 5.1.2.1 Ligands L3, L4 and L5

Ligand modification was based on the idea that *para* substituted pyridines are well known as building blocks for a variety of coordination polymers.<sup>176</sup> L3, L4 and L5 differ from ligands L1 and L2 in the position of one of the pyridyl nitrogen atoms. By the substitution of one pyridyl nitrogen in 2-position by a nitrogen in 3- or 4-position we expected the formation of various coordination polymers when mixed with copper or zinc salts.

While L4 and L5 contain a bispocylamine unit, L3 has a 4-pyridine unit that substitutes one of the 2-pyridine units in the bispicolyl residue (see Figure 76). The difference between the ligands L4 and L5 is located in the pyridyl arm. L5 bears its nitrogen in 3-position, while L4 has a pyridyl nitrogen in 4-position. Therefore L4 can be considered as 4-(dimethylamino)pyridine (DMAP, see Figure 77) derivative, well known for its extraordinary nucleophilicity and catalytic activity.<sup>177</sup> Only recently, Schreiner and co-workers reported about acyltransfer reactions with DMAP derivatives as catalysts.<sup>178</sup>

Thus, we expected a significantly different behavior of the complexes of **L4** compared to that of the other L ligands.

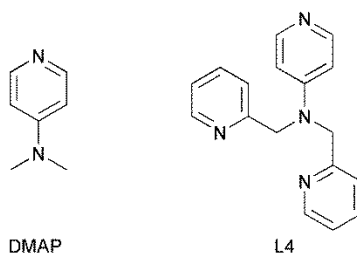


**Fig. 77** Structures of DMAP and the ligand **L4**

The synthesis led to acceptable yields for all ligands. Single crystals were obtained for ligands **L4** and **L5**. Crystallographic details and selected bond lengths are presented in the Supporting Information.

#### 5.1.2.2 Copper(I) Complexes of the Ligands **L3**, **L4** and **L5**

Under inert conditions the ligands **L3**, **L4** and **L5** coordinate readily with several copper(I) salts to form stable complexes. Upon slow ether diffusion into acetone, acetonitrile or DMF solutions of the copper(I) complexes, yellow colored solids formed and single crystals suitable for X-ray crystallographic structure determination of  $[\text{Cu}(\text{L3})(\text{MeCN})]_n(\text{CF}_3\text{SO}_3)_n$  (**1**),  $\text{Cu}_2(\text{L4})_2(\text{CF}_3\text{SO}_3)_2 \cdot \text{DMF}$  (**2**),  $[\text{Cu}(\text{L4})]_n(\text{ClO}_4)_n \cdot n\text{DMF}$  (**3**) and  $[\text{Cu}_2(\text{L5})_2](\text{BPh}_4)_2 \cdot 2\text{CH}_3\text{COCH}_3$  (**4**) were obtained. Selected bond lengths and angles and crystallographic details of **1-4** are given in Table 11 and 12 respectively.

##### 5.1.2.2.1 $[\text{Cu}(\text{L3})(\text{MeCN})]_n(\text{CF}_3\text{SO}_3)_n \cdot \text{MeCN}$ (**1**)

The molecular structure of **1** presented in Figure 78 clearly shows that we obtained a coordination polymer when **L3** was reacted with  $[\text{Cu}(\text{MeCN})_4](\text{CF}_3\text{SO}_3)$  in a stoichiometric ratio in acetonitrile.

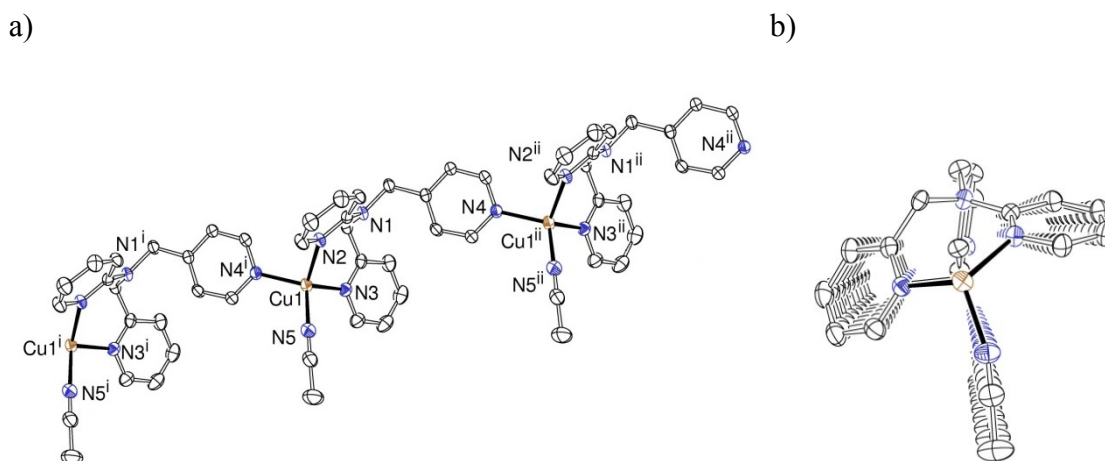


**Fig. 78** a) ORTEP representation of the cationic polymeric chain of **1** with thermal ellipsoids at 50% probability. Hydrogen atoms, not coordinated solvent molecules and anions omitted for clarity. b) view normal to 010.

The copper(I) centers of the polymeric chain are surrounded by four nitrogen atoms forming a distorted tetrahedron. Each of the metal atoms is coordinated by a pyridyl- and a methylpyridyl nitrogen in 2-position (N2 and N3) of one ligand molecule and a methylpyridyl nitrogen in 4-position (N4A) of a second ligand molecule. Thus, one molecule **L3** bridges two copper(I) centers leading to the formation of a polymeric chain. The fourth position of the tetrahedron is occupied by the acetonitrile nitrogen (N5). The methylpyridyl nitrogen atoms N3 and N4<sup>i</sup> form much stronger bonds to the copper(I) atom than the pyridyl nitrogen N2, indicated by bond lengths of 2.018(2) Å for Cu1...N3 and 2.033(2) Å for Cu1...N4<sup>i</sup> that are significantly shorter than Cu1...N2 (2.130(2) Å). The missing methyl bridge between the aliphatic nitrogen N1 and the pyridyl moiety disables N1 to coordinate due to geometric restraints.

The one-dimensional polymeric chain forms a zigzag like structure most likely caused by the ligand structure mainly influenced by the uncoordinated aliphatic “bridgehead” N1 and its close to trigonal planar geometry (see Figure 78a). This enables the methyl pyridine moiety with N4 in 4-position to coordinate to a second metal center and thus form a linear chain. Linearity of the chain is obvious in the view normal to 010 direction (see Figure 78b).

**Table 11** Crystallographic data of 1-5

	[Cu(L3)(MeCN)] <sub>n</sub> (CF <sub>3</sub> SO <sub>3</sub> ) <sub>n</sub> ·nMeCN (1)	[Cu <sub>2</sub> (L4) <sub>2</sub> ](CF <sub>3</sub> SO <sub>3</sub> ) <sub>2</sub> ·DMF (2)	[Cu(L4)] <sub>n</sub> (ClO <sub>4</sub> ) <sub>n</sub> ·nDMF (3)	[Cu <sub>2</sub> (L5) <sub>2</sub> ](BPh <sub>4</sub> ) <sub>2</sub> ·2CH <sub>3</sub> COCH <sub>3</sub> (4)	[ZnDMF) <sub>4</sub> (L4) <sub>2</sub> ](ClO <sub>4</sub> ) <sub>2</sub> (5)	[CuCl <sub>2</sub> L5] (7)
Empirical formula	C <sub>22</sub> H <sub>22</sub> CuF <sub>3</sub> N <sub>6</sub> O <sub>3</sub> S	C <sub>36</sub> H <sub>32</sub> Cu <sub>2</sub> F <sub>6</sub> N <sub>8</sub> O <sub>6</sub> S <sub>2</sub>	C <sub>37</sub> H <sub>39</sub> Cl <sub>2</sub> Cu <sub>2</sub> N <sub>9</sub> O <sub>9</sub>	C <sub>88</sub> H <sub>84</sub> B <sub>2</sub> Cu <sub>2</sub> N <sub>8</sub> O <sub>2</sub>	C <sub>46</sub> H <sub>60</sub> Cl <sub>2</sub> N <sub>12</sub> O <sub>12</sub> Zn	C <sub>34</sub> H <sub>35</sub> Cl <sub>4</sub> Cu <sub>2</sub> N <sub>8</sub> O <sub>1.5</sub>
Formula weight	571.06	977.90	951.75	1434.33	1109.33	848.58
Temperature [K]	200(2)	150(2)	150(2)	193(2)	193(2)	193(2)
Wavelength [Å]	0.71073	0.71073	0.71073	0.71073	0.71073	0.71073
Crystal system, space group	orthorhombic, Pca2(1)	monoclinic, P 21/c	monoclinic, C2	Monoclinic, P2(1)	Triclinic, P-1	Monoclinic, P2(1)/c
Unit cell dimensions [Å, °]	a = 14.3987(10)	a = 11.4322(2)	a = 14.0980(4)	a = 10.761(2)	a = 8.3910(17)	a = 9.3533(19)
	b = 9.5222(6)	b = 8.7293(2)	b = 10.6116(3)	b = 19.885(4)	b = 11.263(2)	b = 29.156(6)
	c = 18.1821(12)	c = 19.0448(3)	c = 13.2446(4)	c = 17.585(4)	c = 13.913(3)	c = 13.143(3)
	α = 90	α = 90	α = 90	α = 90	α = 80.42(3)	α = 90
	β = 90	β = 92.385(2)	β = 90.985(3)	β = 101.42(3)	β = 80.20(3)	β = 95.81(3)
	γ = 90	γ = 90	γ = 90	γ = 90	γ = 89.00(3)	γ = 90
Volume [Å <sup>3</sup> ]	2492.9(3)	1898.93(6)	1981.13(10)	3688.3(13)	1277.6(4)	3565.8(12)
Z, Calculated density [Mg/m <sup>3</sup> ]	4, 1.522	2, 1.710	2, 1.595	2, 1.292	1, 1.442	4, 1.581
Absorption coefficient [mm <sup>-1</sup> ]	1.019	1.319	1.276	0.632	0.658	1.536
F(000)	1168	992	976	1504	580	1732
Crystal size [mm <sup>3</sup> ]	0.40 x 0.40 x 0.20	0.40 x 0.38 x 0.06	0.32 x 0.30 x 0.05	0.36 x 0.24 x 0.08	0.76 x 0.64 x 0.24	0.32 x 0.28 x 0.24
θ range for data collection [°]	2.14 to 28.29	3.10 to 29.99	2.84 to 30.00	2.05 to 25.04	3.01 to 28.15	2.09 to 24.13
Limiting indices	-19<=h<=19	-15<=h<=16	-19<=h<=18	-12<=h<=12	-11<=h<=11	-10<=h<=10
	-12<=k<=12	-12<=k<=12	-11<=k<=14	-23<=k<=23	-14<=k<=14	-33<=k<=33
	-24<=l<=24	-26<=l<=26	-18<=l<=9	-20<=l<=20	-18<=l<=17	-15<=l<=14
Reflections collected / unique	28043 / 6102 [R(int) = 0.0333]	19562 [R(int) = 0.0342]	6024 / 4065 [R(int) = 0.0249]	24983 / 12663 [R(int) = 0.0962]	11702 / 5693 [R(int) = 0.0538]	21054 / 5378 [R(int) = 0.0476]
Completeness to θ	28.29 99.7%	29.99 99.7%	30.00 99.8 %	25.04 99.6 %	28.15 90.9 %	24.13 94.6 %
Absorption correction	multi-scan	semi-empirical	semi-empirical	None	None	None
T min	0.686 (1)	0.6206	0.9390	---	---	---
T max	0.822 (1)	0.9251	0.6857	---	---	---
Refinement method	Full-matrix least-squares on F <sup>2</sup>	Full-matrix least-squares on F <sup>2</sup>	Full-matrix least-squares on F <sup>2</sup>	Full-matrix least-squares on F <sup>2</sup>	Full-matrix least-squares on F <sup>2</sup>	Full-matrix least-squares on F <sup>2</sup>
Data/restraints/parameters	6102 / 1 / 333	5528 / 0 / 271	4065 / 1 / 281	12663 / 1 / 923	5693 / 0 / 403	5378 / 0 / 596
Goodness-of-fit on F <sup>2</sup>	0.987	0.939	0.912	0.832	1.089	0.941
Final R indices [I>2σ(I)]	R1 = 0.0288, wR2 = 0.0679	R1 = 0.0327, wR2 = 0.0672	R1 = 0.0301, wR2 = 0.0561	R1 = 0.0584, wR2 = 0.1195	R1 = 0.0444, wR2 = 0.1298	R1 = 0.0303, wR2 = 0.0799
R indices (all data)	R1 = 0.0358, wR2 = 0.0699	R1 = 0.0518, wR2 = 0.0707	R1 = 0.0372, wR2 = 0.0572	R1 = 0.1214, wR2 = 0.1395	R1 = 0.0509, wR2 = 0.1367	R1 = 0.0421, wR2 = 0.0834
Largest diff. peak and hole	0.276 and -0.316 e·Å <sup>-3</sup>	0.486 and -0.323 e·Å <sup>-3</sup>	0.402 and -0.381 e·Å <sup>-3</sup>	0.670 and -0.443 e·Å <sup>-3</sup>	0.694 and -1.165 e·Å <sup>-3</sup>	0.489 and -0.364 e·Å <sup>-3</sup>

5.1.2.2.2  $[Cu_2(L4)_2](CF_3SO_3)_2 \cdot DMF$  (**2**)

When reacted with copper(I) salts with weakly coordinating anions the ligand L4 forms two different species. One of which was identified as the dimeric compound **2** depicted in Figure 79. The copper atom Cu1 is surrounded by three aromatic nitrogen atoms (N2, N3 and N4<sup>i</sup>) and the aliphatic nitrogen atom N1. With a distance of 2.511(2) Å, N1 does not form a strong coordinative bond with Cu1. Therefore, a bond is not marked in Figure 79 and the coordination environment around Cu1 is best described as distorted trigonal planar with angles of 119.43(5) ° (N2-Cu1-N4<sup>i</sup>), 129.04(6) ° (N2-Cu1-N3) and 111.49(5) ° (N3-Cu1-N4<sup>i</sup>). The triangle around the copper is formed by the aromatic nitrogen atoms with much shorter bond lengths compared to Cu1...N1 with values of 1.965(2) Å (Cu1...N2) and 2.005(2) Å (Cu1...N4<sup>i</sup>).

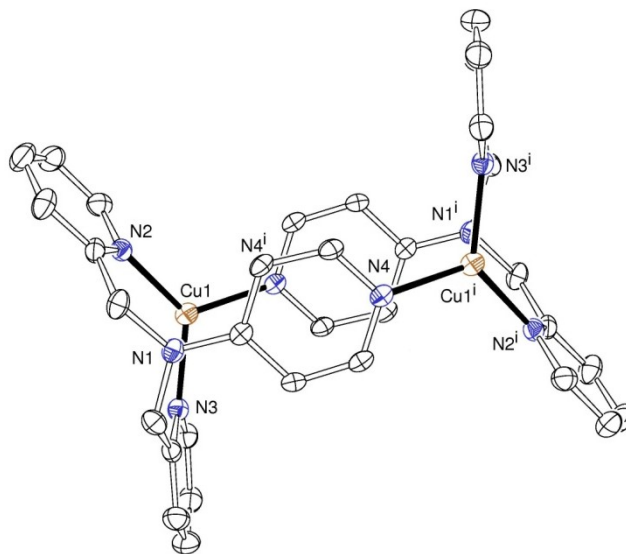


**Fig. 79** ORTEP representation of the molecular structure of **2**. Hydrogen atoms, anion and solvent molecules omitted for clarity. Thermal ellipsoids with 50 % probability.

The cavity between the two pyridine rings is best described with the copper/copper distance Cu1...Cu2 of 6.159(1) Å representing the diagonal, and the distance between the coplanar planes spanned by the atoms of these pyridine rings of 3.310(1) Å. The two coplanar  $\pi$ -systems should enable **2** to intercalate additional transition metals forming sandwich like structures. Cu1 is located 0.668(1) Å out of plane spanned by the atoms of the coordinated pyridine ring bearing the nitrogen in 4-position. This is most likely caused by the weak bonding interaction of the aliphatic N1.

We also obtained single crystals of the PF<sub>6</sub><sup>-</sup> salt from acetone and DMF solutions. The molecular structure is very similar to that of **2** and ORTEP representations, crystallographic details and selected bond lengths for the dimers are reported in the Supporting Information.

**Table 12** Selected bond lengths [Å] and angles [°] of compounds **1-5** and **7**.

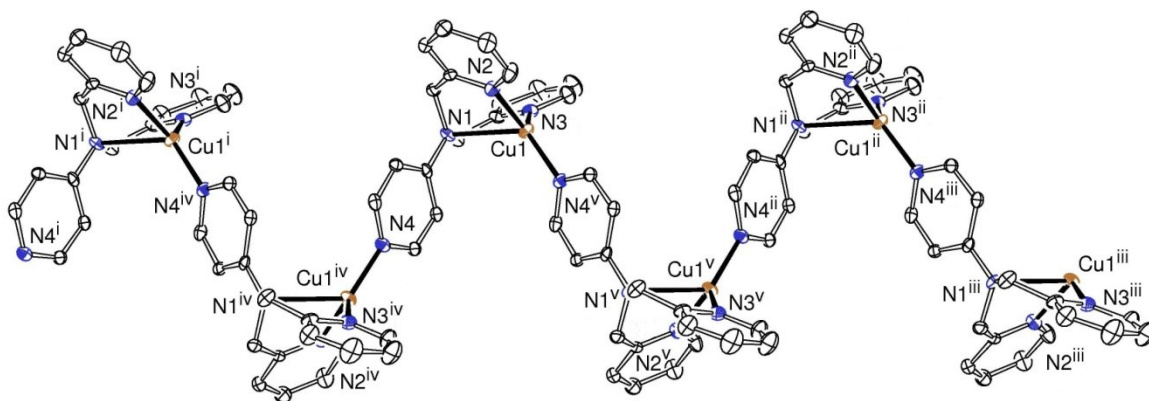
<b>1</b>							
Cu(1)-N(2)	2.130(2)	Cu(1)-N(3)	2.018 (2)	Cu(1)-N(4 <sup>b</sup> )	2.034(2)	Cu(1)-N(5)	2.008(2)
N(3)-Cu(1)-N(2)	105.5(1)	N(3)-Cu(1)-N(4 <sup>b</sup> )	127.0(1)	N(4 <sup>b</sup> )-Cu(1)-N(2)	99.1(1)	N(5)-Cu(1)-N(2)	111.2(1)
N(5)-Cu(1)-N(3)	104.2(1)	N(5)-Cu(1)-N(4 <sup>b</sup> )	109.4(1)	Cu(1)-Cu(1 <sup>b</sup> )	9.522(2)		
symmetry operation used to generate equivalent atoms: i) x,y-1,z b) x,y+1,z							
<b>2</b>							
Cu(1)-N(2)	1.965(2)	Cu(1)-N(3)	1.991(2)	Cu(1)-N(4 <sup>b</sup> )	2.005(2)	Cu(1)-N(1)	2.511(2)
N(2)-Cu(1)-N(4 <sup>b</sup> )	119.43(5)	N(3)-Cu(1)-N(2)	129.04(6)	N(3)-Cu(1)-N(4 <sup>b</sup> )	111.49(5)	N(1)-Cu(1)-N(2)	78.18(5)
N(1)-Cu(1)-N(3)	78.92(5)	N(1)-Cu(1)-N(4 <sup>b</sup> )	115.16(5)	Cu(1)-Cu(1 <sup>b</sup> )	6.159(1)		
symmetry operation used to generate equivalent atoms: i) -x, -y+1, -z							
<b>3</b>							
Cu(1)-N(1)	2.502(2)	Cu(1)-N(2)	2.019(2)	Cu(1)-N(3)	2.000(2)	Cu(1)-N(4 <sup>b</sup> )	1.967(2)
N(2)-Cu(1)-N(1)	76.54(8)	N(3)-Cu(1)-N(1)	76.48(10)	N(4 <sup>b</sup> )-Cu(1)-N(1)	125.36(8)	N(3)-Cu(1)-N(2)	115.92(8)
N(4 <sup>b</sup> )-Cu(1)-N(2)	119.68(8)	N(4 <sup>b</sup> )-Cu(1)-N(3)	123.46(9)				
symmetry operation used to generate equivalent atoms: i) -x+3/2,y+1/2, -z							
<b>4</b>							
Cu(1)-N(1)	2.486(7)	Cu(1)-N(2)	1.927(7)	Cu(1)-N(3)	1.964(6)	Cu(1)-N(8)	2.014(8)
Cu(2)-N(4)	1.993(6)	Cu(2)-N(5)	2.409(7)	Cu(2)-N(6)	1.951(6)	Cu(2)-N(7)	1.944(6)
Cu(1)-Cu(2)	5.483(7)	N(1)-Cu(1)-N(2)	78.3(1)	N(1)-Cu(1)-N(3)	78.9(1)	N(1)-Cu(1)-N(8)	114.1(1)
N(2)-Cu(1)-N(3)	137.2(3)	N(2)-Cu(1)-N(8)	118.4(3)	N(3)-Cu(1)-N(8)	104.0(3)	N(4)-Cu(2)-N(5)	113.2(2)
N(6)-Cu(2)-N(5)	80.2(2)	N(6)-Cu(2)-N(4)	112.5(3)	N(7)-Cu(2)-N(4)	111.0(3)	N(7)-Cu(2)-N(5)	80.6(2)
N(7)-Cu(2)-N(6)	136.4(3)						
<b>5</b>							
O(1)-Zn(1)	2.154(2)	O(2)-Zn(1)	2.117(2)	N(4)-Zn(1)	2.095(2)	O(1)-Zn(1)-O(1 <sup>b</sup> )	180.0 (1)
N(4 <sup>b</sup> )-Zn(1)-N(4)	180.0(1)	N(4)-Zn(1)-O(2)	92.0(1)	N(4)-Zn(1)-O(2 <sup>b</sup> )	88.0(1)	N(4)-Zn(1)-O(1)	89.6(1)
N(4)-Zn(1)-O(1 <sup>b</sup> )	90.4(1)	O(2)-Zn(1)-O(1)	91.6(1)	O(2)-Zn(1)-O(1 <sup>b</sup> )	88.4(1)	O(2 <sup>b</sup> )-Zn(1)-O(2)	180.0(1)
symmetry operation used to generate equivalent atoms: i) -x+1, -y+1, -z+1							
<b>7</b>							
Cl(1)-Cu(1)	2.538(1)	Cl(2)-Cu(1)	2.250(1)	Cl(3)-Cu(2)	2.478(1)	Cl(4)-Cu(2)	2.259(2)
Cu(1)-N(2)	1.991(3)	Cu(1)-N(3)	1.995(3)	Cu(1)-N(1)	2.096(3)	Cu(2)-N(6)	2.017(3)
Cu(2)-N(7)	2.018(3)	Cu(2)-N(5)	2.101(3)	N(2)-Cu(1)-N(1)	80.9(2)	N(3)-Cu(1)-N(1)	81.5(2)
N(2)-Cu(1)-N(3)	160.4(2)	N(1)-Cu(1)-Cl(1)	92.6(1)	N(1)-Cu(1)-Cl(2)	163.2(1)	Cl(4)-Cu(2)-Cl(3)	105.6(1)
N(2)-Cu(1)-Cl(1)	97.0(2)	N(2)-Cu(1)-Cl(2)	96.6(2)	N(3)-Cu(1)-Cl(1)	92.2(1)	N(3)-Cu(1)-Cl(2)	97.8(2)
Cl(2)-Cu(1)-Cl(1)	104.3(1)	N(6)-Cu(2)-N(5)	80.6(2)	N(7)-Cu(2)-N(5)	80.7(2)	N(6)-Cu(2)-N(7)	160.5(2)
N(5)-Cu(2)-Cl(3)	100.2(1)	N(5)-Cu(2)-Cl(4)	154.3(1)	N(6)-Cu(2)-Cl(3)	96.8(1)	N(6)-Cu(2)-Cl(4)	97.1(1)
N(7)-Cu(2)-Cl(3)	91.9(1)	N(7)-Cu(2)-Cl(4)	97.3(1)				

**5.1.2.2.3 [Cu(L4)]<sub>n</sub>(ClO<sub>4</sub>)<sub>n</sub>·nDMF (3)**

From copper complexes with the related ligands L1 and L2 it is known that different anions are able to influence the crystal structure.<sup>151</sup> Thus, we varied the anion used in the dimer **2** in order to synthesize coordination polymers. Using perchlorate as an anion, a polymeric species (**3**) of the copper(I) complex using L4 as a ligand could be successfully obtained. Comparison of complexes **2** and **3** reveals that a cage opening of **2** leads to the formation of the coordination polymer **3**. A part of the polymeric chain shown along the 100 and 010 axes is depicted in Figure 80 a) and b), respectively. The view along the 100 axes reveals the zigzag shaped one-dimensional structure. As expected it is very similar to that of **1** due to the pyridine nitrogen N4 in *para* position located at the “short arm” of the ligand instead of the “long one” in **L3**. An explanation for the zigzag shape is most likely the bonding influence of the aliphatic “bridgehead” nitrogen N1. As described for the dimer in **2** the distance between the copper(I) atom Cu1 and N1 is very long (2.486(7) Å) for a copper...nitrogen coordination bond compared to the other ones in **3** all with values around 2.00 Å. Nevertheless, the bonding

character of the Cu1...N1 interactions leads to the zigzag shape of the polymer. In contrast to **3** the “bridgehead” nitrogen atom N1 in compound **1** remains uncoordinated and is too far away from the metal atom to influence the polymer shape in a similar fashion. Therefore, the zigzag structure motive in **3** is more ideal.

a)



b)

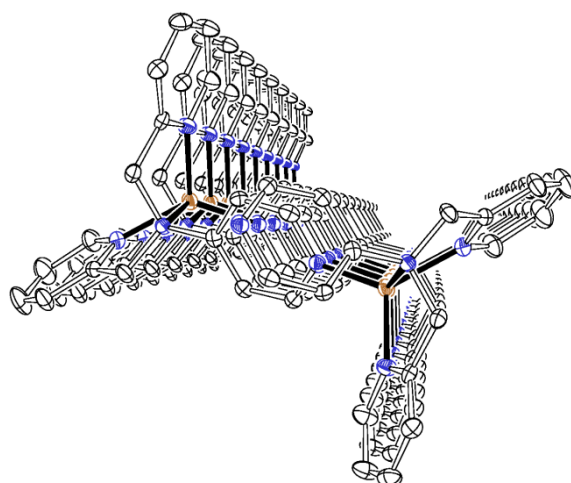


**Fig. 80** Thermal ellipsoid representations of a) a part of the polymeric chain of **3** shown normal to the 100 axes and b) normal to the 010 axes. Probability is set to 50 %, anions, hydrogen atoms and solvent molecules are omitted for clarity.

Linearity of the chain is obvious from Figure 80 b) representing a view along the 010 axes of the unit cell. Due to the long distances between the  $\pi$ -systems of the pyridine rings bonding interactions are not very likely. Ignoring the long bond Cu1...N1, the coordination environment around Cu1 is best described as trigonal planar with angles of 115.92(8) (N(3)-Cu(1)-N(2)), 119.68(8) (N(4<sup>i</sup>)-Cu(1)-N(2)) and 123.46(9) (N(4<sup>i</sup>)-Cu(1)-N(3)).

#### 5.1.2.2.4 $[\text{Cu}_2(\text{L5})_2](\text{BPh}_4)_2 \cdot 2\text{CH}_3\text{COCH}_3$ (**4**)

A representation of the cation dimer of **4** is depicted in Figure 81. Two ligand molecules **L5** coordinate two copper(I) atoms forming a cage like dimer similar to **2**. The Cu1...N1 distance



(2.486(7) Å) is very long compared to the other copper(I)-nitrogen bonds that all have values between 1.95 and 2.00 Å. Thus, as described for **2** a coordinative bond between Cu1 and N1 is not marked in Figure 81. Ignoring the weak coordination of N1 and N4 the environment around the copper atoms is best described as distorted trigonal planar with angles between 111 and 129 °.

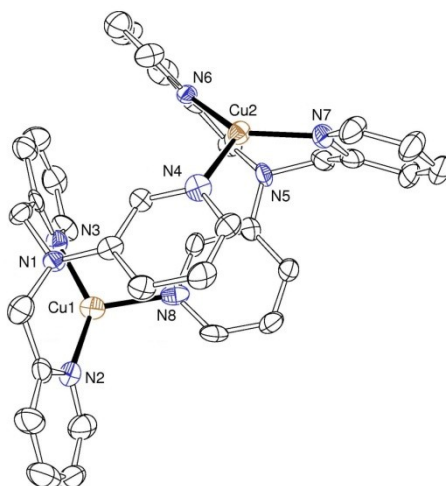


**Fig. 81** ORTEP representation of the molecular structure of **4** with hydrogen atoms, anions and solvent molecules omitted for clarity. Thermal ellipsoids with 50 % probability.

Due to the pyridyl nitrogen in 3-position the connection between the two copper(I) atoms over the bridging pyridyl ring is not linear as demonstrated for **2**. Therefore one side of the dimer is more open for the approach of a molecule to form possible intercalation compounds. With an angle of 22.56 ° the two planes build by the atoms of the two bridging pyridyl rings of **4** are far from being coplanar. A stabilizing interaction of their  $\pi$ -systems is therefore hindered.

#### 5.1.2.2.5 Oxidation Reactions of Copper(I) Complexes

The copper(I) complexes of the ligands **L3**, **L4**, and **L5** react slowly with oxygen. When reacted with air, solutions of the complexes change their color after hours at room temperature from yellow to dark green indicative for the oxidized copper(II) complexes. Unfortunately, it has not been possible to identify reactive intermediates during the reaction with oxygen so far. After the reaction of **2** with oxygen at room temperature the highest signal in the GC-MS spectrum derives from unreacted ligand **L4**. Only very small signals derive from the oxidation products.

The reaction of dihydrogenperoxide with a solution of **2** leads to a nonspecific oxidation and a brown solution. The reaction proceeds too fast to allow detection of “oxygen adduct” intermediates. Even at -90 °C the solution changes its color almost immediately from yellow to dark brown. In nitriles as solvents a possible side reaction has been well known for decades, which forms the related amides.<sup>179</sup> But even in acetone or other solvents that should prevent an oxidation reaction of the solvent, we were not able to identify an oxidation product of this reaction. Upon reaction with *meta*-chlorperbenzoic acid (*m*CPBA) below -95 °C a blue

intermediate, that is observable in very short terms, forms. During our attempts to verify our findings by low temperature stopped-flow techniques only the formation of the oxidation product is detectable through the characteristic copper(II) d-d band around 675 nm and a shoulder in the UV region at 360 nm. Two stopped-flow UV/Vis spectra at 10 °C and the time traces are shown in Figure 82. Additional low temperature stopped-flow spectra are reported in the Supporting Information.

No intensive charge transfer bands were observed at temperatures around -90 °C. Changing the solvent from propionitrile to THF that would have allowed even lower temperatures was not practicable due to the low solubility of the oxidation products. Therefore, so far only speculations about the nature of the observed blue species are possible. Most likely the blue color derives from a typical charge transfer band of a peroxido-species. Nagataki *et al.* proposed a mechanism for the oxidation of a nickel complex with *m*CPBA where such a peroxido-species is the first step in the oxidation reaction.<sup>180</sup> Efforts to verify the observation by crystallizing the possible peroxido intermediate have not been successful so far.

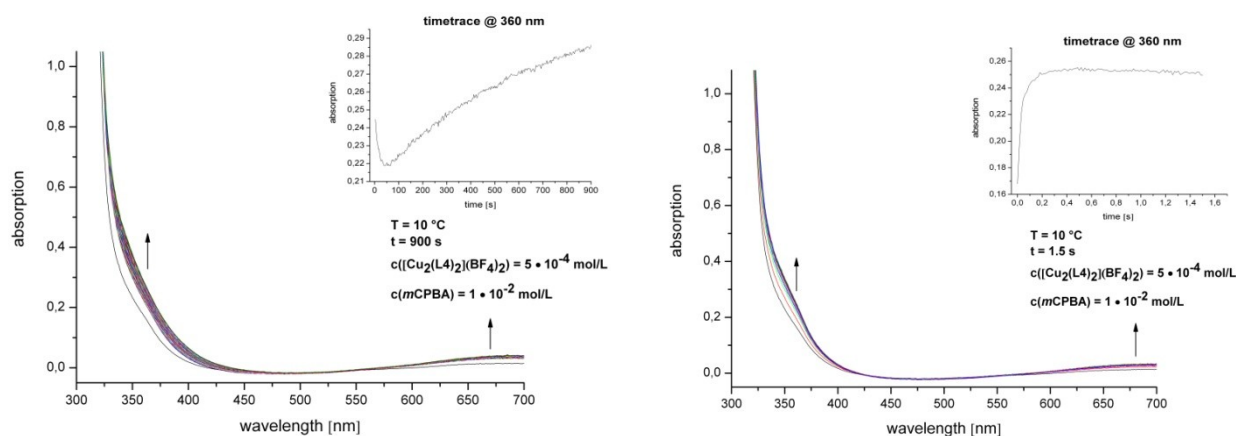


**Fig. 82** Stopped flow spectra at 10 °C of the oxidation reaction of 4 with *m*CPBA. Timetraces of a shoulder at 360 nm.

With rising temperature a consecutive reaction, monitorable with the shoulder at 360 nm in the UV/Vis spectrum, is detectable. Compared to a UV/Vis spectrum of a copper(II) complex with unmodified ligand **L4** with bands at  $\lambda = 350$  nm and  $\lambda = 625$  nm, the bands for the copper(II) complex formed are both shifted to higher wavelengths. With a difference of 50 nm the d-d band shift is the strongest indicator that a different copper(II) species is formed.

Wavelength shifts that occur during the sequential reactions are not detectable. Nevertheless, the considerable difference in the reaction rate obvious from the time traces is a sufficient hint for the proposal of a consecutive reaction (see the insets of Figure 82). The shoulder at 360 nm, obviously characteristic for copper(II) complexes, forms in a fast reaction over a wide temperature range and decays at 10 °C over a period of approximately 50 seconds and forms again with a much slower rate. Most likely this is indicative for a reaction from one copper(II) species to a different copper(II) complex. Warming the solution to room temperature finally leads to a green copper(II) complex solution. The GC-MS spectrum of the oxidized solution only shows a very small signal that derives from unreacted ligand **L4** but nearly quantitative

conversion to the same oxidation product identified from the reaction with oxygen shown in Figure 83 a or the degradation products, respectively (Figure 83 b).

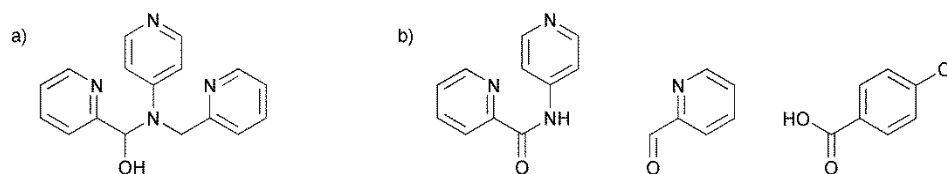


**Fig. 83** a) Proposed oxidation product of the oxidation reaction of the cation of **2** and *m*CPBA. b) Products identified in the GC-MS spectrum of a solution with maximal conversion.

Only recently, Bröhmer *et al.* reported about dipicolylamine as protective group, removable under mild conditions. They were able to demonstrate that the copper(II) coordination is capable of activating the cleavage of the bispicolyl unit from the substrate.<sup>181</sup> In our case the oxidized bispicolyl unit is cleaved, instead of cleaving the protective group bispicolyl amine from an oxidized residue as demonstrated lately by the same authors for numerous examples.<sup>181</sup> The cleavage of the half aminale into pyridinecarboxaldehyde and the remaining amine is most likely also catalyzed by the coordinated copper(II) ion and the associated electron loss of the aliphatic nitrogen atom. The oxidized mother ion signal ( $m/z = 290$ ) could be observed in a solution that reacted significantly shorter where maximal conversion of the ligand was not reached. Therefore, the proposal that a cleavage occurs in solution and not only under GC-MS conditions is most likely the correct description of the reaction. Based on our findings we propose a possible reaction mechanism for the oxidation reaction of **2** with *m*CPBA depicted in Figure 84.

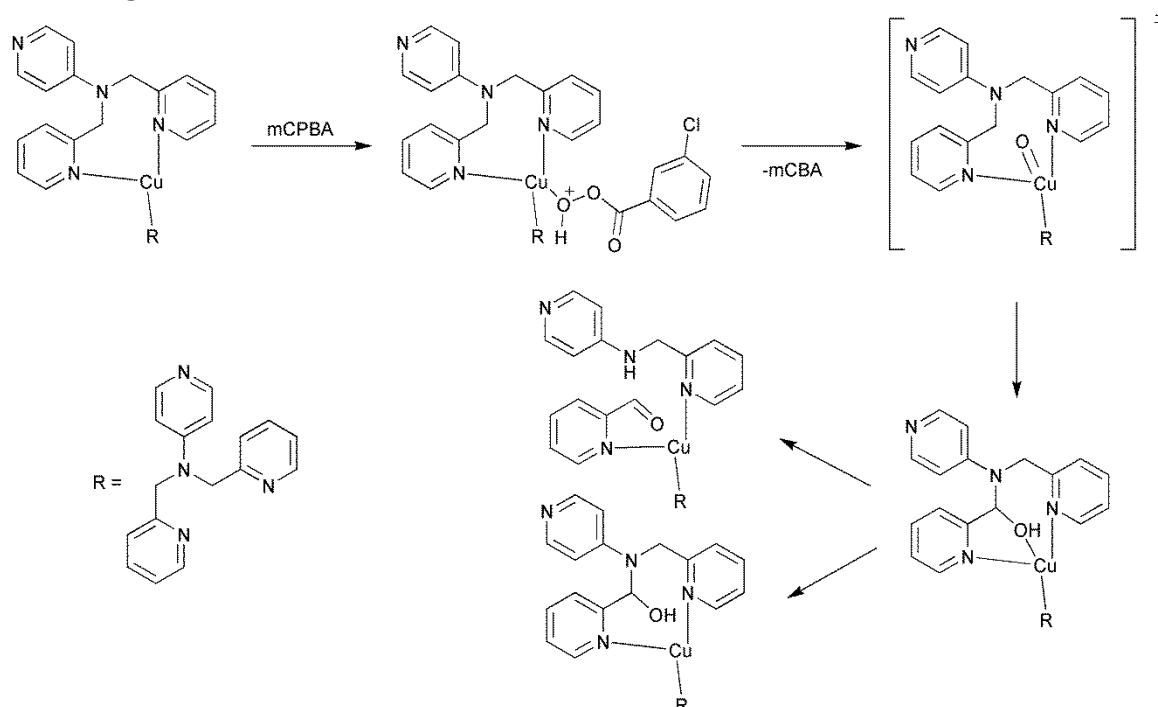


**Fig. 84** Proposed reaction pathway for the oxidation of **2** with *m*CPBA as oxidant.

Unfortunately, a meaningful NMR spectrum of the reaction mixture after the oxidation step could not be obtained so far. The only product identified in solution by NMR spectroscopic measurements, after removing copper(II) ions by complexation with EDTA, is meta-chlorobenzoic acid. The reaction of free ligand **L4** with *m*CPBA only leads to the formation of a

very small amount of oxidation product according to the GC-MS spectrum. The GC-MS spectra are depicted in the Supporting Information.

After the oxidation of a solution of **4** with either oxygen or *m*CPBA no specific oxidation product is detectable. Although the copper(I) dimer using the ligand **L5** in **4** is very similar to that of **2** there is no hint for a ligand hydroxylation in this case. A possible explanation for the different reactivity towards oxidizing agents is the influence of the strong nucleophilicity of the coordinated *para*-nitrogen atom in **L4**.<sup>182</sup> Furthermore, the signal broadening in the NMR spectrum of the copper(I) polymer (see Figure 88) points to a dynamic process in solution, most likely the change between polymer and dimer. In our studies, only the copper(I) complexes with **L4** as a ligand showed hints for such dynamic processes in solution and two different molecular structures in the solid phase. Thus, this solution dynamics is possibly a second point that increases the reactivity towards oxidizing agents compared with copper(I) complexes of **L5**.

### 5.1.2.3 Zinc(II) Complexes of the Ligands L3, L4 and L5

Due to the interesting properties of the zinc(II) complexes using **L1** as ligand (see chapter 4)<sup>175</sup>, we became interested in the zinc(II) complexes of the new ligands **L3**, **L4** and **L5**. Zinc(II) salts containing weakly coordinating anions coordinate readily with the pyridyl ligands, but are less soluble than their copper(I) analogues.

We were able to crystallize a zinc(II) complex containing **L4** from DMF (**5**) and obtained colorless crystals suitable for single crystal X-ray structure determination. The crystallographic details and selected bond lengths and angles are given in Table 11 and 12, respectively. The data for an equivalent complex with a different anion is given in the Supporting Information. Until today, we have unfortunately not been able to obtain single crystals suitable for X-ray crystallography of the zinc(II) complexes of **L3** and **L5**.

#### 5.1.2.3.1 [Zn(DMF)<sub>4</sub>(L4)<sub>2</sub>](ClO<sub>4</sub>)<sub>2</sub> (**5**)

From the zinc(II) complexes of the parent ligand **L2** it is known that the bispicolyl binding site is the preferred coordination sphere for the metal ion. Due to the nitrogen atom in 4-position in the ligand **L4** we expected zinc(II) to form polymeric compounds when reacted with the ligand. Additionally, **L4** has already proved its capability to act as bridging ligand in the copper(I) compound **3** presented above. Unexpectedly, in compound **5** zinc(II) does not coordinate with the methylpyridyl moieties, but is only coordinated by the pyridyl nitrogen in 4-position. A thermal ellipsoid representation of the molecular structure of **5** is shown in Figure 85. The zinc (II) atom is coordinated by the pyridyl nitrogen atoms N4 and N4<sup>i</sup> of two different ligand molecules in the apical positions of the octahedron. The four positions in basal plane of the coordination octahedron are occupied by the oxygen atoms of DMF solvent molecules. The nitrogen atoms N1, N2 and N3 and the equivalent atoms of the second ligand belonging to the bispicolylamine unit remain completely uncoordinated instead of coordinating the next zinc(II) atom. This coordination mode is extremely unusual and highly interesting. There are numerous examples for bispicolyl units as effective binding sites for zinc(II).<sup>16, 183</sup> In contrast, **5** is the first example for an uncoordinated bispicolyl unit in presence

of zinc(II) at least to the best of our knowledge. An explanation for this uncommon behavior of **L4** is the unusual nucleophilicity of the nitrogen atom in 4-position that is possibly accountable for electron deficiency in the remaining system. Thus, the electron donating properties of the bispicolylamine unit are considered to be lowered.

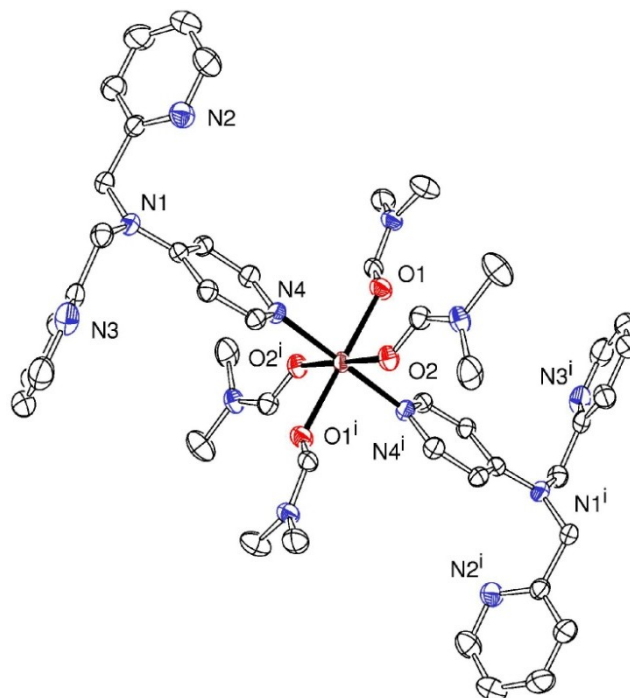


**Fig. 85** ORTEP representation of the molecular structure of **5**. Hydrogen atoms and anions omitted for clarity. Thermal ellipsoids with 50 % probability.

Never the less, the remaining donor atoms should be capable of coordinating additional metal atoms and thereby forming coordination polymers. In contrast to the copper(I) compounds **2** and **3**, we did not observe an indication for the formation of zinc(II) coordination polymers in our studies so far. Attempts to influence the crystal structure by the use of  $\text{SO}_3\text{CF}_3^-$  as a different anion only led to the formation of a compound very similar to **5**. Single crystal X-ray analysis revealed a molecular structure of the cationic complex nearly superimposable to that of **5**. Selected bond lengths and angles, detailed information on the crystallographic measurement and a picture of the molecular structure of the obtained triflate salt are provided as Supporting Information. An influence of the used solvent on the formation of this unusual structure cannot be denied, but is not considered as a main criterion. This is due to the formation of compound **2** from DMF with the isoelectronic copper(I) ion. Here the bispicolylamine units clearly are coordinated to the metal ion and are not substituted by the solvent.

In solution, the complexes of **5** exhibit similar coordinative properties. Even an excess amount of zinc(II) ions does not lead to a coordination of the bispicolyl nitrogen atoms. This description of the solution behavior is based on NMR measurements of stoichiometric solutions of **5** as well as solutions containing an excess amount of zinc(II) ions. Compared to the NMR spectra of the free ligand **L4**, a significant shift is only observable of the pyridyl protons. If coordinated, the protons of the bispicolyl unit should also be shifted to different ppm values. Therefore, the unchanged chemical shifts of the methylpyridyl nitrogen atoms are

indicative for a coordination similar to that in the solid phase. The chemical shifts are listed in Table 13.

#### 5.1.2.4 Copper(II) Complexes of the Ligands L3, L4 and L5

As described for the related ligands L1 and L2, the new ligands L3, L4 and L5 should be able to form polymeric compounds.<sup>151</sup> Therefore we reacted copper(II) salts with coordinating and uncoordinating anions with these ligands. They coordinate in various solvents with all three ligands forming green to blue complexes. We were not able to crystallize a copper(II) species of the ligand **L3** but successfully solved the crystal structures of the chlorido complexes  $[\text{Cu}_3\text{Cl}_6(\text{L4})_2]$  (**6**) (for crystallographic data and selected bond lengths and angles see Supporting Information due to high R-values) and  $[\text{CuCl}_2\text{L5}] \cdot 0.75\text{H}_2\text{O}$  (**7**) of **L4** and **L5**. Selected bond lengths and angles of **7** are listed in Table 12 respectively.

##### 5.1.2.4.1 $[\text{Cu}_3\text{Cl}_6(\text{L4})_2]_n \cdot (x\text{H}_2\text{O})_n$ (**6**)

The X-ray crystallographic structure determination of green single crystals of **6** resulted in the polymeric structure shown in Figure 86. The subunits consist of complexes containing two ligands L4 and three copper(I) atoms. These subunits are bridged by a chloride ion (Cl5) coordinating the central copper(II) (Cu2) and one of the terminal copper(II) ions (Cu3). The chloride bridge leads to the formation of a helical superlattice shown in Figure 86 (b) that additionally reveals a diffusion channel in 010 direction. Due to the poor crystal quality the refinement of the structure led to high R-values. Thus, bond lengths and angles are not reliable and are only given in the Supporting Information. A high amount of electron density is still present in the unit cell, most likely deriving from not definable solvent molecules. Therefore, the formula of **6** is given with x water molecules.

Nevertheless, a helical structure motif, which is more unusual compared to the polymeric structures of **1** and **3**, can be assigned. Until today zigzag structures are much more common than helical ones for one dimensional coordination polymers.<sup>49</sup>

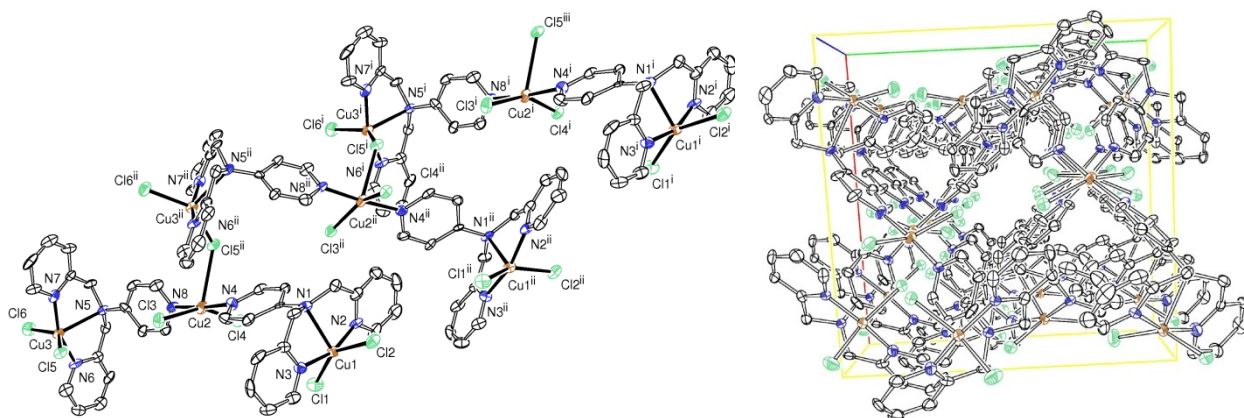


**Fig. 86** ORTEP drawing of (left) part of the polymeric structure of **6** (right) view along the 010 axis of the unit cell of **6**. Thermal ellipsoids at 50% probability, hydrogen atoms and solvent molecules are omitted for clarity.



5.1.2.4.2  $[\text{CuCl}_2\text{L5}] \cdot 0.75 \text{H}_2\text{O}$  (**7**)

Figure 87 shows a thermal ellipsoid representation of the molecular structure of **7**. Unlike the other copper compounds presented, **7** does not crystallize as dimer or polymer. The smallest independent unit consists of two molecules of the monomer **7**. The Cu1 atom is coordinated by the two methyl pyridyl nitrogen atoms and additionally two chloride anions. Due to  $\tau$  values of 0.05 (Cu1) and 0.10 (Cu2), the arrangement around the metal atom is best described as distorted square pyramidal. With a Cu1...N1 distance of 2.095(2) Å, the aliphatic nitrogen atom N1 is bound much stronger than in the presented copper(I) complexes herein. Most likely, this is accountable for the lower strain in compound **7** through the lack of coordination of additional metal atoms. The chloride ions are connected through hydrogen bonded water molecules directing the assembly of the molecules in the crystal structure.

As expected, **7** is very similar to the complexes formed by **L2** and copper(II)chloride published previously.<sup>151</sup>

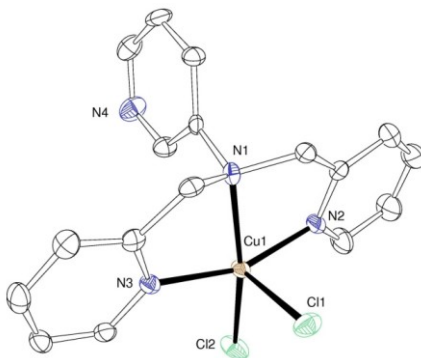


**Fig. 87** Thermal ellipsoid representation of the molecular structure of **7**. Solvent molecules and hydrogen atoms omitted for clarity. Thermal ellipsoids with 50 % probability.

5.1.2.5 *Heterometallic Cu/Zn Complexes*

From a solution containing equimolar amounts of copper(II) salt, a zinc(II) salt crystallized from DMF, and the stoichiometric amount of ligand **L4**, a nearly colorless and a blue species formed. The EDX measurement proves that the colorless species mainly contained zinc(II) and the blue species copper(II). In both complexes, the metal atom is disordered and partly substituted by the other metal. We were able to structurally characterize the colorless species as  $[\text{Zn}(\text{L4})_2(\text{DMF})_4](\text{CF}_3\text{SO}_3)_2$ . Crystallographic details, selected bond lengths and angles and the EDX spectra of this complex cation of **5** with triflate as anion are provided as Supporting Information. When mixing an acetone solution of  $\text{Zn}(\text{ClO}_4)_2$  with  $[\text{Cu}(\text{CH}_3\text{CN})_4](\text{ClO}_4)$  and a stoichiometric amount of the ligand **L4**, yellow single crystals formed. Due to the different coordination modes of copper(I) and zinc(II) in **2** and **5**, we expected a coordination polymer containing zinc and copper(I) in the ratio 1:2. The Single crystal X-ray structure analysis revealed the copper(I) structure of **3** as the only crystallized species. Using triflate as an anion instead of perchlorate led to the dimeric copper(I) compound **2**. Neither crystals of a zinc complex nor a heterometallic coordination polymer could be isolated from the solution.

This finding is in striking contrast to the NMR spectroscopic data in solution that shows different shifts of all signals belonging to the coordinated pyridyl rings in the heterometallic

solution. A comparison of the chemical shifts in the aromatic region of the different species is presented in Figure 88. The values of the chemical shifts are shown in Table 13 accompanied by a full allocation of the signals depicted in Figure 89. The allocation could be determined with two-dimensional NMR experiments performed with the free ligand L4 and the complexes in solution, respectively.

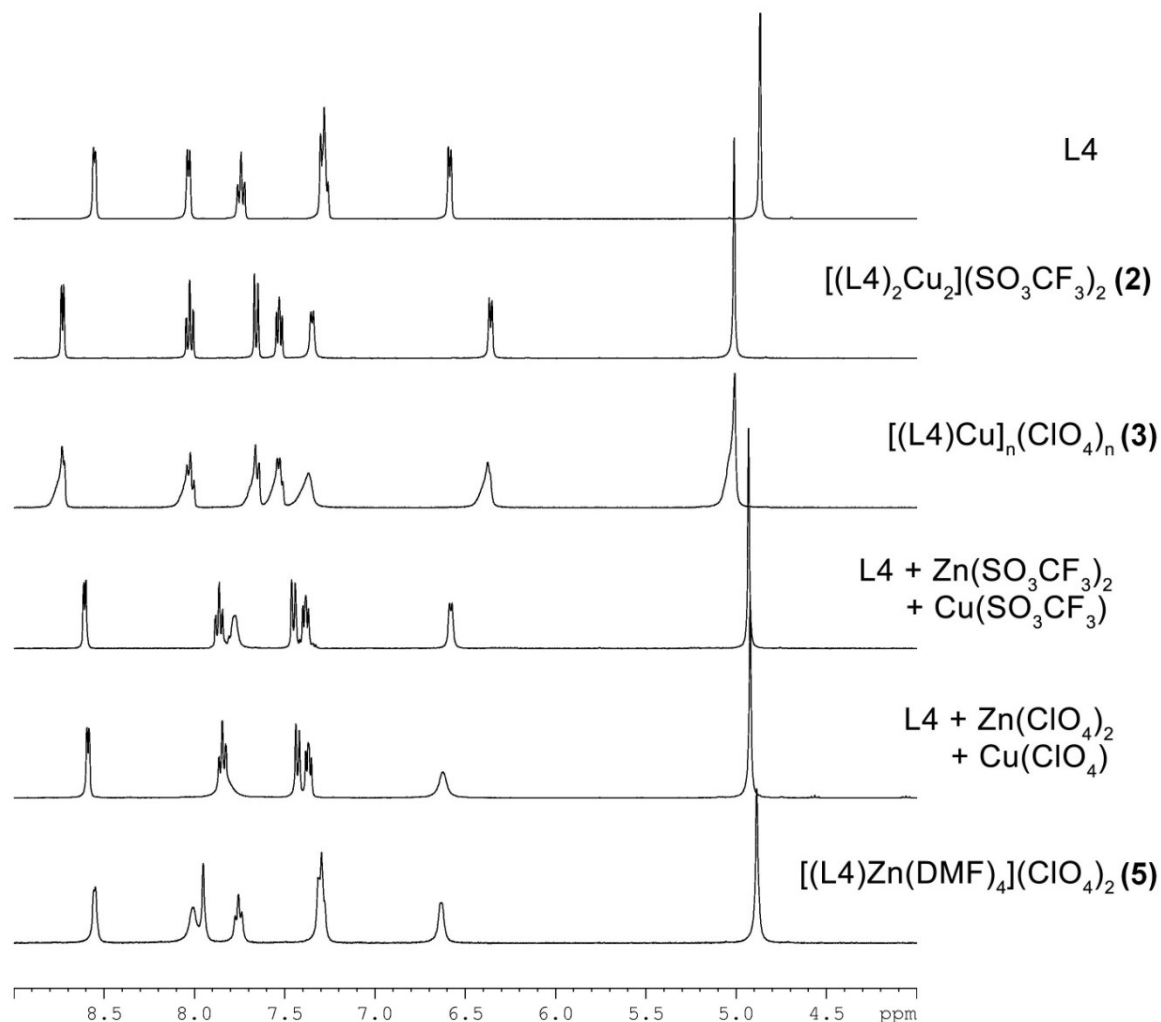


**Fig. 88** NMR spectra of the compounds **2**, **3**, **5**, and the copper zinc mixture in solution.

**Table 13** Chemical shifts [ppm] of the NMR signals depicted in Figure 88

Solution of	H <sub>G</sub>	H <sub>A</sub>	H <sub>F</sub>	H <sub>E</sub>	H <sub>D</sub>	H <sub>B</sub>	H <sub>C</sub>
<b>5</b>	8,55	7,99	7,76	7,32	7,30	6,64	4,89
<b>3</b>	8,73	7,38	7,53	8,03	7,67	6,39	5,02
<b>2</b>	8,74	7,35	7,53	8,03	7,66	6,37	5,02
Cu(ClO <sub>4</sub> ) Zn(ClO <sub>4</sub> ) <sub>2</sub> + L4	8,59	7,81	7,37	7,85	7,43	6,63	4,92
Cu(SO <sub>3</sub> CF <sub>3</sub> ) ZnSO <sub>3</sub> CF <sub>3</sub> ) <sub>2</sub> + L4	8,61	7,78	7,40	7,87	7,46	6,60	4,94



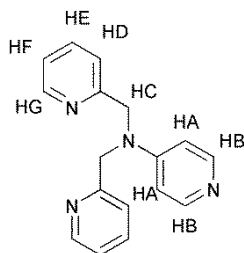


**Fig. 89** Allocation of the NMR chemical shifts to the protons the compounds (see also Table 13).

A differentiation between the possible structures of the dimer **2** and the polymer **3** in solution is difficult due to the similar coordination spheres of the compounds. The only difference is a signal broadening in the NMR spectrum of the polymer in solution. The comparison of the data for solutions of the copper(I) complex **2** and the zinc(II) complex **5** on one hand and the NMR spectra of the mixed solution clearly shows that none of the species found in the homometallic complex solutions is present in the mixture of both metals. This leads to the conclusion that a heterometallic coordination polymer with different coordination spheres of copper(I) and zinc(II) is formed in solution. The possible structure of a polymer with weakly coordinating anions is presented in Figure 90.

A simple disorder of the metal ions in the same coordination sphere should lead to two sets of signals due to the behavior of the different metals. In the shown spectrum only one set of signals is detectable and it therefore supports our proposal concerning the solution behavior.

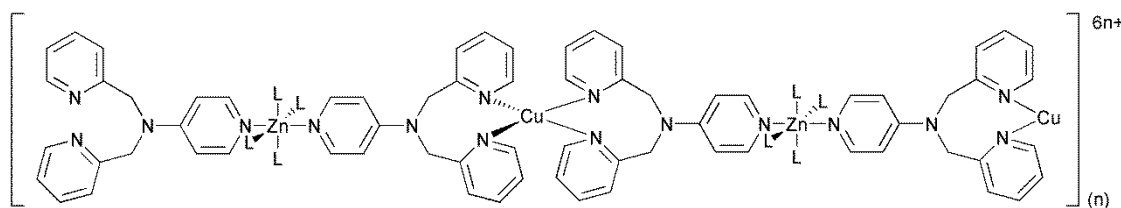


**Fig. 90** Possible structure of the heterometallic polymeric species in solution with **L** as weakly coordinating solvent or anion.

### 5.1.3 Conclusions

We were able to show that the ligands **L3** and **L4** are capable of forming one-dimensional coordination polymers with copper(I) salts with weakly coordinating anions (compounds **1** and **3**). Both compounds exhibit a zigzag shape of the linear chains. The crucial difference of these ligands compared with their close relatives tmpa, **L1** and **L2** is the 4-position of the pyridyl nitrogen atom. A variation as obvious in ligand **L5** with a nitrogen in 3-position did not lead to the formation of a polymer. As expected and already reported for **L1** and **L2**<sup>175</sup>, the copper(I) complexes of **L4** and **L5**, **2** and **4** respectively, form dimers very similar to that of **L1**. Thus, the ligand **L4** has two competing copper(I) species where a bond opening in the dimer **2** and a coordination of an additional copper(I) leads to the formation of the polymer **3**. A possible explanation is the directing influence of the anion, being the only difference in the

preparation of solutions of **2** and **3**. All efforts to obtain a dimer with **L3** or a polymer with **L5** as ligand have not been successful so far.

The substitution of copper(I) by the isoelectronic zinc(II) led to the formation of an unexpected monomeric complex, where only the nitrogen atoms in 4-position of two ligand molecules coordinate the zinc(II) ion. All other nitrogen atoms of the ligand molecules remain uncoordinating. The open positions in the octahedron of the complex are occupied by four solvent molecules. We were not able to obtain complexes with additional metal atoms coordinated at the vacant positions. Neither drastic excess amount of zinc(II) nor the addition of copper(II) or copper(I) led to the formation of coordination polymers incorporating the structure motive of **5**. In compounds **2** and **3** copper(I) is coordinated by the methyl pyridyl moieties of **L4**. Therefore, we would have expected copper(I) as an ideal ion to form heterometallic, polymeric compounds with the zinc(II) complex (**5**). Surprisingly, only the homometallic cationic species of **2**, **3** and **5** with disorders in their solid state structures could be isolated from the mixed metal solutions. Probably, the coordination of zinc(II) by the pyridyl nitrogen in 4-position with its unusual nucleophilicity, known from dmap as a close relative, in an octahedral complex disables the open position to coordinate additional metal centers.

The extraordinary nucleophilicity of the dmap moiety is additionally a possible explanation for the reactivity of the cation of **2** against *m*CPBA compared to **4** and the copper(I) complex of **L3**. As expected all compounds exhibit a sluggish behavior towards oxygen. Nevertheless, with the cation of **2** a significant acceleration of the ligand oxidation compared to free ligand **L4** is observable. Unfortunately, efforts to catalyze oxidation reactions of substrates proceed not very promising most likely due to the catalyzed cleavage of the ligand.

As a legitimate closing remark for the presented work we should be allowed to say that the synthesis of specific coordination polymers by systematic modification of ligands remains a challenging task. In many cases the resulting structures differ from the expected ones and the discovery of new outstanding attributes of one-dimensional polymers is strongly supported by serendipity. Never the less, the presented coordination polymers demonstrate the influence of steric and electronic ligand attributes and anions towards the formation of coordination polymers and their habitus.

#### 5.1.4 Experimental Section

**Caution!** *The syntheses and procedures described below involve compounds that contain perchlorate ions, which can detonate explosively and without warning. Although we have not encountered any problems with the compounds used in this study, they should be handled with extreme caution.*

##### 5.1.4.1 **Materials and Methods**

Reagents and solvents were all used as commercially available if not mentioned otherwise. All <sup>1</sup>H NMR experiments were performed on a Bruker Avance II 400 spectrometer equipped with a 5 mm BBO Z-gradient probe. To obtain the complete <sup>1</sup>H chemical shift assignments for the **L4** compounds the structure elucidation was based on the application of homonuclear

$^1\text{H}$ ,  $^1\text{H}$  correlation spectroscopy (COSY). The data were collected and processed by TOPSPIN software (Bruker) running on a PC with Microsoft Windows<sup>XP</sup>. The two-dimensional experiments were performed using Bruker standard pulse sequences and parameters. The temperatures for all measurements were calibrated with the Bruker methanol sample and were controlled by a Bruker BVT 3000 temperature unit.

Chemical shifts are reported in ppm ( $\delta$  scale) using TMS as internal standard or the solvent signal as secondary standard. Multiplicities of NMR signals are designated as s (singlet), d (doublet), t (triplet), q (quartet), br (broad), m (multiplet, for unresolved lines), etc.

IR spectra were recorded as KBr pellets using a Bruker *IFS* 25.

Gas chromatographic spectra were recorded on a Quadrupol-MS HP MSD 5971(EI) equipped with a J&W Scientific quartz glass GC column (30m  $\times$  0.25 mm, 0.25  $\mu\text{m}$  DB-5 MS). Helium was used as carrier gas on a stationary phase consisting of phenyl- and methylsilane (5:95). Data were collected with HP 5890 GC program.

Room temperature UV/Visible experiments were performed using an Agilent 8453 spectrophotometer using the UV/Visible Chemstation program (Agilent) for collecting and processing of data.

Low temperature stopped-flow spectra were recorded on a Hightec Scientific SF-61SX2 stopped-flow system. Data were collected and processed with the Kinetic Studio (1.12) program by TgK Scientific.

#### **5.1.4.2 X-ray Structure Determination**

The structure determinations for compounds 4, 5 and 7 were performed at 193 K using a STOE IPDS ( $\text{MoK}_{\alpha}$ ,  $\lambda = 0.71073 \text{ \AA}$ , graphite-monochromator) diffractometer equipped with a low temperature unit of the Karlsruher Glastechnisches Werk.

All single crystals were coated with perfluoropolyether and mounted on a glass fiber. The structures were solved by direct methods and refined on  $F^2$  using full-matrix least-squares techniques using the ShelX 97 program package.<sup>113</sup> Space groups were determined by systematic absences. All non-hydrogen atoms were refined anisotropically.

#### **5.1.4.3 Syntheses of the Ligands L3, L4 and L5**

##### **5.1.4.3.1 General Procedure**

Syntheses of the ligands were performed similar to a recently reported literature procedure for the ligand **L2** with slight modifications.<sup>151</sup> The **L3** precursor *N,N*-[(2-pyridyl)methyl(4-pyridyl)methylamine] was prepared according to the literature.<sup>184</sup> Earlier, Wang *et al.* reported an alternative synthesis of the precursor.<sup>185</sup>

##### **5.1.4.3.2 Synthesis of *N,N*-[(2-pyridyl)methyl(4-pyridyl)methyl]-2-pyridylamine (L3)**

Sodium hydride (60% dispersion in mineral oil; 0.13 g, 3.3 mmol) was dissolved in anhydrous DMF (10 mL) in an inert atmosphere. The resulting grey slurry was stirred at room temperature until hydrogen evolution had ceased. A solution of *N,N*-(2-pyridyl)(4-pyridylmethyl)amine (0.50 g, 2.7 mmol) in anhydrous DMF (10 mL) was then added dropwise.

The resulting orange solution was stirred until hydrogen evolution had ceased. To the amine carbanion, a solution of 2-picolyl chloride (derived from 2-picolyl chloride hydrochloride 0.50 g, 3 mmol) in anhydrous diethyl ether (10 mL) was added dropwise at room temperature. The solution was stirred for 14 h and afterwards the reaction was quenched by addition of water (200 mL) and brine (50 mL). The aqueous solution was extracted with dichloromethane (4 × 50 mL). The combined organic phases were dried over anhydrous Na<sub>2</sub>SO<sub>4</sub>. Removal of the solvent in *vacuo* yielded the crude product as brown oil. After days brown crystals derived from the oil and were washed with acetone (0.26 g, 0.9 mmol, 34,9 %) <sup>1</sup>H NMR (δ, ppm; CDCl<sub>3</sub>, 400 MHz): 8.54 (d, 1H, Pyr-H), 8.50 (d, 2H, Pyr-H), 8.18 (d, 1H, Pyr-H), 7.60 (dvt, 1H, Pyr-H), 7.40 (dvdvd, 1H, Pyr-H), 7.22 (d, 1H, Pyr-H), 7.16 (m, 3H, Pyr-H), 6.63 (dvd, 1H, Pyr-H), 6.44 (d, 1H, Pyr-H), 4.91 (s, 2H, -CH<sub>2</sub>-), 4.87 (s, 2H, -CH<sub>2</sub>-); <sup>13</sup>C NMR (δ, ppm; CDCl<sub>3</sub>, 400 MHz): 158.2, 157.9, 149.8, 149.6, 148.0, 137.7, 136.8, 121.2, 122.2, 121.8, 113.1, 105.9, 54.0, 51.1.

#### 5.1.4.3.3 Synthesis of *N,N*-(4-pyridyl)(2-pyridylmethyl)amine

To a solution of 2-pyridinecarboxaldehyde (5.35 g, 49.9 mmol) and 4-aminopyridine (4.70 g, 49.9 mmol) in toluene (100 mL) a catalytic amount p-toluenesulphonic acid was added. The solution was heated under reflux for 24 h using a Dean-Stark trap for the continuous removal of water. The resulting brown solution was washed with aqueous solution of NaHCO<sub>3</sub> (200 mL). The organic phase was separated and dried over anhydrous Na<sub>2</sub>SO<sub>4</sub>.

After removal of toluene in *vacuo*, the resulting oil was redissolved in methanol (100 mL). To this yellow solution, NaBH<sub>4</sub> (3.00 g, 80.0 mmol) was added and the solution was stirred for 18 h at room temperature. The excess amount of NaBH<sub>4</sub> was cautiously quenched by adding 100 mL water and 100 mL brine at 70 °C. After addition of NaOH (10 M), the solvent was again removed in *vacuo* and the residue was redissolved in water (200 mL). The aqueous solution was extracted with ethyl-acetate (3 × 150 mL) and the combined organic fractions were dried over anhydrous MgSO<sub>4</sub>. Removal of the solvent resulted in a yellow residue which solidified after purification by Kugelrohr Apparatus vacuum distillation (6.00 g, 67.0 %, 33.5 mmol). <sup>1</sup>H NMR (δ, ppm; DMSO-d<sub>6</sub>, 400 MHz): 4.41 (d, 2H, -CH<sub>2</sub>-), 6.52 (d, 2H, Pyr-H), 7.15 (t, 1H, NH), 7.26 (t, 1H, Pyr-H), 7.33 (d, 1H, Pyr-H), 7.74 (t, 1H, Pyr-H), 8.53 (d, 1H, Pyr-H). <sup>13</sup>C NMR (δ, ppm; DMSO-d<sub>6</sub>, 400 MHz): 47.3, 107.3, 121.0, 122.1, 136.6, 148.9, 149.6, 153.3, 158.4. IR (KBr): ν = 3278 (br, m), 3155 (m), 3052 (m), 2933 (w), 2859 (w), 1608 (s), 1571 (m), 1527 (m), 1475 (m), 1342 (m), 1322 (m), 1218 (m), 1150 (w), 1119 (w), 1081 (w), 1049 (w), 993 (m), 815 (m), 759 (m), 615 (w), 533 (m).

#### 5.1.4.3.4 Syntheses of *N*-[Bis(2-pyridyl)methyl]-4-pyridylamine (L4)

Sodium hydride (60% dispersion in mineral oil: 0.46 g, 11.5 mmol) was added to anhydrous DMF (30 mL) and stirred in an inert atmosphere until hydrogen evolution had ceased. After dropwise addition of *N,N*-(4-Pyridyl)(2-pyridylmethyl)amine (1.41 g, 7.6 mmol) in anhydrous DMF (10 mL) the resulting orange solution was stirred for 1 h. An ethereal solution of 2-picolyl chloride as a free base was prepared by solving 2-picolyl chloride hydrochloride (1.70 g, 10.3 mmol) and raising the pH to 7 by adding a sodium hydrogen carbonate solution. The red solution was extracted with ether (4 × 40 mL) and dried over anhydrous Na<sub>2</sub>SO<sub>4</sub> and

inspissated to 5 mL. The resulting ethereal solution was then added dropwise to the amine carbanion and stirred over night at room temperature. The brown solution was cautiously quenched by the addition of water (80 mL) and brine (20 mL) and extracted with dichloromethane (4 x 50 mL). The combined organic fractions were dried over anhydrous Na<sub>2</sub>SO<sub>4</sub>. Removal of the solvent yielded the crude product as a brown solid. The solid was recrystallized from dichloromethane to yield pale yellow crystals (1.09 g, 51.3 %, 3.9 mmol), suitable for single crystal X-ray structure analysis. Crystallographic details of **L4** are given in the Supporting Information. <sup>1</sup>H NMR (δ, ppm; DMSO-d<sub>6</sub>, 400 MHz): 4.87 (s, 4H, -CH<sub>2</sub>-), 6.58 (d, 2H, Pyr-H), 7.29 (m, 4H, Pyr-H), 7.74 (t, 2H, Pyr-H), 8.03 (d, 2H, Pyr-H), 8.55 (d, 2H, Pyr-H). <sup>13</sup>C NMR (δ, ppm; DMSO-d<sub>6</sub>, 400 MHz): 55.6, 107.2, 121.1, 122.3, 136.9, 149.4, 152.8, 157.7 IR (KBr): ν = 3089 (w), 3071 (w), 3048 (w), 3006 (w), 2961 (w), 2925 (w), 1590 (s), 1570 (s), 1542 (m), 1518 (s), 1470 (m), 1445 (w), 1434 (s), 1421 (m), 1406 (s), 1357 (m), 1339 (w), 1274 (w), 1255 (w), 1244 (m), 1228 (s), 1178 (m), 1148 (w), 1105 (w), 1092 (w), 1049 (w), 986 (s), 977 (m), 967 (m), 949 (m), 799 (s), 781 (w), 747 (s), 723 (w), 660 (w), 617 (m), 550 (w), 530 (m).

#### 5.1.4.3.5 Syntheses of *N,N*-(3-pyridyl)(2-pyridylmethyl)amine

*N,N*-(3-pyridyl)(2-pyridylmethyl)amine was prepared analogue to the synthesis of *N,N*-(4-pyridyl)(2-pyridylmethyl)amine described above. The procedure yielded the product as brown oil (5.25 g, 58.6 %, 29.3 mmol). <sup>1</sup>H NMR (δ, ppm; DMSO-D<sub>6</sub>, 400 MHz): 4.38-4.39 (d, 2 H, -CH<sub>2</sub>-), 6.56 (t, 1 H, NH), 6.88 (m, 1 H, Pyr-H3), 7.02 (m, 1 H, Pyr-H7), 7.25 (m, 1 H, Pyr-H2), 7.36 (d, 1 H, Pyr-H5), 7.75 (m, 2 H, Pyr-H1 and H6), 8.00 (d, 1 H, Pyr-H4), 8.53 (d, 1 H, Pyr-H8). <sup>13</sup>C NMR (δ, ppm; DMSO-D<sub>6</sub>, 100 MHz): 47.9, 117.7, 121.2, 122.1, 123.5, 135.5, 136.7, 137.1, 144.4, 148.9, 159.0. IR (KBr): ν = 3277 (br, m), 3100 (w), 3051 (m), 2928 (w), 1592 (s), 1507 (m), 1485 (s), 1437 (m), 1419 (m), 1325 (m), 1245 (w), 1188 (w), 1136 (w), 1048 (w), 996 (w), 797 (m), 758 (m), 709 (m), 627 (w).

#### 5.1.4.3.6 Syntheses of *N*-[Bis(2-pyridyl)methyl]-3-pyridylamine (**L5**)

*N*-[Bis(2-pyridyl)methyl]-3-pyridylamine (**L5**) was synthesized analogue to the preparation of **L4** described above. The procedure yielded 0.78 g (50.9 %, 2.8 mmol) of the crude product. The brown solid was recrystallized from an acetone solution by slow ether diffusion to obtain single crystals suitable for X-ray structure analysis. Crystallographic details of **L5** are given in the Supporting Information. <sup>1</sup>H NMR (δ, ppm; DMSO-D<sub>6</sub>, 400 MHz): 4.86 (d, 2 H, -CH<sub>2</sub>-), 7.02 (d, 1 H, Pyr-H3), 7.06 (t, 1 H, Pyr-H2), 7.28 (t, 2 H, Pyr-H7), 7.33 (d, 2 H, Pyr-H5), 7.74 (t, 2 H, Pyr-H6), 7.80 (d, 1 H, Pyr-H1), 8.02 (s, 1 H, Pyr-H4), 8.56 (d, 2 H, Pyr-H8). <sup>13</sup>C NMR (δ, ppm; DMSO-D<sub>6</sub>, 100 MHz): 56.4, 118.4, 121.1, 123.2, 123.2, 134.4, 136.7, 137.1, 143.7, 149.3, 158.2. IR (KBr): ν = 3443 (br, m), 3049 (m), 3012 (m), 2921 (w), 1594 (s), 1586 (s), 1571 (s), 1561 (m), 1495 (s), 1471 (s), 1434 (s), 1383 (m), 1363 (m), 1339 (m), 1299 (w), 1282 (m), 1250 (m), 1240 (m), 1196 (w), 1176 (s), 1150 (w), 1137 (w), 1118(w), 1095 (m), 1064 (w), 1049 (m), 1007 (w), 992 (m), 979 (w), 964 (w), 944 (w), 908 (w), 884 (w), 794 (s), 764 (m), 753 (s), 725 (w), 710 (s), 659 (w), 618 (m), 595 (w), 561 (w), 543 (m), 512 (w), 460 (w), 420 (w), 405 (m).

#### 5.1.4.4 Synthesis of the Copper(I) Complexes of the Ligands L3, L4 and L5

The oxygen sensitive copper(I) compounds were prepared under Argon atmosphere in a glove box using “extra dry” solvents that were distilled under inert atmosphere prior to use.

##### 5.1.4.4.1 Synthesis of $[\text{Cu}(\text{L3})(\text{MeCN})]_n(\text{CF}_3\text{SO}_3)_n$ (1)

Stoichiometric amounts of **L3** and  $[\text{Cu}(\text{CH}_3\text{CN})_4](\text{CF}_3\text{SO}_3)$  were dissolved in MeCN. By slow ether diffusion over several days yellow, block shaped crystals suitable for single crystal X-ray structure analysis could be obtained.

##### 5.1.4.4.2 Synthesis of $[\text{Cu}_2(\text{L4})_2](\text{CF}_3\text{SO}_3)_2 \cdot \text{DMF}$ (2)

**L4** (50.0 mg, 0.18 mmol) dissolved in DMF (1 mL) and  $\text{Zn}(\text{SO}_3\text{CF}_3)_2$  (0.33 g, 0.1 mmol) in DMF (1 mL) was added dropwise. The solution was stirred and  $[\text{Cu}(\text{CH}_3\text{CN})_4](\text{SO}_3\text{CF}_3)$  (0.34 g, 0.1 mmol) in DMF (1 mL) was added. The resulting yellow solution was stirred for 15 min at room temperature and after one day of ether diffusion at -30 °C yellow single crystals suitable for X-ray crystallographic analysis were obtained.

##### 5.1.4.4.3 Synthesis of $[\text{Cu}(\text{L4})]_n(\text{ClO}_4)_n \cdot n\text{DMF}$ (3)

$\text{Zn}(\text{ClO}_4)_2 \cdot 6\text{H}_2\text{O}$  (0.68 g, 0.18 mmol) was dissolved in DMF (2 mL) and added slowly to a solution of **L4** (0.10 g, 0.4 mmol) in DMF (2 mL).  $[\text{Cu}(\text{CH}_3\text{CN})_4](\text{ClO}_4)$  (0.06 mg, 0.2 mmol) in DMF (1 mL) was added after 5 min. Pale yellow crystals suitable for X-ray crystallography formed after several days of ether diffusion at room temperature.

##### 5.1.4.4.4 Synthesis of $[\text{Cu}_2(\text{L5})_2](\text{BPh}_4)_2 \cdot 2\text{CH}_3\text{COCH}_3$ (4)

0.10 g (0.38 mmol) **L5** was dissolved in acetone (2 mL) and a solution of 0.13 g (0.34 mmol)  $[\text{Cu}(\text{CH}_3\text{CN})_4]\text{PF}_6$  in acetone (2 mL) was added. To the resulting yellow solution 0.12 g (0.34 mmol) Na BPh<sub>4</sub> in acetone (2 mL) was added. After several days of ether diffusion at -33 °C yellow single crystals suitable for X-ray analysis formed.

#### 5.1.4.5 Synthesis of Zinc(II) Complexes of the Ligands L3, L4 and L5

##### 5.1.4.5.1 Synthesis of $[\text{Zn}(\text{DMF})_4(\text{L4})_2](\text{ClO}_4)_2$ (5)

$\text{Zn}(\text{ClO}_4)_2 \cdot 6\text{H}_2\text{O}$  (67.3 mg, 0.18 mmol) in DMF (2mL) and a solution of **L4** (50.0 mg, 0.18 mmol) in DMF (2 mL) were combined and diethyl ether was diffused into the solution at -33.5 °C. Colorless crystals suitable for single crystal X-ray structure analysis formed after 1d at room temperature. The crystals were washed with a small amount of diethyl ether and dried at 50 mbar and 50 °C for 1 h. (46.2 mg, 55 %, 0.05 mmol) <sup>1</sup>H NMR (δ, ppm; DMSO-d<sub>6</sub>, 400 MHz): 2.50 (s, 6H, DMF (-NH<sub>2</sub>)), 2.73 (s, 6H, -CH<sub>3</sub>), (-NH<sub>2</sub>)), 4.89 (s, 4H, -CH<sub>2</sub>-), 6.64 (m, 2H, Pyr-H), 7.30 (m, 4H, Pyr-H), 7.76 (t, 2H, Pyr-H), 7.95 (s, 2H, DMF (-CHO)), 8.01 (m, 2 H, Pyr-H), 8.55 (d, 2H, Pyr-H)

#### 5.1.4.6 Synthesis of the Copper(II) Complexes of the Ligands L4 and L5

##### 5.1.4.6.1 Synthesis of $[\text{Cu}_3\text{Cl}_6(\text{L4})_2]_n \cdot (x\text{H}_2\text{O})_n$ (7)

A methanol solution (2 mL) containing equimolar amounts of  $\text{Cu}(\text{ClO}_4)_2 \cdot 6\text{H}_2\text{O}$  (0.03 g, 0.09 mmol) and  $\text{CuCl}_2 \cdot 2\text{H}_2\text{O}$  (0.01 g, 0.09 mmol) was added to 0.05 g L4 (0.18 mmol) in acetonitrile (2 mL). After 2 days of ether diffusion at  $-30^\circ\text{C}$ , green single crystals suitable for X-ray analysis formed.

##### 5.1.4.6.2 Synthesis of $[\text{CuCl}_2(\text{L5})] \cdot \text{H}_2\text{O}$ (8)

To a solution of 0.03 g (18 mmol)  $\text{CuCl}_2 \cdot 2\text{H}_2\text{O}$  in acetonitrile (1 mL), 0.05 g (0.19 mmol) of the ligand L5 in acetonitrile (1 mL) was added. After 15 min at room temperature green, cubic crystals suitable for X-ray analysis formed from the resulting green solution.

#### 5.1.4.7 Preparation of Heterometallic Solutions Used for NMR Experiments

##### 5.1.4.7.1 Preparation of L4 + $\text{Zn}(\text{SO}_3\text{CF}_3)_2$ + $\text{Cu}(\text{SO}_3\text{CF}_3)$

Under inert conditions  $\text{Zn}(\text{SO}_3\text{CF}_3)_2$  (0.07 g, 0.18 mmol) in acetone (1 mL) was slowly added to L4 (0.10 g, 0.36 mmol) solved in acetone (1 mL). A white precipitate formed, that was redissolved with acetonitrile (2 mL). Upon addition of  $[\text{Cu}(\text{CH}_3\text{CN})_4](\text{SO}_3\text{CF}_3)$  (0.07 g, 0.18 mmol) in acetone (1 mL) and diethyl ether (5 mL) a white precipitate formed (0.12 g). It was separated by suction filtration, washed with a small amount of acetone and dried in *vacuo*.

$^1\text{H}$ -NMR ( $\delta$ , ppm;  $\text{dmsO-d}_6$ , 400 MHz): 8,61 (d, 2H, Pyr-H,  $^3J_{\text{H,H}} = 4,7$  Hz), 7,87 (dvt, 2H, Pyr-H,  $^3J_{\text{H,H}} = 7,6$  Hz,  $^4J_{\text{H,H}} = 1,5$  Hz), 7,78 (s, 2H, Pyr-H), 7,46 (d, 2H, Pyr-H,  $^3J_{\text{H,H}} = 7,9$  Hz), 7,40 (t, 2H, Pyr-H,  $^3J_{\text{H,H}} = 6,2$  Hz), 6,60 (s, 2H, Pyr-H), 4,93 (s, 4H,  $-\text{CH}_2-$ )

##### 5.1.4.7.2 Preparation of a Mixture of L4 + $\text{Zn}(\text{ClO}_4)_2$ + $\text{Cu}(\text{ClO}_4)$

$\text{Zn}(\text{ClO}_4)_2 \cdot 6\text{H}_2\text{O}$  (0.07 g, 0.18 mmol) was dried in *vacuo* and solved under inert conditions in acetone (1 mL). The solution was slowly added to an acetone solution (1 mL) L4 (0.10 g, 0.36 mmol). A white precipitate formed, that was redissolved with acetonitrile (2 mL). Upon addition of  $[\text{Cu}(\text{CH}_3\text{CN})_4](\text{ClO}_4)$  (0.06 g, 0.18 mmol) in acetone (1 mL) and diethyl ether (5 mL) a white precipitate formed (0.12 g). It was separated by suction filtration, washed with a small amount of acetone and dried in *vacuo*.

$^1\text{H}$ -NMR ( $\delta$ , ppm;  $\text{dmsO-d}_6$ , 400 MHz): 8,59 (d, 2H, Pyr-H,  $^3J_{\text{H,H}} = 4,6$  Hz), 7,85 (t, 2H, Pry-H,  $^3J_{\text{H,H}} = 7,7$  Hz), 7,81 (s, 2H, Pyr-H), 7,43 (d, 2H, Pyr-H,  $^3J_{\text{H,H}} = 7,7$  Hz), 7,37 (t, 2H, Pyr-H,  $^3J_{\text{H,H}} = 6,0$  Hz), 6,63 (s (b), 2H, Pyr-H), 4,92 (s, 4H,  $-\text{CH}_2-$ )

#### 5.1.5 Acknowledgements

The authors thank Dr. Klaus Peppler of the Institute for Physical Chemistry of the Justus-Liebig-University/Gießen for the REM experiments.

Low temperature stopped flow spectrum of the oxidation of  $[\text{Cu}_2(\text{L4})_2](\text{BF}_4)_2$  with *m*CPBA

## 5.2 Supporting Information for Chapter 5.1

### 5.2.1 Crystal Structures of the Ligands L4 and L5

The so far unknown molecular structures of pale yellow (**L4**) and brown (**L5**) single crystals are depicted in Figures 91 and 92. Crystallographic details are described in Table 14 SI.

Bond lengths and angles of the new ligands are all in expectable ranges for C-C and C-N bonds, respectively.

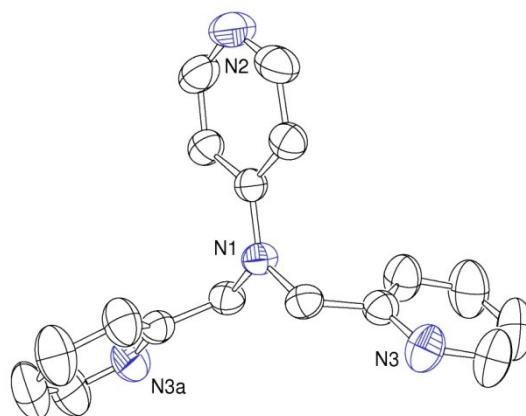


**Fig. 91** Thermal ellipsoid representation of the molecular structure of the ligand **L4** with 50% probability.

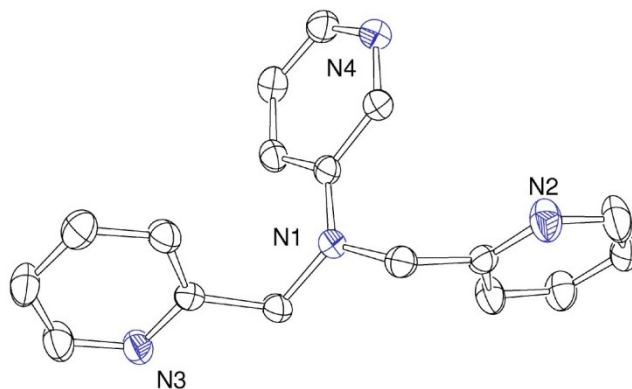


**Fig. 92** Thermal ellipsoid representation of the molecular structure of the ligand **L5** with 50% probability.



**Table 14** Crystallographic data of the molecular structures presented in the Supporting Information paragraph.

	L4	L5	[Cu <sub>2</sub> (L4) <sub>2</sub> ](PF <sub>6</sub> ) <sub>2</sub> ·2CH <sub>3</sub> COCH <sub>3</sub>	[Cu <sub>2</sub> (L4) <sub>2</sub> ](PF <sub>6</sub> ) <sub>2</sub> ·DMF	[Cu <sub>3</sub> Cl <sub>6</sub> (L4) <sub>2</sub> ]·H <sub>2</sub> O	[Zn(DMF) <sub>4</sub> (L4) <sub>2</sub> ](CF <sub>3</sub> SO <sub>3</sub> ) <sub>2</sub>
Empirical formula	C <sub>17</sub> H <sub>16</sub> N <sub>4</sub>	C <sub>17</sub> H <sub>16</sub> N <sub>4</sub>	C <sub>20</sub> H <sub>22</sub> CuF <sub>6</sub> N <sub>4</sub> OP	C <sub>40</sub> H <sub>46</sub> Cu <sub>2</sub> F <sub>12</sub> N <sub>10</sub> O <sub>2</sub> P <sub>2</sub>	C <sub>34</sub> H <sub>32</sub> Cl <sub>6</sub> Cu <sub>3</sub> N <sub>8</sub>	C <sub>48</sub> H <sub>60</sub> F <sub>6</sub> N <sub>12</sub> O <sub>10</sub> S <sub>2</sub> Zn
Formula weight	276.34	2176.34	542.93	1115.89	972.00	1208.57
Temperature [K]	193(2)	200(2)	193(2)	200(2)	193(2)	193(2)
Wavelength [Å]	0.71073	0.71073	0.71073	0.71073	0.71073	0.71073
Crystal system, space group	monoclinic, P2(1)/c	Triclinic, P-1	Triclinic, P-1	Triclinic, P-1	Monoclinic, P2(1)/c	Triclinic, P-1
Unit cell dimensions [Å, °]	a = 18.784(4) b = 8.1377(16) c = 11.694(2) α = 90 β = 123.85(3) γ = 90	a = 6.209(1) b = 9.924(1) c = 11.786(1) α = 90.134(1) β = 102.27(1) γ = 97.267(1)	a = 8.642(2) b = 11.610(2) c = 12.541(3) α = 66.29(3) β = 73.42(3) γ = 76.27(3)	a = 8.3995(7) Å, b = 11.9873(10) Å c = 12.5722(11) Å α = 70.043(1) β = 72.471(1) γ = 79.479(1)	a = 16.055(3) b = 14.890(2) c = 17.374(3) α = 90 β = 113.08(3) γ = 90	a = 8.572(2) b = 12.183(2) c = 14.358(3) α = 111.91(3) β = 100.35(3) γ = 90.15(3)
Volume [Å <sup>3</sup> ]	1484.6(5)	703.75	1093.2(4)	1130.09(17)	3820.8(13)	1364.6(5)
Z, Calculated density [Mg/m <sup>3</sup> ]	4, 1.236	2, 1.304	2, 1.649	1, 1.640	4, 1.690	1, 1.471
Absorption coefficient [mm <sup>-1</sup> ]	0.076	0.081	1.144	1.110	2.116	0.614
F(000)	584	292	552	568	1956	628
Crystal size [mm <sup>3</sup> ]	0.40 x 0.32 x 0.24	0.28 x 0.20 x 0.12	0.76 x 0.44 x 0.32	0.45 x 0.35 x 0.20	0.32 x 0.24 x 0.16	1.46 x 0.12 x 0.08
θ range for data collection [°]	2.82 to 27.97	1.77 to 28.31	2.72 to 28.09	1.78 to 28.31	1.38 to 31.10	2.80 to 28.16
Limiting indices	-24 ≤ h ≤ 24 -10 ≤ k ≤ 10 -15 ≤ l ≤ 15	-8 ≤ h ≤ 8 -12 ≤ k ≤ 12 -15 ≤ l ≤ 15	-11 ≤ h ≤ 11 -15 ≤ k ≤ 15 -16 ≤ l ≤ 16	-11 ≤ h ≤ 11 -15 ≤ k ≤ 15 -16 ≤ l ≤ 16	-23 ≤ h ≤ 23 -19 ≤ k ≤ 19 -21 ≤ l ≤ 21	-10 ≤ h ≤ 10 -16 ≤ k ≤ 16 -19 ≤ l ≤ 18
Reflections collected / unique	6491 / 1717 [R(int) = 0.0333]	8408 / 3352 [R(int) = 0.0272]	9951 / 4859 [R(int) = 0.0652]	12634 / 5352 [R(int) = 0.0246]	46012 / 9449 [R(int) = 0.2536]	12483 / 6091 [R(int) = 0.0485]
Completeness to θ	28.29 99.7%	28.31 95.6 %	28.09 91.1 %	28.31 95.4 %	31.10 76.9 %	28.16 91.0 %
Absorption correction	None	None	None	multi-scan	None	None
Refinement method	Full-matrix least-sq. on F <sup>2</sup>	Full-matrix least-sq. on F <sup>2</sup>	Full-matrix least-sq. on F <sup>2</sup>	Full-matrix least-squares on F <sup>2</sup>	Full-matrix least-sq. on F <sup>2</sup>	Full-matrix least-sq. on F <sup>2</sup>
Data/restraints/parameters	1717 / 0 / 129	3352 / 0 / 194	4859 / 0 / 337	5352 / 0 / 316	9449 / 0 / 471	6091 / 0 / 402
Goodness-of-fit on F <sup>2</sup>	1.005	1.068	1.111	1.044	0.988	0.862
Final R indices [I > 2σ(I)]	R1 = 0.0454, wR2 = 0.1086	R1 = 0.0426, wR2 = 0.1134	R1 = 0.0587, wR2 = 0.1720	R1 = 0.0346, wR2 = 0.0840	R1 = 0.0871, wR2 = 0.2198	R1 = 0.0491, wR2 = 0.1129
R indices (all data)	R1 = 0.0853, wR2 = 0.1227	R1 = 0.0574, wR2 = 0.1194	R1 = 0.0670, wR2 = 0.1804	R1 = 0.0442, wR2 = 0.0905	R1 = 0.2638, wR2 = 0.2771	R1 = 0.0955, wR2 = 0.1298
Largest diff. peak and hole [e·Å <sup>-3</sup> ]	0.142 and -0.113	0.203 and -0.221	0.976 and -1.900	0.443 and -0.389	1.670 and -1.594	0.759 and -0.446

### 5.2.2 $[\text{Cu}_2(\text{L4})_2](\text{PF}_6)_2 \cdot 2\text{CH}_3\text{COCH}_3$

In solid form  $[\text{Cu}_2(\text{L4})_2](\text{PF}_6)_2 \cdot 2\text{CH}_3\text{COCH}_3$  is air stable for several minutes. The use of perfluorated polyether prevented oxidation of the single crystals during the time of preparation. The molecular structure depicted in Figure 93 shows the dimeric cationic copper(I) complex with a  $\text{Cu}(1) \cdots \text{Cu}(1a)$  distance of 6.148(2) Å. This distance represents the diagonal of the cavity formed between the two pyridyl rings and the two dipicolylamine units of the different ligand molecules. The “height” is represented by the distance between the coplanar planes spanned by the atoms of the two pyridyl rings of 3.44(4) Å.

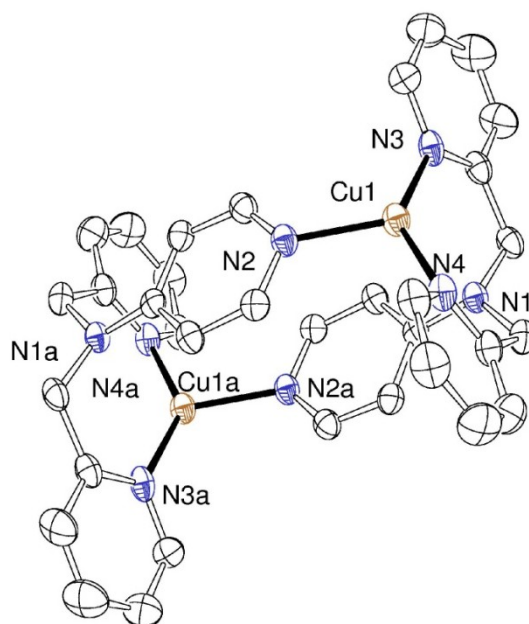


**Fig. 93** Thermal ellipsoid representation of the molecular structure of the cation of  $[\text{Cu}_2\text{L4}_2]\text{PF}_6 \cdot 2\text{CH}_3\text{COCH}_3$  with 50% probability. Solvent molecules are omitted for clarity.

With bond lengths around 2.00 Å (see Table 15 SI) the aromatic nitrogen atoms N2, N3 and N4 bind significantly stronger to the metal atom than the aliphatic nitrogen atom N1. This is indicated by a distance to Cu(1) of 2.508(3) Å. Therefore, a  $\text{Cu}(1) \cdots \text{N}(1)$  bond is not marked in Figure 93.

**Table 15** Selected bond lengths [Å] and angles [°] of the molecular structures presented in the Supporting Information paragraph.

$[\text{Cu}_2(\text{L4})_2](\text{PF}_6)_2 \cdot 2\text{CH}_3\text{COCH}_3$							
Cu(1)-N(2)	2.025(3)	Cu(1)-N(3)	1.959(3)	Cu(1)-N(4)	1.987(3)	Cu(1)-N(1)	2.508(3)
N(2)-Cu(1)-N(4)	106.95(12)	N(3)-Cu(1)-N(2)	115.69(12)	N(3)-Cu(1)-N(4)	137.07(12)	N(1)-Cu(1)-N(2)	117.3(1)
N(1)-Cu(1)-N(3)	78.3(1)	N(1)-Cu(1)-N(4)	78.2(1)	Cu(1)-Cu(1a)	6.148(2)		
symmetry operation used to generate equivalent atoms: a) 2-x, 1-y, -z							
$[\text{Cu}_2(\text{L4})_2](\text{PF}_6)_2 \cdot \text{DMF}$							
Cu(1)-N(2)	1.997(2)	Cu(1)-N(3)	1.971(2)	Cu(1)-N(4a)	2.009(2)	Cu(1)-N(1)	2.539(2)
N(2)-Cu(1)-N(4a)	111.4(1)	N(3)-Cu(1)-N(2)	130.3(1)	N(3)-Cu(1)-N(4a)	118.20(7)	N(1)-Cu(1)-N(2)	77.5(1)
N(1)-Cu(1)-N(3)	77.8(1)	N(1)-Cu(1)-N(4a)	118.0(1)	Cu(1)-Cu(1a)	6.090(2)		
symmetry operation used to generate equivalent atoms: a) -x+1, -y+1, -z							

<b>[Cu<sub>3</sub>Cl<sub>6</sub>(L4)<sub>2</sub>]·H<sub>2</sub>O</b>							
Cu(1)-N(1)	2.291(9)	Cu(1)-N(2)	1.982(10)	Cu(1)-N(3)	2.026(10)	Cu(2)-N(4)	2.066(10)
Cu(2)-N(8)	2.045(9)	Cu(3)-N(6)	1.874(9)	Cu(2)-N(7)	1.864(10)	Cu(1)-Cl(1)	2.301(3)
Cu(1)-Cl(2)	2.410(4)	Cu(2)-Cl(3)	2.393(3)	Cu(2)-Cl(4)	2.313(3)	Cu(3)-Cl(5)	2.204(3)
Cu(3)-Cl(6)	2.328(4)	N(2)-Cu(1)-N(1)	83.8(3)	N(3)-Cu(1)-N(1)	77.0(4)	N(2)-Cu(1)-N(3)	160.8(4)
N(1)-Cu(1)-Cl(1)	117.9(3)	N(2)-Cu(1)-Cl(1)	96.8(3)	N(3)-Cu(1)-Cl(1)	91.0(3)	N(1)-Cu(1)-Cl(2)	94.8(2)
N(2)-Cu(1)-Cl(2)	86.5(3)	N(3)-Cu(1)-Cl(2)	96.4(3)	Cl(1)-Cu(1)-Cl(2)	147.3(2)	N(8)-Cu(2)-N(4)	174.6(4)
N(4)-Cu(2)-Cl(3)	99.1(3)	N(8)-Cu(2)-Cl(3)	81.8(3)	N(4)-Cu(2)-Cl(4)	89.2(3)	N(8)-Cu(2)-Cl(4)	92.6(3)
Cl(4)-Cu(2)-Cl(3)	151.0(2)	N(7)-Cu(3)-N(6)	158.4(5)	N(6)-Cu(3)-Cl(5)	98.1(3)	N(7)-Cu(3)-Cl(5)	89.9(3)
N(6)-Cu(3)-Cl(6)	87.3(3)	N(6)-Cu(3)-Cl(6)	99.1(3)	Cl(5)-Cu(3)-Cl(6)	140.9(2)	Cu(3)-Cu(2a)	4.553(2)
Cu(2a)-Cl(5)	2.820(4)	Cu(2)-Cl(5)-Cu(2a)	129.5(1)				
symmetry operation to generate equivalent atoms: a) x, 1.5-y, -1/2+z							
<b>[Zn(DMF)<sub>4</sub>(L4)<sub>2</sub>](CF<sub>3</sub>SO<sub>3</sub>)<sub>2</sub></b>							
O(1)-Zn(1)	2.195(2)	O(2)-Zn(1)	2.099(2)	N(2)-Zn(1)	2.080(3)	O(1)-Zn(1)-O(1a)	180.000 (1)
N(2a)-Zn(1)-N(2)	180.0	N(2)-Zn(1)-O(2)	89.66(9)	N(2)-Zn(1)-O(2a)	90.34(9)	N(2)-Zn(1)-O(1)	89.12(9)
N(2)-Zn(1)-O(1a)	90.88(9)	O(2)-Zn(1)-O(1)	89.66(8)	O(2)-Zn(1)-O(1a)	90.35(8)	O(2a)-Zn(1)-O(2)	180.00(8)
symmetry operation used to generate equivalent atoms: a) -x+1, -y+1, -z+1							

### 5.2.3 [Cu<sub>2</sub>(L4)<sub>2</sub>](PF<sub>6</sub>)<sub>2</sub>·DMF

We additionally obtained single crystals of the cage-like dimer [Cu<sub>2</sub>(L4)<sub>2</sub>](PF<sub>6</sub>)<sub>2</sub> from a DMF solution. An ORTEP representation of the molecular structure of the cation [Cu<sub>2</sub>(L4)<sub>2</sub>]<sup>+</sup> is shown in Figure 94. Each of the two copper(I) atoms is coordinated by both ligand molecules. The coordination formed by the three nitrogen atoms N2, N3 and N4 around the copper(I) is best described trigonal planar with angles of 115.7(1) ° for N3···Cu1···N2, 107.0(1) ° for N4···Cu1···N2 and 137.0(1) ° for N4···Cu1···N3 indicative for a strong distortion. Cu1 is located in the plane spanned by the three nitrogen atoms. With a distance of 2.539(2) to the copper atom the aliphatic nitrogen atom N1 is not regarded as coordinated.

The coordination of the two methylpyridyl nitrogen atoms N2 and N3 of one ligand molecule at the same copper center the bond lengths Cu1···N3 (1.959(3) Å) and Cu1···N4 (1.987(3) Å) are shorter than the comparable ones for compound **1** that coordinate two different copper(I) centers. The pyridyl nitrogen N4 in 4-position forms a longer coordination bond (2.025(3) Å) to Cu1<sup>i</sup>, the second copper(I) atom of the cage. The two pyridyl bridges form a linear connection between the two metal atoms.

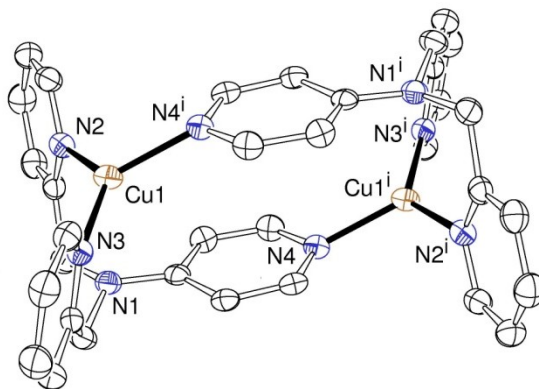


**Fig. 94** Thermal ellipsoid representation of the molecular structure of the cation of [Cu<sub>2</sub>(L4)<sub>2</sub>](PF<sub>6</sub>)<sub>2</sub>·DMF with 50% probability. Hydrogen atoms, anions and solvent molecules are omitted for clarity.

5.2.4  $[\text{Cu}_3\text{Cl}_6(\text{L4})_2]\cdot\text{H}_2\text{O}$  (6)

A thermal ellipsoid representation of the trimeric unit as building block of the coordination polymer described in the main article is shown in Figure 95. These units are bridged by the chloride ion Cl5 coordinating copper atoms Cu3 and a symmetry-equivalent of Cu2.

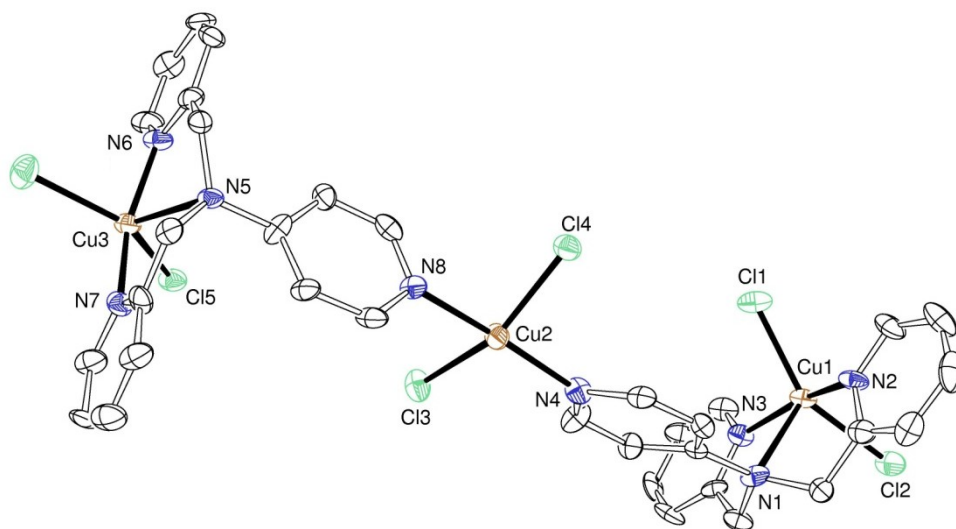


**Fig. 95** Thermal ellipsoid representation of the molecular structure of  $[\text{Cu}_3\text{Cl}_6(\text{L4})_2]\cdot\text{H}_2\text{O}$  with 50% probability. Solvent molecules are omitted for clarity.

The trimeric subunit of compound 6 consists of three copper atoms and two ligand molecules. Furthermore, the copper atoms are coordinated by chloride anions. All three copper atoms are five coordinate with coordination surroundings best described as distorted square pyramidal. Cu1 and Cu3 are coordinated by three nitrogen atoms (N1, N2 and N3 for Cu1 and N5, N6 and N7 for Cu3 respectively) of the two bispicolylamine units. Additionally, two chloride atoms are coordinated in the basal plane of the pyramid. (Cl1 and Cl2 for Cu1 and Cl5 and Cl6 for Cu3 respectively). The third copper atom Cu2 is located in the middle of the trimer, serving as linker between the two ligand molecules. It is *trans*-coordinated by two nitrogen atoms of the 4-pyridyl residues N4 and N8. The basal plane of the square pyramid is formed of two additional chloride atoms Cl3 and Cl4. Not obvious from Figure 95, but noticeable in the polymeric structure (Figure 86) a third chloride atom (symmetry equivalent of Cl5) is coordinated on top of the pyramid. It links to the next trimeric subunit of the superstructure to form the helical coordination polymer described in the main article.

This copper(II) complex is another example for the coordination of both, the bispicolylamine unit and the 4-pyridine nitrogen of the ligand **L4**. This finding is in striking contrast to the zinc(II) complexes **5** and  $[\text{Zn}(\text{DMF})_4(\text{L4})_2](\text{CF}_3\text{SO}_3)_2$  of **L4** only coordinated by the 4-pyridine nitrogen atoms.

### 5.2.5 $[\text{Zn}(\text{DMF})_4(\text{L4})_2](\text{CF}_3\text{SO}_3)_2$

Figure 96 depicts the structure of the complex cation of  $[\text{Zn}(\text{DMF})_4(\text{L4})_2](\text{CF}_3\text{SO}_3)_2$ . The molecular structure of the complex cation is nearly superimposable to that of compound **5**. Only differing in its anion (triflate instead of perchlorate) from compound **5**, this is a second structure demonstrating that only the 4-pyridyl nitrogen atoms do coordinate to the zinc(II) ions. The bispicolylamine nitrogen atoms do not coordinate. Until today, there is no pleasant explanation for this behavior.

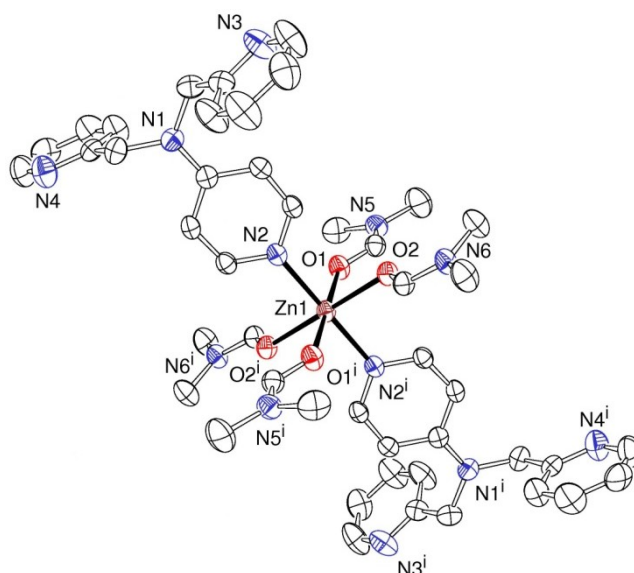


**Fig. 96** Thermal ellipsoid representation of the molecular structure of  $[\text{Zn}(\text{DMF})_4\text{L4}_2](\text{CF}_3\text{SO}_3)_2$  with 50% probability. Anions are omitted for clarity.

### 5.2.6 EDX Measurement

Colorless crystals were separated of a green solution containing copper(II), zinc(II), and  $\text{CF}_3\text{SO}_3^-$  ions and were identified by unit cell determination as  $[\text{Zn}(\text{DMF})_4\text{L4}_2](\text{CF}_3\text{SO}_3)_2$ . In order to determine the metal center, EDX measurements were performed. Its results are shown in Figure 97.

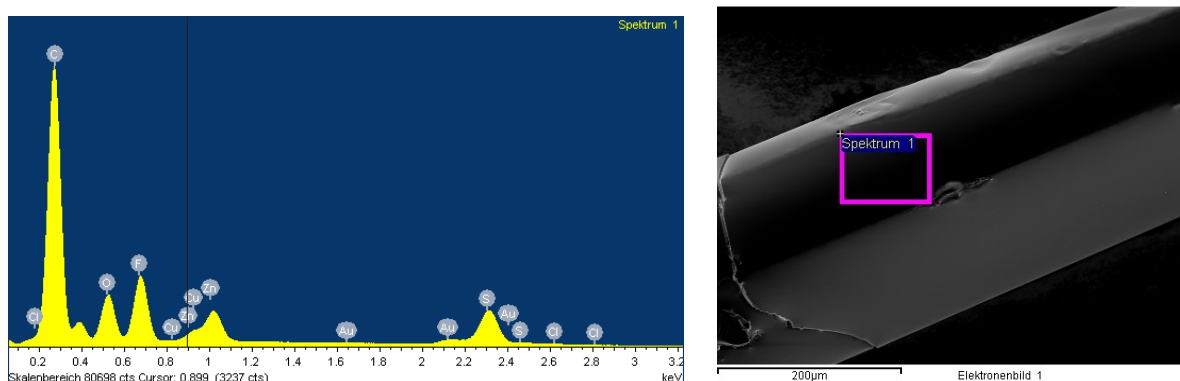


**Fig. 97** EDX spectrum and electron picture of the measured single crystal.

The electron picture in Figure 97 shows a trapeze-like single crystal of  $[\text{Zn}(\text{DMF})_4\text{L4}_2](\text{CF}_3\text{SO}_3)_2$  and the area the EDX measurement was performed in (blue frame). Beside signals for carbon, sulfur, fluorine and oxygen, signals characteristic for zinc atoms as well as that for copper are observable in the EDX. With an atom

percentage of 0.8 % zinc and 0.3 % copper, the compound is mainly consisting of complexes containing zinc disordered with copper atoms. Unfortunately, the EDX method is not reliable in this low atom percentage area. Therefore, the exact zinc/copper ratio cannot be determined for the analyzed compound. Nevertheless, the result of the EDX measurement together with the cell determination *via* single crystal X-ray analysis of the same crystal are strong hints for  $[\text{Zn}(\text{DMF})_4\text{L4}_2](\text{CF}_3\text{SO}_3)_2$  disordered with copper ions. Contamination of the crystal surface with dried solution should not lead to significant signals in the EDX spectrum.

Additionally, EDX measurements were performed with blue crystal species deriving from the same solution. Its results are shown in Figure 98.

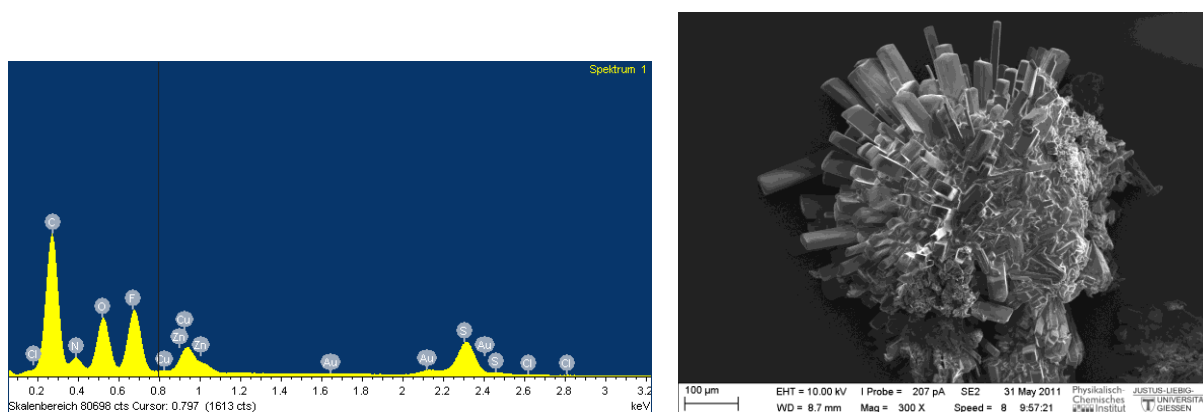


**Fig. 98** EDX spectrum and electron picture of the measured blue species.

As obvious from the electron picture, the blue species was unfortunately polycrystalline. Thus, a structure- or cell determination using single crystal X-ray analysis could not be performed. The EDX spectrum again shows the expected signals of the ligand and the anion and that of both, copper and zinc. A comparison with the spectrum of the  $[\text{Zn}(\text{DMF})_4\text{L4}_2](\text{CF}_3\text{SO}_3)_2$  single crystal above already shows differences in the relative signal intensities of the two metals. With atom percentages of 1.2 % for copper and 0.3 % for zinc, this is most likely a copper(II) complex compound with disordered zinc. Again, the low percentages of the two metal ions prevent an exact analysis. Additional attempts to grow single crystals of this blue species were unsuccessful so far.

### 5.2.7 Low Temperature Stopped Flow Spectrum of the Oxidation Reaction of $[\text{Cu}_2(\text{L4})_2](\text{BF}_4)_2$ with *m*CPBA

At  $-91^\circ\text{C}$  the bands at 360 nm and 680 nm indicative for a copper(II) complex (see room temperature spectra of the corresponding copper(II) complex (Figure 99)) are rising and even over a period of 900 s no second species could be observed. Most likely the hydroxylated species coordinates copper and is responsible for the bands (see Figure 99).

A blue peroxido complex could even at these low temperatures not be observed. Due to the bad solubility of the copper(I) complex in solvents that would allow even lower

temperatures, an observation of the more reactive intermediates *via* low temperature stopped-flow techniques was impossible.

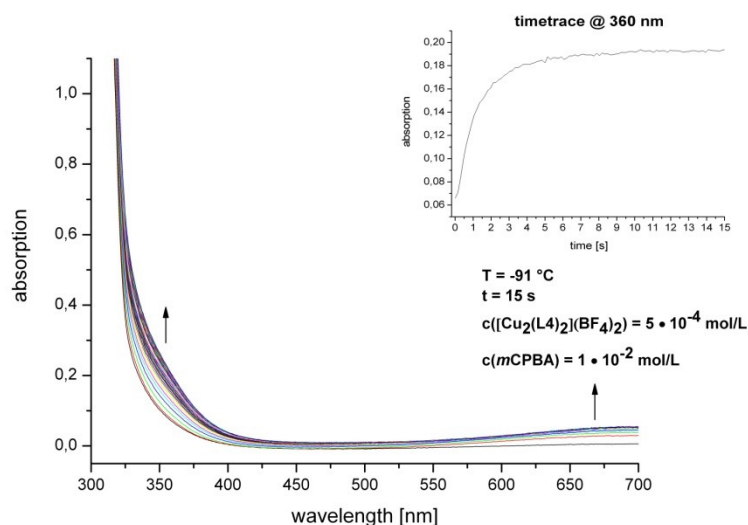


**Fig. 99** Low temperature stopped flow spectrum and timetrace at -91 °C of the oxidation reaction of  $[\text{Cu}_2(\text{L4})_2](\text{BF}_4)_2$  with *m*CPBA

### 5.2.8 UV/Vis Spectra of Copper(II) Complexes

Stoichiometric mixture of  $\text{Cu}(\text{BF}_4)_2$  and L4 at room temperature lead to the formation of a green solution. The UV/Vis spectrum depicted in Figure 100 shows a broad band with an absorption maximum at 625 nm. It is most likely deriving from metal centered dd transitions that are typical for copper(II) complex compounds.

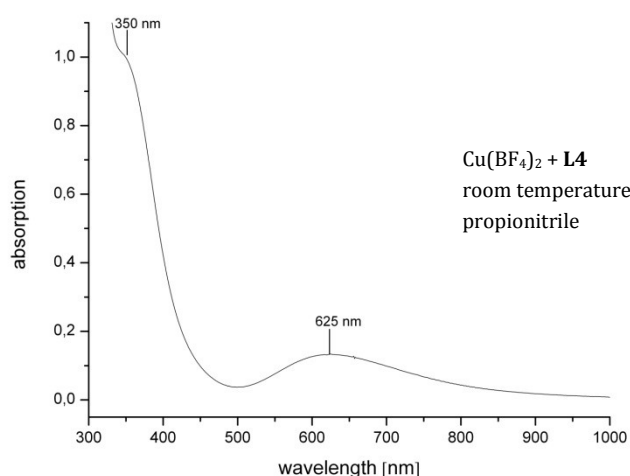


**Fig. 100** Room temperature UV/Vis spectrum of a solution containing  $\text{Cu}(\text{BF}_4)_2$  and the ligand L4 using propionitrile as solvent.



### **5.2.9 Experimental Section of the Supporting Information**

#### **5.2.9.1 Synthesis of Ligands L4 and L5**

Purification and syntheses of pale yellow (**L4**) and brown (**L5**) single crystals of both ligands were carried out as described in the main article.

#### **5.2.9.2 Synthesis of $[\text{Cu}_2(\text{L4})_2](\text{PF}_6)_2 \cdot 2\text{CH}_3\text{COCH}_3$**

Yellow crystals suitable for X-ray structure analysis formed from an acetone solution prepared according to the described procedure for **2** (see chapter 5.1.4.4).

#### **5.2.9.3 Synthesis of $[\text{Cu}_2(\text{L4})_2](\text{PF}_6)_2 \cdot \text{DMF}$**

To a solution of **L4** (0.10 g, 0.38 mmol) in DMF (2 mL)  $[\text{Cu}(\text{CH}_3\text{CN})_4]\text{PF}_6$  (0.13 g, 0.34 mmol) in DMF (2 mL) was added. After 15 min at room temperature, yellow crystals suitable for X-ray structure analysis formed from the resulting yellow solution.

#### **5.2.9.4 Synthesis of $[\text{Zn}(\text{DMF})_4(\text{L4})_2](\text{CF}_3\text{SO}_3)_2$**

To (0.091 g, 0.34 mmol) **L4** solved in 1.0 mL acetone a solution of  $\text{Cu}(\text{CF}_3\text{SO}_3)_2$  (0.060 g, 0.34 mmol) and  $\text{Zn}(\text{CF}_3\text{SO}_3)_2$  (0.060 g, 0.34 mmol) in 1.5 mL acetone was added dropwise. A white precipitate formed, that was resolved by adding 1.0 mL DMF. After 2 days of ether diffusion at room temperature, blue and colorless crystals formed. The colorless species was separated and structurally characterized by single crystal X-ray diffractometry. Additionally, EDX measurements with both species were performed.

#### **5.2.9.5 Low Temperature Stopped Flow Spectrum of the Oxidation Reaction of $[\text{Cu}_2(\text{L4})_2](\text{BF}_4)_2$ with mCPBA**

Low temperature stopped flow measurements were performed as described in the main article. The copper(I) solution was prepared under inert atmosphere with stoichiometric amounts of  $[\text{Cu}(\text{CH}_3\text{CN})_4]\text{BF}_4$  and **L4** resulting in a yellow  $1 \times 10^{-3}$  mol/L propionitrile solution of  $[\text{Cu}_2(\text{L4})_2](\text{BF}_4)_2$ . After mixture with a  $2 \times 10^{-2}$  mol/L mCPBA propionitrile solution at  $-91^\circ\text{C}$  the spectra depicted in Figure 99 were recorded.

#### **5.2.9.6 UV/Vis Measurement of Copper(II) Complexes**

Using propionitrile as solvent, a  $1 \times 10^{-2}$  mol/L solution containing stoichiometric amounts of  $\text{Cu}(\text{BF}_4)_2$  and the ligand **L4** was prepared. The spectrum was recorded with an agilent 8463 spectrophotometer at room temperature. The solution was diluted with additional propionitrile until the absorption adjusted in an acceptable range and the dd-band was still clearly visible.



## 6 Summary/Zusammenfassung

### 6.1 Summary

Copper and zinc complexes with dipicolylamine as binding motif (Figure 101) attracted growing interest with regard to their extraordinary properties. There are examples of transition metal complexes using derivatised bispic compounds as ligands in many fields of chemical research. Zinc(II) complexes as fluorescence sensors in biological processes, copper(I) complexes for the activation of small molecules like carbon dioxide or coordination polymers with highly interesting properties, the opportunities included in the synthesis and characterization of so far unknown transition metal complexes using this ligand class are very promising. Hence studies on selected derivatives of bispic and their copper and zinc complexes were initialized and the results that could be achieved are presented in this work.

Extending the bispic binding unit with a fourth nitrogen atom leads to a tripodal ligand class well known for their stabilization of reactive oxygen intermediates of copper coordination compounds and thus enabling studies on metalloenzymatic oxygenation reactions. Unspenp affords the opportunity to combine an extraordinary binding site for copper and zinc ions with additional functionalities such as bridging units or extended  $\pi$ -systems for instance. Coordination compounds using functionalized derivatives of unspenp as ligands are supposed to exhibit extraordinary properties with regard to studying and activating reactive oxygen intermediates of their copper(I) complexes. A minor part of this work focused on the synthesis and characterization of copper(I) complexes and their reactivity towards dioxygen of selected representatives of this ligand family.

The structures of the parent amines bispic and unspenp are depicted in Figure 101. The reported results are all based on the derivatisation of these ligands and the synthesis and characterization of their copper and zinc coordination compounds.

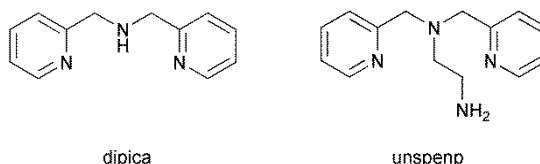


**Fig. 101**                      Structure of the parent amines bispic and unspenp.

The interesting properties with regard to magnetism, emission behavior and the formation of one-dimensional coordination polymers of selected compounds could be reported. Chapter 6 is supposed to provide a condensed insight into the results of this work.

### 6.1.1 Unspenp Relatives as Ligands

Yellow solutions of copper(I) complexes using xylyl-bridged unspenp units as ligands were prepared and the reactivity towards dioxygen was studied using low temperature stopped-flow techniques. Reactive superoxido- and peroxido species could be successfully identified. For the imine the results reported earlier by Garcia-Bosch *et al.* for perchlorate salts could be confirmed.<sup>123</sup> Upon reaction with dioxygen at  $-90\text{ }^{\circ}\text{C}$  in propionitrile as solvent the copper(I) complex of Imxyl-unspenp forms a typical, metastable  $\mu-(\eta^1:\eta^1)$ -peroxido intermediate represented by intensive charge transfer bands at 502 and 637 nm respectively. The imine band located at 378 nm shows unsteady behavior during the first reaction period, which is not clearly explainable. The identified reactive oxygen adduct species of the copper(I) complexes of Imxyl-unspenp and Hxyl-unspenp are depicted in Figure 102.

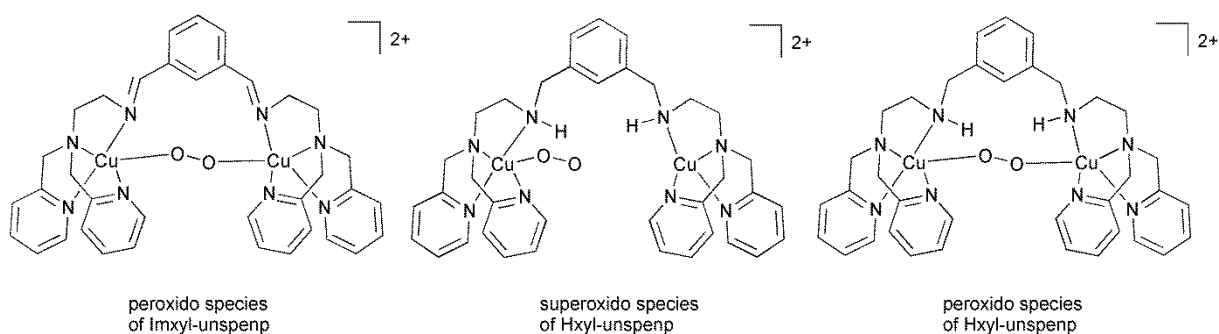


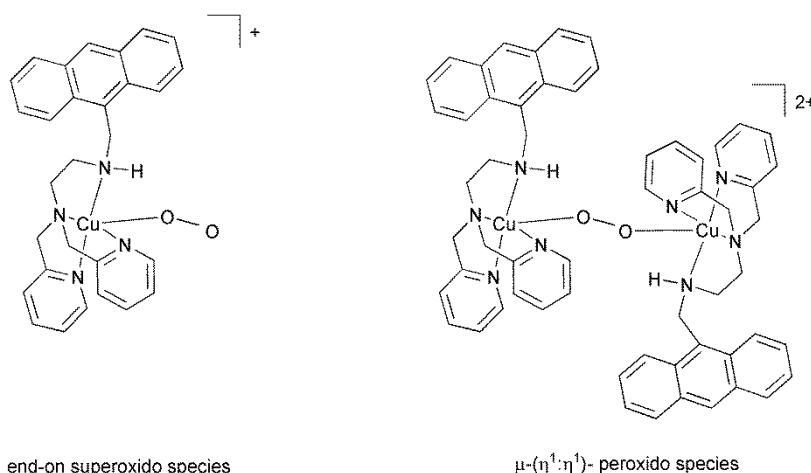
**Fig. 102** Reactive intermediates identified during the reaction of dioxygen with solutions of  $[\text{Cu}_2(\text{Imxyl-unspenp})]^{2+}$  and  $[\text{Cu}_2(\text{Hxyl-unspenp})]^{2+}$ , respectively.

The copper(I) complex of Hxyl-unspenp forms similar UV/Vis bands at 517 and 602 nm assignable to the  $\mu-(\eta^1:\eta^1)$ -peroxido species. In contrast to the imine coordination compound a third intensive band at 422 nm is detectable at  $-93\text{ }^{\circ}\text{C}$  that decays within seconds most likely assignable to an end-on superoxido species known from unspenp studies. Therefore, the protonated species is assumed to stabilize the superoxido species, disfavored by the second intramolecular copper(I) atom with high binding affinity. All discussed species are highly reactive, but unfortunately more detailed kinetic studies could not be performed so far.

First hints of reactivity towards carbon dioxide from air were reported. A crystal structure with high R-values could be presented, revealing coordinated carbonate anions that were most likely formed from air. Due to the high R-values the crystal structure is unfortunately not reliable, but the coordinating carbonate anion motif is never the less assignable and legitimates further studies in that direction.

Furthermore, initial results concerning the reactivity of yellow solutions of the copper(I) complex of Hant-unspenp towards dioxygen were reported. Highly reactive oxygen adduct species could be successfully identified (Figure 103).

A superoxido species is the initially formed oxygen adduct species upon reaction of the copper(I) complex of Hant-unspenp with dioxygen indicated by a UV/Vis band at 422 nm.

**Fig. 103**

Oxygen adduct species identified during the reaction of acetone solutions of [Cu(Hant-unspen)]<sup>+</sup> with dioxygen.

The reaction of this species with a second [Cu(Hant-unspen)]<sup>+</sup> cation leads to the formation of the typical  $\mu$ -( $\eta^1$ : $\eta^1$ )-peroxido adduct observed *via* UV/Vis bands at 524 nm and a broad one around 600 nm. The equilibrium concentrations are very low compared to other unspenp relatives, possibly due to the interaction with the large  $\pi$ -system of the anthracene residue.

## 6.1.2 Bispic Relatives as Ligands

### 6.1.2.1 1,3-tpbd Coordination Compounds

Studies on the reactivity of copper(I) complexes of 1,3-tpbd towards oxygen using nitriles as solvent revealed a red (525 nm/propionitrile) intermediate that could unfortunately not be characterized so far. The “non-innocent” nature of the ligand itself accounts most likely for the sluggish behavior of its copper(I) complexes towards dioxygen, preventing more detailed studies. Attempts to structurally characterize a zinc(II) complex of 1,3-tpbd with an open coordination position remained unsuccessful. These attempts led to an interesting dimeric structure linked by hydroxy or water oxygen atoms unfortunately only solvable with high R-values.

Novel copper(II) complexes using 1,3-tpbd were successfully synthesized and structurally characterized in order to tune the magnetic properties. The use of the tetradentate ligands AsO<sub>4</sub><sup>3-</sup> and PO<sub>4</sub><sup>3-</sup> lead to the formation of uncommon tetranuclear coordination compounds with a  $\mu_4$ -XO<sub>4</sub> (X = P, As) binding motif. Figure 104 depicts the tetrakis monodentate binding mode of [Cu<sub>4</sub>(1,3-tpbd)<sub>2</sub>(AsO<sub>4</sub>)(ClO<sub>4</sub>)<sub>3</sub>(H<sub>2</sub>O)]<sup>2+</sup>. In case of arsenate, it is the first reported copper coordination compound of this type and one out of three using phosphate. Influencing the structure by introducing bulky organic residues, lead to the formation of a polymeric chain, where the copper centers are linked *via* bridging diphenylphosphate units, and a dimeric structure motif using monophenylphosphate as an anion.

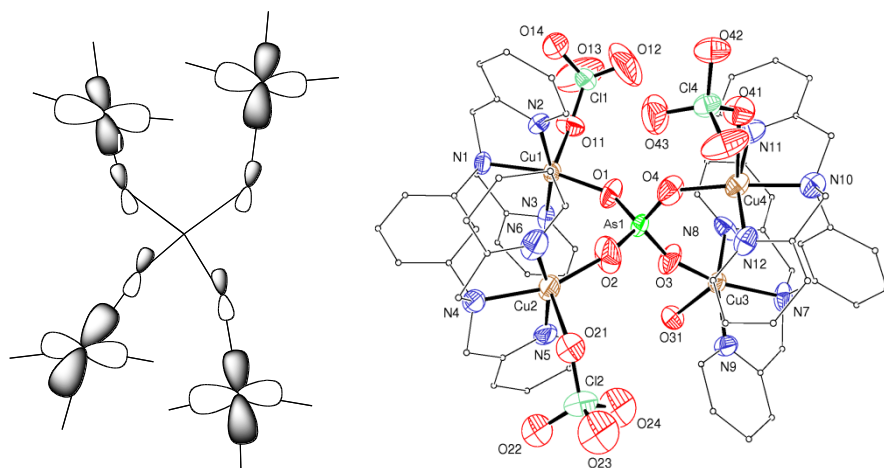


**Fig. 104** Structure of the cation  $[\text{Cu}_4(1,3\text{-tpbd})_2(\text{AsO}_4)(\text{ClO}_4)_3(\text{H}_2\text{O})]^{2+}$  and orbital considerations of one possible pathway for magnetic coupling over the arsenate bridge.

Using nitrate as an anion, also lead to the formation of a coordination polymer. The study of the magnetic properties of selected compounds showed weak antiferromagnetic coupling that is explainable through orbital considerations and structural knowledge of the possible pathways.

Nevertheless, the study demonstrates methods to increase the nuclearity and dimensionality of the presented compounds by varying the nature of the co-ligand and thus creating new possible pathways for magnetic coupling between copper(II) atoms in order to achieve stronger effects.

#### 6.1.2.2 Coordination Compounds Using Ligands Related to *tmpa*

The first copper(I) compounds using the ligands **L1** and **L2** could be successfully synthesized and structurally characterized. With weakly coordinating anions, the complexes tend to form dimeric compounds containing two copper(I) centers, as is demonstrated with the presented single crystal X-ray structures.

The isoelectronic zinc(II) ion forms monomeric, four or five coordinated species with either coordinating anions like chloride or weakly coordinating anions like triflate using the ligands **L1**, **L2** and **Mebispic**. This could be demonstrated again with the presented single crystal structures. In methanol, as a protic, coordinating solvent, the only octahedral zinc(II) complex using **L1** as ligand formed during this study. This is most likely due to the stabilization with hydrogen bridges between the two coordinated methanol molecules and unbound pyridine nitrogen atoms of the coordinated ligands.

This structural knowledge supported the explanation of the unusual fluxional behavior of the zinc(II) complexes of **L1**. Detailed emission studies in aprotic solvents successfully demonstrated the dependence of the emission and the electronic and structural properties of the studied compounds. The protonated ligand exhibits an unusual high bathochromic shift of the emission of  $6000\text{ cm}^{-1}$ . This is due to the protonation of the pyridine nitrogen forming a hydrogen bridge to the second pyridine residue of **L1** and thus forcing the rings into a coplanar configuration. Figure 105 depicts the structure of protonated **L1** and the observed emission spectra in dichloromethane as solvent.

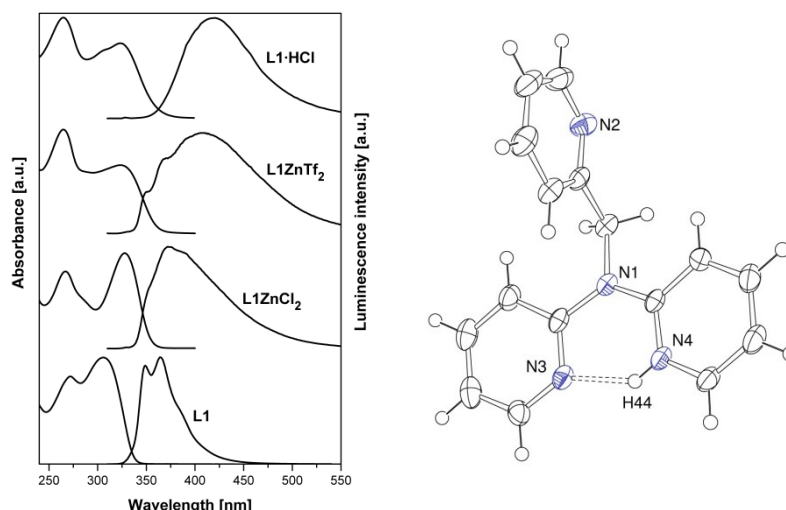


**Fig. 105** Structure of protonated ligand **L1** and absorbance/emission spectra of L1 compounds using dichloromethane as aprotic solvent.

The studied zinc(II) complexes can be regarded as intermediate situation between the free ligand **L1** and the protonated species. The solvent has a strong influence on the emission behavior among other things due to essential structural changes shown in methanol solution.

Additionally an interesting rotation mechanism is occurring in the coordination sphere of the zinc(II) complexes in solution that could be proved by detailed one and two dimensional variable temperature NMR studies. All signals could be successfully assigned to the protons of the studied compounds. The exchange mechanism is depicted in Figure 106.

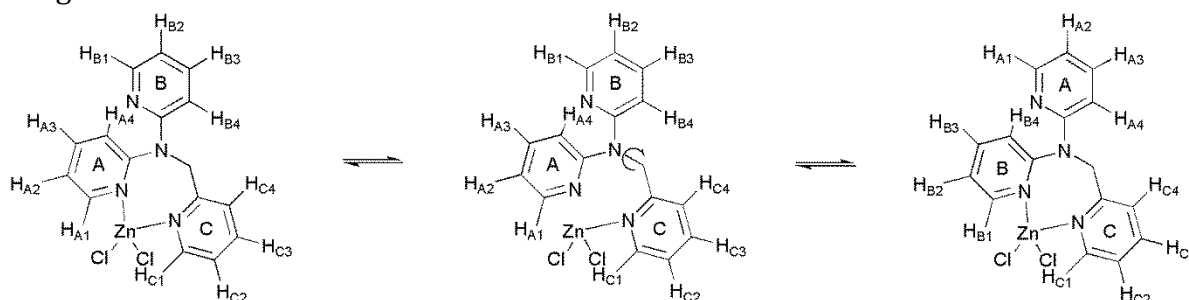


**Fig. 106** Rotation mechanism in the coordination sphere of zinc(II) complexes using **L1** as a ligand (here [ZnL1Cl<sub>2</sub>]).

### 6.1.2.3 Coordination Polymers Using Derivatives of bispic as Ligands

The derivatisation of ligand **L2** in order to study coordination polymers of copper and zinc, lead to the synthesis and characterization of three new ligands: **L3**, **L4** and **L5** (Figure 107). Copper(I) complexes with the ligands exhibit sluggish behavior towards dioxygen. Studies with regard to the reactivity towards *m*CPBA revealed an enhanced ligand oxidation reaction upon addition of copper(I) to **L4** that could unfortunately not be specified unambiguously so far.

One-dimensional coordination polymers of copper(I) using the ligands **L3** and **L4** could be structurally characterized. The crucial difference between these two ligands and **L5** is

the pyridyl nitrogen atom in 4-position favoring the formation of coordination polymers. It was possible to structurally characterize cage like copper(I) dimers of **L4** and **L5** also obtained with **L1** as ligand. These two ligands have the dipicolylamine binding unit in common, not present in **L3**.

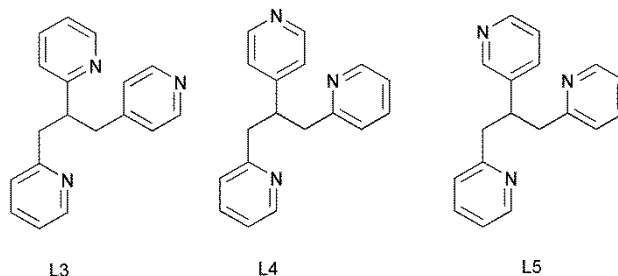


**Fig. 107** Structures of the new ligands **L3**, **L4** and **L5**

The use of zinc did unexpectedly not lead to the formation of coordination compounds with **L4**. All attempts resulted in the formation of an octahedral complex, where one zinc(II) ion is solely coordinated by the nitrogen in 4-position of two different ligand molecules, and not as one would expect by the excellent bispic binding site. Figure 108 depicts an ORTEP representation of the structure of the  $[\text{Zn}(\text{L4})_2(\text{DMF})_2]^{2+}$  ion.

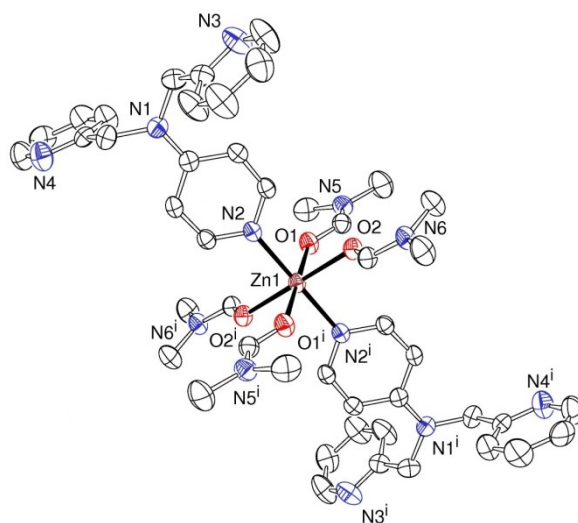


**Fig. 108** ORTEP representation of the  $[\text{Zn}(\text{L4})_2(\text{DMF})_2]^{2+}$  ion. Hydrogen atoms were omitted for clarity.

The combination of copper and zinc ions and **L4** to form heterobimetallic coordination polymers, with copper coordinating the bispic binding site and zinc preferring the nitrogen atom in 4-position, only lead to the formation of the known homometallic species. In contrast, NMR studies in solution point to the formation of a polymeric species with all pyridine nitrogen atoms coordinated.

## 6.2 Zusammenfassung

Kupfer- und Zink-Koordinationsverbindungen mit Bispicolylamin als Bindungsmotiv (Abbildung 109) erwecken aufgrund ihrer aussergewöhnlichen und vielfältigen Eigenschaften steigendes Interesse. Beispiele für Übergangsmetallkomplexe mit bispic Derivaten als Liganden finden sich in vielen Bereichen chemischer Forschung. Zink(II) Komplexe als Fluoreszenzsensoren in biologischen Prozessen, Kupfer(I)-Verbindungen zur Aktivierung kleiner Moleküle wie Kohlendioxide oder Koordinationspolymere mit besonderen Eigenschaften, die Möglichkeiten bislang unbekannter Verbindungen dieser Art sind sehr viel versprechend. Studien mit ausgewählten bispic Derivaten und deren Kupfer und Zink-Komplexen bilden die Grundlage der vorliegenden Arbeit.

Eine Erweiterung der bispic Bindungseinheit um einen vierten Stickstoff Donor führt zu einer tripodalen Ligandenklasse, die für die Stabilisierung reaktiver Metall-Sauerstoff Intermediate bekannt ist. Dies ermöglicht Studien zu Reaktionsmechanismen von metallenzymatisch katalysierten Oxidationsreaktionen. Unspenp (siehe Abbildung 109) als gut erforschter Ligand dieser Klasse ist leicht zu derivatisieren und eröffnet daher die Möglichkeit der Kombination der starken Bindungsaffinität zu Kupfer- und Zink-Ionen mit zusätzlichen Funktionalitäten wie zum Beispiel verbrückende Einheiten oder konjugierte  $\pi$ -Systemen. Koordinationsverbindungen funktionalisierter Derivate des Liganden unspenp sollten besondere Eigenschaften bei der Aktivierung von Sauerstoff und Stabilisierung dieser reaktiven Sauerstoffspezies haben. Daher wird in einem Teil dieser Arbeit die Synthese und Charakterisierung von Kupfer(I)-Komplexen mit Vertretern der unspenp-Familie und deren Reaktivität gegenüber Sauerstoff berichtet.

Die Strukturen der Liganden bispic und unspenp sind in Abbildung 109 dargestellt. Die präsentierten Ergebnisse gründen alle auf der Derivatisierung dieser Liganden und der Synthese und Charakterisierung ihrer Kupfer- und Zink-Koordinationsverbindungen.

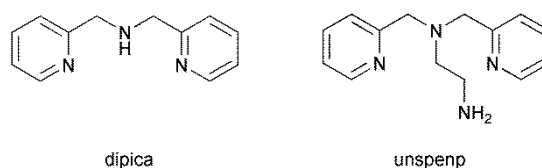


**Fig. 109** Strukturformel der Liganden bispic und unspenp.

In der vorliegenden Arbeit konnten bisher unbekannter Komplexverbindungen synthetisiert und interessante Eigenschaften bezogen auf Magnetismus, Emissionsverhalten und die Bildung eindimensionaler Koordinationspolymere beschrieben werden. Kapitel 6 fasst die voranstehenden Kapitel zusammen, um einen Überblick der erzielten Ergebnisse zu bieten.

### 6.2.1 Unspenp verwandte Verbindungen als Liganden

Gelbe Lösungen von Kupfer(I)-Komplexen mit xylylverbrückten unspenp Einheiten als Liganden konnten dargestellt und ihre Reaktivität gegenüber Sauerstoff mittels Tieftemperatur „stopped-flow“ Techniken untersucht werden. Dabei wurden erfolgreich reaktive Superoxido- und Peroxido-Spezies identifiziert. Im Falle des Imin Liganden konnten die bereits früher publizierten Ergebnisse von Garcia-Bosch *et al.* für Perchloratsalze bestätigt werden.<sup>123</sup> Der Kupfer(I)-Imxyl-unspenp-Komplex bildet bei der Reaktion mit Sauerstoff bei  $-90^{\circ}\text{C}$  in Propionitril ein typisches, metastabiles  $\mu$ -( $\eta^1:\eta^1$ )-Peroxido Intermediat aus. Identifizierbar ist das Intermediat anhand intensiver „charge-transfer“ Banden bei Wellenlängen von 502 und 637 nm. Die Imin Bande bei 378 nm zeigt ein unerklärliches, unstetes Verhalten während der ersten Reaktionsperiode. Die erfolgreich durch Tieftemperatur „stopped-flow“ Messungen identifizierten Sauerstoffintermediate der Kupfer(I) Komplexe von Imxyl-unspenp und Hxyl-unspenp sind in Abbildung 110 dargestellt.

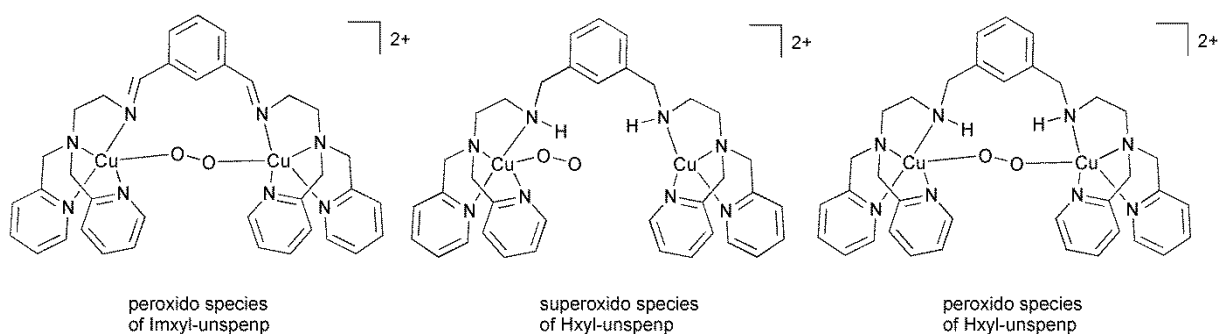


**Fig. 110** Reaktive Sauerstoffintermediate der Komplexe  $[\text{Cu}_2(\text{Imxyl-unspenp})]^{2+}$  bzw.  $[\text{Cu}_2(\text{Hxyl-unspenp})]^{2+}$ .

Der Kupfer(I)-Hxyl-unspenp Komplex bildet ähnliche UV/Vis Banden bei 517 und 602 nm aus. Diese sind ebenfalls der  $\mu$ -( $\eta^1:\eta^1$ )-Peroxido Spezies zuzuordnen. Anders als bei der Imin Verbindung ist bei  $-93^{\circ}\text{C}$  eine dritte intensive Bande bei 422 nm beobachtbar, die innerhalb von Sekunden wieder verschwindet. Sie ist am wahrscheinlichsten einer „end-on“ Superoxido Spezies, welche bereits aus Studien mit dem Liganden unspenp bekannt ist, zuzuordnen. Daher wird vermutet, dass der protonierte Ligand die Superoxido Spezies stabilisiert. Der schnelle Abbau ist auf das zweite intramolekulare Kupfer(I)-Zentrum zurück zu führen, da dieses eine hohe Bindungsaffinität zum Sauerstoff besitzt. Alle hier diskutierten Intermediate sind hoch reaktiv, was detailliertere kinetische Untersuchungen bis dato verhindert hat.

Es konnten erste Hinweise auf eine Reaktivität dieser Komplexe gegenüber Kohlendioxid aus der Luft gefunden werden. Eine Kristallstruktur mit hohen Fehlerindizes wurde präsentiert, die koordinierte Carbonat-Ionen zeigt, die durch die Reaktion mit Kohlendioxid aus der Luft entstanden sein müssen. Aufgrund des großen Fehlers ist diese Kristallstruktur leider nicht verlässlich, gibt aber durch die trotzdem klar erkennbaren Carbonat-Ionen Anlass zu weitergehenden Studien.



Desweiteren konnten erste Ergebnisse zur Reaktivität von gelben Kupfer(I)-Hant-unspenp Lösungen gezeigt werden. Auch hier wurden hoch reaktive Sauerstoff Addukt Komplexe mittels Tieftemperatur "stopped-flow" Messungen identifiziert (Abbildung 111).

Bei der Reaktion mit Sauerstoff wird im ersten Schritt eine Superoxido Spezies geformt, die eine UV/Vis Bande bei 422 nm hervorruft.

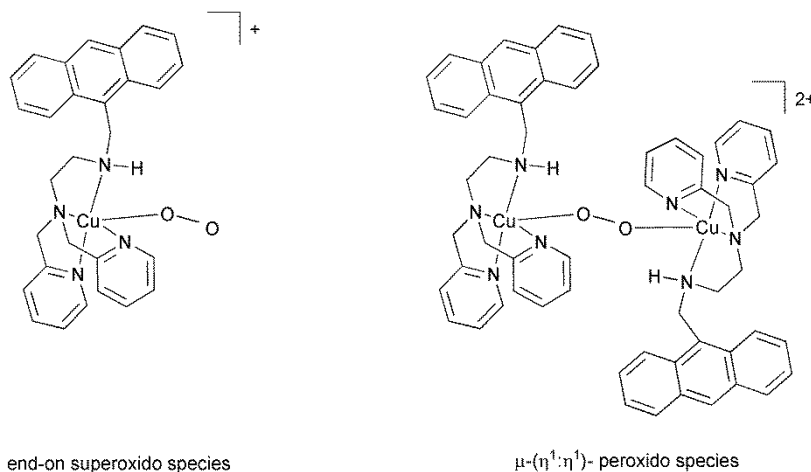


**Fig. 111** Sauerstoff Addukt Spezies bei der Reaktion von  $[\text{Cu}(\text{Hant-unspenp})]^+$  mit Sauerstoff.

Die Reaktion des Superoxidokomplexes mit einem zweiten  $[\text{Cu}(\text{Hant-unspenp})]^+$ -Kation führt zur Bildung des typischen  $\mu$ -( $\eta^1:\eta^1$ )-peroxido Addukts, identifizierbar durch eine UV/Vis Bande bei 524 nm und eine breite Bande bei 600 nm. Verglichen mit anderen unspenp Komplexen sind die Gleichgewichtskonzentrationen sehr gering, was möglicherweise auf die Interaktion mit dem großen  $\pi$ -Systems des Anthracenrestes zurück zu führen ist.

## 6.2.2 Bispic verwandte Verbindungen als Liganden

### 6.2.2.1 1,3-tpbd Koordinationsverbindungen

Studien zur Reaktivität der in Nitrilen gelösten Kupfer(I)-Komplexe des Liganden 1,3-tpbd gegenüber Sauerstoff zeigten das auftreten eines roten Intermediates (525 nm/Propionitril). Die wahrscheinliche Beteiligung des Liganden Moleküls an der Reaktion hat die Charakterisierung, sowie eine detailliertere Untersuchungen bis dato unmöglich gemacht. Versuche einen Zink(II)-1,3-tpbd-Komplex mit nicht oder schwach koordinierenden Anionen herzustellen, führten zu einem interessanten dimeren Molekül, in welchem die Metallatome über Hydroxidoionen oder Wassermoleküle miteinander verknüpft sind. Eine genauere Zuordnung der Brücken wurde durch die unzureichende Bestimmung der Struktur, erkennbar an den hohen Fehlerindizes, verhindert.

Um die magnetischen Eigenschaften der Verbindungen zu analysieren, konnten bis dahin unbekannte Kupfer(II)-1,3-tpbd-Komplexe synthetisiert und strukturell charakterisiert werden. Die Verwendung der tetradentaten Liganden Arsenat ( $\text{AsO}_4^{3-}$ ) und Phosphat ( $\text{PO}_4^{3-}$ ) führten zur Bildung sehr ungewöhnlicher  $\mu_4\text{-XO}_4$  ( $\text{X} = \text{P}, \text{As}$ )

Bindungsmotive. Abbildung 112 zeigt den tetrakis-monodentaten Bindungsmodus von  $[\text{Cu}_4(1,3\text{-tpbd})_2(\text{AsO}_4)(\text{ClO}_4)_3(\text{H}_2\text{O})]^{2+}$ . Im Fall des Arsenats stellt diese Struktur die erste Kupferkoordinationsverbindung dieses Bindungstyps dar. Die Phosphatverbindung ist nach bestem Wissen die dritte ihrer Art. Die Beeinflussung der Struktur durch die Verwendung sterisch anspruchsvoller organischer Reste führte zur Bildung einer Polymerkette, in der die Kupferzentren durch Diphenylphosphat Einheiten verknüpft sind. Desweiteren bildete sich bei der Verwendung von Monophenylphosphat ein dimeres Strukturmotiv aus.

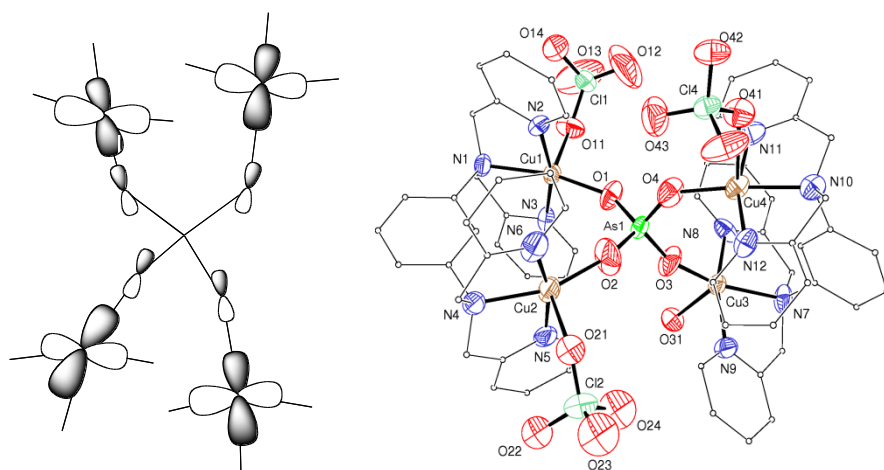


**Fig. 112** Molekülstruktur des Kations  $[\text{Cu}_4(1,3\text{-tpbd})_2(\text{AsO}_4)(\text{ClO}_4)_3(\text{H}_2\text{O})]^{2+}$  und Orbitalbetrachtungen zu einem möglichen Weg zur magnetischen Kopplung über die Arsenat Brücke hinweg.

Nitrat als Anion führte ebenfalls zur Bildung eines Koordinationspolymeres. Anhand theoretischer Orbitalbetrachtungen und der gewonnenen strukturellen Kenntnisse, erscheint eine schwach antiferromagnetische Kopplung möglich.

Auch wenn die erwarteten magnetischen Kopplungen nicht beobachtet werden konnten, zeigt die Studie neue Wege zur Verringerung der Nuklerität und Dimensionalität der gezeigten Koordinationsverbindungen durch die Variation der co-Liganden auf. Diese führen zu möglichen neuen Pfaden um stärkere Effekte zur magnetischen Kopplung zweier Kupfer(II)atome zu erzielen.

### 6.2.2.2 Koordinationsverbindungen mit Liganden verwandt mit *tmpa*

Es konnten die ersten Kupfer(I)-Komplexe der Liganden L1 und L2 erfolgreich synthetisiert und strukturell charakterisiert werden. Diese neigen bei der Verwendung von schwach koordinierenden Anionen zur Ausbildung von Dimeren mit zwei Kupfer(I)atome. Dies konnte mit Hilfe von Einkristallstrukturen der Verbindungen demonstriert werden.

Das isoelektronische Zink(II)-Ion bildet mit den Liganden L1, L2 und Mebispic monomere, vier- oder fünffach koordinierte Komplexverbindungen aus. Als Anionen wurden sowohl koordinierende Anionen wie Chlorid, sowie schwach koordinierende Anionen wie Triflat verwendet. Auch hier konnten Einkristallstrukturen der Verbindungen erhalten werden. Der einzige oktaedrische Zink(II)-Komplex dieser

Studie konnte mit dem Liganden **L1** in Methanol als protischem, koordinierendem Lösungsmittel dargestellt werden. Die Geometrie ist durch die Stabilisierung des Oktaeders durch Wasserstoffbrückenbindungen zwischen koordinierten Methanolmolekülen und ungebundenen Pyridin Stickstoffatomen der koordinierten Liganden zu erklären.

Diese gute strukturelle Kenntnis des Moleküls stützt die Erklärung des ungewöhnlichen Emissionsverhaltens der Zink(II)-Komplexe des Liganden **L1**. Detaillierte Studien zum Emissionsverhalten in aprotischen Lösungsmitteln konnten erfolgreich die Abhängigkeit der Emission von den elektronischen und strukturellen Eigenschaften der untersuchten Verbindungen zeigen. Der protonierte Ligand zeigte eine auffallend große bathochrome Verschiebung von  $6000\text{ cm}^{-1}$ , was auf die Protonierung eines Pyridin-Stickstoffes zurück zu führen ist. Dies bedingt die Ausbildung einer Wasserstoffbrückenbindung zum zweiten Pyridin Rest, die beide Ringe in eine coplanare Anordnung zwingt. Abbildung 113 zeigt die Molekülstruktur des protonierten Liganden **L1** und die beobachteten Emissionsspektren der untersuchten Verbindungen in Dichlormethan.

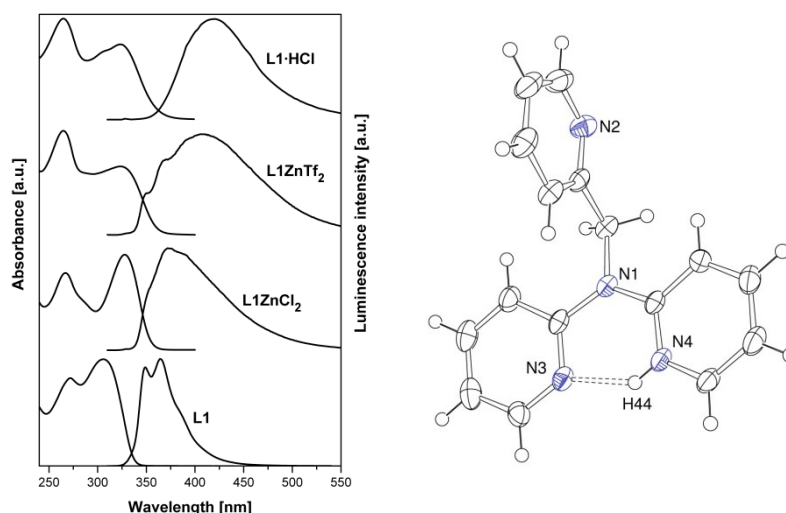


**Fig. 113** Struktur des protonierten Liganden **L1** und Absorptions/Emissions Spektren der untersuchten **L1** Verbindungen.

Die Zink(II)-Komplexe können hier als Übergangszustände zwischen dem freien Liganden **L1** und der protonierten Form betrachtet werden. Neben anderen Faktoren hat das Lösungsmittel einen starken Einfluß auf das Emissionsverhalten der Zinkkomplexe. Ursache dafür sind die gezeigten strukturellen Veränderungen der Komplexe in methanolischer Lösung.

Zusätzlich konnte ein interessanter Rotationsmechanismus in der Koordinationssphäre der Zink(II)-Komplexe in Lösung gezeigt werden. Belegt werden konnte dieser Mechanismus durch umfangreiche ein- und zweidimensionale NMR-Studien bei variabler Temperatur. Alle auftretenden Signale konnten eindeutig den Protonen der untersuchten Verbindungen zugeordnet werden. Der Austauschmechanismus ist in Abbildung 114 verdeutlicht.

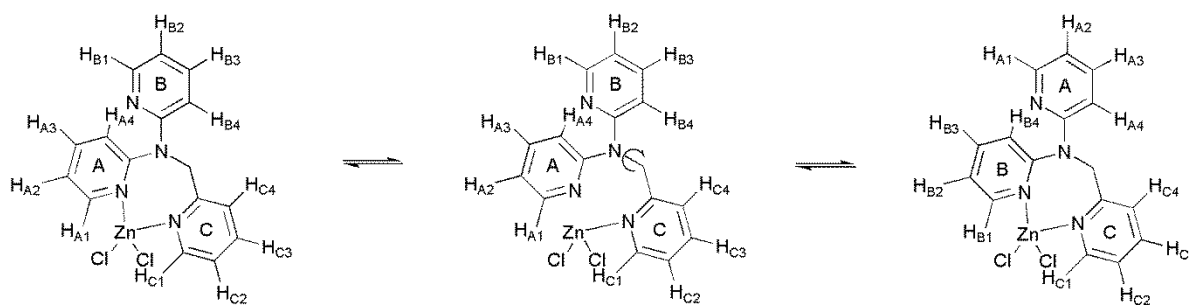


**Fig. 114** Rotationsmechanismus in der Koordinationssphäre von Zink(II)-Verbindungen mit dem Liganden **L1** (hier [ZnL1Cl<sub>2</sub>]).

### 6.2.2.3 Koordinationspolymere mit Derivaten des Liganden bispic

Die Derivatisierung des Liganden **L2** zur Untersuchung von Koordinationspolymeren mit Kupfer und Zink, führten zur Synthese und Charakterisierung der bis dahin unbekannten Liganden **L3**, **L4** und **L5** (Abbildung 115). Die untersuchten Kupfer(I)-Komplexe dieser Liganden zeigen ein undefinierbares Verhalten gegenüber Sauerstoff. Studien zur Reaktivität gegenüber *m*CPBA zeigten eine Ligandenhydroxylierungsreaktion, die bei der Zugabe von Kupfer(I)-Ionen zu dem reinen Liganden **L4** deutlich beschleunigt ablief. Der Reaktionsmechanismus, sowie die Produkte konnten noch nicht zweifelsfrei identifiziert werden.

Mit Kupferkomplexen der Liganden **L3** und **L4** konnten eindimensionale Koordinationspolymere strukturell charakterisiert werden. Der entscheidende Unterschied zum Liganden **L5** bildet der Pyridyl-Stickstoff in 4-Position, der eine Bildung eines Polymeres begünstigt. Es ist gelungen, käfigartige Kupfer(I) Dimere mit den Liganden **L4** und **L5** strukturell zu charakterisieren, die auch schon mit dem Liganden **L1** nachgewiesen werden konnten. Diese beiden Liganden haben die Bispicolylamin-Bindungseinheit gemein, die im Liganden **L3** nicht vorhanden ist.

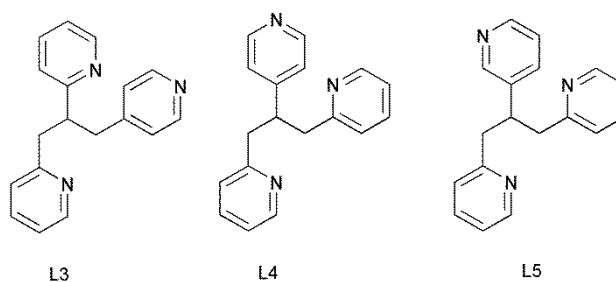


**Fig. 115** Strukturen der neuen Liganden **L3**, **L4** und **L5**

Die Verwendung von Zink als Zentralatom führte überraschenderweise nicht zur Bildung einer Koordinationsverbindung in der der Ligand **L4** über die affine bispic-Einheit an das Zink koordiniert. Alle Darstellungsversuche resultierten in der Bildung eines oktaedrischen Komplexes in dem ein Zinkion lediglich durch die Stickstoffatome in 4-Position koordiniert ist. Abbildung 116 zeigt eine ORTEP-Darstellung der Molekülstruktur des [Zn(L4)<sub>2</sub>(DMF)<sub>2</sub>]<sup>2+</sup> Ions.

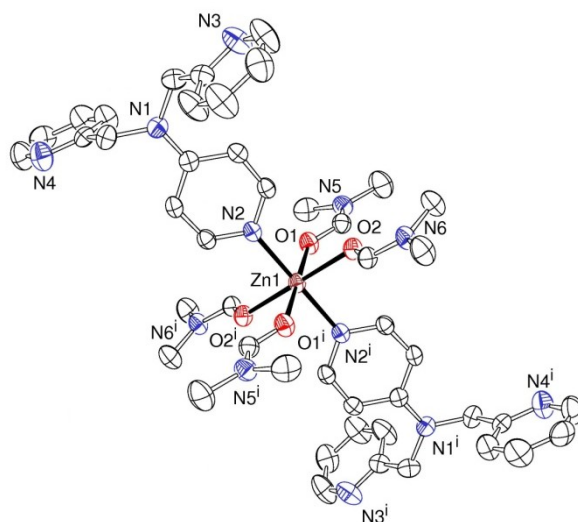


**Fig. 116** ORTEP Darstellung des  $[\text{Zn}(\text{L4})_2(\text{DMF})_2]^{2+}$  Ions. Wasserstoffatome wurden gelöscht.

Die Kombination von Kupfer und Zink Ionen und **L4** mit der Absicht heterobimetallische Koordinationspolymere zu erzeugen in denen Kupfer von der bispic Einheit und Zink von den Pyridin-Stickstoffen in 4-Position koordiniert wird führte zur Bildung der bekannten homometallischen Spezies. Im Gegensatz dazu weisen NMR Studien in Lösung auf polymere Spezies hin in der alle Pyridin-Stickstoffe koordinieren.

## 7 Publications

### 7.1 Journal Articles

*Synthesis and Characterization of Iron(II) Thiocyanate Complexes with Derivatives of the Tris(pyridine-2-ylmethyl)amine (tmpa) Ligand*

S. Kisslinger, H. Kelm, S. Zheng, A. Beitat, C. Würtele, R. Wortmann, S. Bonnet, S. Herres-Pawlis, H.-J. Krüger, and S. Schindler, *Zeitschrift für Anorganische und Allgemeine Chemie*, **2012**, DOI: 10.1002/zaac.201200237

*Syntheses, Characterisation and Magnetic Studies of Copper(II) Complexes with the Ligand N,N,N',N'-Tetrakis(2-pyridylmethyl)-1,3- benzenediamine (1,3-tpbd) and a Phenol Derivative*

S. Turba, S. P. Foxon, A. Beitat F. W. Heinemann, K. Petukhov, P. Müller, O. Walter, F. Lloret, M. Julve and S. Schindler, *Inorg. Chem.* **2012**, 51(1), 88-97.

*Syntheses, Emission Properties and Intramolecular Ligand Exchange of Zinc Complexes with Ligands Belonging to the tmpa Family*

A. Beitat, S. P. Foxon, C.-C. Brombach, H. Hausmann, F. W. Heinemann, F. Hampel, U. Monkowius, C. Hirtenlehner, G. Knör and S. Schindler, *Dalton Trans.*, **2011**, 40, 5090.

*Synthesis, Characterization and Properties of Iron(II) Complexes with a Series of Tripodal Ligands Based on the Parent Ligand tris(2-pyridylmethyl)amine*

S. Kisslinger, H. Kelm, A. Beitat, C. Würtele, H.-J. Krüger and S. Schindler, *Inorg. Chim. Acta*, **2011**, 374, 540.

*Iron and Cobalt Complexes with the Ligand (2-aminoethyl)bis(2-pyridyl- methyl)amine (uns-penp) and Derivatives*

T. Nebe, J.-Y. Xu, A. Beitat, C. Würtele, O. Walter, M. Serafin, S. Schindler, *Inorg. Chim. Acta*, 2010, 363, 2965.

*Reinvestigation of the Formation of a Mononuclear Fe(III) Hydroperoxido Complex Using High Pressure Kinetics*

T. Nebe, A. Beitat, C. Würtele, C. Dücker-Benfer, R. van Eldik, C. J. McKenzie and S. Schindler, *Dalton Trans.*, **2010**, 39, 1.

*Synthesis of Proline-Based Diketopiperazine Scaffolds*

N. Deppermann, A. H. G. P. Prenzel, A. Beitat and W. Maison, *J. Org. Chem.*, **2009**, 74, 4267.

### 7.1.1 Articles in Preparation

*Reversible Binding of Dioxygen by Copper(I) Complexes with Tripodal Tetraammine Ligands*

C. Würtele, I. Kerezsi, A. Beitat, M. Weitzer, S. P. Foxon, P. K. Wick, M. Holthausen and S. Schindler, Inorg. Chem., **2012**, ready for submission.

*Ligand Effects on the Formation of Coordination Polymers Containing Copper and Zinc Complexes with Derivatives of Tris(2-pyridylmethyl)amine (tmpa) as Ligands*

A. Beitat, J.-Y. Xu, C.-C. Brombach, H. Kelm, C. Würtele, and S. Schindler, Inorg. Chem., **2012**, ready for submission.

\* Underlined articles are part of this dissertation

### 7.2 Oral Presentations

*Zink Komplexe mit tripodalen Liganden der tmpa Familie*

Koordinationschemie – Treffen 2011, 27.02. – 01.03.2011, Stuttgart/D

*Zinc Complexes as Possible Phosphate Sensors*

2nd GGL Conference on Life Sciences, 30.09. - 01.10.2009, Gießen/D

### 7.3 Poster Presentations

*Studies on Zinc Complexes with Derivatives of tmpa*

IRMG Meeting 2010, Kloster Banz/D

*Studies on Zinc Complexes with Tripodal Amine Ligands of the tmpa Family*

Wissenschaftsforum Chemie, 30.08. – 02.09.2009, Frankfurt am Main/D

*Emission Studies on Zinc Complexes*

Wissenschaftsforum Chemie, 16. – 19.09.2007, Ulm/D

## 8 References

1. Turba, S. Syntheses, structures and properties of metal complexes of bis(2-pyridylmethyl) derivatives of o-, m-, and p- phenylenediamine and aniline. Justus-Liebig-Universität-Gießen, Gießen, 2007.
2. Auld, D. S., *BioMetals* **2001**, *14*, 271-313.
3. Auld, D. S., *BioMetals* **2009**, *22*, 141-148.
4. Mirica, L. M.; Ottenwaelder, X.; Stack, T. D. P., *Chem. Rev.* **2004**, *104*, 1013-1045.
5. Maret, W.; Li, Y., *Chem. Rev.* **2009**, *109*, 4682 - 4707.
6. Rubino, F. T.; Franz, K. J., *J. Inorg. Biochem.* **2012**, *107*, 129 - 143.
7. Solomon, E. I.; Chen, P.; Metz, M.; Lee, S.-K.; Palmer, A. E., *Angew. Chem., Int. Ed.* **2001**, *40*, 4570 - 4590.
8. Kaim, W.; Schwederski, B., *Bioanorganische Chemie-Zur Funktion chemischer Elemente in Lebensprozessen*. 3rd ed.; B. G. Teubner Verlag 1991.
9. Lippard, S. J.; Berg, J. M., *Bioanorganische Chemie*. Spektrum Verlag: Heidelberg, 1995.
10. Fridovich, I., *J. Biol. Chem.* **1997**, *272*, 18515 - 18517.
11. Sayre, L. M.; Perry, G.; Smith, M. A., *Chemical Research Toxicology* **2008**, *21*, 172 - 188.
12. Ohtsu, H.; Fukuzumi, S., *Angew. Chem., Int. Ed.* **2000**, *39*, 4537 - 4539.
13. Ohtsu, H.; Fukuzumi, S., *Chem.--Eur. J.* **2001**, *7*, 4947 - 4953.
14. Riley, D. P., *Chem. Rev.* **1999**, *99*, 2573 - 2587.
15. Que Jr., L.; Tolman, W. B., *Angew. Chem.* **2002**, *114*, 1160 - 1185.
16. Ojida, A.; Sakamoto, T.; Inoue, M.-a.; Fujishima, S.-h.; Lippens, G.; Hamachi, I., *J. Am. Chem. Soc.* **2009**, *131*, 6543 - 6548.
17. Angamuthu, R.; Byers, P.; Lutz, M.; Spek, A. L.; Bouwman, E., *Science* **2010**, *327*, 313-315.
18. Peterson, R. L.; Himes, R. A.; Kotani, H.; Suenobo, T.; Tian, L.; Siegler, M. A.; Solomon, E. I.; Fukuzumi, S.; Karlin, K. D., *J. Am. Chem. Soc.* **2011**, *133*, 1702-1705.
19. Suzuki, M., *Acc. Chem. Res.* **2007**, *40*, 609-617.
20. Cramer, C. J.; Tolman, W. B., *Acc. Chem. Res.* **2007**, *40*, 601-608.
21. Chufan, E. E.; Puiu, S. C.; Karlin, K. D., *Acc. Chem. Res.* **2007**, *40*, 563-572.
22. Würtele, C. End-On "Copper Dioxygen Adduct Complexes". Justus-Liebig-Universität Gießen, Gießen, 2008.
23. Jacobsen, R. R.; Tyeklár, Z.; Farooq, A.; Karlin, K. D.; Liu, S.; Zubieta, J., *J. Am. Chem. Soc.* **1988**, *110*.
24. Würtele, C.; Sander, O.; Lutz, V.; Waitz, T.; Tuczec, F.; Schindler, S., *J. Am. Chem. Soc.* **2009**, *131*, 7544-7545.
25. Caron, S.; Dugger, R. W.; Ruggeri, S. G.; Ragan, J. A.; Brown Ripin, D. H., *Chem. Rev.* **2006**, *106*, 2943-2989.
26. Que, L.; Tolman, W. B., *Nature* **2008**, *455*, 333-340.



27. Donoghue, P. J.; Tehranchi, J.; Cramer, C. J.; Sarangi, R.; Solomon, E. I.; Tolman, W. B., *J. Am. Chem. Soc.* **2011**, *133*.
28. Wendlandt, A. E.; Suess, A. M.; Stahl, S. S., *Angew. Chem.* **2011**, *123*, 11256-11283.
29. Benson, E. E.; Kubiak, C. P.; Sathrum, A. J.; Smieja, J. M., *Chem. Soc. Rev.* **2009**, *38*, 89-99.
30. Saveant, J.-M., *Chem. Rev.* **2008**, *108*, 2348-2378.
31. *Physiol. Rev.* **1993**, *73*, 79-118.
32. Tomat, E.; Lippard, S. J., *Curr. Opin. Chem. Biol.* **2010**, *14*, 225-230.
33. Buccella, D.; Horowitz, J. A.; Lippard, S. J., *J. Am. Chem. Soc.* **2011**, *133*, 4101-4114.
34. Valeur, B.; Leray, I., *Coord. Chem. Rev.* **2000**, *205*, 3-40.
35. Wong, B. A.; Friedle, S.; Lippard, S. J., *J. Am. Chem. Soc.* **2009**, *131*, 7142-7152.
36. Nolan, E. M.; Lippard, S. J., *Acc. Chem. Res.* **2009**, *42*, 193-203.
37. Katayev, E. A.; Ustynyuk, Y. A.; Sessler, J. L., *Coord. Chem. Rev.* **2006**, *250*, 3004-3037.
38. Lipscomb, W. N.; Sträter, N., *Chem. Rev.* **1996**, *96*, 2375-2433.
39. Sakamoto, T.; Ojida, A.; Hamachi, I., *Chem. Commun.* **2009**, 141-152.
40. Huang, X.-h.; Lu, Y.; He, Y.-b.; Chen, Z.-h., *European Journal of Organic Chemistry* **210**, 1921-1927.
41. Kim, K. M.; Oh, D. J.; Ahn, K. H., *Chem.--As. J.* **2011**, *6*, 122-127.
42. Bailar Jr., J. C.; Jolly, W. L. E., *Preparative Inorganic Reactions*. In Interscience: New York, 1964; Vol. 1, pp 1-25.
43. Chen, C.-T.; Suslick, K. S., *Coord. Chem. Rev.* **1993**, *128*, 293-322.
44. Hoskins, B. F.; Robson, R., *J. Am. Chem. Soc.* **1989**, *111*, 5962-5964.
45. Hoskins, B. F.; Robson, R., *J. Am. Chem. Soc.* **1990**, *112*, 1546-1554.
46. Jiang, H.-L.; Xu, Q., *Chem. Commun.* **2011**, *47*, 3351-3370.
47. Cundy, C., *Chem. Rev.* **2003**, *13*.
48. Stock, N.; Biswas, S., *Chem. Rev.* **2012**, *112*, 933-969.
49. Long, W. L.; Vittal, J. J., *Chem. Rev.* **2011**, *111*, 688-764.
50. Khlobystov, A. N.; Blake, A. J.; Champness, N. R.; Lemenovskii, D. A.; Majouga, A. G.; Zyk, N. V.; Schröder, M., *Coord. Chem. Rev.* **2001**, *222*, 155-192.
51. Li, G.; Zhu, C.; Xi, X.; Cui, Y., *Chem. Commun.* **2009**, 2118-2120.
52. Lee, *Angew. Chem., Int. Ed.* **2004**, *43*.
53. McManus, G. J.; Perry IV, J. J.; Perry, M.; Wagner, B. D.; Zaworotko, M. J., *J. Am. Chem. Soc.* **2007**, *129*, 9094-9101.
54. Mas-Balleste, R.; Gomez-Herrero, J.; Zamora, F., *Chem. Soc. Rev.* **2010**, *39*, 4220-4233.
55. Cao, R.; McCarthy, B. D.; Lippard, S. J., *Inorg. Chem.* **2011**, *50*, 9499-9507.
56. Verdaguer, M.; Linert, W., *Molecular Magnets: Recent Highlights*. 1 ed.; Springer: Wien, 2003; p 220.
57. Kahn, O., *Molecular Magnetism*. Wiley VCH: Weinheim, 1993.
58. Willet, R. D.; Gatteschi, D.; Kahn, O., *Magneto-Structural Correlations in Exchange Systems*. Reidel: Dordrecht, 1985.

59. Ruiz, E.; Alemany, P.; Alvarez, S.; Cano, J., *J. Am. Chem. Soc.* **1997**, *119*, 1297-1303.
60. Ruiz, E.; Alemany, P.; Alvarez, S.; Cano, J., *Inorg. Chem.* **1997**, *36*, 3683-3688.
61. Ruiz, E.; Cano, J.; Alvarez, S.; Alemany, P., *J. Am. Chem. Soc.* **1998**, *120*, 11122-11129.
62. Cano, J.; Alemany, P.; Alvarez, S.; Verdaguer, M.; Ruiz, E., *Chem. Eur. J.* **1998**, *4*, 476-484.
63. Cano, J.; Ruiz, E.; Alemany, P.; Lloret, F.; Alvarez, S., *J. Chem. Soc., Dalton Trans.* **1999**, 1669-1676.
64. Rodríguez-Forte, A.; Alemany, P.; Alvarez, S.; Ruiz, E., *Chem. Eur. J.* **2001**, *7*, 627-637.
65. Ruiz, E.; Rodríguez-Forte, A.; Alvarez, S.; Verdaguer, M., *Chem. Eur. J.* **2005**, *11*, 2135-2144.
66. Venegas-Yazigi, D.; Aravena, D.; Spodine, E.; Ruiz, E.; Alvarez, S., *Coord. Chem. Rev.* **2010**, *254*, 2086-2095.
67. Canadillas-Delgado, L.; Fabelo, O.; Pasan, J.; Delgado, F. S.; Lloret, F.; Julve, M.; Ruiz-Perez, C., *Dalton Trans.* **2010**, *39*, 7286-7293.
68. Schindler, S.; Szalda, D. J.; Creutz, C., *Inorg. Chem.* **1992**, *31*, 2255-2264.
69. Foxon, S.; Xu, J.-Y.; Turba, S.; Leibold, M.; Hampel, F.; Heinemann, F. W.; Walter, O.; Würtele, C.; Holthausen, M.; Schindler, S., *Eur. J. Inorg. Chem.* **2007**, 429-443.
70. Foxon, Simon P.; Torres, Gemma R.; Walter, O.; Pedersen, Jens Z.; Toftlund, H.; Hüber, M.; Falk, K.; Haase, W.; Cano, J.; Lloret, F.; Julve, M.; Schindler, S., *Eur. J. Inorg. Chem.* **2004**, 335-343.
71. Foxon, Simon P.; Walter, O.; Koch, R.; Rupp, H.; Müller, P.; Schindler, S., *Eur. J. Inorg. Chem.* **2004**, 344-348.
72. Turba, S.; Walter, O.; Schindler, S.; Nielsen, L. P.; Hazell, A.; J. McKenzie, C.; Lloret, F.; Cano, J.; Julve, M., *Inorg. Chem.* **2008**, *47*, 9612-9623.
73. Li, D.; Tian, J.; Kou, Y.; Huang, F.; Chen, G.; Gu, W.; Liu, X.; Liao, D.; Cheng, P.; Yan, S., *Dalton Trans.* **2009**, 3574-3583.
74. Li, D.-D.; Huang, F.-P.; Chen, G.-J.; Gao, C.-Y.; Tian, J.-L.; Gu, W.; Liu, X.; Yan, S.-P., *J. Inorg. Biochem.* **2010**, *104*, 431-441.
75. Chakrabarti, S.; Natarajan, S., *Angew. Chem. Int. Ed.* **2002**, *41*, 1224-1226.
76. Rao, V. K.; Chakrabarti, S.; Natarajan, S., *Inorg. Chem.* **2007**, *46*, 10781-10790.
77. de Hoog, P.; Gamez, P.; Lüken, M.; Roubeau, O.; Krebs, B.; Reedijk, J., *Inorg. Chim. Acta* **2004**, *357*, 213-218.
78. Gómez-Saiz, P.; García-Tojal, J.; Díez-Gómez, V.; Gil-García, R.; Pizarro, J. L.; Arriortua, M. I.; Rojo, T., *Inorg. Chem. Commun.* **2005**, *8*, 259-262.
79. Grove, H.; Sletten, J.; Julve, M.; Lloret, F.; Cano, J., *J. Chem. Soc., Dalton Trans.* **2001**, 259-265.
80. Addison, A. W.; Rao, T. N.; Reedijk, J.; van Rijn, J.; Verschoor, G. C., *J. Chem. Soc., Dalton Trans.* **1984**, 1349-1356.
81. Doyle, R. P.; Kruger, P. E.; Julve, M.; Lloret, F.; Nieuwenhuyzen, M., *CrystEngComm* **2002**, *4*, 13-16.

82. Hou, Y.; Wang, S.; Shen, E.; Xiao, D.; Wang, E.; Li, Y.; Xu, L.; Hu, C., *J. Mol. Struct.* **2004**, *689*, 81-88.
83. Li, Y.; De, G.; Yuan, M.; Wang, E.; Huang, R.; Hu, C.; Hu, N.; Jia, H., *Dalton Trans.* **2003**, 331-334.
84. Soumahoro, T.; Burkholder, E.; Ouellette, W.; Zubieta, J., *Inorg. Chim. Acta* **2005**, *358*, 606-616.
85. Krebs, B.; Schepers, K.; Bremer, B.; Henkel, G.; Althaus, E.; Mueller-Warmuth, W.; Griesar, K.; Haase, W., *Inorg. Chem.* **1994**, *33*, 1907-1914.
86. Lim, J.-S.; Aquino, M. A. S.; Sykes, A. G., *Inorg. Chem.* **1996**, *35*, 614-618.
87. True, A. E.; Scarrow, R. C.; Randall, C. R.; Holz, R. C.; Que, L., *J. Am. Chem. Soc.* **1993**, *115*, 4246-4255.
88. Neves, A.; de Brito, M. A.; Vencato, I.; Drago, V.; Griesar, K.; Haase, W., *Inorg. Chem.* **1996**, *35*, 2360-2368.
89. Finn, R.; Zubieta, J., *Chem. Commun.* **2000**, 1321-1322.
90. Kawafune, I.; Matsubayashi, G.-e., *Bull. Chem. Soc. Jpn.* **1994**, *67*, 694-698.
91. Neier, R.; Trojanowski, C.; Mattes, R., *J. Chem. Soc., Dalton Trans.* **1995**, 2521-2528.
92. Pohl, M.; Lin, Y.; Weakley, T. J. R.; Nomiya, K.; Kaneko, M.; Weiner, H.; Finke, R. G., *Inorg. Chem.* **1995**, *34*, 767-777.
93. Bu, X.; Feng, P.; Stucky, G. D., *J. Chem. Soc., Chem. Comm.* **1995**, 1337-1338.
94. Soghomonian, V.; Chen, Q.; Haushalter, R. C.; O'Connor, C. J.; Tao, C.; Zubieta, J., *Inorg. Chem.* **1995**, *34*, 3509-3519.
95. Zhang, Y.; Clearfield, A.; Haushalter, R. C., *Chem. Mater.* **1995**, *7*, 1221-1225.
96. Cargill Thompson, A. M. W.; Bardwell, D. A.; Jeffery, J. C.; Ward, M. D., *Inorg. Chim. Acta* **1998**, *267*, 239-247.
97. Raidt, M.; Neuburger, M.; Kaden, T. A., *Dalton Trans.* **2003**, 1292-1298.
98. Tobey, S. L.; Anslyn, E. V., *J. Am. Chem. Soc.* **2003**, *125*, 14807-14815.
99. Tobey, S. L.; Anslyn, E. V., *Org. Lett.* **2003**, *5*, 2029-2031.
100. Tobey, S. L.; Jones, B. D.; Anslyn, E. V., *J. Am. Chem. Soc.* **2003**, *125*, 4026-4027.
101. Zhang, T.; Anslyn, E. V., *Tetrahedron* **2004**, *60*, 11117-11124.
102. Wall, M.; Hynes, R. C.; Chin, J., *Angewandte Chemie International Edition in English* **1993**, *32*, 1633-1635.
103. Moreno, Y.; Vega, A.; Ushak, S.; Baggio, R.; Pena, O.; Le Fur, E.; Pivan, J.-Y.; Spodine, E., *J. Mat. Chem.* **2003**, *13*, 2381-2387.
104. Phuengphai, P.; Youngme, S.; Pakawatchai, C.; van Albada, G. A.; Quesada, M.; Reedijk, J., *Inorg. Chem. Commun.* **2006**, *9*, 147-151.
105. Fernández, I.; Ruiz, R.; Faus, J.; Julve, M.; Lloret, F.; Cano, J.; Ottenwaelder, X.; Journaux, Y.; Muñoz, M. C., *Angew. Chem. Int. Ed.* **2001**, *40*, 3039-3042.
106. Yuste, C.; Ferrando-Soria, J.; Cangussu, D.; Fabelo, O.; Ruiz-Pérez, C.; Marino, N.; De Munno, G.; Stiriba, S.-E.; Ruiz-García, R.; Cano, J.; Lloret, F.; Julve, M., *Inorg. Chim. Acta* **2010**, *363*, 1984-1994.

107. Pardo, E.; Ferrando-Soria, J.; Dul, M.-C.; Lescouëzec, R.; Journaux, Y.; Ruiz-García, R.; Cano, J.; Julve, M.; Lloret, F.; Cañadillas-Delgado, L.; Pasán, J.; Ruiz-Pérez, C., *Chem. Eur. J.* **2010**, *16*, 12838-12851.
108. Hatfield, W. E.; Estes, W. E.; Marsh, W. E.; Pickens, M. W.; ter Haar, L. W.; Weller, R. R., In *Extended Linear Chain Compounds*, Miller, J. S., Ed. Plenum: New York, 1983; Vol. 3, p 43.
109. Cano, J. *VP MAG package*, University of Valencia, Spain, 2003.
110. Doyle, R. P.; Bauer, T.; Julve, M.; Lloret, F.; Cano, J.; Nieuwenhuyzen, M.; Kruger, P. E., *Dalton Trans.* **2007**, 5140-5147.
111. Earnshaw, A., *Introduction to Magnetochemistry*. Academic Press: London, 1968.
112. Sheldrick, G. M. *SHELXTL NT*, 6.12; Bruker AXS, Inc.: Madison, WI, USA, 2002.
113. Sheldrick, G. M. *ShelX-97*, Universität Göttingen, 1997.
114. Turba, S.; Foxon, S. P.; Beitat, A.; Heinemann, F. W.; Petukhov, K.; Müller, P.; Julve, M.; Schindler, S., *Inorg. Chem.* **2012**, *51*, 88-97.
115. Müller, J.; Würtele, C.; Walter, O.; Schindler, S., *Angew. Chem., Int. Ed.* **2007**, *46*.
116. Li, L.; Narducci Sarjeant, A. A.; Vance, M. A.; Zakharov, L. N.; Rheingold, A. L.; Solomon, E. I.; Karlin, K. D., *J. Am. Chem. Soc.* **2005**, *127*, 15360-15361.
117. Li, L.; Narducci Sarjeant, A. A.; Karlin, K. D., *Inorg. Chem.* **2006**, *45*, 7160-7172.
118. Addison, A. W.; Rao, T. N.; Reedijk, J.; van Rijn, J.; Verschoor, G. C., *J. Chem. Soc., Dalton Trans.* **1984**, 1349-1356.
119. Hollemann, A. F.; Wiberg, N., *Lehrbuch der Anorganischen Chemie*. 102 ed.; de Gruyter: Berlin, 1900; p 241.
120. *Purification of laboratory chemicals*. 6th ed.; Elsevier Inc.: Burlington, MA, USA, 2009; p 176.
121. Schindler, S., *Eur. J. Inorg. Chem.* **2000**, 2311-2326.
122. Würtele, C. Untersuchungen zur Aktivierung von Sauerstoff an tripodalen ein- und mehrkernigen Kupfer(I)-Komplexen. Justus-Liebig-Universität Gießen, Gießen, 2005.
123. Garcia-Bosch, I.; Company, A.; Frisch, J. R.; Torrent-Sucarrat, M.; Cardallach, M.; Gamba, I.; Güell, M.; Casella, L.; Que Jr., L.; Ribas, X., *Angew. Chem., Int. Ed.* **2010**, *49*, 2406-2409.
124. Berggren, G.; Huang, P.; Eriksson, L.; Styring, S.; Anderlund, M. F.; Thapper, A., *Dalton Trans.* **2010**, *39*, 11035-11044.
125. Drewry, J. A.; Gunning, P. T., *Coord. Chem. Rev.* **2011**, *255*, 459-472.
126. Beitat, A. Synthetische und spektroskopische Untersuchungen von Zinkkomplexen mit tripodalen Liganden. Justus-Liebig-Universität Gießen, Gießen, 2007.
127. Hoffmann, N., *ChemSusChem* **2012**, *5*, 352 - 371.
128. Wang, M.; Na, Y.; Gorlov, M.; Sun, L., *Dalton Trans.* **2009**, 6458 - 6467.
129. Inagaki, A.; Akita, M., *Coord. Chem. Rev.* **2010**, *254*, 1220 - 1239.
130. Esswein, A. J.; Nocera, D. G., *Chem. Rev.* **2007**, *107*, 4022 - 4047.

131. Schatz, M.; Leibold, M.; Foxon, S. P.; Weitzer, M.; Heinemann, F. W.; Hampel, F.; Walter, O.; Schindler, S., *Dalton Trans.* **2003**, 1480-1487.
132. Weitzer, M.; Schatz, M.; Hampel, F.; Heinemann, F. W.; Schindler, S., *Dalton Trans.* **2002**, 5, 686-694.
133. Weitzer, M.; Schindler, S., *Inorg. Chem.* **2003**, 42, 1800-1806.
134. Schatz, M.; Becker, M.; Thaler, F.; Hampel, F.; Schindler, S.; Jacobsen, R. R.; Tyeklar, Z.; Murthy, N. N.; Gosh, P.; Chen, Q.; Zubieta, J.; Karlin, K. D., *Inorg. Chem.* **2001**, 40, 2312-2322.
135. Karlin, K. D.; Wei, N.; Jung, B.; Kaderli, S.; Niklaus, P.; Zuberbühler, J., *J. Am. Chem. Soc.* **1993**, 115, 9506-9514.
136. *Inorg. Chim. Acta* 331, 208-.
137. *Inorg. Chim. Acta* 324, 232-.
138. van Albada, G. A.; Mutikainen, I.; Roubeau, O.; Turpeinen, U.; Reedijk, J., *Inorg. Chim. Acta* **2002**, 331, 208-215.
139. Riduan, S. N.; Zhang, Y., *Dalton Trans.* **2010**, 39, 3347-3357.
140. Kubas, G. J.; Monzyk, B.; Crumbliss, A. L., *Inorg. Synth.* **1979**, 19.
141. Li, Y.; Maret, W., *Chem. Rev.* **2009**, 109, 4682-4707.
142. Mareque Rivas, J. C.; Torres Martin de Rosales, R.; Parsons, S., *Dalton Trans.* **2003**, 2156-2163.
143. Mareque Rivas, J. C.; Torres Martin de Rosales, R.; Parsons, S., *Dalton Trans.* **2003**, 4385-4386.
144. Mareque-Rivas, J. C.; Prabakaran, R.; Parsons, S., *Dalton Trans.* **2004**, 1648-1655.
145. Mareque-Rivas, J. C.; Torres Martin de Rosales, R.; Parsons, S., *Chem. Commun.* **2004**, 610-611.
146. Rivas, J. C. M.; Prabakaran, R.; de Rosales, R. T. M.; Metteau, L.; Parsons, S., *Dalton Trans.* **2004**, 2800-2807.
147. Rivas, J. C. M.; Salvagni, E.; de Rosales, R. T. M.; Parsons, S., *Dalton Trans.* **2003**, 3339-3349.
148. Rivas, J. C. M.; Salvagni, E.; Parsons, S., *Dalton Trans.* **2004**, 4185-4192.
149. Szajna, E.; Makowska-Grzyska, M. M.; Wasden, C. C.; Arif, A. M.; Berreau, L. M., *Inorg. Chem.* **2005**, 44, 7595-7605.
150. Szajna-Fuller, E.; Ingle, G. K.; Watkins, R. W.; Arif, A. M.; Berreau, L. M., *Inorg. Chem.* **2007**, 46, 2353-2355.
151. Foxon, S. P.; Walter, O.; Schindler, S., *Eur. J. Inorg. Chem.* **2002**, 111-121.
152. Yang, W. Y.; Schmider, H.; Wu, Q. G.; Zhang, Y. S.; Wang, S. N., *Inorg. Chem.* **2000**, 39, 2397-2404.
153. Dick, S.; Weiss, A., *Z. Naturforsch. B* **1997**, 52, 188-192.
154. Jensen, K. B.; McKenzie, C. J.; Simonsen, O.; Toftlund, H.; Hazell, A., *Inorg. Chim. Acta* **1997**, 257, 163-172.
155. Nelson, S. M.; Rodgers, J., *J. Chem. Soc. A* **1968**, 272-276.
156. Astner, J.; Weitzer, M.; Foxon, S. P.; Schindler, S.; Heinemann, F. W.; Mukherjee, J.; Gupta, R.; Mahadevan, V.; Mukherjee, R., *Inorg. Chim. Acta* **2008**, 361, 279-292.

157. Chomitz, W. A.; Minasian, S. G.; Sutton, A. D.; Arnold, J., *Inorg. Chem.* **2007**, *46*, 7199-7209.
158. Murthy, N. N.; Karlin, K. D., *J. Chem. Soc. Chem. Commun.* **1993**, 1236-1238.
159. Adams, H.; Bailey, N. A.; Fenton, D. E.; He, Q.-Y., *J. Chem. Soc. Dalton Trans.* **1995**, 697-699.
160. Allen, C. S.; Chuang, C.-L.; Cornebise, M.; Canary, J. W., *Inorg. Chim. Acta* **1995**, *239*, 29-37.
161. Mao, Z.-W.; Hang, Q.-W.; Tang, W.-X.; Liu, S.-X.; Wang, Z.-M.; Huang, J.-L., *Polyhedron* **1996**, *15*, 321-325.
162. Adams, H.; A. Bailey, N.; E. Fenton, D.; He, Q.-Y., *J. Chem. Soc. Dalton Trans.* **1997**, 1533-1540.
163. Nielsen, A.; Veltze, S.; Bond, A. D.; McKenzie, C. J., *Polyhedron* **2007**, *26*, 1649-1657.
164. Wang, S. N., *Coord. Chem. Rev.* **2001**, *215*, 79-98.
165. Ni, J.; Xie, Y.; Liu, X.; Liu, Q., *Appl. Organomet. Chem.* **2002**, *17*, 315-316.
166. Hoorn, H. J.; deJoode, P.; Driessen, W. L.; Reedijk, J., *Recl. Trav. Chim. Pays-B.* **1996**, *115*, 191-197.
167. Palaniandavar, M.; Butcher, R. J.; Addison, A. W., *Inorg. Chem.* **1996**, *35*, 467-471.
168. Palaniandavar, M.; Mahadevan, S.; Köckerling, M.; Henkel, G., *J. Chem. Soc. Dalton Trans.* **2000**, 1151-1154.
169. Wirbser, J.; Vahrenkamp, H., *Z. Naturforsch. B* **1992**, *47b*, 962-968.
170. Mandel, J. B.; Maricondi, C.; Douglas, B. E., *Inorg. Chem.* **1988**, *27*, 2990-2996.
171. Weisstuch, A. C.; Testa, J., *J. Phys. Chem. A* **1968**, *72*, 1982-1987.
172. Monkman, A. P.; Palsson, L.-O.; Higgins, R. W. T.; Wang, C.; Bryce, M. R.; Batsanov, A. S.; Howard, J. A. K., *J. Am. Chem. Soc.* **2002**, *124*, 6049-6055.
173. Ho, K.-Y.; Yu, W.-Y.; Cheung, K.-K.; Che, C.-M., *Chem. Commun.* **1998**, 2101-2102.
174. Montalti, M.; Credi, A.; Prodi, L.; Gandolfi, M. T., *Handbook of Photochemistry*. 3 ed.; CRC: Boca Raton, 2006.
175. Beitat, A.; Foxon, S. P.; Brombach, C.; Hausmann, H.; Heinemann, F. W.; Monkowius, U.; Hirtenlehner, C.; Knör, G.; Schindler, S., *Dalton Trans.* **2011**, *40*, 5090-5101.
176. Wang, S.; Xiong, S.; Wang, Z.; Du, J., *Chem.-Eur. J.* **2011**, *17*, 8630 - 8642.
177. Baidya, M.; Kobayashi, S.; Brotzel, F.; Schmidhammer, U.; Riedle, E.; Mayr, H., *Angew. Chem., Int. Ed.* **2007**, *46*, 6176-6179.
178. Müller, C. E.; Schreiner, P. R., *Angew. Chem.* **2011**, *123*, 6136-6167.
179. Radziszewski, B., *Chem. Ber.* **1885**, *18*, 355-356.
180. Nagataki, T.; Ishii, K.; Tachi, Y.; Itoh, S., *Dalton Trans.* **2007**, 1120-1128.
181. Bröhmer, M. C.; Mundinger, S.; Bräse, S.; Bannwarth, W., *Angew. Chem.* **2011**, *123*, 6299-6301.
182. Baidya, M.; Brotzel, F.; Mayr, H., *Org. Biomol. Chem.* **2010**, *8*, 1929-1935.
183. Azuma, Y.; Imai, H.; Yoshimura, T.; Kawabata, T.; Imanishi, M.; Futaki, S., *Org. Biomol. Chem.* **2012**, *10*, 6062 - 68.

184. Brown, K.; Zolezzi, S.; Aguirre, P.; Venegas-Yazigi, D.; Paredes-Garcia, V.; Baggio, R.; Novak, M. A.; Spodine, E., *Dalton Trans.* **2009**, 1422-1427.
185. Wang, Z.; Xiong, R.-G.; Foxman, B. M.; Wilson, S. R.; Lin, W., *Inorg. Chem.* **1999**, 38, 1523-1528.

## **Versicherung**

Ich erkläre: Ich habe die vorgelegte Dissertation selbständig und ohne unerlaubte fremde Hilfe und nur mit den Hilfen angefertigt, die ich in der Dissertation angegeben habe. Alle Textstellen, die wörtlich oder sinngemäß aus veröffentlichten Schriften entnommen sind, und alle Angaben, die auf mündlichen Auskünften beruhen, sind als solche kenntlich gemacht. Bei den von mir durchgeführten und in der Dissertation erwähnten Untersuchungen habe ich die Grundsätze guter wissenschaftlicher Praxis, wie sie in der „Satzung der Justus-Liebig-Universität Gießen zur Sicherung guter wissenschaftlicher Praxis“ niedergelegt sind, eingehalten.

Alexander Beitat